ENERGY BASIS OF DISASTERS AND THE CYCLES OF ORDER AND DISORDER

By

JOHN FRANKLIN ALEXANDER, JR.

A DISSERTATION PRESENTED TO THE GRADUATE COUNCIL OF
THE UNIVERSITY OF FLORIDA
IN PARTIAL FULFILLMENT OF THE REQUIREMENTS FOR THE
DEGREE OF DOCTOR OF PHILOSOPHY

UNIVERSITY OF FLORIDA

1978

ACKNOWLEDGEMENTS

Appreciation is expressed to Dr. Howard T. Odum, my committee chairman, for his inspiration, knowledge, and deep insight into ecological problems of man and nature. I am greateful for having worked under Dr. Odum on many exciting projects and study in his systems ecology program in the Department of Environmental Engineering Sciences from which I have developed a keen sense of appreciation for ecological and energy principles which organize the world.

Many contributions were made by members of my committee: Dr. Paul Doughty in the field after the Guatemala earthquake; Dr. Jim Burns with simulation; Dr. Wayne Huber with global energies; Dr. Charles Roessler with ionizing radiation. Also, assistance was provided by Dr. Jerome Milliman's advice on economic aspects of disasters. Professor Byron Spangler advised on the engineering aspects of disasters.

Investigation was carried out under the sponsorship of the United States Department of Energy (contract EY-76-S-05-4398) project entitled "Energy Analysis and Models of the United States" and the United States Nuclear Regulatory Commission (contract NRC-04-77-123) project entitled "The Energy Analysis of Environmental Values," H. T. Odum, principal investigator. Work in Guatemala was sponsored by the United States Agency for International Development (contract AID 520-268) project entitled "A Comprehensive Plan for the Reconstruction of El Progreso, Guatemala," John F. Alexander, Jr., principal investigator.

Thanks are extended to Joan Breese and Linda Yates for assisting in typing drafts, David Jass for drafting of figures, Diane Goddard for editing, and Rossina Fernandez for final typing the manuscript.

TABLE OF CONTENTS

Page

ACKNOWLEDGEMENTS. ii

LIST OF TABLES. vii

LIST OF FIGURES viii

ABSTRACT. xi

INTRODUCTION. 1

- Theory of Order, Disorder, and Material Cycling. 2
    - Catastrophic Consumption and Pulsing. 5
    - Secondary Disorder and Cascading. 8
- Global Model 11
- The Global Energy Web and Natural Disasters. 11
- Energy Quality and Embodied Energy 14
- Energy Embodied in Radiation 16
- Previous Work on the Theory of Order, Disorder, and Pulsing. 18
- Previous Work on Natural Disasters 20
- Description of Study Situations and Previous Work. 24
    - Global Models of Atmospheric, Oceanic, Biological, Geological, and Urban Systems 24
    - The Tropical Rain Forest at El Verde, Puerto Rico and the Effect of Radiation 28
    - Johnstown, Pennsylvania, and the Failure of the South Dam 32
    - Guatemala and the Earthquake of February 4, 1976. . . . 36

METHODS 43

- Description of Modeling Language and Symbols 43
- Development of Models. 48
- Limiting Factors and Differential Equations. 49
- Data Assembly and Evaluation of Models 52
- Simulation Procedures. 53
- Calculation of Ratios. 54
- Calculation of Spatial Distribution of Seismic Energy. . . . 55
- Plan of Study. 59

RESULTS 61

- Simulation and Analysis of Order-Disorder Models 61
    - Switching Pulse Models. 71

Page

Exponential Surge Model 71
Evaluation of Global Energy Web and Disasters. 79
Atmospheric Circulation and Storms. 83
Oceanic Circulation 92
Photosynthetic Production, Animals, and Fire. 99
Plate Tectonics, Volcanoes, and Earthquakes 105
Urban Structure, Fire, Disasters, and War 113
The Global Energy Web and Energy Quality of Disasters . 121
Evaluation and Simulation of the Radiation Stress on a Tropical Rain Forest at El Verde, Puerto Rico 122
Evaluation of the Rain Forest Model 126
Simulation of the Order-Disorder Process in the Rain Forest Ecosystem. 134
Calculation of Order-Disorder Energy Ratios for the Rain Forest 134
Evaluation and Simulation of the Johnstown Flood of 1889 . . 136
Evaluation of the Model 139
Simulation of the South Fork Dam Failure and the Destruction of Johnstown 143
Disaster-Amplifier Ratios for Johnstown and the Flood . 146
Evaluation and Simulation of the Guatemala Earthquake of 1976 146
Evaluation of the Model 149
Simulation of the Earthquake and Secondary Distribution 154
Calculation of Disaster-Amplifier Ratios. 154

DISCUSSION 164

The Dynamics of Pulsing Systems. 164
The Cycling of Matter 164
Energy Convergence and Storage. 165
Exponential Surges and Energy Pulses. 165
System Control through Cascading. 166
Dynamic Behavior of Energy Cycling Models 166
Global Energy Web. 166
Energy Quality, A Universal Energy Conversion Factor. . 167
Embodied Solar Energy, A Universal Measure. 168
Disaster-Amplifier Ratios, A Measure of Control 168
The Frequency of Pulsing and Control. 169
Control of Global Cycles by Solar Pulses. 169
Disasters. 170
The Energy Cost and Benefit of Disasters. 170
The Distribution of Disaster Pulses as a Control Device 173
Common Aspects of Disaster and Disorder in Different Systems 175
Pulsing and Maximum Power. 175
Disaster Planning and Future Research. 176

Page

APPENDIX I NOTES TO TABLES 2-7, 9, 10 AND 11. 182

APPENDIX II DYNAMO PROGRAMS. 217

LIST OF REFERENCES. 221

BIOGRAPHICAL SKETCH 232

LIST OF TABLES

Table Page

1 STEADY-STATE SOLUTIONS AND STEADY-STATE VALUES FOR THE ORDER-DISORDER MINIMODELS IN FIGURE 14. 69

2 EVALUATION, NAME, AND DESCRIPTION OF ENERGY FLOWS AND STORAGES FOR GLOBAL ATMOSPHERIC SECTOR MODEL IN FIGURE 19. 86

3 EVALUATION, NAME AND DESCRIPTION OF ENERGY FLOWS AND STORAGES FOR THE OCEANIC SECTOR OF THE MODEL IN FIGURE 21. 95

4 EVALUATION, NAME, AND DESCRIPTION OF ENERGY FLOWS AND STORAGES FOR BIOSPHERE MODEL IN FIGURE 22 102

5 EVALUATION, NAME, AND DESCRIPTION OF ENERGY FLOWS IN GEOLOGICAL SECTION OF GLOBAL MODEL IN FIGURE 23. . . 108

6 EVALUATION, NAME, AND DESCRIPTION OF ENERGY FLOWS AND STORAGES FOR FLOODS AND CITIES OF FIGURE 24 116

7 GLOBAL DISASTER-AMPLIFIER RATIOS FOR CITIES AND NATURAL DISASTERS 120

8 ENERGY QUALITY FACTORS FOR GLOBAL PROCESSES AND DISASTERS 123

9 GAMMA RADIATION AND SOLAR RADIATION STORAGES AND FLOWS FOR MODEL OF RAIN FOREST IN FIGURE 27 129

10 EVALUATION, NAME, AND DESCRIPTION OF ENERGY FLOWS AND STORAGES FOR JOHNSTOWN FLOOD MODEL. 140

11 EVALUATION, NAME, AND DESCRIPTION OF ENERGY FLOWS AND STORAGES FOR EARTHQUAKE MODEL IN FIGURE 32. 150

12 ENERGY ABSORBED PER SQUARE METER OF ADOBE HOUSE BY ISOSEISMAL INTENSITY ZONES FOR GUATEMALA EARTHQUAKE OF FEBRUARY 4, 1976 153

13 DISASTER-AMPLIFIER FACTORS FOR SECONDARY DISASTERS IN VARIOUS CITIES IN GUATEMALA. 162

LIST OF FIGURES

Figure		Page
1	Energy circuit models of order and disorder.	4
2	Energy circuit models of order-disorder cycle with catastrophic energy pulsing in the disordering loop. . .	7
3	Energy circuit model of concept of cascading of energy pulses which may be regarded as disasters, to smaller elements of the systems	10
4	Model of the global crust composed of energy flows of atmosphere, ocean, biological, geological, and urban subsystems	13
5	Energy circuit translation of economic model of risk . .	22
6	Location maps and diagram of Puerto Rico and El Verde Experiment	31
7	Location map of Johnstown and the South Fork Dam	34
8	Location maps of Guatemala, El Progreso, and the Motagua Fault.	39
9	Maps of damage to adobe structures and earthquake intensity in Guatemala	41
10	Energy circuit language group symbols.	45
11	Energy circuit language mathematical symbols used to construct modules in Figure 8.	47
12	Order-disorder model in energy circuit language, illustrating the incorporation of internal and external limiting factors.	51
13	Order-disorder model illustrating energy flows used in calculating the order-disorder ratio and the disaster-amplifier ratio.	57
14	A comparison of several order-disorder models and their simulation results	64

Figure Page

15 Energy circuit disorder model of disaster typical of previous fire and epidemic models of other researchers. 73

16 Order-disorder energy circuit model with catastrophic energy, pulse generated by consumer module. 75

17 Results of simulation of pulse model in Figures 15 and 16. 78

18 Web model of global energy. 81

19 Energy circuit diagrams of atmospheric system 85

20 Global distribution of solar energy with latitude . . . 90

21 Energy circuit models of the oceanic systems of the earth 94

22 Energy circuit models of biological energy concentration process of the world. 101

23 Energy circuit model of earth's geological system . . . 107

24 Urban order-disorder model with depreciation, fire, war, and natural disasters in disorder process 115

25 Global energy web model diagramed in energy circuit language. 119

26 Order-disorder model of gamma ray stress on tropical rain forest at El Verde, Puerto Rico. 125

27 Evaluated order-disorder model of gamma ray radiation stress on tropical rain forest in El Verde, Puerto Rico. 128

28 Gamma radiation field and effects on tropical rain forest at El Verde. 131

29 Results of simulation of order-disorder gamma ray model in Figure 27. 133

30 Energy circuit model of Johnstown, Pennsylvania, 1889, and the disruption generated by the catastrophic failure of the South Fork Dam 138

31 Simulation results of failure of the South Fork Dam model in Figure 30. 145

32 Earthquake order-disorder model for Guatemala earthquake 148

Figure Page

33 Energy distribution in Guatemala from the major event, February 4, 1976 earthquake. 156

34 Simulation results of earthquake model in Figure 32. . 158

35 Structural damage of towns in Guatemala as a function of earthquake energy dissipated by the adobe houses. . 160

36 Conceptual model illustrating possible mechanisms for control of global energy cycles by Solar Pulsing . . . 172

37 A test of the effect of pulsing on the principle of maximum power. 178

Abstract of Dissertation Presented to the Graduate Council
of the University of Florida in Partial Fulfillment of the
Requirements for the Degree of Doctor of Philosophy

ENERGY BASIS OF DISASTERS AND THE CYCLES OF ORDER AND DISORDER

By

John Franklin Alexander, Jr.

August 1978

Chairman: Howard T. Odum
Major Department: Environmental Engineering Science

A quantitative theory of cycles order and disorder was applied to the earth and evaluated to form an energy basis for the global cycles, surges, and disasters. Energy circuit language was used to diagram the world system and show a common pattern in the order-disorder processes.

Storms, floods, forest fires, volcanic eruptions, earthquakes, urban fires, and wars were modeled as the catastrophic release of energy previously converged and stored. Released energy disordered and recycled material available to stimulate a new cycle of growth. Cascading of catastrophic processes of disasters was modeled with a world web. The feedback in the global energy web was provided by the control action of disaster pulses. The global model was presented in both diagrammatic and differential equation form with the energy flows and storages evaluated. Order-disorder models of the atmospheric, oceanic, biological, geological, and urban systems of earth were connected to form an energy convergence network.

The global energy model was used to calculate energy quality factors (ratio of energy of one type generating energy of another type) for the earth's major energy transformations. The ratio of solar energy required to produce a catastrophic event to the energy released in the event (Calories per Calorie) was found to be $1 \times 10^{7}:1$ for volcanoes, $5 \times 10^{6}:1$ for earthquakes, $1 \times 10^{5}:1$ for urban fires, floods, and wars, $2 \times 10^{4}:1$ for forest fires, and $2 \times 10^{3}:1$ for storms. The energy quality factors of stored energy were used to calculate embodied solar energy.

The hypothesis of selection for maximum power was used to explain the prevalence of systems that recycle structure by the catastrophic release of energy pulses generated in disasters. The solar energy embodied in the disordered city structure was found to be 1.4, 1.3, and 1.7 times the solar energy embodied in storm, flood, and seismic pulses of the global web.

The dynamic properties of several configurations of models of the cycles order-disorder were analyzed by solving the model in differential equation form and through computer simulation. The most suitable model has a production function supplying energy to a consumer that alternately shifts from linear flow to a surge of exponential growth causing an oscillation.

Suitability of order-disorder models were further tested by application to three case studies: (a) effect of gamma radiation stress on a tropical rain forest in Puerto Rico; (b) the disordering of Johnstown, Pennsylvania, by the great flood of 1889; and (c) the destruction of El Progreso, Guatemala, by the earthquake of 1976. The dynamic effects of the flood on Johnstown and the earthquake on El Progreso were modeled with two order-disorder models in cascade and simulated. The resulting graphs of the destruction of the towns studied compared favorably with observed results.

The energy flows that produced order in the radiation, flood, and earthquake case were 13,000, 970, and 7,700 times the energy flows required to generate disorder when measured in heat equivalents. When expressed in embodied solar equivalents, the ratio of ordering energy to disordering energy was found to be 4:1 for radiation disordering and from 25:1 to 85:1 for pulse disordering.

The theory provided suggestions for land-use policy. Energy ratios that provide a quantitative basis for disaster planning can be developed for a local environment of pulsing energy.

Possibilities were considered that cycles of order and disorder of the earth are synchronized by cycles of sunspots. Energy quality and pulse amplifier ratios of solar flares may be high enough to control many global cycles.

INTRODUCTION

A major problem in environmental science is the nature of cycles of order, disorder, and disasters. How are these related to the solar energies that drive most processes on earth? How do the patterns of the biosphere limit the roles of humanity and provide planning principles? In this dissertation, energy analysis, energy systems concepts, and simulation methods are used to test theories relating order and disorder. Included are evaluations of earthquakes, floods, ionizing radiation, solar flares, and the world energy web. Specific case studies include the gamma irradiation of a tropical rain forest, the Johnstown flood of 1889, and the Guatemala earthquake of 1976.

The ability to converge energy in space and time by cycling matter may be a fundamental principle of all systems of man and nature. As systems build structure by concentration of energy in the form of ordered matter, potential energy gradients are created. The storages of energy that are formed become sources of even steeper potential gradients. Extensive competition exists for the use of concentrated forms of energy. The principle of selection for maximum power suggests that the system that can process storages most effectively will out compete the other systems. When energy is processed at very high rates,pulses are generated that are transmitted against the concentration gradient performing a control on the surrounding areas and on the energy convergence web. These surges are often regarded as disasters.

Theory of Order, Disorder, and Material Cycling

Figure 1a is the basic configuration of the order-disorder model diagramed in energy circuit language (H. T. Odum, 1971) that was used throughout this research (see Methods section). The system converges energy to power the production of structure by transforming disordered matter into ordered state (lower entropy); however, the entropy of the total process increases as much as the energy required to power the production process is degraded as waste heat. The structure built up in the production process continuously undergoes depreciation in such a manner that the stored energy is dissipated as waste heat and the material recycles to form disordered matter.

The energy circuit model in Figure 1b is similar, except an external energy source drives the consumption-recycle process. In this model the rate of material recycle is proportional to the magnitude of the stress energy source. In both of the models in Figure 1, the matter is cycled as energy flow through the system. In one the energy driving recycle is only from its own storages.

A basic question, analyzed in this dissertation and illustrated by the order-disorder model in Figure 1, is "what relationship, if any, exists between the energy required to order a system versus that required to disorder it." In order to address this question, the model was evaluated using data from several examples and simulated. Examples included irradiation of a tropical rain forest at El Verde, Puerto Rico, and the catastrophic

Figure 1. Energy circuit models of order and disorder.

(a) Energy circuit of basic process of order and disorder believed to be characteristic of all systems of man and nature; recycle uses stored energy.

(b) Basic order-disorder model with disordering process driven by external energy source.

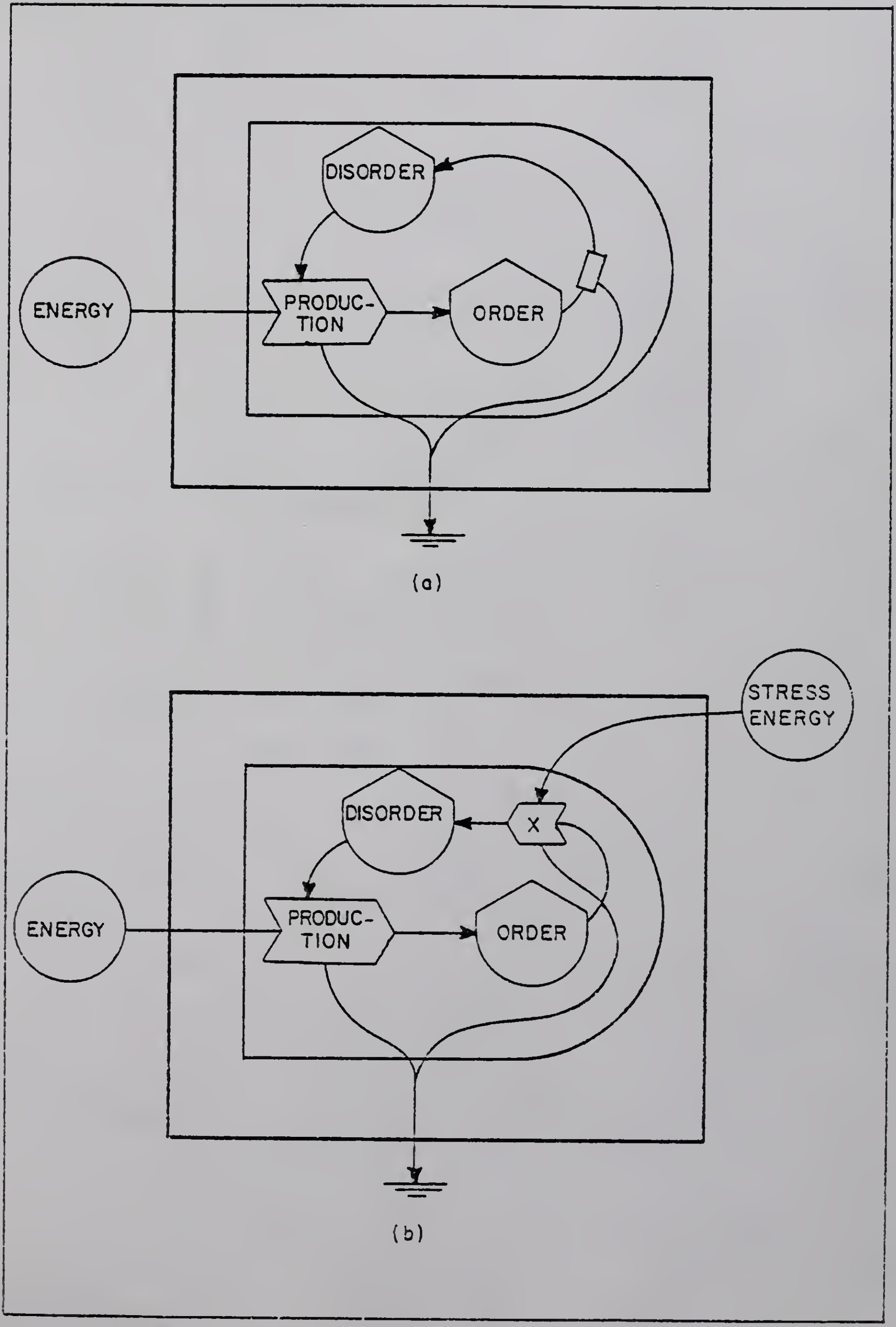
DISORDER
ENERGY
PRODUCTION
ORDER
(a)
STRESS ENERGY
DISORDER
X
ENERGY
PRODUCTION
ORDER
(b)

destructions of Johnstown, Pennsylvania, and El Progreso, Guatemala.

Catastrophic Consumption and Pulsing

As systems build up substantial storages of energy in the structure form of ordered matter, massive potential gradients are formed. As the gradient becomes larger, the production of order by the system often exceeds the loss due to depreciation through linear processes such as diffusion. This, therefore, increases the possibility and opportunity for a consumer system to form that will further concentrate the stored energy and release a pulse of energy in a control action. To explain this concept, the order-disorder models in Figure 2, similar to the previously introduced model, were developed. An autocatalytic or self-generating consumer system was added in the disordering energy flow path to further concentrate stored energy. In the system diagramed in Figure 2a, a trigger pulse, or seed, is required to start the consumer system; however, once triggered the system will grow at an exponential rate until the energy storage in the form of order in the producer system is consumed. This growth of the consumer system produces an energy control pulse that is exponential at first and fades as the storages are exhausted.

The model in Figure 2b is similar except the system is capable of self-triggering; that is, when the energy storage in the producer system reaches threshold, the consumer system self-activates. Consumer systems that can process large quantities of energy at high rates produce catastrophic pulses of energy when activated. The order-disorder models in Figure 2 are suggested as a dynamic system that can simulate the concentration, storage, and catastrophic release process found in many systems of man and nature, of which natural disasters are a special

Figure 2. Energy circuit models of order-disorder cycle with catastrophic energy pulsing in the disordering loop.

(a) Externally triggered disaster.

(b) Self-triggered disaster.

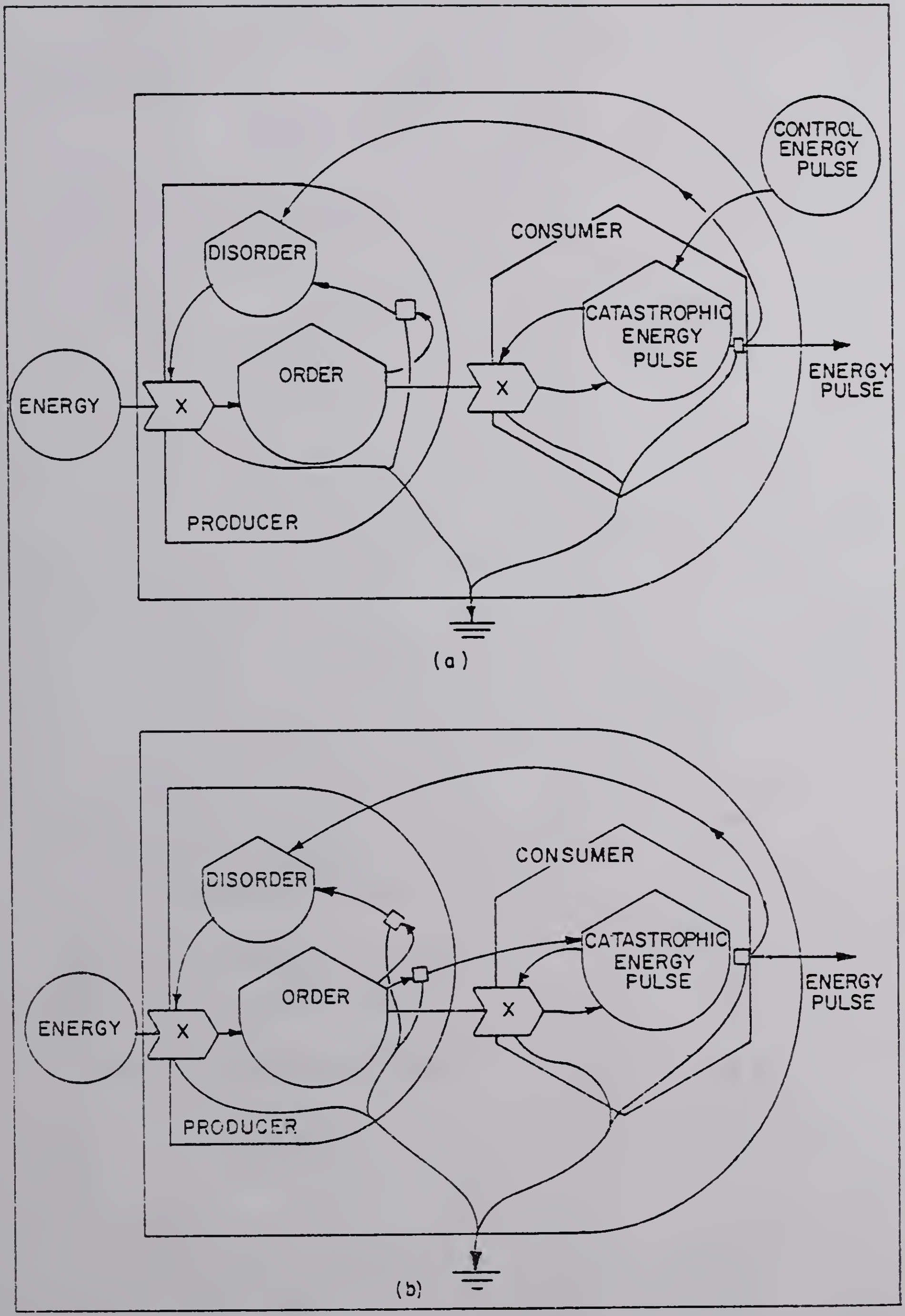
CONTROL ENERGY PULSE
DISORDER
CONSUMER
CATASTROPHIC ENERGY PULSE
ORDER
ENERGY
X
X
ENERGY PULSE
PRODUCER
(a)
DISORDER
CONSUMER
CATASTROPHIC ENERGY PULSE
ORDER
ENERGY
X
X
ENERGY PULSE
PRODUCER
(b)

case. Data from the catastrophic collapse of a dam resulting from the exponential growth of turbulence were used to evaluate the model. Simulations were performed and the results compared to field observation for the Guatemala earthquake and the Johnstown flood.

Secondary Disorder and Cascading

Two order-disorder models with catastrophic consumer systems were cascaded to extend the theory to explain and simulate the secondary disruptions created by a major disaster pulse such as an earthquake. Once the surge of consumption starts it may generate waves of disordering energy spreading into surrounding energy convergence systems. Figure 3 is an energy circuit diagram of this concept. In the model, the energy storage increases until the energy flow in the disordered loop is great enough to generate a dynamic structure, which feeds back some of the energy to pump more. This results in exponential growth of the storage of kinetic energy until the potential energy is effectively exhausted. When sufficient energy is coupled to the structure of the impacted system, the potential energy stored in the impacted system is released causing a secondary disaster. Some notable examples of secondary events triggered by earthquakes are given by Ayre (1975): (1) failure of man-made structures such as buildings and bridges; (2) avalanches, landslides, rockslides, and other natural disruptions; (3) fire; (4) floods and flash floods from tidal waves and ruptured dams; and (5) volcanic eruption. Note that each of the above events involves the cascaded release of potential energy stored in the structure of the secondary source. The cascading of disasters is believed to be of considerable importance in understanding the dynamic behavior of systems under the high stress of natural disaster pulses.

Figure 3. Energy circuit model of concept of cascading of energy pulses which may be regarded as disasters, to smaller elements of the systems.

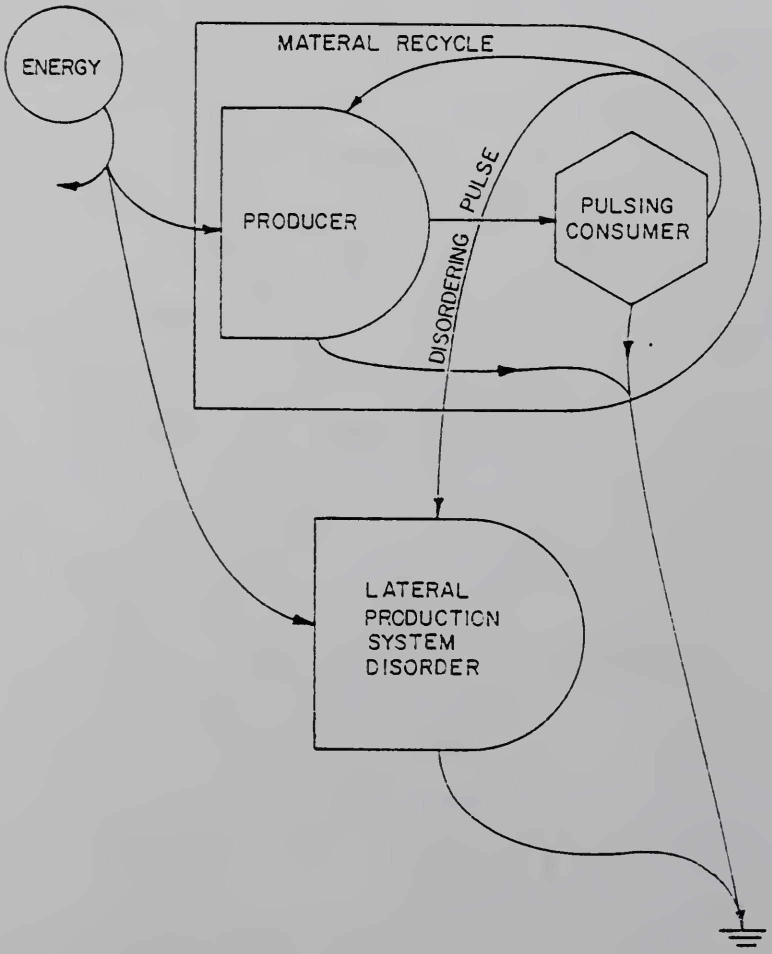
ENERGY
MATERAL RECYCLE
PRODUCER
PULSE
DISORDERING
PULSING CONSUMER
LATERAL PRODUCTION SYSTEM DISORDER

The multiple hazard phenomena must be included in a disaster theory to make it plausible for application to real world cases.

This theory was tested by evaluation of the model with data from an earthquake and the secondary destruction of several towns. Simulations were performed and compared to observed destruction.

Global Model

The global model in Figure 4 connects energy concentration, storage, and consumer subsystems into a web. This energy web provides a framework that helps to explain the nature and function of disasters in a global context. The model also outlines a conceptual network for evaluating the flows and storages of energy that power various global processes. The web is composed of self-regulating units that successfully converge energy of the sun. Each module produces order and releases it with a pulsed consumption that forms a temporary high energy system. To survive in competition this pulse of energy must couple with or feed back to other systems. Pulsing the energy that is fed back in a control action produces an amplifier effect in disordering and recycling other systems. Systems that survive are those that become organized and adapted to operate in a regime of pulses and use these pulses to power recycling processes and other means to achieve maximum power.

The Global Energy Web and Natural Disasters

Natural disasters have been a subject of great interest to humanity throughout recorded history. Earthquakes, volcanoes, floods, storms, fires, and epidemics take a great toll in life and property. Hazards in the United States currently generate an economic loss in excess of one

Figure 4. Model of the global crust composed of energy flows of atmosphere, ocean, biological, geological, and urban subsystems. Each system is modeled to include energy concentration, storage, and catastrophic release processes.

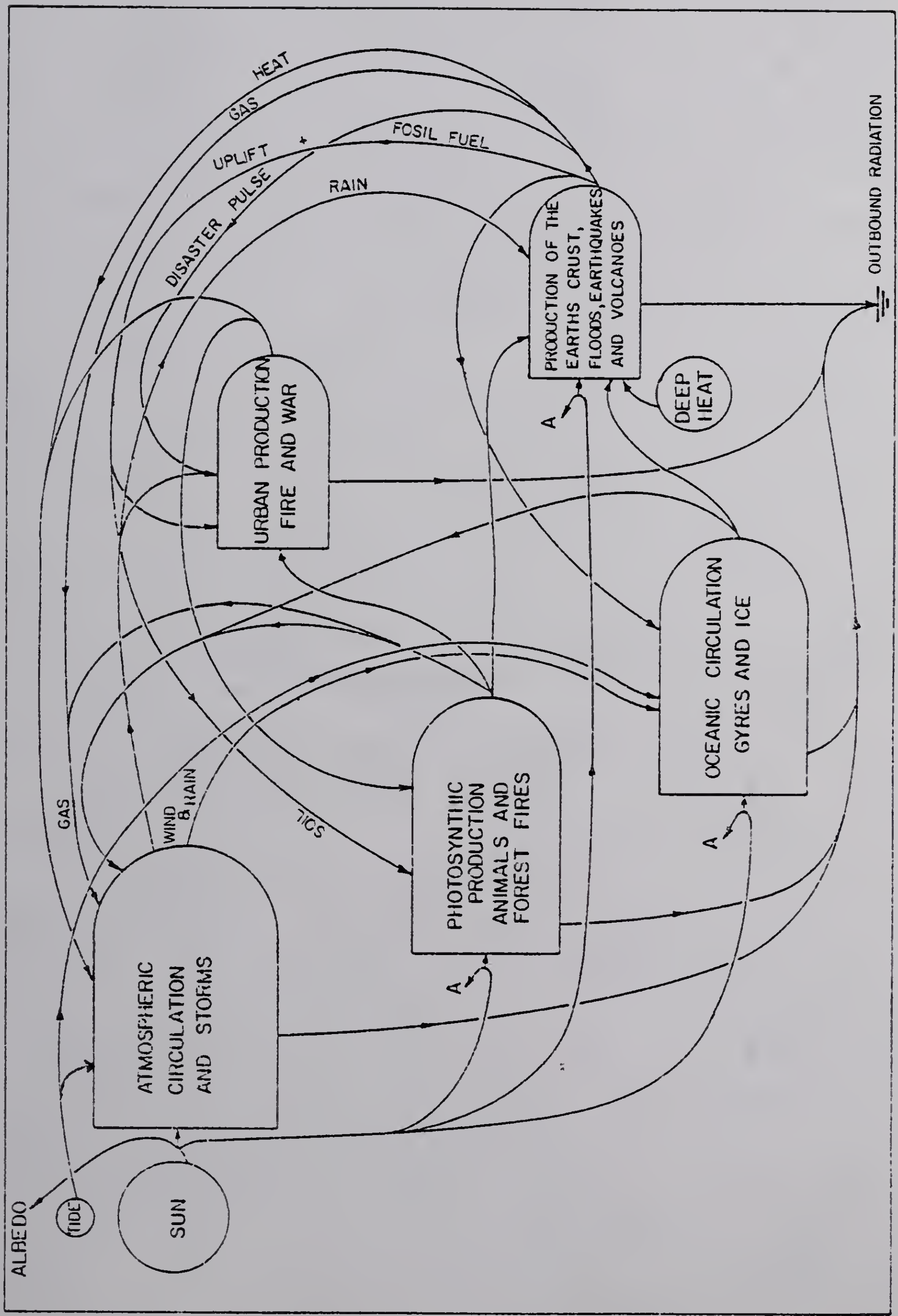
ALBEDO
TIDE
SUN
ATMOSPHERIC CIRCULATION AND STORMS
GAS
WIND & RAIN
SOIL
PHOTOSYNTHETIC PRODUCTION ANIMALS AND FOREST FIRES
A
URBAN PRODUCTION FIRE AND WAR
DISASTER PULSE
UPLIFT
GAS
HEAT
FOSIL FUEL
RAIN
PRODUCTION OF THE EARTHS CRUST, FLOODS, EARTHQUAKES AND VOLCANOES
A
DEEP HEAT
OCEANIC CIRCULATION GYRES AND ICE
A
OUTBOUND RADIATION

billion dollars per year, with all data indicating that this will become an ever-growing problem (White and Haas, 1975). Pulse disasters are a major part of all systems of nature with catastrophic energy releases, often with cascading effects, causing many smaller systems to be disordered. Energy concepts of order and disorder provide a systematic means of disaster analysis and help explain and generalize about natural disasters. The theory is that global processes concentrate, store, and catastrophically release energy according to a common pattern, thus creating natural disasters.

Energy Quality and Embodied Energy

Energy quality theory as developed by H. T. Odum (1971) and recently amplified (Odum, 1978) was built on the laws of energy. The law of energy conservation provides the basic underpinnings for all energy circuit diagrams. In a first law energy diagram, the average heat equivalent stored or flowing per unit of time is used to evaluate the model. When evaluated in heat equivalents, all systems of man and nature conserve energy, that is, the sum of all the flows into a system less the flows of energy out must equal the net changes in the energy storages. The system models in this dissertation meet the first law requirement. Unfortunately, heat equivalent measures provide no information relating to the potential value of energy flow or storage for performing work or controlling a system.

Working with the law of energy degradation provides insight into assigning a value to a particular energy flow or storage. The law of energy degradation states that in all useful processes some energy must be degraded, thus losing its ability to do work. The concept is incorporated into energy circuit language by requiring heat sinks or energy degradation pathways on all energy flows, processes, and storages. The quantity of energy dissipated by each energy concentration process is also evaluated in heat equivalents in energy circuit diagrams, even though these energy pathways can do no useful work on this earth.

The concept of energy quality places an embodied energy measuring cost in energy units on the concentrated flows and storages which are a resultant of the energy convergence property of systems. Energy quality factors for systems are defined to be the ratio of the heat equivalent energy produced or upgraded by a system to the quantity of energy required to power the system.

The maximum power principle makes it possible to relate value calculated on a basis of energy used to value based on effect of energy flow. The maximum power principle proposes that systems that maximize their flows of energy survive in competition (Lotka, 1922). The theoretical relationship between cost quality and effect quality is grounded in the idea that the surviving system must effectively use its energy flows and storages to survive in competition. Hence, in the long run, energy cost must equal energy effect.

Solar energy is used as the basis for all energy quality calculations in this dissertation. By constructing a global energy web model, which was evaluated in heat equivalent, the energy quality of the major energy convergence and control processes of the world were calculated based on the quantity of solar energy required to power the system as suggested by Odum (1978).

Energy Embodied in Radiation

A method is proposed for calculating the energy embodied in electromagnetic radiation. For calculations in the biosphere web energy quality factors are calculated based on the quantity of energy required to produce a certain energy in open systems flow. Embodied energy is then calculated by multiplying measured energy flows in heat calories by the energy quality factor (Odum, 1978).

In the proposed method for the energy embodied in electromagnetic radiation, energy quality factors are based on the absolute temperature of the radiation energy source. The concept is based on the fact that more energy is required per degree Kelvin to raise the temperature of the population of molecules. The mean energy of the photon emitted from radiation peak of the energy source is proportional to the temperature of the source. Wien's displacement law states that the photon wavelength maximum emission λ_{max} is related to absolute temperature of the radiating body by

$$\lambda_{max} = \frac{R}{T\ (K°)} \tag{1}$$

where $R = 2.89 \times 10^{-3}$ m °K (Rosenberg, 1974). Given the wavelength of electromagnetic radiation, the energy per photon e may be calculated from Planck's constant.

$$e_{max} = h \frac{c}{\lambda_{max}} \tag{2}$$

where Planck's constant $h = 1.58 \times 10^{-3}$ Cal sec and c is the velocity of light ($c = 3 \times 10^{8}$ m sec^{-1}).

Substituting equation 2 into equation 1 produces a direct relationship between the energy of the photons emitted from the peak of the electromagnetic spectrum and the absolute temperature of the radiating body.

$$e_{mac} = k_2 \, T \, (°K) \text{ Cal} \tag{2a}$$

where $k_2 = 1.6 \times 10^{-20}$ Cal $°K^{-1}$. Thus the average energy of the photons emitted from the peak of the radiation spectrum of a blackbody is in proportion to the temperature and the constant of proportionality is known.

It is postulated that in order to build a system that can support and sustain high temperature, some form of molecular energy convergence chain must be formed. The total energy required to support the system increases in proportion to the temperature obtained.

Since the energy per photon is proportional to the temperature of the source, it may be possible to relate the energy quality of certain energy photons to the energy in the population of molecules required to produce the photons.

The blackbody temperature of the sun, 6,000°K (9.8×10^{-17} Cal photons) formed a reference for energy quality calculations per photon. For example the earth's mean surface temperature is about 300°K; thus, at its spectral peak it gives off 4.92×10^{-18} Cal photons, which have an energy quality factor 0.05. A 60,000°K sunspot would emit photons with a relative energy quality factor of 10.

Divergence of radiation is not directly addressed by the proposed method of calculating the embodied energy of radiation. The question of the relationship between photon flux density and the quantity of energy required to produce the radiation is not answered.

Previous Work on the Theory of Order, Disorder, and Pulsing

Previous study of order-disorder theory was developed with energy circuit language, a systems diagram and a mathematical framework, by H. T. Odum (1971). A general model of order and disorder was recognized as Michaelis-Menton Kinetics. Odum and fellow researchers have used energy circuit language to study and model specific catastrophic events previously. Jeff Richey (1970) disordered microcosms; Odum (1970c) measured order-disorder relations with the irradiation of a tropical rain forest and considered order-disorder model of war and the effects of herbicides in South Vietnam (1974). Energy in food chains and webs were found to maximize power for survival by conserving and storing energy in high quality consumers and releasing energy in pulses.

A massive report on the Rain Forest Research Project was prepared under H. T. Odum's direction by the multidisciplinary scientific field team. Two parts of the report relate directly to the concept of order and disorder as applied to a natural ecosystem. Dienes (1970) developed a kinetic model of the radiation response of the forest ecosystem to field irradiation based on a chemical reaction type system of equilibrium equations as in equation 3:

$$X_1 \underset{K_{-1}}{\overset{K_1}{\rightleftarrows}} X_2 \xrightarrow{K_2} X_3 \qquad (3)$$

where X_1 = normal state; X_2 = partially damaged state; X_3 = lethal state; K_1 and K_2 = rate constant corresponding to radiation induced chance; and K_{-1} = radiation independent rate constant describing recovery of the system. Dienes used the model to calculate survival versus distance from radiation source for various sets of hypothetical coefficients. In H. T.

Odum's (1970c) ecological analysis of the system at El Verde, the classic washout curve of the chemostat was used to explain the effect of the radiation stress, yielding similar results to Dienes' model and the observed effect on natural system. Probably more significantly, however, from the standpoint of this research, the ratio of disordering energy P_1 to potential energy flux for reordering the system was calculated by Odum who found that in a zone where destructive action balanced repair rates the gamma ray energy input was only about 1/10,000 of that due to photosynthesis (Odum, 1970c).

A recent innovation in mathematics is a catastrophe theory by Rene Thom (1975). In Thom's theory, models for elementary catastrophes are constructed from higher order differential equations. Surfaces are generated from all the points of the functions where the first derivative is equal to zero. Thom produced fold, cusp, sallowtail, butterfly, hyperbolic, elliptic, and parabolic surfacesin this manner. Possibly the interesting point of Thom's work is the use of higher order terms in the differential equations describing the surface that are similar to the result of interacting several energy flows in a web model.

A theory related to the theory of order and disorder developed herein is the theory of risk as it is used in economics. Hirshlerfer and Shapiro (1970) analyzed the appropriate discount rate for capital investments. In this paper risk of catastrophic loss is treated as a depreciation flow similar to technological obsolescence and physical depreciation. Risk probabilities are based on historical or perceived probabilities of disaster, such as depression, war, or drought. In mathematical form Hirshleifer and Shapiro incorporate risk into the standard calculation of the present value of one dollar of future money, as given in equation 4, by increasing the standard discount rate by risk factor.

$$P = \frac{1}{(1 + i + r)} \tag{4}$$

Where i = rate of interest and r is the rate of risk.

Thurow and Taylor (1966) proposed a model for generation of the capital stock K as given in equation 5:

$$\dot{K} = I - dK - \alpha K \tag{5}$$

where I is investment, d is physical depreciation, and α is technological obsolescence. Incorporating risk into Thurow and Taylor's model yields equation 6:

$$\dot{K} = I - dK - \alpha K - rK \tag{6}$$

where r is the rate of risk.

Figure 5 is a translation of the Thurow and Taylor model into energy circuit language drawn in the format of an order-disorder model of Figure 1. Note that depreciation and obsolescence are driven by internally built accumulation of capital assets while risk is an externally powered process.

Previous Work on Natural Disasters

Relatively few studies provide a basic theory of natural disasters. Most research has dealt with descriptions and analyses of specific events, such as reports on the Alaska earthquake and tsunami on Good Friday, March 27, 1964 (Rogers, 1970), Hurricane Agnes of June 1972 (National Advisory Committee on Oceans and Atmospheres, 1972), and the Lubbock, Texas, storm of May 11, 1970 (Thompson, 1970). Another common

Figure 5. Energy circuit translation of economic model of risk. The diagram is based on Thurow and Taylor (1966) capital stock generation model.

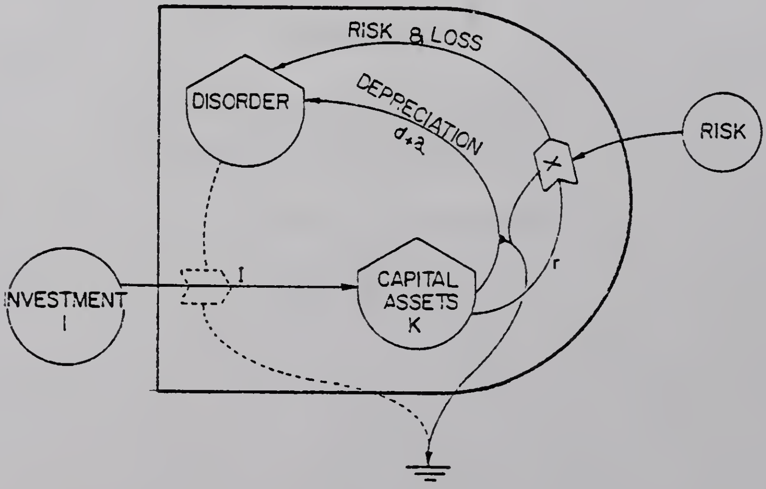
RISK & LOSS
DISORDER
DEPRECIATION
d+a
RISK
×
r
INVESTMENT
I
I
CAPITAL
ASSETS
K

$$\dot{K} = I - (d+a)K - rK$$

disaster research procedure is to look at one component in several types of disasters. Notable examples would be Dacy and Kunreuther's (1969) economic analysis of natural disaster economic disruption and Cochrane's (1975) analysis of the disrupting effects of natural hazards. Dacy and Kunreuther developed an economic framework for analyzing the economic problems resulting from disasters, analyzed short-term recovery across several case catastrophes, looked at empirical evidence of long-term disaster recovery, and tried to describe the report of federal policy on disaster mitigation. Cochrane focused on what populations were destroyed and how much of the burden of loss and reconstruction was borne by whom.

Approaches that are not disaster theory per se do merit recognition including Ericksen's (1975) scenario methodology for natural hazard research and Friedman's (1975) computer simulation of natural hazard assessments. Ericksen synthesizes observed results from cross-sectional analysis of disasters at progressive longitudinal steps to qualitatively describe what might happen to specific communities in future disasters. Ericksen's methodology was based on the work of Kahn and Wiener (1967). Friedman (1975) had a similar but more quantitative approach in using computer mapping to simulate the possible risk of destruction of future earthquakes, hurricanes, and inland flooding for various geographic areas of the United States. Friedman's interest was stimulated by his employment by the Traveler's Insurance Company and their concern over the spatial distribution of loss of life and property in the future.

Description of Study Situations and Previous Work

In this section previous work on energy cycles of the earth are reviewed and related to natural disasters. The sites and systems of special study and the disordering events of interest are described including the tropical rain forest at El Verde, Puerto Rico, and the disordering effects of radiation; the setting for the City of Johnstown, Pennsylvania, 1889, and the disastrous effects of the failure of the South Fork Dam; and the town of El Progreso, Guatemala, and the catastrophic effect of the earthquake of February 4, 1976.

Global Models of Atmospheric, Oceanic, Biological, Geological, and Urban Systems

General circulation models of the atmosphere are normally developed using a grid technique integrating the equations over large regions, often a hemisphere or the whole globe, using a finite differencing scheme with as small as practical integration step. The grid might be 200 km square horizontally and divided into as many as 18 layers vertically (Frisken, 1973). Significant examples of uses of this technique are found in Smagorinsky (1969) and Oliger *et al*., (1970). General circulation models attempt to simulate the daily dynamic process of the earth's atmosphere, while climatological models generally tend to concentrate more heavily on modeling annual means.

Houghton (1954) developed a schematic representation of the flows of energy in the atmosphere. Houghton estimated that the transport of energy toward the poles by the atmosphere and by the sea would reach a maximum of 1×10^{17} Cal d^{-1} across the 40°N latitude circle. Budyko (1969) and Sellers (1969) expanded Houghton's schematic model to a mathematical mean annual zonally averaged energy balance model. The effect of solar radiation on variations on the climate of the earth is a central feature of the model. Further development of the theory of energy balance climate models by North (1975) has shown that a small variation of the solar mean can trigger an ice age in the model. Somewhat parallel to the developments of climate models, considerable attention has been placed on the development of global biological productivity estimates.

Estimates of global production by Liebig (1862), which were extrapolated from a single community, were refined by Schroeder (1919) by distinguishing four land community types. Helmut Lieth (1975) developed a spatial model of the primary productivity of the biological systems of the earth-based world climate data that included 20 vegetation types. These were not dynamic; that is, there is no feedback from the vegetation cover of the earth to the global climate. The patterns of vegetation of the earth that were analyzed and tabulated by Whittaker and Likens (1975) provided a useful summary of the production and stocks in the global system.

Another approach to global biological system modeling has been in the carbon balance of the world. Bolin (1970) diagramed a carbon model of the biosphere, finding the vast majority of carbon trapped in sediments amounting to 39 metric tons per square meter of the earth's surface. However, only a few tenths of a percent of the immense mass of carbon is on or near the earth's surface. By estimating detritus by ecosystem type for the earth, Schlesinger (1977) found 2.8 kg m^{-2} of carbon for the world's surface in detritus.

Mathematical models of the sea are usually restricted to individual components of marine systems running on very large data bases with little effort toward development of a comprehensive model (Walsh, 1972). Ekman (1905) showed wind stress, acting at the sea's surface, put momentum into the ocean in a thin boundary layer. Ekman's theory is normally included in general circulation models of the sea (Holland, 1977). Sverdrup (1947) developed a vorticity balance theory to which Stommel (1948) added bottom friction to explain closed basis circulation. Holland and Sverdrup's work was the basis for general circulation models of the sea. Models of the ocean's tide were based on the incorporation of Newton's second law by Laplace in 1776 to explain the action of gravity on the sea (Hendershott, 1977). Seasonal models of the thermoclines attempt to explain the heat exchange between the atmosphere and the ocean that produces large horizontal-scale changes at the temperature structure in surface layers of the ocean (Niler, 1977). Charney (1955), who developed a theory to explain geostrophic adjustment, used the theory coastlines known as the costal jets such as the Gulf Stream.

Modeling of the sea is often fragmented among circulation, waves, nutrient, productivity, zooplankton, and phytoplankton models as if they were independent processes. Odum (1975) considered ways of combining physical, chemical, and biological units in a single model of the sea.

Sand transport on beaches and shoreline evolution geological simulation techniques have been documented by Harbaugh and Bonham-Carter (1970). The processes of erosion, transport, deposition, and consolidation form the basis for models of marine sediment models.

Dynamic modeling of the earth's crust, supported by the Vine-Matthews Hypothesis, proposes that anomalies in the earth's magnetic field are due to cycles in the earth's magnetic field. The cycles set the magnetic properties of the basaltic rocks of the earth's ocean crust as they formed on the ocean ridges. Magnetic patterns in basaltic rocks in the crust underlying the sea floor and the age of sediments on the sea floor provide conclusive evidence of the sea floor's spreading from the ocean ledges at approximately 2 cm yr^{-1} (Clark, 1971). Hayakawa (1976) included continental drift, midocean ridge, volcanoes, orogenesis, and other geological phenomena in a pictoral energy balance model of the earth's crust. Hayakawa's model was evaluated by estimating energy flows from geophysical data.

A dynamic global web model of human systems and resources was made by J. Forrester (1970) with the support and encouragement of the Club of Rome. Forrester's work with world modeling was followed by an extensively documented work by Meadows et al. (1974). Both models were diagramed in systems dynamics language (Forrester, 1970) and simulated with DYNAMO (Pugh, 1970).

Hubbert (1971) evaluated a schematic global energy web highlighting flows in the atmospheric system with some attention to aggregate biological, geological, and oceanic energy flows. In Hubbert's work, concentration and storages of energy are central, especially those in fossil fuels. However, the only catastrophic releases of energy considered are geologic in nature. H. T. Odum has developed several global energy models (Odum, 1972; 1973). A global minimodel was developed, evaluated, and simulated by Alexander et al. (1976) to estimate long-term United States fossil fuel availability. A recent energy web model of the biosphere (Odum, 1978) treats storms and volcanoes as high quality control mechanisms which consume energy concentrated by the atmospheric and continental sedimentary cycles, respectively.

The Tropical Rain Forest at El Verde, Puerto Rico and the Effect of Radiation

As part of a major postwar research effort by the United States to quantify the effects of irradiation on the environment, a field experiment was set up at El Verde, Puerto Rico, by the Atomic Energy Commission in 1963. A goal of the research was to perform a detailed study of the disordering effect of gamma radiation on a tropical rain forest ecosystem.

Radiation studies with similar design were done at Brookhaven National Laboratory and at Rhinelander, Wisconsin. At Brookhaven, the chronic effects of irradiation on terrestrial ecosystems were studied (Woodwell, 1963). Woodwell and Rebuck (1967) analyzed the effects of chronic gamma irradiation on oak and pine forests. Canoy (1972), writing a dissertation under the direction of H. T. Odum, measured the deoxyriboncicleic acid (DNA) of radiated vegetation at Brookhaven and at El Verde by relating molecular order and information to the pattern of stress. Highest DNA levels were found at boundary where ordering and disordering rates were similar.

The radiation source used in Puerto Rico under Dr. Odum's direction was later moved to Enterprise Radiation Forest near Rhinelander, Wisconsin, where a similar exposure of a major northern forest type (aspen) was conducted (Rudolph, 1974; Zavitkovski, 1977). In the pre-irradiation study, detailed analyses of the ecological community--including solar radiation, lichens, flora, plant communities, temporal and spatial patterns, leaf-litter production, and vertebrates and small-mammal populations--were performed. The effects of gamma irradiation on northern forest communities was predicted by Zavitkovski *et al*.

(1974). In the recently completed radioecological studies, extensive investigations were made into the ecological effects of gamma radiation. Of special interest to this research was the radiation effect on biomass production of ground vegetation studied by Zavitkovski and Salmonson (1977) and the response of the forest ecotone to ionizing radiation studied by Murphy _et al_. (1977). A result of their research, which relates directly to the theory of order and disorder, was the large increase in the number of seedlings they found in the irradiation recycled area.

Puerto Rico is a Caribbean island located between 18°N and 19°N latitude and 65°W longitude. El Verde station was constructed in the tropical rain forest region of the Luquillo Mountains of eastern Puerto Rico (see Figure 6a). The steady flow of warm, moist air from the 1.2 m sec^{-1} prevailing easterly trade wind provides a uniformly wet climate with a mean temperature of 22.6°C, a relative humidity of 91 percent, an absolute humidity of 18.7 g m^{-3}, an insulation of 3,830 Cal m^{-2} d^{-1}, and an annual rainfall of 3,750 mm. Climate fluctuations were found to be small, for example temperature had only a 21° to 25°C diurnal range and a 2° seasonal mean fluctuation (Odum _et al_., 1970).

The vegetation of the area is the lush tropical forest traditionally characteristic of rain forest, with high diversity of plants and insects, buttress roots, broad thin leaves, bromeliads, lianas, trunk bark heavy with growth, and an open ground story in deep shade. The area is known as the Tabanuco Forest after the principal tree, the tabanuco. With a rainfall of greater than 102 mm every month, droughts were not experienced

Figure 6. Location maps and diagram of Puerto Rico and El Verde experiment.

(a) Map of Puerto Rico showing east location of El Verde (Odum, 1970a).
(b) Main base map for studies at the El Verde site (Odum, 1970a).
(c) El Verde station and vicinity showing some principal locations of activity (Odum, 1970a).

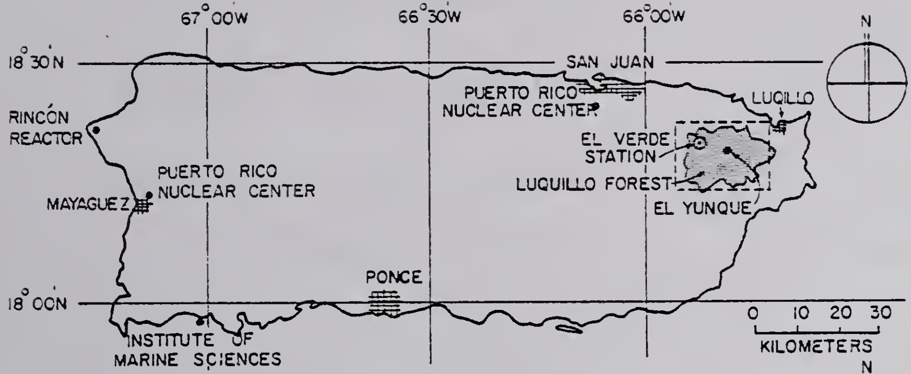
67° 00W
66° 30W
66° 00W
N
18° 30N
SAN JUAN
PUERTO RICO
NUCLEAR CENTER
LUQUILLO
RINCÓN
REACTOR
EL VERDE
STATION
PUERTO RICO
NUCLEAR CENTER
LUQUILLO FOREST
MAYAGUEZ
EL YUNQUE
PONCE
18° 00N
0 10 20 30
KILOMETERS
INSTITUTE OF
MARINE SCIENCES

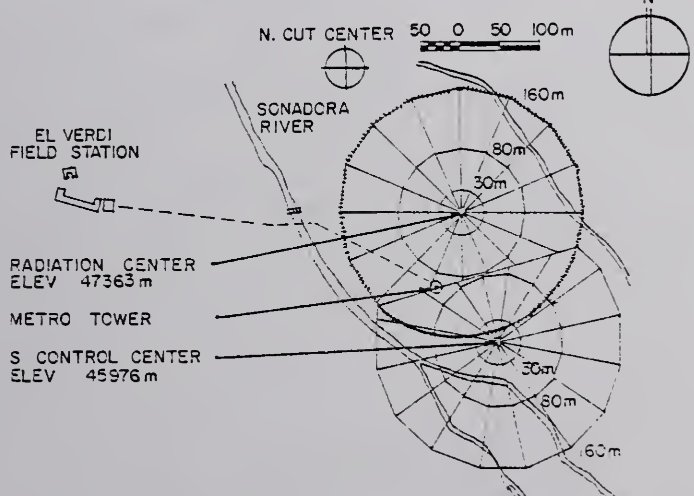
N
N. CUT CENTER
50 0 50 100m
SONADORA
RIVER
160m
EL VERDI
FIELD STATION
80m
30m
RADIATION CENTER
ELEV 47363 m
METRO TOWER
S CONTROL CENTER
ELEV 45976 m
30m
80m
160m

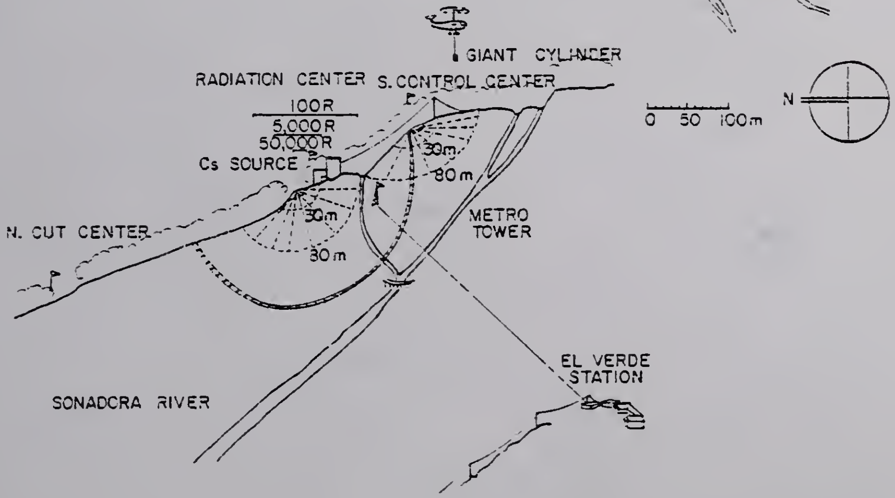
GIANT CYLINDER
RADIATION CENTER
S. CONTROL CENTER
100R
5,000R
50,000R
Cs SOURCE
N
0 50 100m
30m
80m
30m
80m
METRO
TOWER
N. CUT CENTER
EL VERDE
STATION
SONADORA RIVER

by the forest ecosystems. For example, the tropical rain forest in the El Verde study area had never experienced fire (Odum, 1970a).

The rain forest project study was concentrated around the radiation source and two control locations. Figure 6b is a plan view of the irradiation and the south control area while Figure 6c diagrams the ecological and irradiation experiment. The irradiation was provided by a 10,000 curie cesium source for 93 days in early 1965. Another 6 years were required for analyzing the results of the irradiation stress on the ecosystem, including comparison studies with two control sites. The south control site was undisturbed while the north control was denuded of vegetation to resemble the irradiation site. Substantial stress was imposed on the ecosystem by the high field gamma radiation.

Johnstown, Pennsylvania, and the Failure of the South Fork Dam

Johnstown, Pennsylvania, is a heavily industrialized city located 121 km east of Pittsburg, Pennsylvania, in a valley of the Allegheny Mountains (see Figure 7a). The town was founded at the confluence of two medium-sized mountain streams, Stony Creek and the Little Conemaugh River, which join at central Johnstown to become the Conemaugh River. Above Johnstown, the two streams and their tributaries drain 650 sq mi of valley and mountainside (Gilbert, 1977). The point of confluence provided water transport and the level floodplain encouraged development. These coupled with the area's rich coal deposits made Johnstown a natural place for eighteenth-century European settlers to start a town (Figure 7b).

Johnstown received national attention when on May 31, 1889, 6 to 8 in of rain sent Stony Creek and the Little Conemaugh into the streets of the town and breached what was then the world's largest earthen dam,

Figure 7. Location map of Johnstown and the South Fork Dam.

(a) Map of Pennsylvania showing location of Johnstown in relationship to other major Pennsylvania cities.

(b) General map of the region of the Johnstown disaster and the watershed of the South Forks. This map is the first correct one published, the decided differences between it and those which have yet appeared elsewhere being due to inaccuracies in the latter. It reproduces by kindness of G. W. Colton & Co. from an old and scarce county map of 1867, on a scale of 1 1/4 in per mi. The topography on this map is made accurately to scale from sketches made on the ground (Engineering News, 1889a).

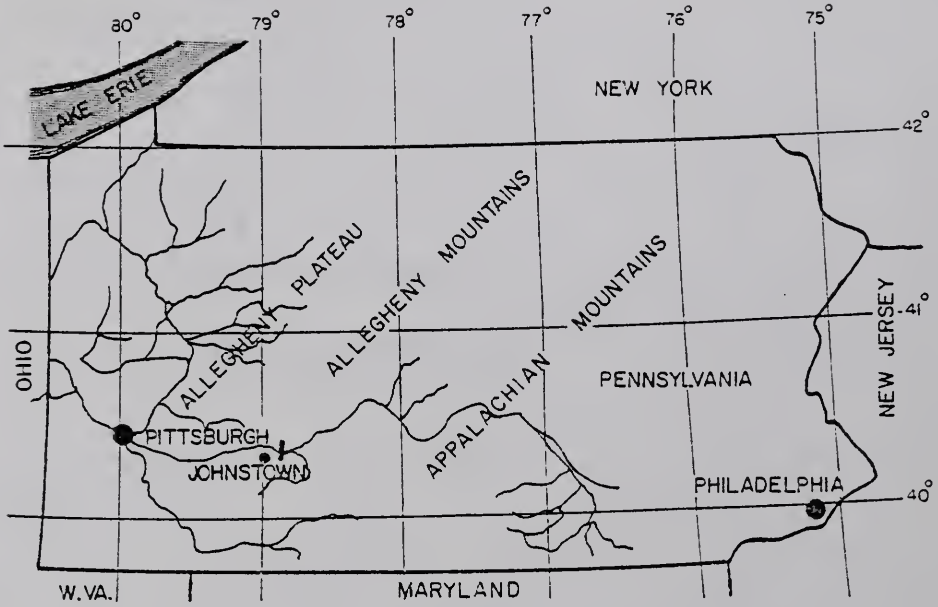
80°
79°
78°
77°
76°
75°
LAKE ERIE
NEW YORK
42°
41°
40°
ALLEGHENY PLATEAU
ALLEGHENY MOUNTAINS
APPALACHIAN MOUNTAINS
PENNSYLVANIA
NEW JERSEY
OHIO
PITTSBURGH
JOHNSTOWN
PHILADELPHIA
W.VA.
MARYLAND

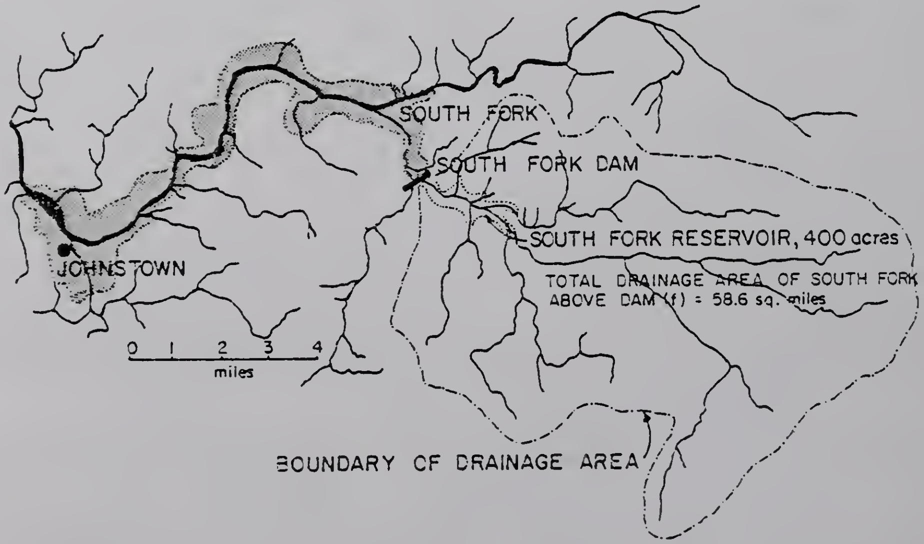
SOUTH FORK
SOUTH FORK DAM
SOUTH FORK RESERVOIR, 400 acres
TOTAL DRAINAGE AREA OF SOUTH FORK ABOVE DAM (f) = 58.6 sq. miles
JOHNSTOWN
0 1 2 3 4
miles
BOUNDARY OF DRAINAGE AREA

14 mi up the Little Conemaugh at South Fork, releasing a 420-acre lake, which was 65 ft deep at places (Engineering Society of Western Pennsylvania, 1889). The water in the lake overflowed the dam in a low spot in the center and eroded the entire 900-ft-long, 70-ft-high earthen structure on the down river side, allowing the earthen wall to fail under the extreme pressure, and sending a wave descending into Johnstown. The entire 540 million cu ft of water was released behind a 40-ft wave that took approximately one hour to reach Johnstown. Very large quantities of energy were released as the wave roared down the valley carrying buildings, trees, houses, factories, and even locomotives. It hit the town with virtually no warning, scouring most of the town to bedrock, drowning 2,200 people, and creating $17 million property damage. Figure 6b shows the path of the floodwave.

Floods are nothing new for Pennsylvania, for of 2,800 communities in the state, 2,468 are located in proven flood zones (Gilbert, 1977). However, Johnstownians, believing this to be a freak accident, rebuilt on the same floodplain only to be hit by another torrential rainstorm on March 17, 1936. The amount of rain water was compounded by melting snow from the mountains. In the 1936 flood no dams broke, but the flood crest took 25 lives and did $41 million in property damage to a city which had more than doubled in size. With two floods in 50 years the U.S. Army Corps of Engineers spent $7 million on a flood control project to make Johnstown the "flood free city" (Gilbert, 1977).

On July 19, 1977, Johnstown experienced a rainstorm which was expected to move away by midnight but stopped, releasing an incredible 11.87 in of water between July 19 at 9 pm and 4 am on July 20, creating a severe flash flood and breaching five small earthen dams. The most serious was the Laurel Run Dam, which was 42 ft high and impounded 22 acres, generating a 15-ft wave directly into to the Comenaugh River. This third Johnstown flood took approximately 100 lives and was responsible for $350 million in property damage (Gilbert, 1977).

Excellent field documentation of the 1889 failure of the South Fork Dam make the test of constructing and evaluating a dynamic model for the event feasible. The Engineering Record (1891) and Engineering News (1889b) provided detailed engineering descriptions of the failure of the South Fork Dam, the path of the flood wave, and the destruction of Johnstown. In addition, several authoritative historical accounts of the flood have been published. The most notable are a Ph.D. dissertation by Shappee (1940) and a book by McCullough (1968).

Reports on the 1936 flood are much more sketchy even though property damage as measured in dollars was greater. However, some water flow data were compiled by the United States Geological Survey. The 1977 flood has brought Johnstown new fame and several rather extensive scientific fact collections are now available from the National Oceanic and Atmospheric Administration (1977) and United States Geological Survey (Ambruster, 1978; Brua and Humphries, 1978).

Gilliland (1975) modeled the failure of a slime pond dam and the disordering effect of the phosphorus spill on the Peace River in energy circuit language.

Guatemala and the Earthquake of February 4, 1976

The Guatemala earthquake of February 4, 1976, and the catastrophic destruction of El Progreso was used as the field test of the theory of energy concentration, storage, and catastrophic release triggering secondary catastrophic events. Much of the supporting fieldwork in this research was done in the Department of El Progreso with a land area of 19,922 km^2 which is mapped in Figures 6, 8, and 9. Detailed analysis was performed on the capital of the department, also named El Progreso, which has a municipal land area of 220 km^2 and a central urban area of approximately 1.5 km^2.

The source of energy in the Guatemalan earthquake was the 2 cm per year annual westerly motion of the North American Plate of the earth crust with respect to the Caribbean Plate. The plate movement had stored great quantities of potential energy in stress built up in the Motagua Fault over the past two centuries. Figure 8c is a map of the junction of the North American Plate and Caribbean Plate of the tectonic system of the earth (Tarr and King, 1976).

El Progreso experienced almost total destruction by the earthquake of February 4, 1976, due to its relatively close proximity to the Motagua Fault rupture and earthquake epicenter and to the softness of the alluvial soil on which the adobe structures of the town were constructed.

Previous research on the Guatemala earthquake has been primarily concerned with scientific documentation of the geological characteristics of the event, its size, magnitude, and the geographic distribution of the destruction generated by the earthquake. The most useful scientific summary studies were carried out by the Comite de Emergencia, Guatemala (1976) and the United States Geological Survey (Espinosa *et al*., 1976). The maps in Figure 9 summarize the data on the damage to adobe structure and the estimated earthquake intensity distribution in Guatemala (Espinosa *et al*.,1976). In addition to development of a reconstruction plan for El Progreso (Alexander and Sipe, 1977), many other

Figure 8. Location maps of Guatemala, El Progreso, and the Motagua Fault.

(a) Map of Guatemala showing the location of the department of El Progreso (Alexander and Sipe, 1977).

(b) Map of the Department of El Progreso showing the location of the municipality in relation to the other seven municipalities (Alexander and Sipe, 1977).

(c) Motagua fault zone junction of Caribbean and North American Plate. Jordan (1975) modified by Tarr and King (1976).

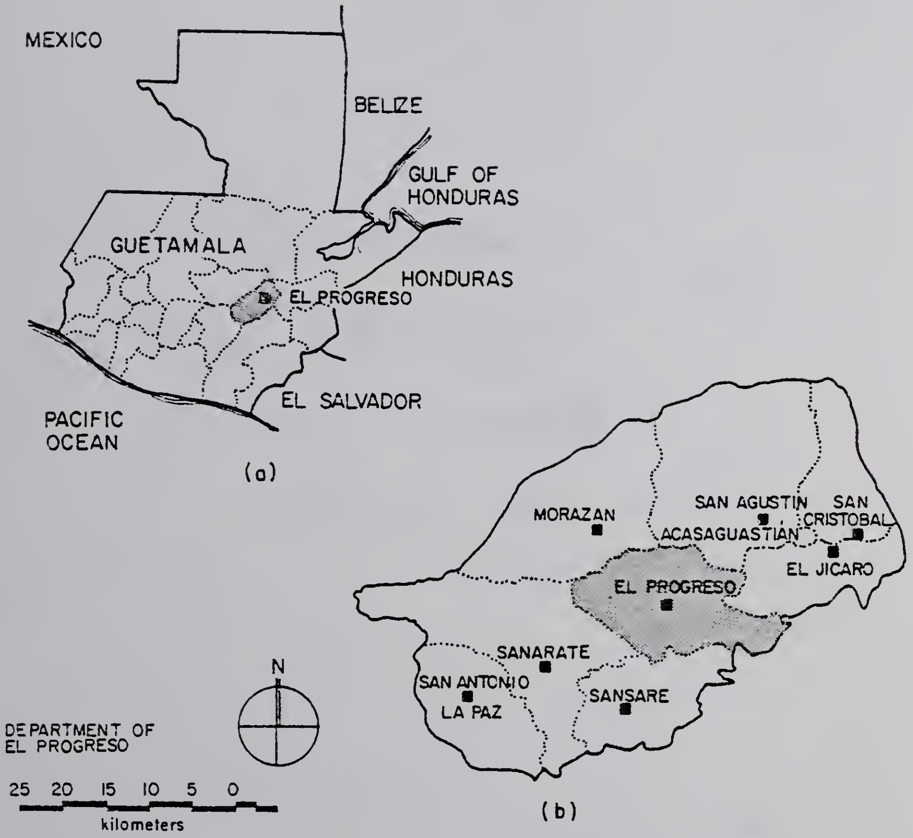
MEXICO
BELIZE
GULF OF HONDURAS
GUETAMALA
HONDURAS
EL PROGRESO
EL SALVADOR
PACIFIC OCEAN
MORAZAN
SAN AGUSTIN ACASAGUASTIAN
SAN CRISTOBAL
EL JICARO
EL PROGRESO
SANARATE
SAN ANTONIO LA PAZ
SANSARE
N
DEPARTMENT OF EL PROGRESO
25 20 15 10 5 0
kilometers

(a)

(b)

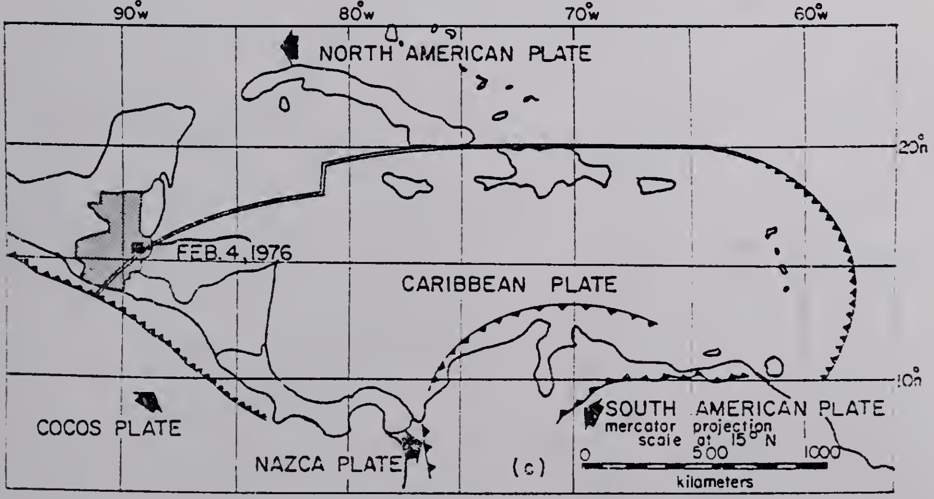
90°w
80°w
70°w
60°w
20°n
10°n
NORTH AMERICAN PLATE
FEB. 4, 1976
CARIBBEAN PLATE
COCOS PLATE
NAZCA PLATE
SOUTH AMERICAN PLATE
mercator projection
scale at 15° N
0 500 1000
kilometers

(c)

Figure 9. Maps of damage to adobe structures and earthquake intensity in Guatemala.

(a) Contour map showing damage to adobe-type structures caused by the February 4 earthquake (Espinosa *et al*., 1976).

(b) Isoseismal map of intensity distribution from spread of the main event. Intensity is measured by the Modified Mercialli Scale (Espinosa *et al*., 1976).

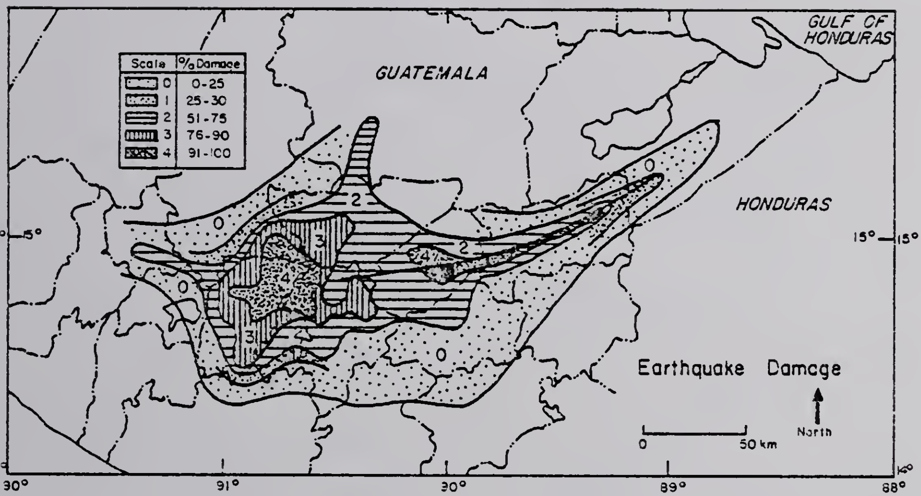
GULF OF HONDURAS
GUATEMALA
HONDURAS
Scale | % Damage
0 0-25
1 25-30
2 51-75
3 76-90
4 91-100
0
1
2
3
4
Earthquake Damage
0 50 km
North
15°
14°
90°
91°
90°
89°
88°

■ EL PROGRESO

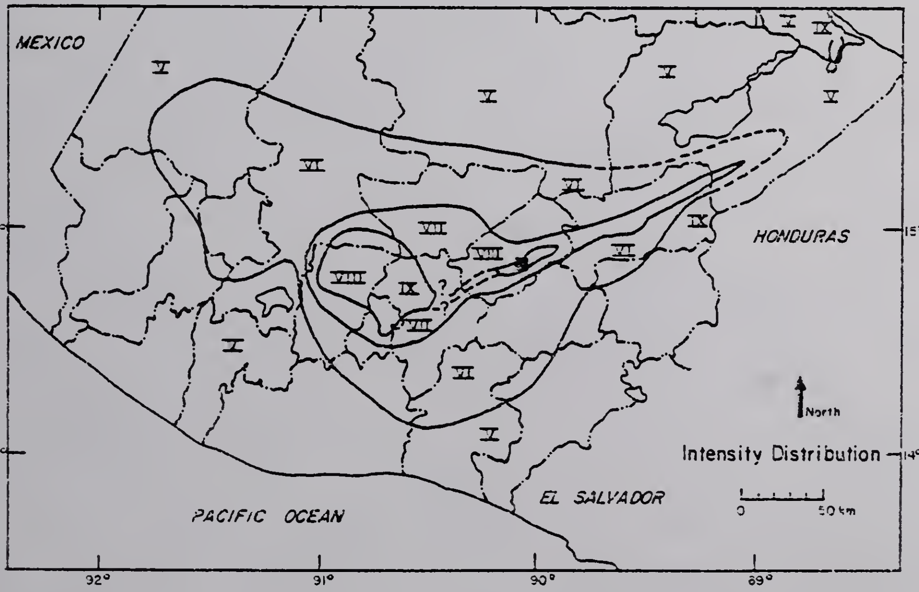
MEXICO
HONDURAS
EL SALVADOR
PACIFIC OCEAN
V
VI
VII
VIII
IX
?
North
Intensity Distribution
0 50 km
15°
14°
92°
91°
90°
89°

foreign governments are sponsoring reconstruction projects throughout Guatemala. The only other formal study of the effect of the Guatemala earthquake on El Progreso was a cadastre mapping project sponsored by the Guatemalan National Geographic Institute (Giron, 1976). The destruction was so great that identification of landmarks to identify property ownership was a substantial problem. El Progreso was studied in detail by the author (Alexander and Sipe, 1977).

METHODS

Description of Modeling Language and Symbols

The symbols used in the systems diagrams were established by Howard T. Odum (1971) and are part of the energy circuit language. The language combines several powerful approaches which show energetics and provide insight into the mathematical description of a system, while also illustrating the process under study in a holistic manner. Energy circuit language contains a hierarchy of symbols, which allow the diagraming of several levels of complexity in one model.

Aggregate symbols are summarized in Figure 10. They consist of the cycling receptor module, the self-maintaining module, the production module, and the logic module. The modules are constructed by combining members of the set of mathematical symbols presented in Figure 11.

Energy circuit models are normally constructed by arranging mathematical symbols within group symbols to show systems and to facilitate comprehension of the concepts embedded in the model. Standard convention also calls for arranging the model so that subsystems, which concentrate dilute energy, are at the left while energy flows increase in quality toward the right of the diagram. Heat sinks are always used to show loss of degraded energy from the system. This creative use of symbols and organization provides several levels of hierarchy. The highest level is formed by arranging the diagram by energy concentration or quality, the intermediate by use of group symbols, while the

Figure 10. Energy circuit language group symbols (H.T. Odum,1971). Each group symbol is made up of a set of mathematical symbols.

(a) The cycling receptor has the condition of conservation of matter that is ordered by input energy flow and is degraded and recycled with output of energy.
(b) The self-maintaining consumer module processes energy and feeds back control to other parts of the system.
(c) The production module fixes low quality energy and the control of a consumer module.
(d) The logic module performs discrete operations based on control inputs.

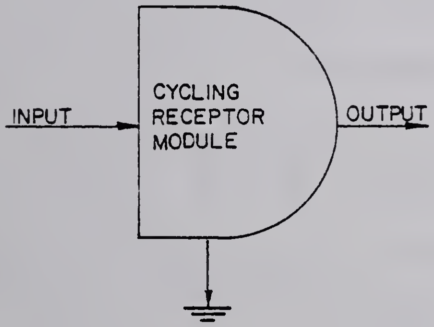
INPUT
CYCLING RECEPTOR MODULE
OUTPUT

(a)

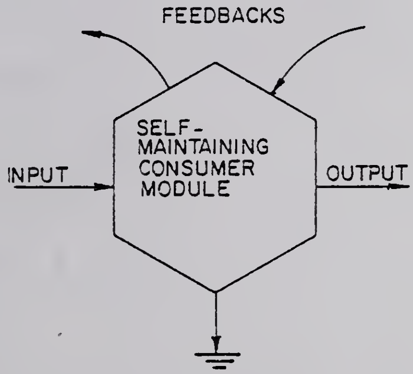
FEEDBACKS
INPUT
SELF-MAINTAINING CONSUMER MODULE
OUTPUT

(b)

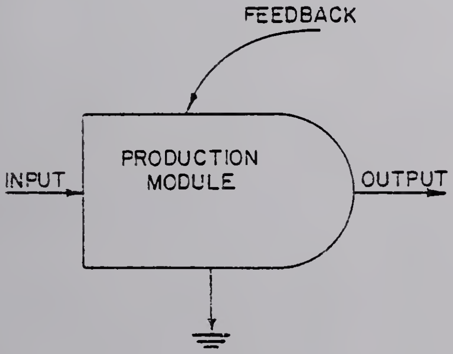
FEEDBACK
INPUT
PRODUCTION MODULE
OUTPUT

(c)

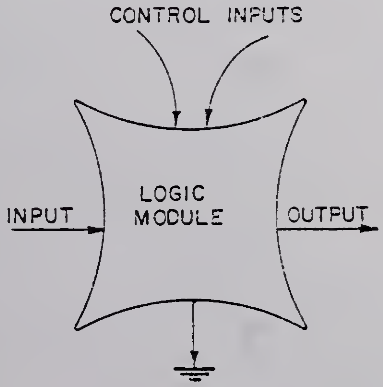
CONTROL INPUTS
INPUT
LOGIC MODULE
OUTPUT

(d)

Figure 11. Energy circuit language mathematical symbols used to construct modules in Figure 8 (H. T. Odum, 1971).

(a) Outside source of energy supply to the system controlled by external system and not affected by energy demand on the internal system; a forcing function E.
(b) Constant flow source of energy from outside the system.
(c) A pathway whose flow is proportional to the quantity in the upstream storage; $J = K_1E$.
(d) Storage of some quantity in the system. The rate of change of the storage Q with time equals the inflows minus outflows; $Q = J - KQ$.
(e) Interaction of two flows to produce an output, which is a function of the two flows or storages driving the flows. For multiplicative interaction; $f(X,Y) = KXY$.
(f) Transactor symbol for which money flows in one direction and energy flows in the other with price (P) adjusting one flow J_1 in proportion to the other; $J_1 = PH$.
(g) Sensor of the magnitude of flow, J symbol also used to sense storages Q; $J_2 = RJ$.
(h) Constant gain amplifier multiplies the inflow J_1 by a constant A. Power is extracted from energy source E; $J_2 = AN$.
(j) Logic switch turns flow on or off based on logic such that the output equals the input when logic is one and zero when logic is off; on $J_2 = J_1$, off $J_2 = 0$.
(k) Logic comparitor compares A with B to provide a logic signal C; if $A \geq B$ $C = 1$; if $A \leq B$ $C = 0$.

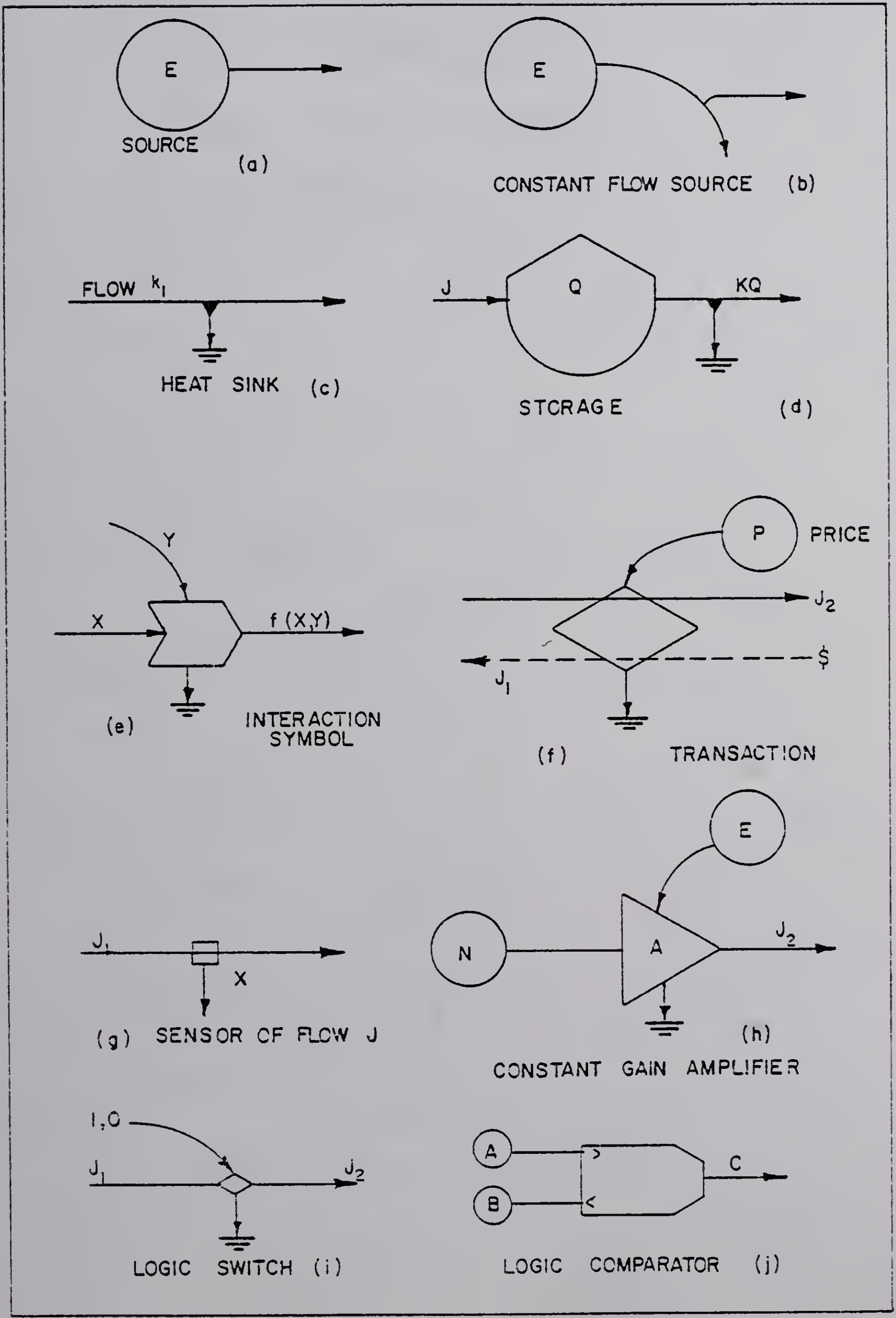
E
SOURCE
(a)
E
CONSTANT FLOW SOURCE
(b)
FLOW k_1
HEAT SINK
(c)
J
Q
KQ
STORAGE
(d)
Y
X
f (X,Y)
(e)
INTERACTION SYMBOL
P
PRICE
J_2
$
J_1
(f)
TRANSACTION
E
J_1
X
(g)
SENSOR OF FLOW J
N
A
J_2
(h)
CONSTANT GAIN AMPLIFIER
1,0
J_1
J_2
LOGIC SWITCH
(i)
A
B
>
<
C
LOGIC COMPARATOR
(j)

the dynamic and kinetic detail is constructed with the mathematical symbols.

Development of Models

The models in this dissertation were developed in a sequential order starting with the basic order-disorder model in Figure 1. A family of this type of models was constructed and analyzed mathematically by setting up each model in differential equation form, setting the rate of change equal to zero, and solving for the steady-state solutions. Dynamic characteristics were next tested by simulating each model in the family of order-disorder models as depicted by Figure 1. A preferred order-disorder model was tested by modeling the previous studies on the effect of gamma radiation stress of a tropical rain forest at El Verde, Puerto Rico.

A catastrophic consumer pathway was added to the basic order-disorder as shown in Figure 2. The family of similar models was analyzed and simulated to test the models' dynamic behavior. The model of catastrophic energy release was tested by simulating the failure of the South Fork Dam (which generated the Johnstown flood of 1889) and the Guatemala earthquake of 1976.

Next, two order-disorder models were connected in cascade and tested by simulation of the Guatemala earthquake and the secondary destruction of El Progreso and the Johnstown flood and the secondary destruction of Johnstown. Figure 3 describes the basic configuration. By connecting units in a web, a more general model was developed as a methodological guide for calculation of a power spectrum for global disasters and for estimation of quantity of solar energy embodied in generic types of natural hazards and their disruptive pulses of energy. The model summarized in Figure 4 is a global energy budget model that relates the atmospheric, oceanic, biological, geological, and urban processes responsible for concentration and storage of solar energy to power storms, floods, earthquakes, fires, and volcanoes.

Limiting Factors and Differential Equations

The energy circuit models developed in this research incorporate internal and external limiting factors. Internal limits result from the shortage of disordered matter in the cycling modules. External limits are provided by energy flow sources such as solar radiation. Both limits to growth are incorporated in diagrammatic and differential equation form of the models. Figure 12 is a typical example, illustrating the use of internal and external limits to growth in the same order-disorder model. The differential equation for the energy storage term Q_1 is given below:

$$\dot{Q}_1 = J_r K_1 Q_2 - K_2 Q_1 \tag{7}$$

The energy flow J is split between J_0 and J_r as in equation 8:

$$J = J_0 + J_r. \tag{8}$$

The energy consumption of the system is given by equation 9:

$$J_0 = K_0 J_r Q_2. \tag{9}$$

Substituting equation 9 into equation 8 and solving for J_r yields equation 10:

$$J_r = \frac{J}{K_0 Q_2 + 1}. \tag{10}$$

Figure 12. Order-disorder model in energy circuit language, illustrating the incorporation of internal and external limiting factors. The internal limit is provided by conservation of matter in the order-disorder loop. The external limits to growth are a result of the use of a constant flow energy source.

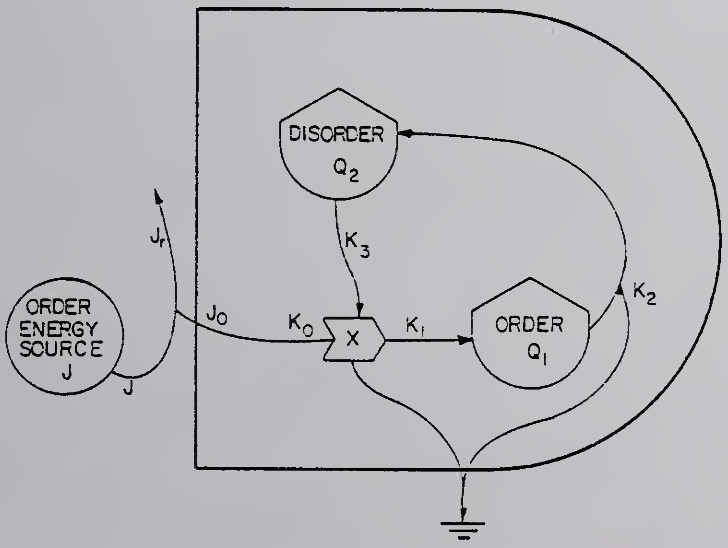

$$\dot{Q}_1 = \frac{K_1 J\ Q_2}{1 + K_0 Q_2} - K_2 Q_1$$

$$Q_2 = C - K_3 Q_1$$

Substituting equation 10 into equation 1 yields the desired results in equation 11:

$$\dot{Q}_1 = \frac{K_1\, J\, Q_2}{K_0\, 0_2 + 1} - K_2\, Q_1. \qquad (11)$$

Rearranging equation 9 defines K_0

$$K_0 = \frac{J_0}{J_r\, Q_2}. \qquad (12)$$

Requiring conservation of mass such that the total mass in the storages Q_1 and Q_2 to constant C yield equation 13:

$$C = K_3\, Q_1 + Q_2, \qquad (13)$$

where K is the mass per unit energy for the system under study. Solving for Q yields equation 14:

$$Q_2 = C - K_3\, Q_1. \qquad (14)$$

Substituting equation 14 into equation 11 to remove Q_2 yields equation 15:

$$\dot{Q}_1 = \frac{K_1 JC - K_1 J K_3 Q_1}{1 + K_0 C - K_\theta K_3 Q_1} - K_2 Q_1. \qquad (15)$$

Equation 15 is a differential equation describing the behavior of the model in Figure 12 and incorporating the internal limit imposed by conservation of matter and the external limit of a constant flow energy source.

Data Assembly and Evaluation of Models

The energy circuit models in Figures 1 to 4 were used as a guide for collection and organization of data. Data were assembled from literature for evaluation of global models. A table was constructed for each energy flow and storage in the model. The table contains the energy value of the flow or storage with each calculation documented by a note in Appendix I. Each data source was referenced to the appropriate research and, when possible, several measures or estimates were used for each reference value.

Simulation Procedures

A set of simultaneous nonlinear differential equations was developed for each of the energy circuits models of the case study disasters. Initial conditions and coefficients for each model were calculated from the table of energy flows and storages that was constructed to document the model. Mathematical solutions were used to develop the behavioral properties of the basic order-disorder model used as a basis for this research. However, this was not feasible for more complex models.

Numerical approximation techniques and solution by analogous system were used to study and simulate the dynamic behavior of the disaster models. Numerical approximation was the most straightforward simulation method. During early stages of model development, simulations were tested on a Hewlett Packard 25 programmable calculator. However, more extensive computer runs were performed with the simulation language DYNAMO (Pugh, 1970). Working with DYNAMO offered the advantages of a large, dynamic range of modern digital computers. Thus, the models could be simulated without going through a scaling procedure necessary with analog simulation. DYNAMO models were developed directly from the energy circuit diagram so that one level equation was written for each state variable (storage tank), while one rate equation was written for each energy flow pathway. Digital computer programs such as DYNAMO, simulate nonlinear differential equation solutions by mathematical approximation. To insure reasonable accuracy with Euler integration technique, a time step of 0.1 percent of the disaster duration was used as a maximum. Thus, many computations are required for one simulation run, rendering the digital much slower than analog computer methods that continuously solve the set of nonlinear equations. A Tektronix digital computer terminal and time-sharing techniques were used to carry out model development and simulation. Some of the models were scaled and wired on the analog computer to provide hands-on immediate response. Analog simulation was used for sensitivity analysis to study relative response of the system to each parameter. Information gained from analog simulation was used to plan runs on the DYNAMO version of the model. The data for storages and flows that were determined to be sensitive by analog or digital simulation were reverified and checked for accuracy with a second or third reference, and when possible by several independent techniques of calculating the energy flows and storages used in evaluating the models.

Calculation of Ratios

In addition to evaluation and simulation, the energy circuit models in this dissertation were used as systematic guides to energy analysis of energy flows. Several types of ratios of energy flows were calculated to add to the quantitative understanding of natural hazards and their disruptive effects. As explained in this section, three important ratios calculated are energy quality, embodied energy, order-disorder ratios, and disaster amplifier ratios.

Energy quality factors were calculated from the evaluated biosphere web as diagramed in Figure 4 (Odum, 1978). Under the web concept all of the energy flows are interrelated in such a way that each is produced as a by-product of all the others. Taking this point of view, the total incident solar energy to the world is required to produce all energy flows and build all the structures. In the example of global net primary production, rain, wind, dry air, and nutrients of the soil are all known to be necessary energy flows as direct radiant solar energy. Once the global energy web is evaluated, the energy flow in a specific process is divided by the total solar energy necessary to power the earth. For this research the mean solar incident radiation was used as the basis for all energy quality calculation except for electromagnetic radiation.

Embodied energy factors were calculated by multiplying an energy flow in a specific case by the global quality factor, which was developed from the energy web model in Figure 4.

The order-disorder model diagramed in Figure 13 illustrates the energy flows used in calculating the ratio of the energy required to produce order to the energy required to produce disorder in the system. The ratio was calculated by dividing flow A by flow C in Figure 13. When the ratio of the storage of order, which is recycled to disorder (flow B), to the flow of energy required to pump the recycling process is calculated, flow B is then divided by flow C. For purposes of clarity, the first is referred to as the order-disorder ratio, while the second is designated as the disaster-amplifier ratio.

Calculation of Spatial Distribution of Seismic Energy

A method is proposed for calculation of the spatial distribution of seismic energy from observed field intensities measured on the

Figure 13. Order-disorder model illustrating energy flows used in calculating the order-disorder ratio and the disaster-amplifier ratio.

Order-disorder ratio

$$\frac{\text{Energy required to produce order}}{\text{Energy required to produce disorder}} = \frac{A}{C}$$

Disaster amplifier ratio

$$\frac{\text{Storage of order disordered externally}}{\text{Energy required to produce disorder}} = \frac{A}{C}$$

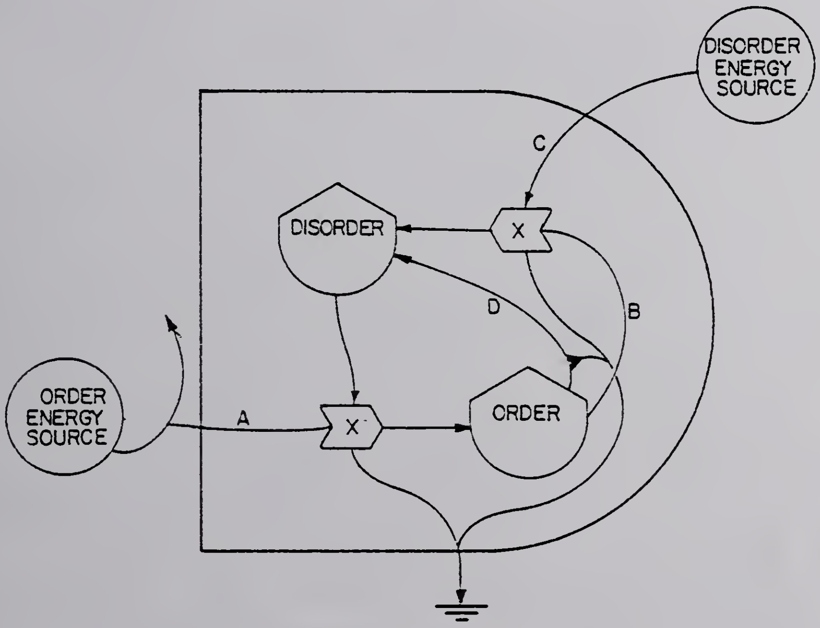

ORDER-DISORDER RATIO = $\frac{A}{C}$

DISASTER-AMPLIFIER RATIO = $\frac{B}{C}$

Modified Mercalli scale. Intensity is a subjective numerical index describing the effect of an earthquake on man, on structure, and on the surface of the earth. The Modified Mercalli scale of 1931 has intensity rankings from I to XII (see legend on Figure 30b for definition of scale; Espinosa *et al*., 1976; Richter, 1958). Acceleration A was calculated from the intensities discussed above using equation 16 (Gutenberg and Richter, 1969).

$$\log a = I/3 - 1/2 \qquad (16)$$

If energy was distributed uniformly, one could find the dissipation per unit of land area by dividing the total energy by the total land area affected; however, this is not a realistic assumption. For the calculations, it was assumed that energy was uniformly distributed in each isoseismal zone. Equation 17 mathematically gives this relationship:

$$e_i = E_{si}/A_i, \qquad (17)$$

where e_i is the energy dissipated per unit area of zone, i, E_{si} is the total seismic energy dissipated in zone i, and A_i is the land area of zone i. Energy was related to acceleration by combining the following two equations (Gutenberg and Richter, 1969):

$$E_{si} = c\ t\ (A_i/T)^2 \qquad (18)$$

where c is a transmission constant, t is the duration of the wave group, and T is the period of vibration, all of which were constant for the case under study. A_i is the amplitude of the ground motion for zone i. Amplitude A_i was related to acceleration a_i as shown in equation 19 (Gutenberg and Richter, 1969):

$$a_i = (A_i/T)\ 4\pi^2/T \tag{19}$$

and then substitute equation 19 into equation 18, combining constants to form a new constant c, which yields equation 20.

$$e_i = c\ a_i^2. \tag{20}$$

The constant of proportionality c was then evaluated by substituting equation 17 into equation 20 to get equation 21.

$$c = E_s/(\sum_{i=1}^{n} A_i a_i^2) \tag{21}$$

Substituting equation 16 into equation 21 and rearranging, yields the desired relationship between energy distribution and earthquake intensity:

$$E_s = (\sum_{i=1}^{n} C\ A_i^{0.66\ I-1}). \tag{22}$$

Plan of Study

The theory of cycles of order and disorder was first developed by analyzing several possible configurations of order-disorder models. The analysis was carried out by calculation of the steady-state solution to the models in differential equation form. The dynamic properties of the model were tested using simulation techniques. As a refinement of the order-disorder concept, a consumer module was added to the order-disorder model. The catastrophic energy release properties of the model were initially analyzed for steady-state properties of the differential equation form of the family of models. Dynamic characteristics were analyzed using simulation techniques.

An energy basis for disasters was developed by connecting order-disorder models to form a global energy web model with pathways for cascading of catastrophic release processes. The resulting model was then used to evaluate the energy quality of natural disasters and to illustrate the control action of their pulsing. The first section of the results develops, evaluates, and documents this model by diagraming the atmospheric, oceanic, biological, geological, and urban systems of the world, their energy flows, and their interconnection. Then energy ratios were calculated from energy flows in the evaluated models. Quantitative comparison of order-disorder ratios were made with all of the energy flows involved in a common unit of measure as calories of solar equivalent energy.

To verify the theory of cycles of order and disorder, three disasters were studied with models, energy evaluation, and simulation data from an irradiation disordering experiment in a tropical rain forest was used to evaluate a pulsing order-disorder system. The model was simulated and compared to field observations. An order-disorder model containing a catastrophic consumer module was evaluated for the failure of the dam, which created the major disaster at Johnstown. Two models were connected, so their effect could be cascaded and evaluated for a major earthquake and the secondary disruption of several cities. The flood and earthquake were simulated and the results were compared to field observation. Finally ratio of ordering and disordering energies were assembled to consider theories of energy flow in disasters.

RESULTS

Simulation and Analysis of Order-Disorder Models

Results of the study of several possible order-disorder models are presented in this section, starting with a simple model and progressing to more complex examples. Differential equations to describe the behavior of each are also presented along with time simulations of each model. All of these models have the common characteristic of materials cycling as a mechanism to capture, concentrate, and store energy and are mathematically constrained to conserve matter. Figure 14a is the basic order-disorder model which was first applied in enzyme reactions (Michaelius-Menton, 1913). The behavior of the level of order Q_1 is described by differential equation 22.

$$\dot{Q}_1 = k_1 E_1 Q_2 - k_2 Q_1 \tag{22}$$

Requiring conservation of matter yields equation 23.

$$Q_2 = Q_T - Q_1 \tag{23}$$

Substituting equation 23 in equation 22 yields a single differential equation which describes the model behavior of equation 24.

$$\dot{Q}_1 = k_1 E(Q_T - Q_1) - K_2 Q_1 \tag{24}$$

To find the steady-state solution, $\dot{Q}_1$ was set equal to zero and equation 24 was solved for Q_{1ss}, yielding equation 25.

$$Q_{1ss} = \left(\frac{k_1E_1}{k_1E_1 + k_2}\right) Q_T \qquad (25)$$

Assuming E constant and substituting k_1 for k_1E in equation 25, produces equation 26. Let $Q_T = 1$, $K_3 = 0.6$, $K_2 = 0.2$, and $E_1 = 1$

$$Q_{1ss} = \frac{k}{k + k_2} Q_T = \frac{0.6}{0.6 + 0.2} = 0.75. \qquad (26)$$

This form of the solution appears often in problems involving distribution of a resource between two states. Figure 14a also shows the result of a DYNAMO (Pugh, 1970) simulation of this order-disorder model. Note that the steady-state value determined both mathematically and by simulation is the same.

Similar analysis and simulation were performed for each model in Figures 14b through h. The analyses are summarized in Table 1, while the simulation results of each model with the same pathway coefficients and energy source values were shown parallel to the energy circuit model diagram. The documentation of each simulation model is contained in Appendix II.

The series of models presented in this section all used only one differential equation in the simulation model. The second equation dropped out when the constraint of holding total matter constant was applied.

The order-disorder model in Figure 14b incorporates the addition of a feedback of some of the order, Q_1 to pump more energy. The conservation of matter imposed gives this model logistic characteristics as seen in the simulation results. This model has two steady-state solutions. Figure 14c incorporates an external energy source, E_2 to pump the recycle process. The simulation results are the same as

Figure 14. A comparison of several order-disorder models and their simulation results. In all simulations the following values were used:

$$E_1 = 1, E_2 = 1, K_1 = 0.6, K_2 = 0.2.$$

Also conservation of matter was imposed on each model.

(a) Simple order-disorder model and simulation results with one energy source E_1.

(b) Order-disorder model and simulation results with autocatalytic feedback and one energy source E_2.

(c) Order-disorder model and simulation results with an ordering energy source E_1 and a disordering energy source E_2.

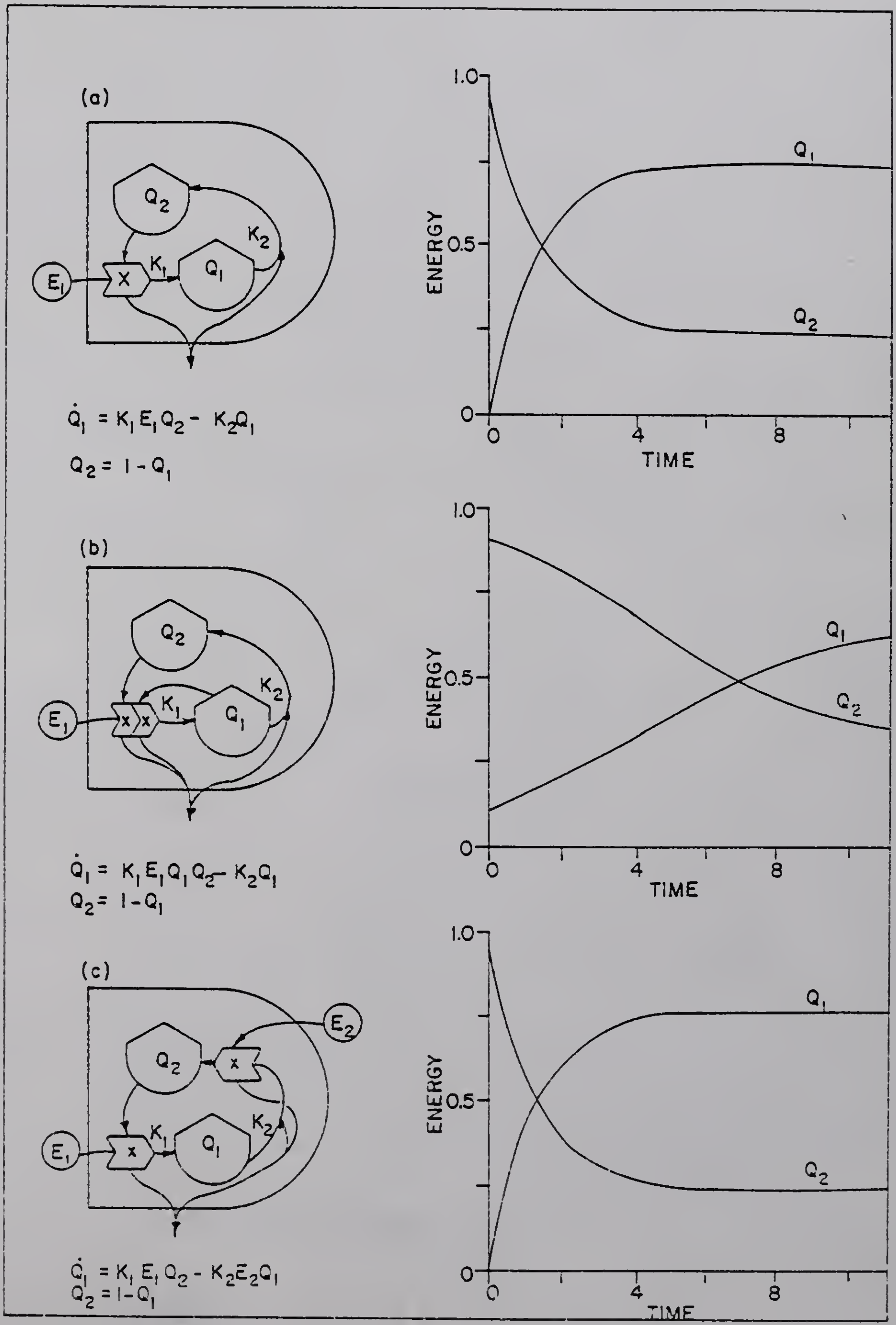

(a)

$$\dot{Q}_1 = K_1 E_1 Q_2 - K_2 Q_1$$

$$Q_2 = 1 - Q_1$$

(b)

$$\dot{Q}_1 = K_1 E_1 Q_1 Q_2 - K_2 Q_1$$

$$Q_2 = 1 - Q_1$$

(c)

$$\dot{Q}_1 = K_1 E_1 Q_2 - K_2 E_2 Q_1$$

$$Q_2 = 1 - Q_1$$

Figure 14. Continued

(d) Autocatalytic order-disorder model and simulation results ordering energy source E_1 and disordering energy source E_2.

(e) Autocatalytic order-disorder model and simulation results with cooperation feedback in order loop and cubic drain on disorder loop.

(f) Autocatalytic order-disorder model and simulation results with square drain in disorder loop and an disordering energy source.

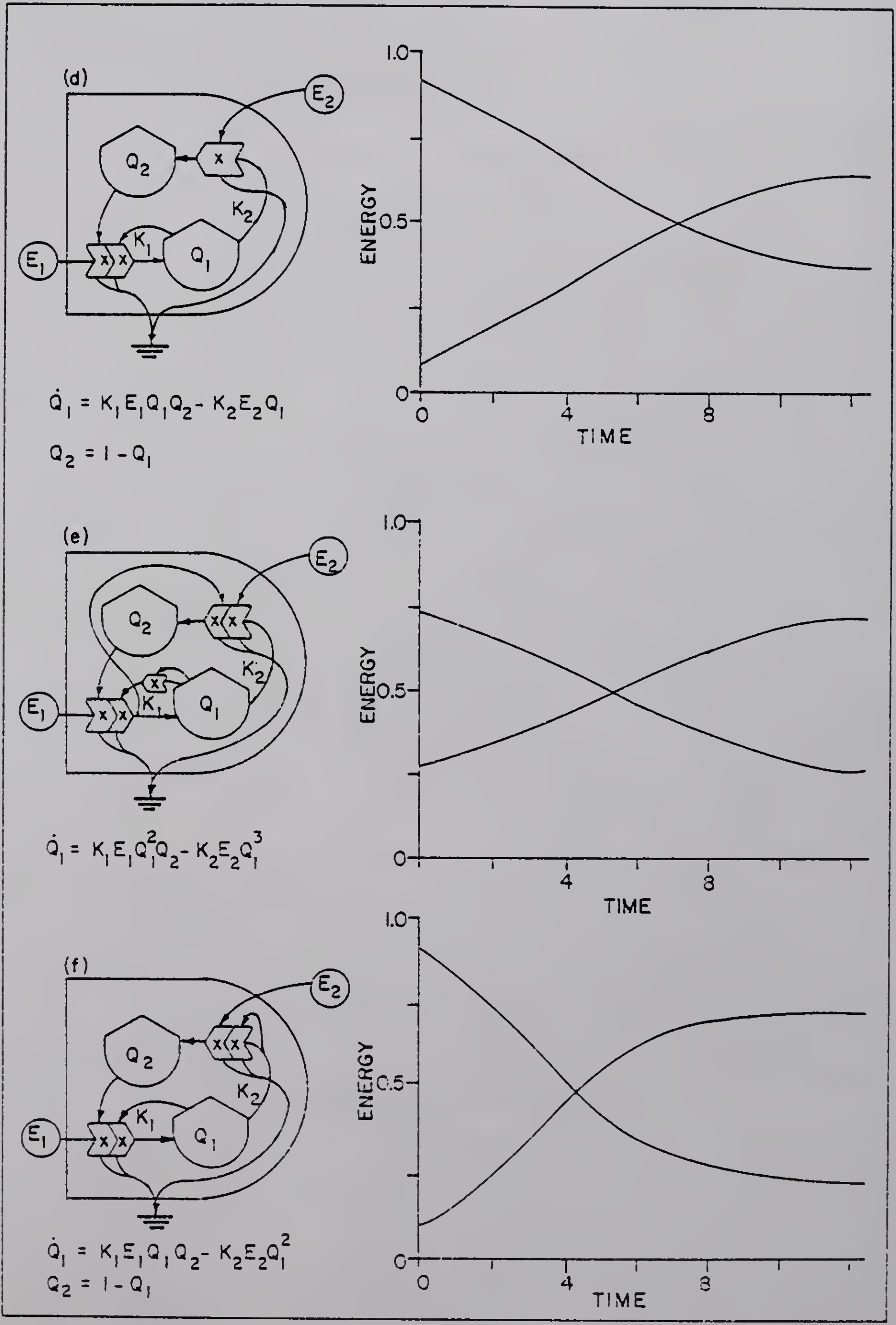

(d)

$$\dot{Q}_1 = K_1E_1Q_1Q_2 - K_2E_2Q_1$$

$$Q_2 = 1 - Q_1$$

(e)

$$\dot{Q}_1 = K_1E_1Q_1^2Q_2 - K_2E_2Q_1^3$$

(f)

$$\dot{Q}_1 = K_1E_1Q_1Q_2 - K_2E_2Q_1^2$$

$$Q_2 = 1 - Q_1$$

Figure 14. Continued

(g) Dual autocatalytic order-disorder model and simulation results which behaves like a flip-flop.

(h) Autocatalytic order-disorder model and simulation results with constant flow energy source.

(i) Simple order-disorder model simulation results with two differential equations.

(g)

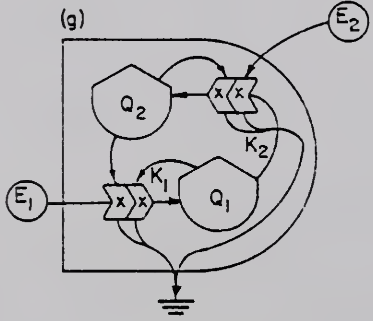

$$\dot{Q}_1 = K_1E_1Q_1Q_2 - K_2E_2Q_1Q_2$$
$$Q_2 = Q_T - Q_1$$

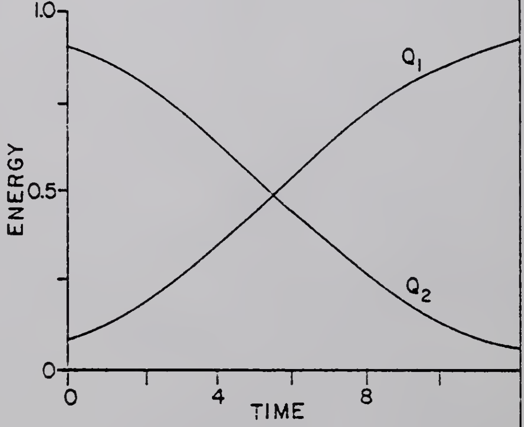

(h)

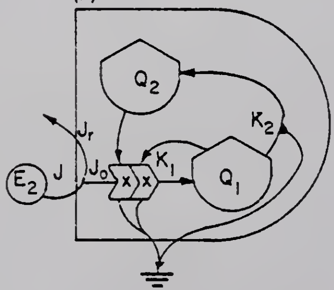

$$\dot{Q}_1 = \frac{K_1J_0Q_1Q_2}{1 + K_0Q_1Q_2} - K_2Q_1E_2$$
$$Q_2 = Q_T - Q_1$$

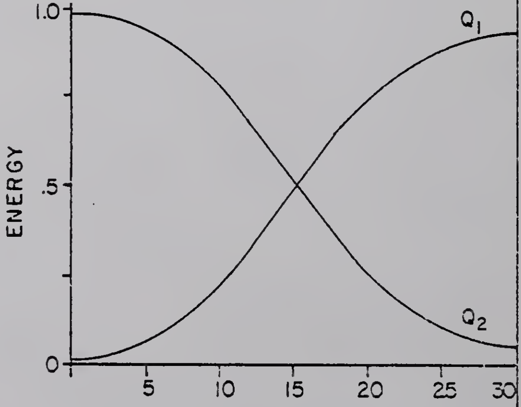

(i)

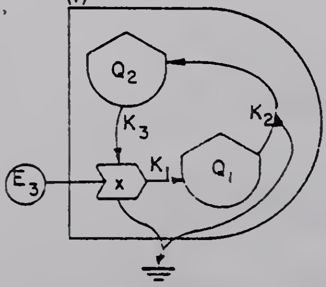

$$\dot{Q}_1 = K_1E_1Q_1 - K_2Q_1$$
$$\dot{Q}_2 = K_2Q_1 - K_3E_1Q_2$$

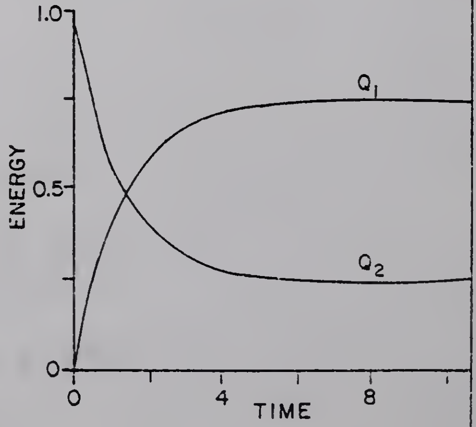

TABLE 1. STEADY-STATE SOLUTIONS AND STEADY-STATE VALUES FOR THE ORDER-DISORDER MINIMODELS IN FIGURE 14.

Model No.	Steady-state Solution	Steady-state Value
a	$Q_{1ss} = \frac{k_1E \quad Q_r}{k_1E + k_2}$	0.75
b	$Q_{1ss} = \frac{k_1 \, E_1Q_T \; - K_2}{k_1 \, E_1}$ or 0	0.67 or 0
c	$Q_{1ss} = \frac{k_1E_1 \, Q_T}{k_1E_1 + k_2E_2}$	0.75
d	$Q_{1ss} = \frac{K_1 \, E_1Q_T - k_2E_2}{k_1E_1}$ or 0	0.67 or 0
e	$Q_{1ss} = \frac{K_1 \, E_1 \, Q_T}{K_1 \, E_1 + k_2E_2}$ or o	0.75 or 0
f	$Q_{1ss} = \frac{E_1Q_T}{E_1 + k_2E_2}$ or 0	0.75 or 0
g	$Q_{1ss} = \frac{E_1 - k_2E_2}{E_1 - k_2E_2}$ or 0	1 to 0

Figure 14a, thus this is another form of the Michaelius-Menton kinetics. Figure 14d is the logistic model with the addition of an external energy source to pump the recycle process. Figure 14e illustrates the effect of using the square of the order Q_1 to pump order and disorder with two external energy sources. Figure 14f is another configuration of the order-disorder model which has logistic behavior and also uses dual energy sources for order and disorder processes. Figure 14g is an unusual order-disorder model, which behaves as a flip-flop circuit. This may be unrealistic for there is no depreciation on the storages except through the dual production functions of order and disorder. Figure 14h incorporates internal and external limits to form a logistic behavior. The external limit is provided by a constant flow energy source and the internal limit provided by material cycling.

To determine that this mathematical manipulation would not affect the simulation result, the model in Figure 14i was simulated. The model diagramed in Figure 14i is the same as Figure 14a. This simulation was performed using differential equations 27 and 28.

$$\dot{Q}_1 = K_1E_1Q_2 - K_2Q_1 \tag{27}$$

$$\dot{Q}_2 = K_2Q_1 - K_3E_1Q_2 \tag{28}$$

To insure stability in the model, (K_1) was set equal to (K_3) as in a Lotka Loop. Figure 14i also shows the result of the simulation, and it was identical to the results obtained in Figure 14q. Thus identical simulation results were obtained for the order-disorder models with two differential equations in Figure 14i when the coefficients were balanced as with one differential equation and the conservation of matter constraint in Figure 14q.

Switching Pulse Models

A previous energy circuit model used a threshold approach to modeling disasters or disorder in processes, such as fire or epidemic. A switch controlled by a logic threshold was used to model the disruption process (Odum, 1974). Two logic configurations of the model are given in Figure 15. The behavior of the model is simple and adequate for a first order approximation to modeling catastrophic events. When the level in the storage Q_1 exceeds a present threshhold T, the disaster pathway K_3 is logically switched on and remains conductive until the energy storage Q_i is depleted below its self-extinguishing threshhold, T_2. Also, the model may be triggered by applying a logic pulse at P. The limitations of this model are apparent when the simulation is examined over the period of the disaster. However, this model does not explain the dynamic behavior of the diaster. It simply replicates observed results' destruction.

Exponential Surge Model

To facilitate the simulation of actual disaster processes such as fire, earthquakes, and floods, a dynamic model was developed capable of explaining energy concentration, storage, and catastrophic release in the disaster process. As a minimum, the model needed the long-term characters of the logically switched one in Figure 15. Previous work by other researchers with fire has shown the energy in the fire to increase exponentially until the source of fuel is consumed by the fire (Byram et al., 1966). These previous findings suggested that an exponential growth model would be appropriate for modeling the fire. Figure 16q is an energy circuit order-disorder model with the logic pathway replaced by an autocatalytic consumer, fire. In this model, the fire was triggered by an energy pulse applied to the fire energy storage Q_3. Once initiated,

Figure 15. Energy circuit disorder model of disaster typical of previous fire and epidemic models of other researchers. Disorder process is logically switched.
(a) Model with external trigger required.
(b) Model with internal threshold trigger mechanism.

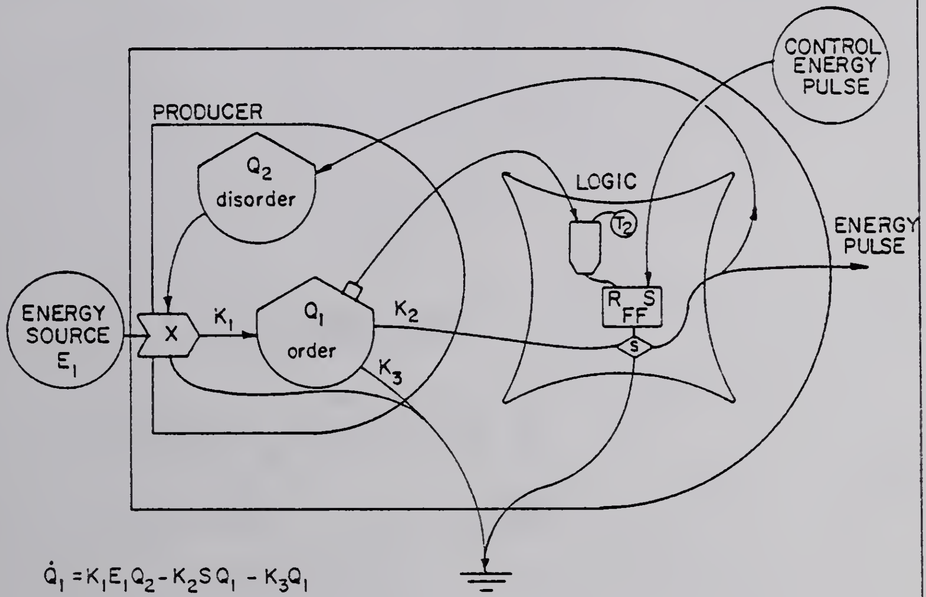

$\dot{Q}_1 = K_1E_1Q_2 - K_2SQ_1 - K_3Q_1$

$Q = Q_T - Q_1$

S = 1 if flip-flop is set

S = 0 if flip-flop is reset

(a)

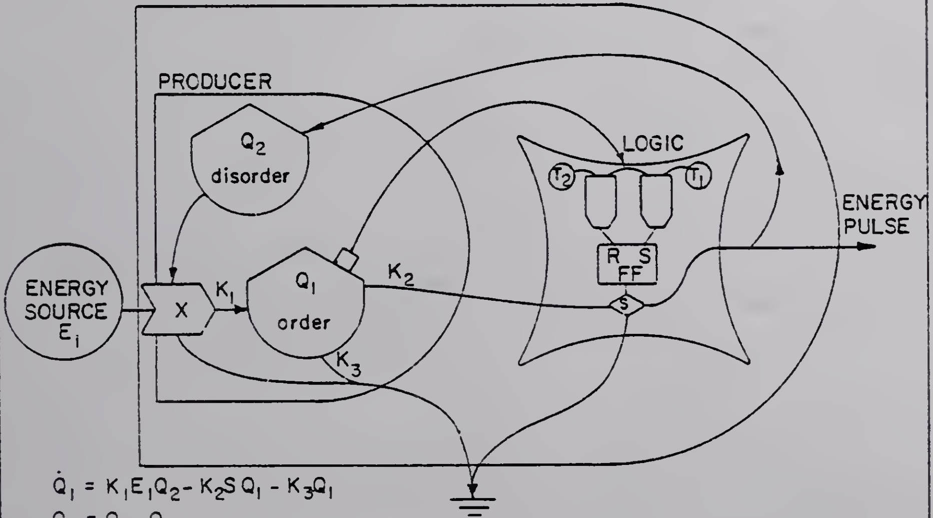

$\dot{Q}_1 = K_1E_1Q_2 - K_2SQ_1 - K_3Q_1$

$Q_2 = Q_T - Q_1$

S = 1 if flip-flop is set

S = 0 if flip-flop is reset

(b)

Figure 16. Order-disorder energy circuit model with catastrophic energy, pulse generated by consumer module.

(a) Model with external control pulse required.

(b) Model with internal threshold for pulse generation.

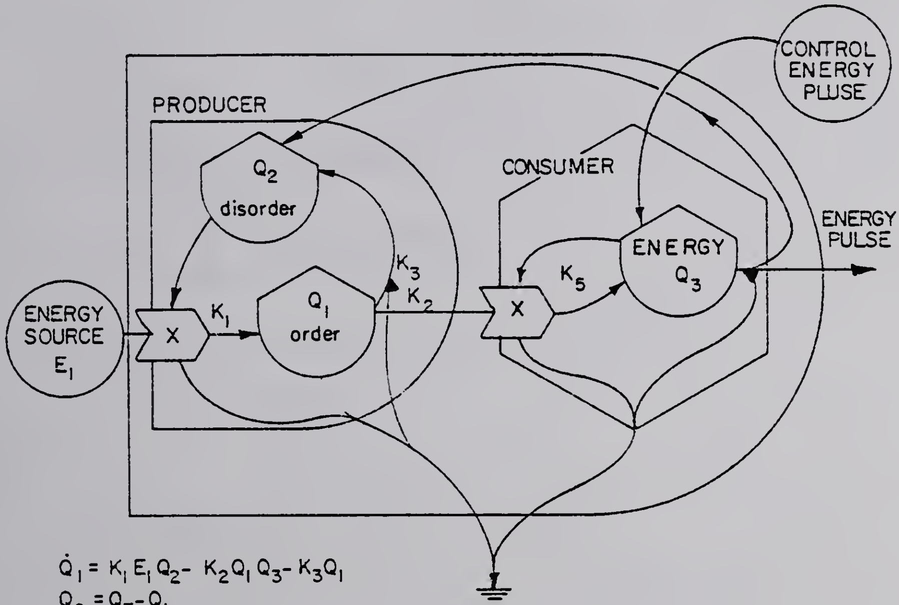

$$\dot{Q}_1 = K_1E_1Q_2 - K_2Q_1Q_3 - K_3Q_1$$
$$Q_2 = Q_T - Q_1$$
$$\dot{Q}_3 = K_5Q_1Q_3 - K_6Q_3 + E_2$$

(a)

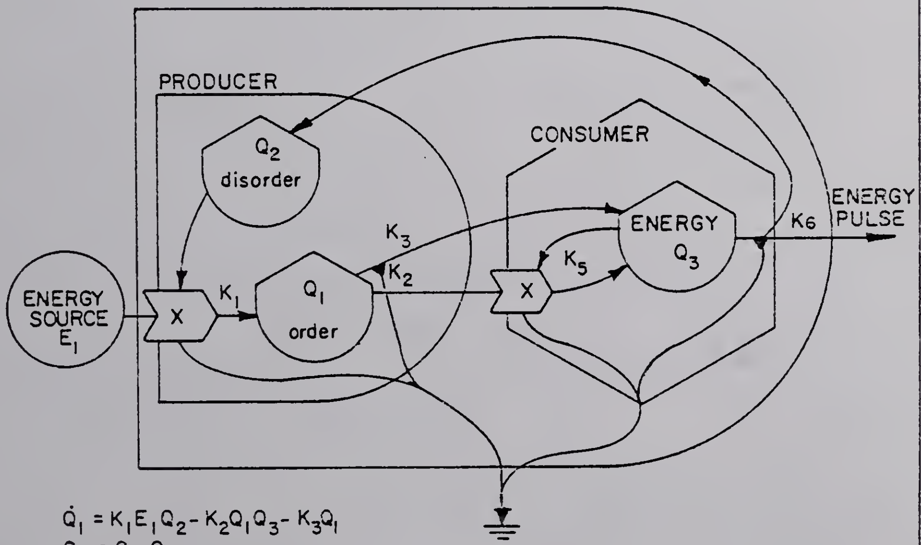

$$\dot{Q}_1 = K_1E_1Q_2 - K_2Q_1Q_3 - K_3Q_1$$
$$Q_2 = Q_T - Q_1$$
$$\dot{Q}_3 = K_5Q_1Q_3 - K_6Q_3 + K_3Q_1$$

(b)

the fire grew exponentially until the fuel source was consumed to the point of self-extinction. However, this model could not self-start.

To incorporate the self-starting characteristic into the model, the linear drain pathway, which represents depreciation, was fed into the disaster energy storage Q_3. As long as the drain or depreciation of Q_3 is greater than the inflows, the model was stable, and the order or potential energy in Q_1 could be increased. However, if Q_1 became large enough so that the depreciation of Q_1 exceeded the losses from Q_3, the autocatalytic fire model reached a critical point where it could self-start and grow until the energy source Q_1 was consumed. This model was also capable of periodic oscillation as shown in Figure 16. The storage of energy grows to a threshold and periodically discharges.

This model has several advantages over the logic model in addition to replication of upper and lower thresholds. Because it actually models the disaster, if preventive measures can be taken in time, the disaster may be extinguished. For example, the fire may be controlled or extinguished by cooling the disaster energy storage Q_3 as is done in fire fighting with water. It is also possible to control the disaster growth and extinguishing rate based on the characteristics of the stored fuel.

The order-disorder model in Figure 16b had good dynamic characteristic for disaster model used in this research. The model conforms to the convention of conservation of matter such that the sum of storages are constant Q_T as in equation 29.

$$Q_1 + Q_2 = Q_T. \qquad (29)$$

The level of order or stress in the disaster Q_1 was described by equation 30.

Figure 17. Simulation of the periodic buildup and pulse generation property of the exponential surge model in Figure 16b.

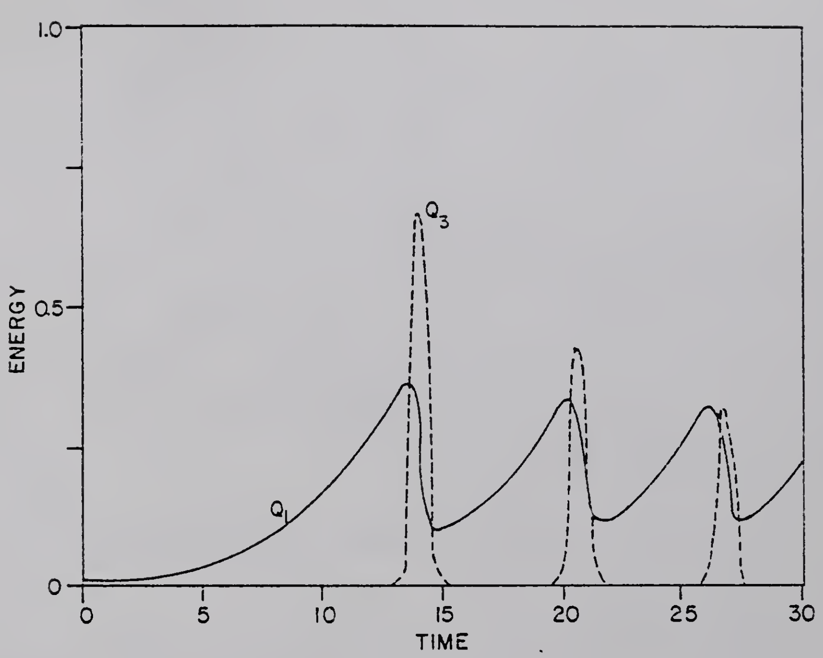
1.0
0.5
0
ENERGY
0
5
10
15
20
25
30
TIME
Q_3
Q_1

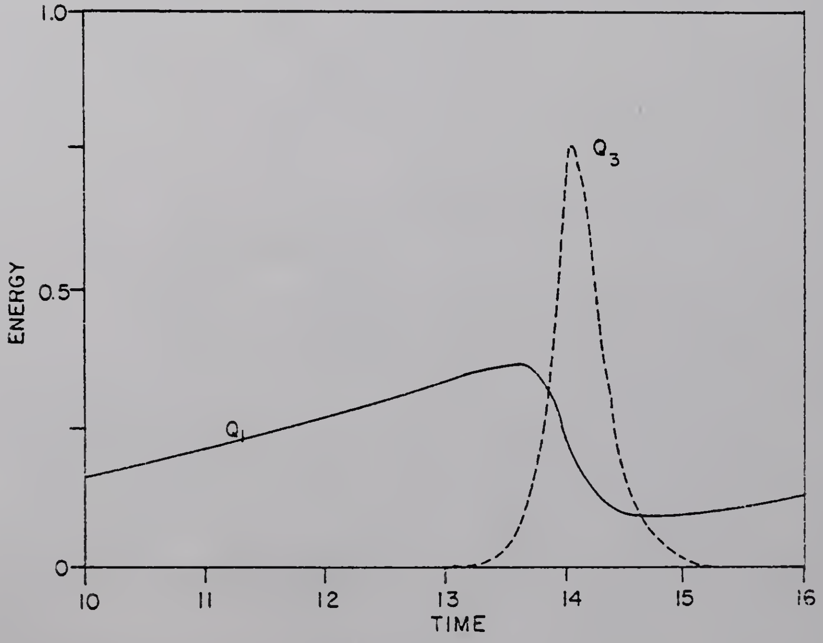
1.0
0.5
0
ENERGY
10
11
12
13
14
15
16
TIME
Q_3
Q_1

$$\dot{Q}_1 = k_1EQ_2 - k_2 (Q_1 + Q_1Q_3). \qquad (30)$$

Catastrophic energy release was controlled by the autocatalytic energy release pathway $k_2(Q_1 + Q_1Q_3)$. When Q_3 is small, this term is dominated by the linear depreciation k_2Q_1. The value of energy storage in the decay pathway Q_3 is described by equation 31.

$$\dot{Q}_3 = (k_4 - k_3)Q_1Q_3 - k_5Q_3 + K_6Q_1 \qquad (31)$$

Equations 30 and 31 may be used to solve for steady-state values of Q_1 and Q_3 by setting the Q_1 and Q_3 equal to zero, yielding equations 32 and 33.

$$Q_{1ss} = \frac{k_1EQ_T}{k_1E - k_1 - k_1Q_{3(ss)}} \qquad (32)$$

$$Q_{1ss} = \frac{k_5Q_{1(ss)}}{k_3Q_{1(ss)} + k_5 - k_4Q_{1(ss)}} \qquad (33)$$

Also, threshold for catastrophic release is given by equation 34:

$$Q_{1t} = \frac{k_5Q_3}{(k_3 - k_4)\ (Q_3 + k_6)} \qquad (34)$$

that is, if $Q_1 > Q_{1t}$, the model will catastrophically switch to the disorder state.

The decay path of the disaster is controlled by the value of k_5, which is the time constant of the catastrophic decay.

Evaluation of Global Energy Web and Disasters

Figure 18 is an energy circuit model that attempts to synthesize concepts about the earth using concepts from geology, meteorology,

Figure 18. Web model of global energy. In this energy circuit, diagram units of coupled order and disorder are connected to form a world web of energy concentration and material cycling. For purposes of clarity, group symbols were used to divide the global energy web into the atmospheric, economic, oceanic, geological, and biological subsystems of the earth. The solar and tidal energy provide the power to build in the system. The continuous degeneration of the ordered storages released an equal amount of infrared radiation thus maintaining the global energy balance. This model is diagramed by sector.

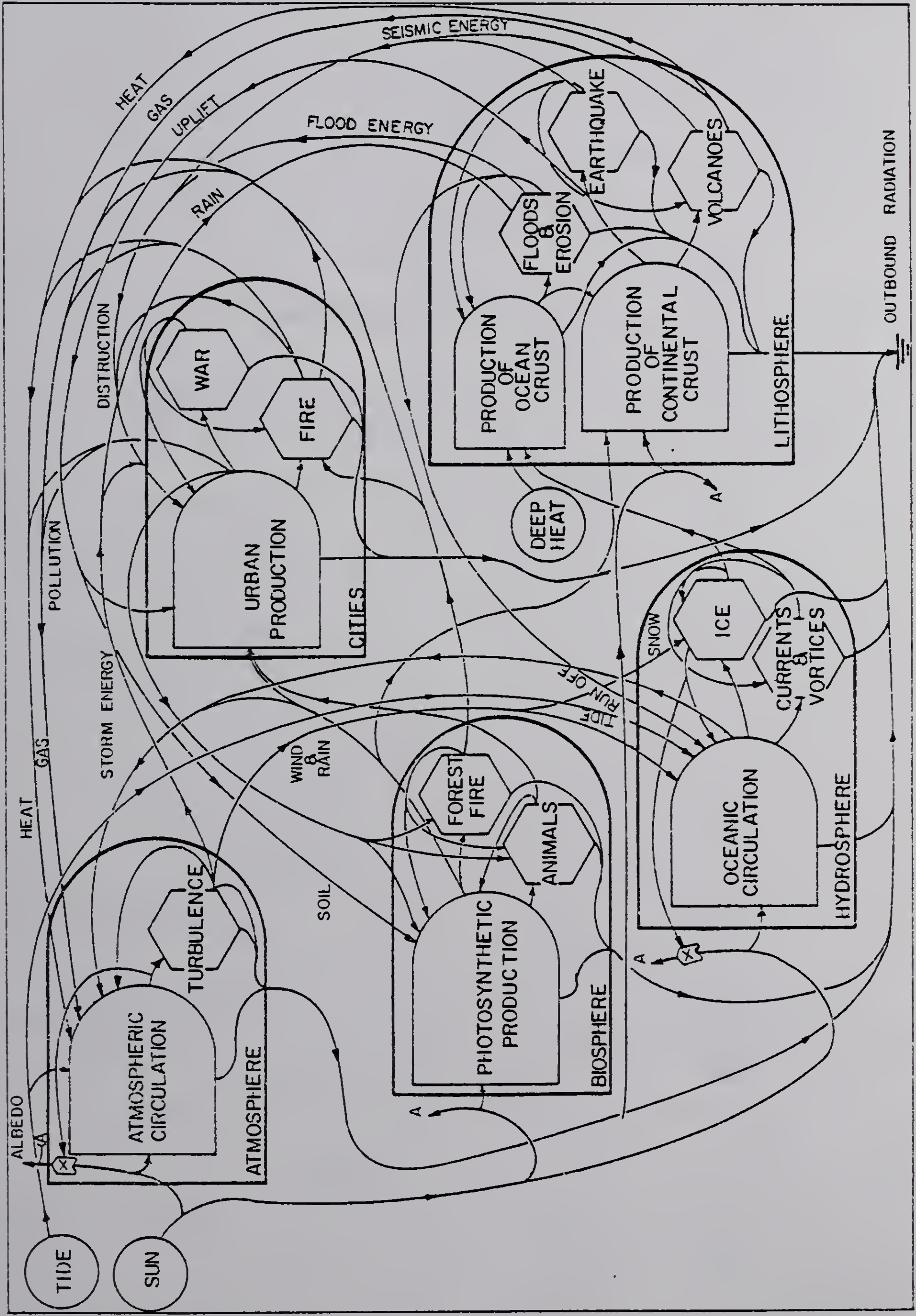
TIDE
SUN
ALBEDO
A
ATMOSPHERIC CIRCULATION
TURBULENCE
ATMOSPHERE
HEAT
GAS
STORM ENERGY
POLLUTION
DISTRUCTION
RAIN
UPLIFT
GAS
HEAT
SEISMIC ENERGY
FLOOD ENERGY
WAR
FIRE
URBAN PRODUCTION
CITIES
WIND & RAIN
SOIL
FOREST FIRE
ANIMALS
PHOTOSYNTHETIC PRODUCTION
BIOSPHERE
A
DEEP HEAT
PRODUCTION OF OCEAN CRUST
PRODUCTION OF CONTINENTAL CRUST
FLOODS & EROSION
EARTHQUAKE
VOLCANOES
LITHOSPHERE
A
OUTBOUND RADIATION
ICE
CURRENTS & VORTICES
SNOW
RUN OFF
TIDE
OCEANIC CIRCULATION
HYDROSPHERE
A

oceanography, economics, and ecology. It shows the global structural mechanisms that concentrate energy in space and time, store energy, and eventually release the energy in catastrophic pulses that seem natural disasters to people.

Studies of energy flow and concentration processes in the biosphere are usually constrained by the boundaries of the discipline. Parts of the global energy model developed in this section have been studied by meteorologists, oceanographers, ecologists, geologists, and economists, with each group concentrating on kinetics, energy flows, and catastrophic phenomena in their respective fields. However, energy is known to flow across the areas covered by disciplines in the real world. A catastrophic event in one field often triggers secondary disruptions in many fields.

Modeling the concentration, storage, and catastrophic release mechanism produced fundamental insight into the behavior of disasters. Conceptually, each natural disaster occurrence is viewed as a disruption of a storage following a peak in the normal global energy cycle. Earthquakes, volcanoes, tidal waves, rock slides, and other disruptive geological hazards are viewed as momentary nonlinear pulses of energy generated by bottlenecks, which produce a temporary concentration of potential energy. Floods, lightning, hurricanes, and tornados result from a rapid release of excess potential energy stored in atmospheric systems. Forest fire is the result of catastrophic release of chemical potential energy stored by biological systems in organic matter. Urban fire and war can be modeled as releases from storages of society, often disordered by earthquakes, floods, storms, tsunamies, and volcanoes.

The world model suggests interrelationships of natural disasters and the energy trajectory required for them. It allows energy flows from various energy sources to be compared.

Rational quantitative comparison of sectors, disaster phenomena, and ratios of flow can be made if all of the energy flows involved are put in a common unit of measure such as heat equivalents, Calories of embodied solar energy, and energy quality factors. These were evaluated for the world model and are given by sector next.

Atmospheric Circulation and Storms

Figure 19 is the atmospheric sector of the global natural hazard model in Figure 18, which was the web used for calculation of the solar energy quality of rain, wind, and storms. To calculate the energy quality of storms, it was first necessary to evaluate the model from the available global energy data. Figure 19a presents the model in conceptual form, while 19b is in mathematical form with differential equations. Table 2 documents the energy flow and storage evaluation of the world's atmospheric system with detailed calculations provided in Appendix I.

Storms, such as cyclones, hurricanes, tornados, and thunderstorms, are powered by warm moist air conducted toward polar latitudes of the earth as excess heat from tropical latitudes. Storms are formed by the atmospheric systems acting as a mechanism to release excessive quantities of potential energy that could not be released in a competitive way by simple diffusion. The release of excess energy built up across fronts produces turbulence. The wind pumps more energy through the atmospheric system. The turbulence also provides a positive feedback to the ocean by producing waves which in turn supply more water vapor energy to power the storm and to provide rain for the land systems of the earth.

The advent of the satellite made direct measurement of global parameters possible. Measurements from space platforms essentially confirm

Figure 19. Energy circuit diagrams of atmospheric system.

(a) Conceptual drawing of energy circuit model of atmosphere used to illustrate energy quality calculation for weather and wind. Energy flows are in Cal $m^{-2}d^{-1}$ while storages are in Cal m^{-2}.

(b) Atmospheric sector of global energy web model in Figure 18 with differential equations. This energy circuit cycling receptor module was evaluated for the major flows of energy in the atmosphere. Table 1 provides documentation for the model.

$$\dot{Q}_1 = \frac{K_1 R_h Q_2}{1 + K_{80} Q_2} + \frac{K_2 R_w Q_5}{1 + K_{81} Q_5} - K_3 Q_1 Q_3 - K_4 Q_1 - K_5 Q_1$$

$$Q_2 = C_1 - K_{56} Q_1$$

$$\dot{Q}_3 = K_3 Q_1 Q_2 - K_6 Q_3 - K_7 Q_3 - K_8 Q_3$$

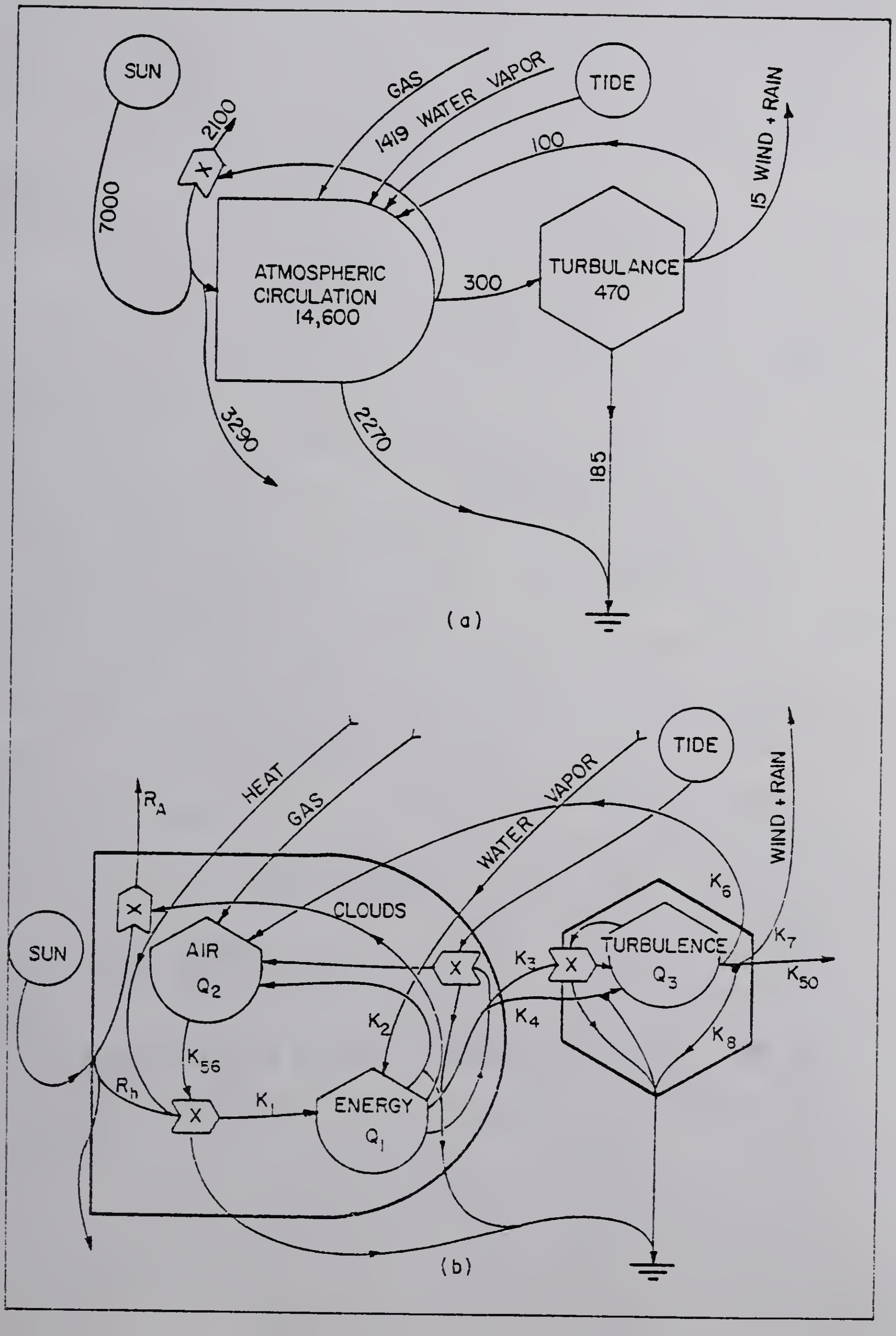
SUN
7000
2100
X
GAS
1419 WATER VAPOR
TIDE
100
15 WIND + RAIN
ATMOSPHERIC CIRCULATION 14,600
300
TURBULANCE 470
3290
2270
185
(a)
R_A
HEAT
GAS
WATER VAPOR
TIDE
WIND + RAIN
X
CLOUDS
SUN
AIR Q_2
X
K_2
K_3
X
TURBULENCE Q_3
K_6
K_7
K_50
K_4
K_8
K_56
R_h
X
K_1
ENERGY Q_1
(b)

TABLE 2. EVALUATION, NAME, AND DESCRIPTION OF ENERGY FLOWS AND STORAGES FOR GLOBAL ATMOSPHERIC SECTOR MODEL IN FIGURE 19.

Coefficients	Values	Coefficient Name	Descriptive Comment	Note[a]
I_o	7,000 Cal $m^{-2}d^{-1}$	Solar radiation	Solar radiation incident to earth	1
R_n	4,900 Cal $m^{-2}d^{-1}$	Net radiation	Solar radiation absorbed by earth	2
R_a	2,100 Cal $m^{-2}d^{-1}$	Albedo	Solar radiation reflected	3
R_w	3,290 Cal $m^{-2}d^{-1}$	Surface radiation	Solar radiation available to plants and land surface	4
R_h	1,610 Cal $m^{-2}d^{-1}$	Atmosphere	Solar radiation consumed in atmosphere system	5
R_L	4,900 Cal $m^{-2}d^{-1}$	Infrared radiation	Infrared radiation radiated outward from earth	6
Q	14,600 Cal $m^{-2}d^{-1}$	Latent heat	Latent heat storage of energy in atmospheric water	7
Q	10,400 kg m^{-2}	Air	Mass of atmosphere	8
Q	470 Cal m^{-2}	Circulation and turbulence	Energy stored in turbulence and circulation	9
$\frac{K_1\ Q_2\ R_h}{1 + K_{80}\ Q_2}$	1,610 Cal $m^{-2}d^{-1}$	Atmosphere	Solar energy consumed in atmosphere	10

---

[a] The calculations that document this table are shown in Appendix I.

TABLE 2. CONTINUED

Coefficients	Values	Coefficient Name	Descriptive Comment	Note[a]
$\frac{K_2\ Q_5\ R_W}{1 + K_{81}\ Q_5}$	1,440 Cal $m^{-2}d^{-1}$	Evaporation	Energy delivered by water vapor	11
$K_3\ Q_1\ Q_3$	150 Cal $m^{-2}d^{-1}$	Turbulence	Energy consumed by eddy flux	12
$K_4\ Q_1$	150 Cal $m^{-2}d^{-1}$	Circulation	Energy consumed in circulation	13
$K_5\ Q_1$	2,720 Cal $m^{-2}d^{-1}$	Cooling	Energy loss by cooling	14
$K_6\ Q_3$	100 Cal $m^{-2}d^{-1}$	Weather	Poleward energy flow in weather system	15
$K_7\ Q_3$	15 Cal $m^{-2}d^{-1}$	Wind and rain	Energy flow in wind and rain	16
$K_8\ Q_3$	185 Cal $m^{-2}d^{-1}$	Heat loss	Turbulent energy dissipated in atmosphere	17
$K_{50}\ Q_3$	4.1 Cal $m^{-2}d^{-1}$	Hurricanes	Energy dissipated by hurricanes	18

the Smithsonian mean value of the solar radiation to be 1.94 g-Cal cm^{-2} min^{-1} or 27,940 Cal $m^{-2}d^{-1}$(Byers, 1974). The world model shows the relation. Solar flares, which have been shown to have an 11-year cycle (Eddy, 1976), release high quality cosmic radiation which is responsible for a 2 percent fluctuation around this mean (Schneider and Mass, 1975), sometimes called the "solar constant." The solar radiation incident to the earth was taken to be 7,000 Cal $m^{-2}d^{-1}$. This was calculated by dividing the solar mean by the ratio of the area of the earth's plane to the area of the earth's surface.

Working with 5 years of data from satellites (1962-1966), Vonder Haar and Suomi (1971) found the global annual average solar radiation to be 7,000 Cal $m^{-2}d^{-1}$, and the radiation absorbed to be 4,900 Cal $m^{-2}d^{-1}$. Radiation hitting the earth was either absorbed or reflected by the clouds, land surface, and plants. The difference between the energy absorbed and the incident energy, known as albedo, was found to be 2,100 Cal $m^{-2}d^{-1}$. The global average infrared radiation was also measured by Vonder Haar and Suomi (1971) from satellite data and found to be 4,900 Cal $m^{-2}d^{-1}$. Houghton (1954) found 23 percent of the solar energy incident to the globe was directly consumed in powering the hydrological cycle to 1,610 Cal $m^{-2}d^{-1}$, while the majority of the remaining energy, 3,290 Cal $m^{-2}d^{-1}$, was used in direct heating land and sea and powering the photosynthetic cycle. Indirect forms of solar energy, however, are equally important to the operation of the earth's energy web. The energy flows evaluated above were global averages; however, the solar radiation was shown by Houghton (1954) to be distributed in such a way that the incident radiation per square meter of surface area drops as latitude increases. Figure 20a is an early plot of this

Figure 20. Global distribution of solar energy with latitude.

(a) Distribution with latitude of absorbed and outgoing radiation as computed by Houghton; solar radiation absorbed by earth and atmospheres; long-wave radiation leaving the atmosphere. The abscissa is scaled by the cosine of latitude (Houghton, 1954).

(b) Mean meridional profiles (averages within latitude zones) of components of the earth's radiation budget measured during the period 1962-66. The abscissa is scaled by the cosine of latitude (Vonder Haar and Soumi, 1971).

(c) Total poleward energy transport required by the radiation budget (RT) and its major components. The free energy transport by ocean currents is ΔF, LΔC is the transport of energy in latent form of water vapor and ΔC, the sensible heat plus potential energy transported by the atmosphere (Vonder Haar and Suomi, 1971).

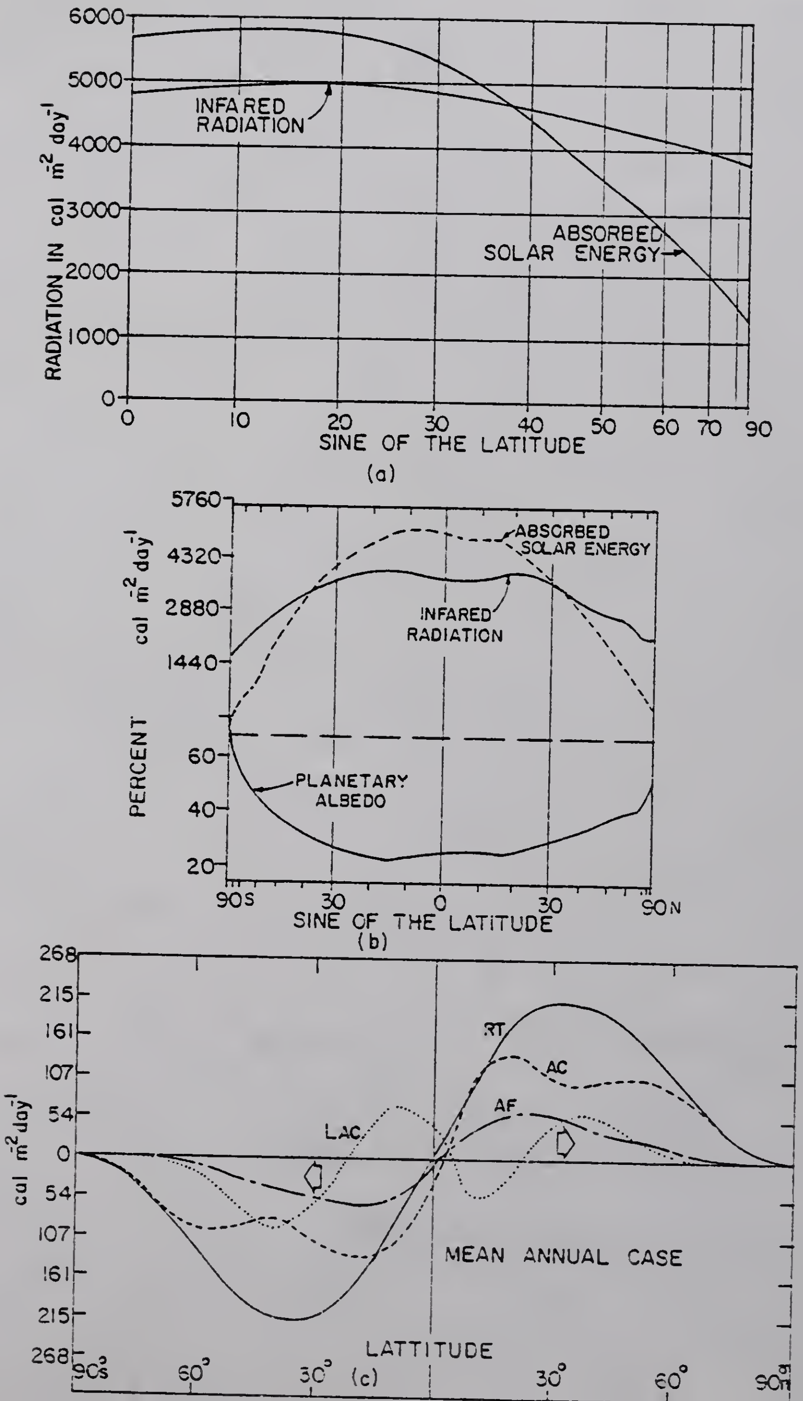
6000
5000
4000
3000
2000
1000
0
RADIATION IN cal m^{-2} day^{-1}
INFARED RADIATION
ABSORBED SOLAR ENERGY
0
10
20
30
40
50
60
70
90
SINE OF THE LATITUDE
(a)
5760
4320
2880
1440
cal m^{-2} day^{-1}
ABSORBED SOLAR ENERGY
INFARED RADIATION
PERCENT
60
40
20
PLANETARY ALBEDO
90S
30
0
30
90N
SINE OF THE LATITUDE
(b)
268
215
161
107
54
0
54
107
161
215
268
cal m^{-2}day^{-1}
RT
AC
AF
LAC
MEAN ANNUAL CASE
LATTITUDE
90°S
60°
30°
(c)
30°
60°
90°N

phenomenon developed by Houghton (1954). Note that there was a net flux of energy toward the poles necessary to offset the cooling processes at the polar region. Houghton's findings indicate that below 40° latitude heating exceeded cooling, and above 40° the reverse was true. A more accurate estimation of the relationship was available from satellite data and was plotted in Figure 20b (Vonder Haar and Suomi, 1971). The planetary albedo was also plotted on Figure 20b. The net result of the imbalance of heating and cooling was a poleward energy transport, R_t, required to balance the budget and is shown in Figure 20c. Vonder Haar and Suomi divided the total energy transport among three major components; the free energy transport of the ocean with a mean of 50 Cal $m^{-2}d^{-1}$, the transport of energy in the latent heat of water vapor with a mean of 25 Cal $m^{-2}d^{-1}$, and the sensible heat plus potential energy transported by the atmosphere with a mean of 75 Cal $m^{-2}d^{-1}$. Thus approximately 100 Cal $m^{-2}d^{-1}$ is atmospherically transported towards the poles.

The buildup of potential gradients of energy was released in the model through the mean circulation flux of meridional motion and eddy flux. The 100 Cal $m^{-2}d^{-1}$ transported to higher latitudes was used as the energy source for the consumptive processes. Byers (1974) suggested that the split was approximately equal between the circulation flux of the atmosphere and the eddy flux between the equator and 30° latitude, the net direct effect was from the circulation flux while at higher latitudes, the eddy flux term was dominant. Thus 50 Cal $m^{-2}d^{-1}$ were pumped from the order to disorder storages in the model to represent circulation flux while the other 50 Cal $m^{-2}d^{-1}$ was used to power the eddy flux of storms in the disorder pathway.

Oceanic Circulation

Figure 21a presents the oceanic systems of the world in conceptual form with the primary energy flows evaluated. Sluggish general circulation over much of the earth converges into fast currents and associated vortices in a few zones, especially in the Gulf Stream and its counterparts in other oceans. Figure 21b is the oceanic model in mathematical form with differential equations. Table 3 documents the evaluation of energy flows and storages in the model supported by calculations and references in Appendix I.

The oceanic system of the world was modeled as a reservoir of water and chemicals in continuous circulation. Solar energy in the form of radiation, wind, and rain, plus the tidal pull of the sun and moon are the principal energy sources responsible for the cycling of matter in the sea. Excess heat, built up at lower latitudes in the ocean by solar heating, is transported towards the poles' tide driven by deep currents and wind-driven waves and surface currents.

Solar energy provided the major energy input to power the oceanic system by delivering 3,280 Cal $m^{-2}d^{-1}$ (Weyl, 1970). The sea reflected back an average of 350 Cal $m^{-2}d^{-1}$ to the sky (Weyl, 1970), consumed 1,570 Cal $m^{-2}d^{-1}$ to power the evaporation process, fixed 2 Cal $m^{-2}d^{-1}$ in photosynthesis (Whittaker and Likens, 1975) and transported 50 Cal $m^{-2}d^{-1}$ toward the pole (Vonder Haar and Suomi, 1971). This left 1,318 Cal $m^{-2}d^{-1}$, which was lost to the atmosphere as heat. On the average, 3.4×10^5 Cal m^{-2} was stored in the sea in the form of heat (Weyl, 1970). The evaporation process consumes 2.9 kg $m^{-2}d^{-1}$ of water, which was replaced by 2.6 kg $m^{-2}d^{-1}$ of precipitation and 0.3 kg $m^{-2}d^{-1}$ of runoff from the land masses of the earth.

Figure 21. Energy circuit models of the oceanic systems of the earth.

(a) Conceptual diagram of energy concentration of sea that illustrates energy flows necessary for quality calculations. Energy flows are in Cal $m^{-2}d^{-1}$ and storages in Cal^{-2}.

(b) Energy circuit model of oceanic system of global model in Figure 18 with differential equations. Solar, wind, and tidal energy produce global currents to transport excess heat at lower latitudes thus aiding in equalizing global energy distribution and powering the cycles of the sea.

$$\dot{Q}_4 = \frac{R_W\ K_{10}\ Q_5}{1 + K_{82}\ Q_5} - K_{14}\ Q_4\ K_{11}\ TQ_4 - K_{12}\ Q_4\ Q_3\ K_{13}\ Q_4\ Q_6\ Q_{20}$$

$$Q_5 = C_2 - K_{56}\ Q_4$$

$$\dot{Q}_6 = K_{13}\ Q_4\ Q - K_{72}\ Q_6\ Q_{20} - K_{15}\ Q_6 - K_{17}\ Q_6$$

$$\dot{Q}_{20} = K_{70}\ Q_3 - K_{71}\ Q_6\ Q_{20}.$$

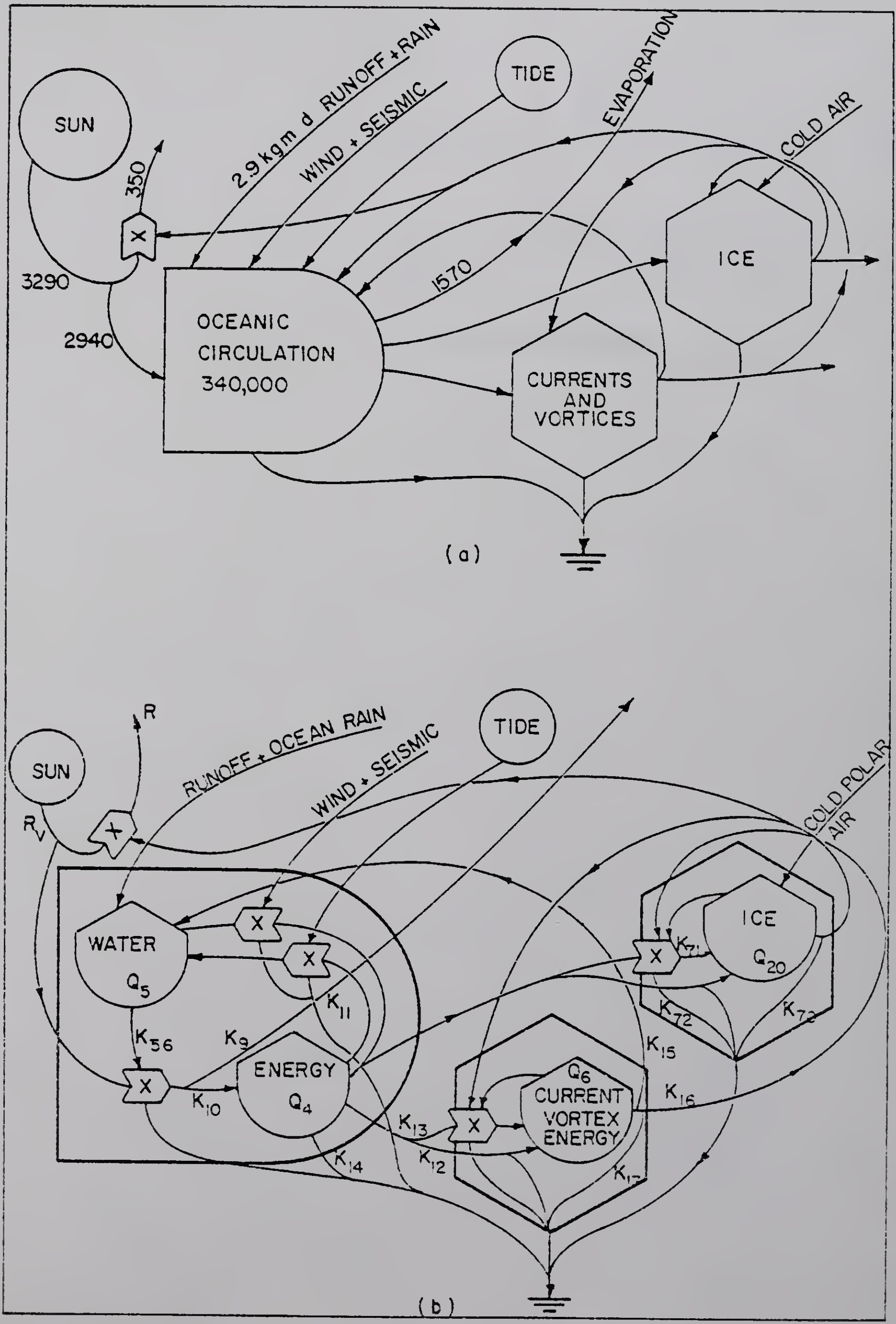
SUN
TIDE
2.9 kgm d RUNOFF + RAIN
WIND + SEISMIC
EVAPORATION
COLD AIR
350
3290
2940
1570
OCEANIC
CIRCULATION
340,000
ICE
CURRENTS
AND
VORTICES
(a)
SUN
R
R_V
RUNOFF + OCEAN RAIN
WIND + SEISMIC
TIDE
COLD POLAR
AIR
WATER
Q_5
K_{56}
K_9
K_{11}
K_{10}
ENERGY
Q_4
K_{13}
K_{14}
K_{12}
ICE
Q_{20}
K_{71}
K_{72}
K_{72}
K_{15}
K_{16}
Q_6
CURRENT
VORTEX
ENERGY
K_{17}
(b)

TABLE 3. EVALUATION, NAME, AND DESCRIPTION OF ENERGY FLOWS AND STORAGES FOR THE OCEANIC SECTOR OF THE MODEL IN FIGURE 21.

Coefficient	Value	Coefficient Name	Descriptive Comment	Note[a]
R_W	3,290 Cal $m^{-2}d^{-1}$	Solar energy	Mean solar radiation at sea surface	1
R_{wa}	350 Cal $m^{-2}d^{-1}$	Reflection	Mean solar radiation reflected by sea	2
Q_4	3.4 x 10^4 Cal m^{-2}	Stored heat	Mean solar energy stored in ocean as heat	3
Q_5	3.88 x 10^6 kg m^{-2}	Mass of ocean	Mean mass of water in ocean	4
Q_6	0.55 Cal m^{-2}	Kinetic energy	Energy stored in sea gyers	5
$\frac{R_W K_9 Q_5}{1 + K_{81} Q_5}$	1,570 Cal $m^{-2}d^{-1}$	Evaporation	Mean solar energy used in evaporation	6
$\frac{R_W K_{10} Q_5}{1 + K_{82} Q_5}$	1,370 Cal $m^{-2}d^{-1}$	Heating	Mean solar energy consumed in heating of sea	7
$K_{11} Q_4 T$	25 Cal $m^{-2}d^{-1}$	Tide transport	Mean transport of heat energy by tide	8
$K_{12} Q_4$	25 Cal $m^{-2}d^{-1}$	Surface current	Wind pumped surface current	9
$K_{13} Q_4 Q_6 Q_3$	620 Cal $m^{-2}d^{-1}$	Heat pumped by wind	Heat loss due to wind turbulence	10

---

[a] The calculations that document this table are shown in Appendix I.

TABLE 3. CONTINUED

Coefficent	Value	Coefficient Name	Descriptive Comment	Note[a]
$K_{14}\ Q_4$	700 Cal $m^{-2}d^{-1}$	Dissipate heat	Mean solar dissipated as heat	11
$K_{15}\ Q_6$	25 Cal $m^{-2}d^{-1}$	Surface current	Wind driven surface heat transfer poleward	12
$K_{16}\ Q_6$	0.13 Cal $m^{-2}d^{-1}$	Wave dissipation	Energy transferred from wind to waves	13
$K_{17}\ Q_6$	620 Cal $m^{-2}d^{-1}$	Wind cooling	Cooling of sea by wind act of waves	14
$K_8\ Q_{13}$	2633 g $m^{-2}d^{-1}$	Precipatation	Mean rainfall on ocean	15
T	1.34 Cal $m^{-2}d^{-1}$	Tide	Energy dissipated in sea from tide	16
$K_7\ Q_3$	15 Cal $m^{-2}d^{-1}$	Wind	Energy from wind	17
$K_{13}\ Q_4\ Q_6\ Q_{30}$	3 x 10^{-4} Cal $m^{-2}d^{-1}$	Gyer energy	Energy consumed by gyers	18
$K_{14}\ Q_4$	3 x 10^{-4} Cal $m^{-2}d^{-1}$	Gyer energy dissipation	Energy dissipated by sea gyers	19
Q_{20}	5.7 x 10^7 g m^{-2}	Ice	Water stored in polar ice and glaciers	20
$K_{70}\ Q_3$	3.9 g $m^{-2}d^{-1}$	Snow	Buildup of ice from rain and snow	21

TABLE 3. CONTINUED

Coefficient	Value	Coefficient Name	Descriptive Comment	Note[a]
K_{71} Q_4 Q_{26}	3.9 g $m^{-2}d^{-1}$	Melting	Melting of ice by land and sea heat	22
K_{22} Q_7 Q_{20}	0.39 Cal $m^{-2}d^{-1}$	Energy	Energy consumed in melting of ice	23

Wind and tide provided the necessary energy sources to transport the excess heating at the equator toward the poles by delivering 15 Cal $m^{-2}d^{-1}$ of wind energy of which 0.44 Cal m^{-2} was stored in the potential kinetic energy transfer of waves, while 0.13 Cal $m^{-2}d^{-1}$ was dissipated on the shores of the continental land masses. The tide driven by the gravitational pull of the sun and moon contributed 1.5 Cal $m^{-2}d^{-1}$ to the ocean system by powering the deep currents of the sea. The net effect of the wind and tide was a transfer of 50 Cal $m^{-2}d^{-1}$ poleward and a substantial mixing of the sea.

Just as the global imbalance of temperature generates large scale patterns of circulation in the atmospheric system, excess heating of the sea produces gigantic anticyclonic gyers. The strongest ocean currents are found at the western peripheries of gyres, such as the Gulf Stream and the Kuroshio. The gyres of the hemispheres of the earth converge by colliding equatorial currents. The mean radius of gyres is approximately 2,500 km and the average velocity of the current at the periphery is about 0.1 m sec^{-1}, thus the period of circulation is approximately 5 years (Monin _et_ _al_., 1977). The mean current velocity for oceans is 0.035 m sec^{-1} thus 0.55 Cal m^{-2} is stored in the kinetic energy of sea circulation (Monin _et_ _al_., 1977).

The glaciers and polar ice cap store 2.9×10^{7} km (Skinner and Turekian, 1973), which is equivalent to 5.7×10^{7} g m^{-2} of ice. The turnover time for the ice of the earth was estimated at 4×10^{4} yr^{-1} (Skinner and Turekian, 1973). Therefore, the rate of new ice formation is 4 g $m^{-2}d^{-1}$, which is offset by melting of an equal amount if the global ice storage is in equilibrium. This melting of the polar ice cap and glaciers requires 0.4 Cal $m^{-2}d^{-1}$ of heat from the sea.

Photosynthetic Production, Animals, and Fire

Figure 22 is a conceptual model of the order-disorder model of the biosphere with animal life and fire in the consumer role. Figure 22b is the model in mathematical form with the storages and flows of energy evaluated and documented in Table 4. Note the strong similarity between the application of the theory of order, disorder, and pulsing to biological, atmospheric, and oceanic systems of the world energy web in Figure 18.

Many fundamental similarities exist between the biological process of material cycles that form ordered structure, the structures continual disordering process, and the atmospheric and oceanic systems of the earth previously diagramed.

The photosynthetic system of the biosphere forms the solar energy concentration system, while animals, microorganisms, and forest fire were in continual competition to consume the excess storages of energy in the plant community, to aid in recycling matter, and to perform many necessary control actions by feeding back part of their concentrated energy.

Sun, heat, wind, rain, and geological minerals were the primary energy sources for the production of organic matter by plant life. The global average of 4,900 Cal $m^{-2}d^{-1}$ of solar energy was the dominant energy source when measured in heat Calories. Wind and rain delivered approximately 15 Cal $m^{-2}d^{-1}$. Organic and geologic minerals contributed a flow of 0.25 g $m^{-2}d^{-1}$, or 1 Cal $m^{-2}d^{-1}$.

Lieth and Whittaker (1975) have made extensive quantitative studies of the primary production of the photosynthetic processes of the biosphere and compiled extensive data on global net primary production.

Figure 22. Energy circuit models of biological energy concentration process of the world.

(a) Conceptual version of order-disorder process in biosphere with energy flows in Cal $m^{-2}d^{-1}$ and energy storages in Cal m^{-2}.

(b) Biological section of global energy web model in mathematical form. This cycling receptor module was evaluated for energy flows in biological systems. The differential equation form of the model is also included.

$$\dot{Q}_7 = \frac{R_W\ (K_{18} - K_{19})\ Q_3\ Q_7\ Q_8}{1 + K\ Q_3\ Q_7\ Q_8} - K_{29} - Q_7 - K_{22}\ Q_9\ Q_7 - K_{21}\ Q_7\ Q_{20}$$

$$Q_8 = C_3 - K_{55}\ Q_7$$

$$\dot{Q}_9 = K_{22}\ Q_7\ Q_9 - K_{23}\ Q_9 - K_{26}\ Q_9\ Q_{10}$$

$$\dot{Q}_{10} = K_{21}\ Q_7\ Q_{10} - K_{24}\ Q_{10} - K_{30}\ Q_9\ Q_{10}$$

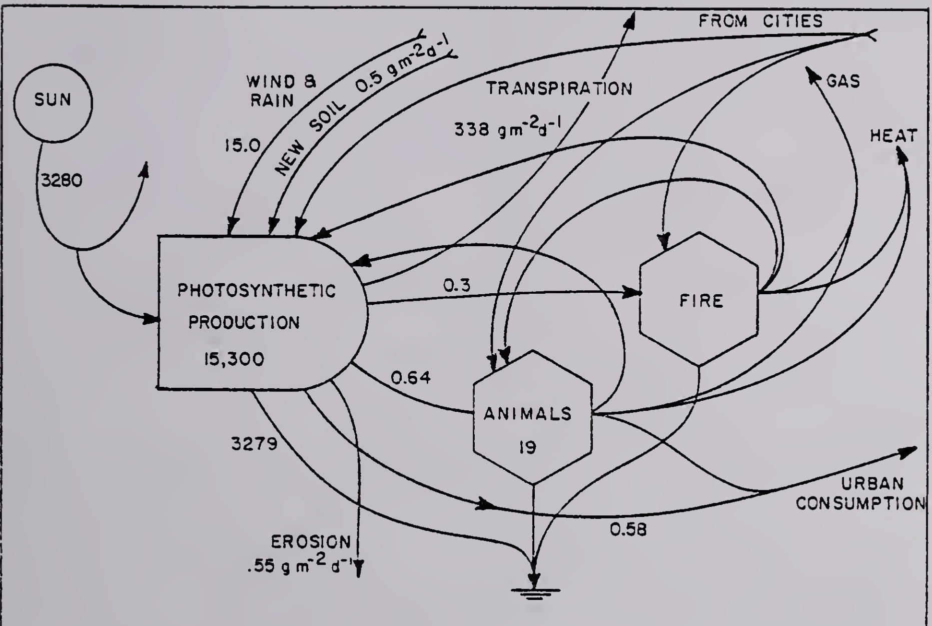
SUN
3280
WIND & RAIN
15.0
NEW SOIL 0.5 gm-2d-1
TRANSPIRATION
338 gm-2d-1
FROM CITIES
GAS
HEAT
PHOTOSYNTHETIC PRODUCTION
15,300
0.3
FIRE
0.64
ANIMALS
19
3279
EROSION
.55 g m-2 d-1
URBAN CONSUMPTION
0.58

(a)

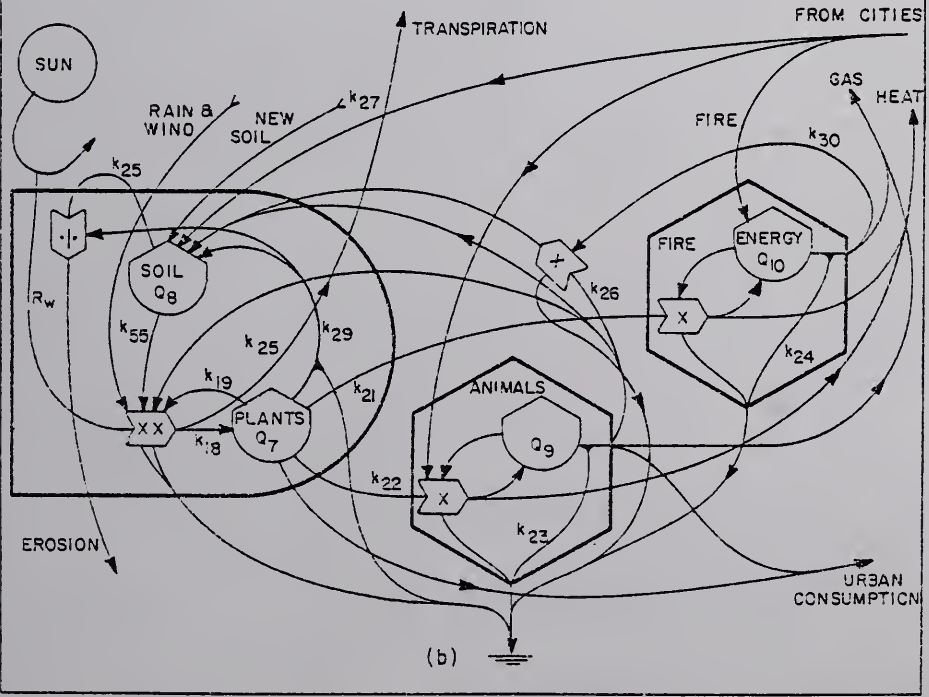
TRANSPIRATION
FROM CITIES
SUN
RAIN & WIND
NEW SOIL
k27
GAS
HEAT
FIRE
k30
k25
SOIL
Q8
Rw
k55
k25
k29
k26
FIRE
ENERGY
Q10
X
k24
k19
XX
k18
PLANTS
Q7
k21
ANIMALS
Q9
k22
X
k23
EROSION
URBAN CONSUMPTION

(b)

TABLE 4. EVALUATION, NAME, AND DESCRIPTION OF ENERGY FLOWS AND STORAGES FOR BIOSPHERE MODEL IN FIGURE 22.

Coefficients	Value	Coefficient Name	Descriptive Comment	Note[a]
Q_7	15,300 Cal m^{-2}	Plant biomass	Standing stock of plants	1
Q_9	19 Cal m^{-2}	Animal biomass	Global stock of annual	2
Q_{10}	2×10^{14} Cal m^{-2}	Forest fire	Energy stored in fire	3
Q_8	650 kg m^{-2}	Soil	Mean mass of soil	4
R_w	3290 Cal $m^{-2}d^{-1}$	Surface radiation	Energy available to plants	5
$K_{18}R_wQ_3Q_8Q_9$	7.8 Cal $m^{-2}d^{-1}$	Gross primary production	Total plant production	6
$K_{19}R_wQ_3Q_5Q_8$	3.90 Cal $m^{-2}d^{-1}$	Respiration of plants	Energy consumed by plants	7
$\frac{(K_{18}-K_{19})R_wQ_3Q_7Q_8}{1 + K_{83}Q_3Q_7Q_8}$	3.90 Cal $m^{-2}d^{-1}$	Net primary production	Energy fixed by plants	8
$K_{22}Q_7Q_9$	0.62 Cal $m^{-2}d^{-1}$	Consumption	Energy consumed by herverores	9

---

[a] The calculations that document this table are shown in Appendix I.

TABLE 4. CONTINUED

Coefficients	Value	Coefficient Name	Descriptive Comment	Note[a]
$K_{21}Q_7Q_{10}$	0.3 Cal $m^{-2}d^{-1}$	Forest fire	Energy consumed by fire	10
$\frac{K_{25}R_WQ_3Q_7Q_8}{1+K_{34}Q_2Q_7Q_8}$	338 g $m^{-2}d^{-1}$	Transpiration	Water evaporated from plants	11
$K_{24}Q_{10}$	0.3 Cal $m^{-2}d^{-1}$	Fire dissipation	Mean energy dissipated in fire	12
$K_{23}Q_9$	0.62 Cal $m^{-2}d^{-1}$	Animal respiration	Mean respiration of animals	13
$K_{26}Q_9Q_{10}$	1 x 10^{-4} Cal $m^{-2}d^{-1}$	Animal burned	Mean animal consumed in fire	14
$K_{27}Q_{18}Q_{16}$	0.51 g $m^{-2}d^{-1}$	New soil minerals	Uplift from geologic system	15
$K_{28}Q_{11}$	0.55 g $m^{-2}d^{-1}$	Erosion	Loss of soil due to wind and rain	16
$K_{21}Q_{11}$	2.13 Cal $m^{-2}d^{-1}$	Detrius	Buildup of detrius	17

Based on annual statistics of the U.S. Fire Service, it was estimated that 0.3 Cal $m^{-2}d^{-1}$ of biological material was consumed by fire.

A third use of organic matter is through the sedimentary cycle. Schlesinger (1977) estimated the input of carbon into the world detritus pool at 3.75×10^{13} kg C yr^{-1}, which is an energy input of 2.1 Cal $m^{-2}d^{-1}$. The world stock of carbon in detritus was estimated 1.4×10^{15} kg C which is equivalent to 2.4×10^{4} Cal m^{-2}. This gives a turnover time for the carbon stock of about 40 years. Hubbert (1971) estimated a world fossil fuel net production rate of 0.1 Cal $m^{-2}d^{-1}$. It is likely that some detritus is degraded in the fossil fuel production process. A minimal consumption of detritus by the earth's fossil fuel production system is about 0.3 Cal $m^{-2}d^{-1}$ or approximately 10 percent of the total detritus produced. They found the net primary production of the biosphere to be 0.92 g $m^{-2}d^{-1}$ dry matter, or 3.9 Cal $m^{-2}d^{-1}$, of chemical energy photosynthetically fixed by the biosphere. This estimate was found to be in reasonable agreement with the findings of other researchers (Golley, 1972; Olson, 1970; Ryther, 1969; SCEP, 1970; Whittaker, 1970; and Whittaker and Likens, 1973). Leith (1975) suggested that these estimates may not need major revision unless human interference changes the global primary production drastically. The total estimated biomass for plant life was also found by Leith and Whittaker (1975) to be 3,600 g m^{-2} of dry matter or 15,300 Cal m^{-2} of chemical energy.

Consumer systems of the world model, which were powered by organic matter, were also responsible for recycling minerals and controlling the function of the photosynthetic producer systems. Whittaker and Likens (1973) found consumption of organic matter by herbivorous animals to be 0.62 Cal $m^{-2}d^{-1}$, and the consumption of man to be about 0.27 Cal $m^{-2}d^{-1}$, for a total consumption of 0.9 Cal $m^{-2}d^{-1}$. They also estimated the world animal biomass to be 4.5 g m^{-2} (dry matter) or 19 Cal m^{-2} which was only .13 percent of the standing stock of plants.

Forest fire was of considerable importance to the control of both plant and animal populations. Of all plant biomass, 99.8 percent was found in the terrestrial systems of the world, leaving virtually all of the chemical potential energy stored in the standing stock of plants exposed to fire (Whittaker and Likens, 1973).

Plate Tectonics, Volcanoes, and Earthquakes

Figure 23a presents the global geological submodel in conceptual form while Figure 23B is the mathematical form with differential equations. Table 5 documents the model and summarizes the calculations of this section.

The geologic processes of the earth are of considerable importance in the cycles of the biosphere and in the causes of disasters. As the tectonic plates of the earth collide, stress energy is stored in the vicinity of the plate junctions. Earthquakes were modeled as a catastrophic release of energy, which then feeds back to pump more energy to drive the global geologic process. As the plates of the earth's crust collide the thinner oceanic plates may be driven under the thicker continental plates, folding under the eroded organic matter from the land and the sediments deposited on the continental shelf.

The extreme pressures and heat transform the organic matter to fossil fuel, which was modeled as an energy source for the earth's volcanic system, the continental uplift process, and the cities of the

Figure 23. Energy circuit model of earth's geological system.

(a) Conceptual energy circuit model of geological system, which forms the basis for energy quality of geological systems of the earth. Energy flows are in Cal $m^{-2}d^{-1}$ and storages in Cal m^{-2}.

(b) Energy circuit model of the plate tectonic system of concentrates energy of lissosphere to power volcanoes and earthquakes. The interaction of rain to produce floods is also shown.

$$\dot{Q}_{12} = \frac{H_0 K_{30} Q_5 Q_{13}}{1 + K_{50} Q_6 Q_{15}} - K_{31} Q_{12} Q_{18} - K_{33} Q_{12} + K_{32} Q_8/Q_7$$

$$Q_{13} = C_4 - K_{54} Q_{13}$$

$$\dot{Q}_{14} = K_{42} Q_{12} Q_{14} Q_5 - K_{41} Q_{14} - K_{46} Q_{14} Q_{17} - K_{43} Q_{14}$$

$$\dot{Q}_{15} = \frac{K_{34} Q_{16} R_W Q_{12}}{1 + K_{51} Q_{16} Q_{12}} - K_{39} Q_{15} - K_{35} Q_{15} Q_{18} - K_{36} Q_{15}$$

$$\dot{Q}_{16} = C_5 - K_{52} Q_{14} - K_{53} Q_{16}$$

$$\dot{Q}_{17} = K_{46} Q_{14} Q_{17} - K_{45} Q_{17} - K_{44} Q_{17} + K_{38} Q_{18}$$

$$\dot{Q}_{18} = K_{35} Q_{15} Q_{18} - K_{37} Q_{18} - K_{37} Q_{18} - K_{38} Q_{18}$$

$$\dot{Q}_{11} = \frac{K_{57} Q_3 Q_8 Q_{11}}{Q_7} + K_{58} Q_{11} - K_{59} Q_{11} - K_{60} Q_{11}.$$

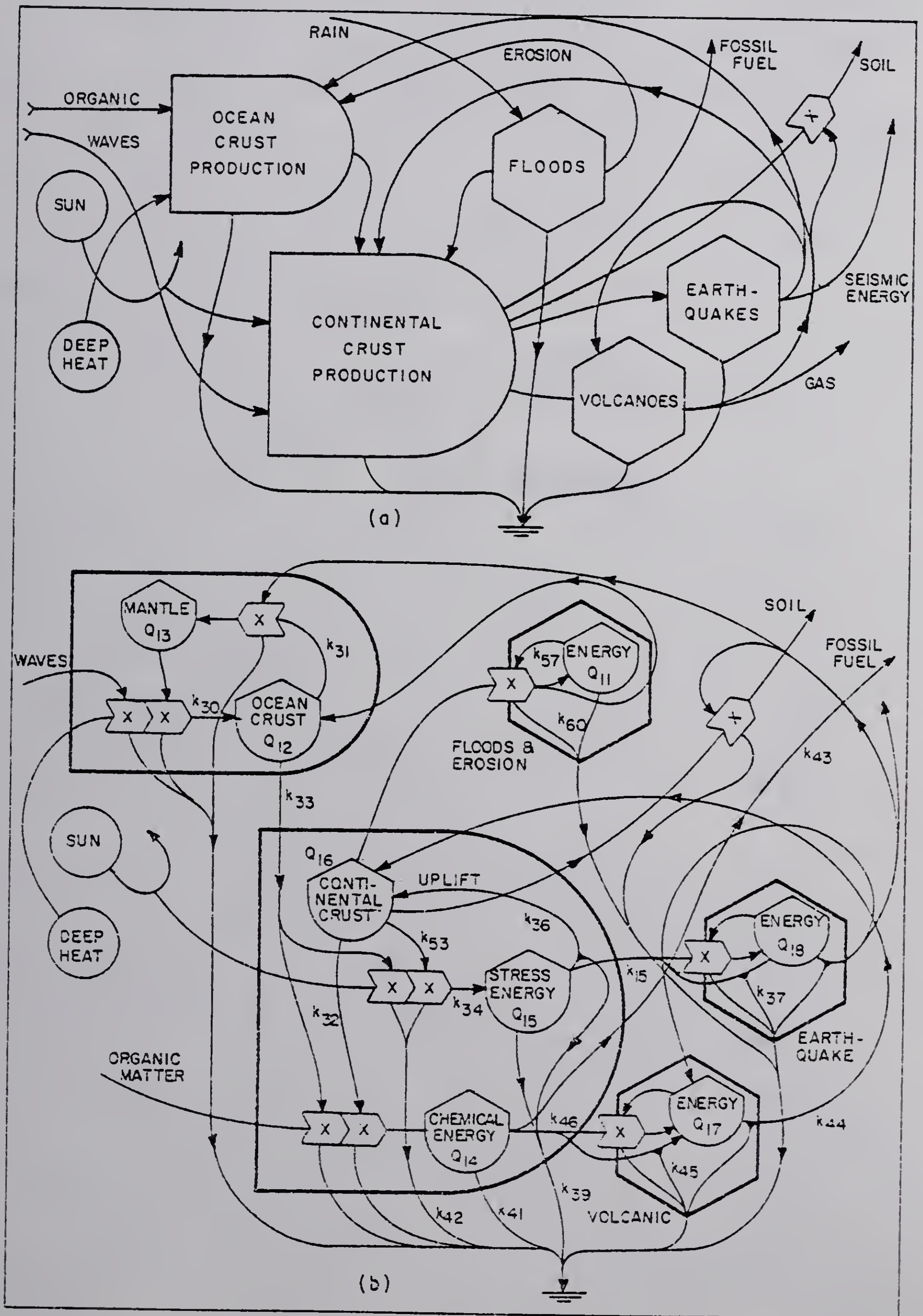
RAIN
EROSION
FOSSIL FUEL
SOIL
ORGANIC
WAVES
OCEAN CRUST PRODUCTION
FLOODS
SUN
DEEP HEAT
CONTINENTAL CRUST PRODUCTION
EARTH-QUAKES
SEISMIC ENERGY
VOLCANOES
GAS
(a)
MANTLE Q_{13}
X
k_{31}
WAVES
X
X
k_{30}
OCEAN CRUST Q_{12}
k_{57}
ENERGY Q_{11}
X
k_{60}
FLOODS & EROSION
SOIL
FOSSIL FUEL
k_{43}
k_{33}
SUN
DEEP HEAT
Q_{16}
CONTI-NENTAL CRUST
UPLIFT
k_{36}
k_{53}
X
X
k_{34}
STRESS ENERGY Q_{15}
k_{15}
X
ENERGY Q_{18}
k_{37}
EARTH-QUAKE
k_{32}
ORGANIC MATTER
X
X
CHEMICAL ENERGY Q_{14}
k_{46}
X
ENERGY Q_{17}
k_{44}
k_{45}
k_{39}
k_{42}
k_{41}
VOLCANIC
(b)

TABLE 5. EVALUATION, NAME, AND DESCRIPTION OF ENERGY FLOWS IN GEOLOGICAL SECTION OF GLOBAL MODEL IN FIGURE 23.

Coefficients	Value	Coefficient Name	Descriptive Comment	Note[a]
Q_{12}	1.94×10^{10} g m^{-2}	Ocean crust	Mass of ocean crust	1
Q_{13}	7.8×10^{12} g m^{-2}	Mantle	Mass of mantle	2
Q_{14}	19,000 Cal m^{-2}	Fossil fuels	Chemical energy storage of earth's crust	3
Q_{15}	4.6 Cal m^{-2}	Stress energy	Seismic energy storage of earth's crust	4
Q_{16}	1.07×10^{11} g m^{-2}	Continental crust	Mass of continental crust of earth	5
Q_{17}	2.2×10^{-5} Cal m^{-2}	Volcanic energy	Storage of energy in active volcanoes	6
Q_{18}	8×10^{-7} Cal m^{-2}	Seismic energy	Storage of energy in active earthquake	7
$\frac{H_0 K_{30} Q_6 Q_{13}}{1 + K_{50} Q_6 Q_{13}}$	0.35 g $m^{-2}d^{-1}$	New ocean crust	Mantle solidified into ocean crust	8
$K_{31} Q_{12} Q_{18}$	0.58 g $m^{-2}d^{-1}$	Ocean crust lost	Ocean crust folded into mantle	9

---

[a] The calculations that document this table are shown in Appendix I.

TABLE 5. CONTINUED

Coefficients	Value	Coefficient Name	Descriptive Comment	Note[a]
$K_{32}\ Q_8/Q_7$	$0.23\ g\ m^{-2}d^{-1}$	Sediments	Deposit of sediments from land	10
$K_{33}\ Q_{12}$	$2\ cm\ yr^{-1}$	Ocean crust stress	Pressure on continental crust by ocean crust	11
$\frac{K_{34} R_W\ Q_{12}\ Q_{16}}{1 + K_{51}\ Q_{16}\ Q_{12}}$	$0.155\ Cal\ m^{-2}d^{-1}$	Stress	Buildup of stress in earth crust	12
$K_{35}\ Q_{15}\ Q_{18}$	$0.055\ Cal\ m^{-2}d^{-1}$	Earthquake consumption	Stress energy consumed by earthquakes	13
$K_{36}\ Q_{15}$	$0.05\ Cal\ m^{-2}d^{-1}$	Uplift	Dissipation of stress energy as uplift	14
$K_{37}\ Q_{18}$	$5.4 \times 10^{-3}\ Cal\ m^{-2}d^{-1}$	Earthquake dissipation	Seismic energy dissipated in earthquake	15
$K_{38}\ Q_{18}$	$1.15 \times 10^{-3}\ Cal\ m^{-2}d^{-1}$	Seismic energy	Global mean flow of siesmic energy	16
$K_{39}\ Q_{15}$	$0.1\ Cal\ m^{-2}d^{-1}$	Stress dissipated	Stress dissipated as heat in rock fracture	17
$K_{40}\ Q_{16}$	$0.51\ g\ m^{-2}d^{-1}$	Soil	Formation of new soil	18
$K_{41}\ Q_{14}$	$0.22\ Cal\ m^{-2}d^{-1}$	Fossil fuel loss	Energy loss in fossil product	19

TABLE 5. CONTINUED

Coefficient	Values	Coefficient Name	Descriptive Comment	Note[a]
$K_{42}\ Q_5\ Q_{12}\ Q_{14}$	0.33 Cal $m^{-2}d^{-1}$	Gross production	Organic matter consumed in fossil fuel	20
$K_{43}\ (Q_7 + Q_9)\ Q_{14}Q_{19}$	0.2 Cal $m^{-2}d^{-1}$	Consumption, city	Mass use of fossil fuel	21
$K_{44}\ Q_{17}$	5.1×10^{-4} Cal $m^{-2}d^{-1}$	Volcanic energy	Energy released by volcanoes	22
$K_{45}\ Q_{17}$	1×10^{-3} Cal $m^{-2}d^{-1}$	Volcanic loss	Heat loss in volcanic process	23
$K_{56}\ Q_{14}\ Q_{17}$	1.5×10^{-3} Cal $m^{-2}d^{-1}$	Volcanic consumption	Energy consumed by volcanoes	24
H	1 Cal $m^{-2}d^{-1}$	Deep heat	Low quality heat loss of earth's crust	25
Q_{11}	1.7×10^{-3} Cal m^{-2}	Energy storage in floods	Mean energy stored in floods of world	26
$\frac{K_{57}\ Q_3\ Q_8\ Q_{11}}{Q_7}$	0.04 Cal $m^{-2}d^{-1}$	Floods consumption	Energy consumed in powering floods	27
$K_{58}\ Q_{11}$	753 g $m^{-2}d^{-1}$	Runoff	Water transported to sea	28
$K_{59}\ Q_{11}$	0.23 g $m^{-2}d^{-1}$	Sediments	Sediments transported to sea	29
$K_{60}\ Q_{11}$	0.04 Cal $m^{-2}d^{-1}$	Flood dissipation	Energy dissipated by floods	30

world. As the ocean plates are consumed under the continental plates, new plates are formed in the deep trenches of the ocean from uplift of molten mantle material. In some cases the formation of ocean crust produces sea earthquakes and volcanoes. These catastrophic events dissipated some of their energy through tsunami or seismic sea waves, which accelerated continental erosion.

Conceptually, the material cycling process of the geologic system of the earth was viewed as two interlocked order-disorder loops. In the first loop, the ocean crust was continuously recycled into the ocean crust mantel of the earth by folding the ocean crust under the continental crust at the plate junctions by production of new crust at the ocean trenches by the mantle. Scientific evidence exists to prove that the ocean plates are in constant motion. The ocean plates slide away from ocean ridges at a rate of approximately 2 cm yr^{-1}, so that approximately 0.35 g $m^{-2}d^{-1}$ of new ocean plate material was formed from hot material flowing up from the mantle of the ocean ridge (Clark, 1971). As the ocean plates were created by the ridge, the plates become larger, applying great pressure to the continental plates, which were about five times thicker and several hundred times older than the older ocean plate. Sediments from the continental plates also contribute 0.2 g m^{-2} d^{-1} to the mass of the ocean plates. The rate of creation of ocean crust was balanced by a loss of 0.58 g $m^{-2}d^{-1}$ as the ocean plates folded under the continental plates.

The fact that the continental crust was several hundred times older than any ocean crust also supports the concept that plates of the earth were part of a separate but related order-disorder cycle in which the erosion process of the atmosphere wore down continental plates as they were rebuilt by geostatic forces. The continental crust was worn down over time by climatic forces such as rain and wind and transported to the sea by the world's streamflow. An average of 2.6 kg $m^{-2}d^{-1}$ of precipitation falls on the ocean annually, while 1.8 kg $m^{-2}d^{-1}$ falls on land. Using the 1,450 Cal $m^{-2}d^{-1}$, which was consumed by evaporation systems, yields 0.6 Cal g^{-1} of rain. That is, 1,000 Cal $m^{-2}d^{-1}$ was used to drive the erosion of land processes. The annual runoff to the sea amounts to 19.3 g $m^{-2}d^{-1}$, which carries 0.15 g $m^{-2}d^{-1}$ of material from the continental plate to form sediment on the ocean crust. Note that the ocean crust was 2.4 times larger than the continental crust; therefore, 0.51 g $m^{-2}d^{-1}$ of continental erosion equals 0.21 g $m^{-2}d^{-1}$ of ocean sedimentation and the 0.51 g $m^{-2}d^{-1}$ loss of the continental crust was offset by geostatic and volcanic uplift of an equal amount. The energy required to lift this material to an average height of 20 km from an average height of 3.5 km was computed to be 0.05 Cal $m^{-2}d^{-1}$. Hayakawa (1976) found geologic uplift to consume 0.025 Cal $m^{-2}d^{-1}$, which was in reasonable agreement with the agreement with the calculation in equation 13.

Because of the relatively rigid nature of the plates of the earth by comparison to the fluid ocean or atmosphere, it was believed that the geological process of floods, glaciers, volcanoes, and earthquakes perform an important role in plate recycling. Floods were modeled as an interaction of the atmosphere process of rain, ocean waves, and the continental plates. The role of floods in the global web was modeled as a prime transporter of material from the continental crust to the ocean crust, thus, accelerating the cycling of the geologic system of the earth.

Flood waters have very high soil-carrying capacity, so that turbulence built up in floods moves very large quantities of land to lower elevations. Assuming that 1 percent of all rain was involved in flooding (yields 1.8 g $m^{-2}d^{-1}$ global average of flood water elevated an average of 1,000 m) results in a gravitational potential energy of 0.04 Cal $m^{-2}d^{-1}$ for floods.

Volcanoes provide an offsetting force in the contribution to continental uplift process. The average global energy flow was estimated by Hayakawa (1976) to be 5×10^{-5} Cal $m^{-2}d^{-1}$. The volcanoes in the model were powered by organic sediments, solar heating, and the interaction of deep heat flowing out of the continental surface. An equally important geological process was the seismic energy release of earthquakes. Richter (1958) estimated the seismic energy global average to be 1×10^{-4} Cal $m^{-2}d^{-1}$. Earthquakes were modeled as the catastrophic release of strain energy built up by the interaction of the ocean and the continental plates driven by the creation of new ocean plates and the convention of the mantle. Earthquakes were fed back to accelerate the erosion process by fracturing continental plate material.

Urban Structure, Fire, Disasters, and War

Figure 24 is an energy circuit submodel of the urban sector of the world system showing the internal disordering effect of depreciation, obsolescence, fire, and war and the external disordering effect of floods, storms, earthquakes, volcanoes, and forest fires. Table 6 documents the energy flows and storages in the model.

The cities of the earth formed the fifth order-disorder system included in the global model. The structure or capital assets of the urban systems, including all structures, machinery, and human assets, were

Figure 24. Urban order-disorder model with depreciation, fire, war, and natural disasters in disorder process. Table 5 documents the evaluation of the flows and storages in the model.

(a) Conceptual model with energy flows Cal $m^{-2}d^{-1}$ and storages in Cal m^{-2}.

(b) Mathematical form of model with differential equations.

$$\dot{Q}_{14}=K_{61}Q_{21}Q_{19}(Q_7+Q_9)Q_{14}Q_{16}-K_{65}Q_{22}Q_{19}-K_{67}Q_{19}Q_{23}-K_{64}Q_{19}$$

$$-K_{65}Q_{19}(Q_{23}+Q_{18}+Q_{10}+Q_6+Q_{20})$$

$$Q_{22}=C_5-K_{53}Q_{14}$$

$$\dot{Q}_{23}=K_{67}Q_{23}-K_{68}Q_{23}-K_{65}Q_{19}Q_{23}.$$

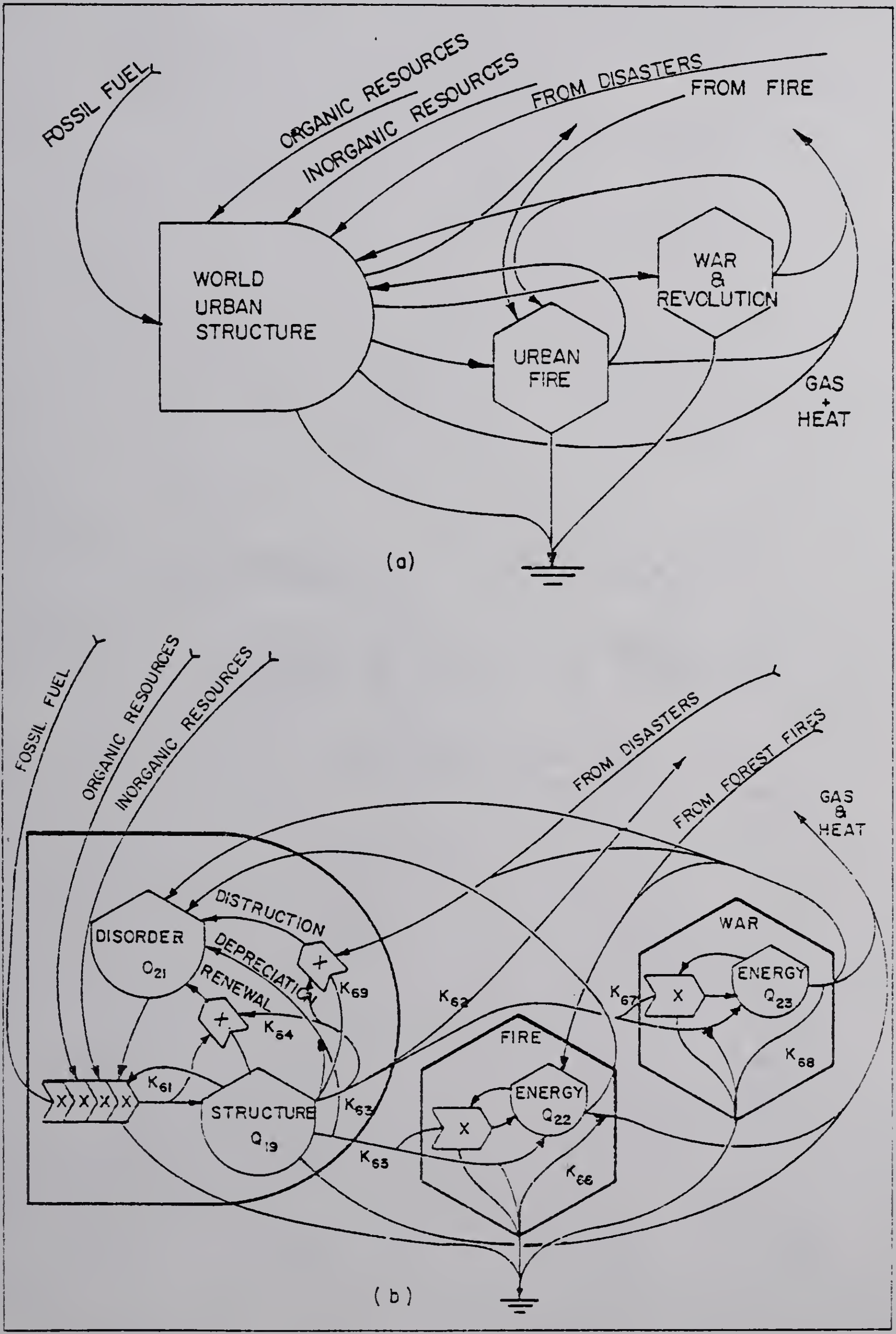
FOSSIL FUEL
ORGANIC RESOURCES
INORGANIC RESOURCES
FROM DISASTERS
FROM FIRE
WORLD URBAN STRUCTURE
WAR & REVOLUTION
URBAN FIRE
GAS + HEAT
(a)
FOSSIL FUEL
ORGANIC RESOURCES
INORGANIC RESOURCES
FROM DISASTERS
FROM FOREST FIRES
GAS & HEAT
DISORDER Q_{21}
DISTRUCTION
DEPRECIATION
RENEWAL
K_{69}
K_{64}
K_{61}
K_{62}
K_{63}
K_{65}
K_{66}
K_{67}
K_{68}
STRUCTURE Q_{19}
FIRE
ENERGY Q_{22}
WAR
ENERGY Q_{23}
X
(b)

TABLE 6. EVALUATION, NAME, AND DESCRIPTION OF ENERGY FLOWS AND STORAGES FOR FLOODS AND CITIES OF FIGURE 24.

Coefficients	Value	Coefficient Name	Descriptive Comment	Note[a]
Q_{19}	1,400 Cal m^{-2}	Energy storage in	Mean energy storages in cities of	1
$K_{61}Q_{14}(Q_7+Q_9)Q_{19}$	0.45 Cal $m^{-2}d^{-1}$	Urban consumption	Energy consumed by cities	2
K_{62} Q_{19}	0.1 g $m^{-2}d^{-1}$	Pollution	Gas returned to atmosphere system	3
K_{63} Q_{19}	0.45 Cal $m^{-2}d^{-1}$	Respiration	Energy dissipated by cities	4
K_{64} Q_{19}	0.31 Cal $m^{-2}d^{-1}$	Depreciation	Depreciation and oblescence of urban structure	5
K_{65} Q_{22} Q_{19}	0.065 Cal $m^{-2}d^{-1}$	Fire loss	Urban energy storage consumed by fire	6
K_{66} Q_{22}	0.065 Cal $m^{-2}d^{-1}$	Fire dissipation	Energy dissipated by fire	7
Q_{23}	0.003 Cal m^{-2}	Fire storage	Energy stored in urban fire	8
K_{67} Q_{19} Q_{23}	0.05 Cal $m^{-2}d^{-1}$	War consumption	Energy consumed by world millions	9
K_{68} Q_{23}	0.05 Cal $m^{-2}d^{-1}$	War dissipation	Energy dissipated by military activity	10
Q_{23}	90 Cal m^{-2}	War assets	Energy stored in war equipment	11
$K_{69}Q_{19}(Q_3+Q_{11}+Q_{18})$	0.006 Cal $m^{-2}d^{-1}$	Disaster loss	Energy loss due to disasters	12

[a] The calculations that document this table are shown in Appendix I.

modeled as order. The disordering forces modeled were depreciation, obsolescence and urban renewal, urban fire, disasters, and war. The combined action of these destructive forces was used to cycle ordered matter in the form of city structure to disorder.

Cities were modeled as a consumer of fossil fuel and biological material. The urban fossil fuel consumption of the world in 1937 was only 0.056 Cal $m^{-2}d^{-1}$ (Oxford Economic Atlas of the World, 1965). By 1974, the world fossil fuel consumption had grown to 0.23 Cal $m^{-2}d^{-1}$ (United Nations Statistical Year Book, 1975, 1976).

The world consumption of biological material by humans was estimated by Whittaker and Likens (1975) to be 0.27 Cal $m^{-2}d^{-1}$, yielding a total chemical energy consumption for man of 0.45 Cal $m^{-2}d^{-1}$. The energy storage in urban structure of the world was calculated from depreciation rates of assets. Solow (1962) showed that incorporating technical obsolescence and physical depreciation gave an average annual loss of approximately 8 percent of capital stocks. Based on an energy consumption of 0.45 Cal $m^{-2}d^{-1}$, a depreciation rate of the capital stock of the world cities was calculated to be 2,000 Cal m^2. By comparison this was 13 percent of the biological standing stock of the globe. The biological material and fossil fuel consumed by the urban sector were primarily carbon and thus vented in the form of gas back to the atmosphere. Urban renewal was modeled as an internal recycle process, which used energy from the production function of the urban sector to recycle structure.

Urban fire was the largest destructive force with an estimated magnitude of four times the total of all other catastrophic losses. Based on fire statistics for the United States, it was estimated that urban fire consumes at least 4 percent of the total productivity and 1 percent

Figure 25. Global energy web model diagramed in energy circuit language. The atmospheric, oceanic, biological, and geologic systems are documented in Tables 2, 3, 4, and 5, respectively, with cities documented in Table 6.

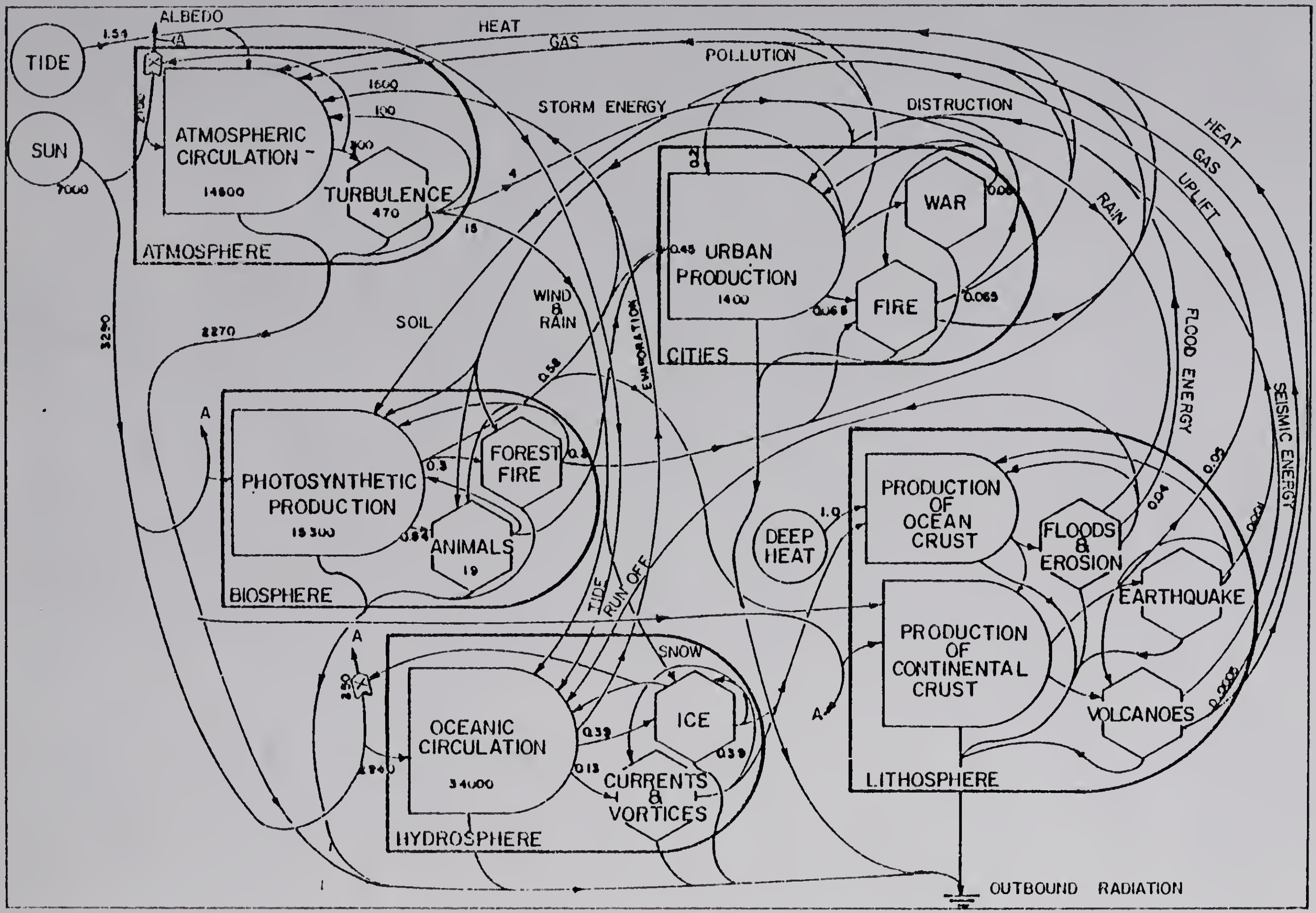
TIDE
SUN
1.54
7000
ALBEDO
A
3290
ATMOSPHERIC CIRCULATION
14600
TURBULENCE
470
1600
100
300
ATMOSPHERE
HEAT
GAS
POLLUTION
STORM ENERGY
DISTRUCTION
4
18
2870
SOIL
WIND & RAIN
EVAPORATION
0.58
URBAN PRODUCTION
1400
0.45
WAR
0.08
FIRE
0.068
0.065
CITIES
HEAT
GAS
UPLIFT
RAIN
FLOOD ENERGY
SEISMIC ENERGY
PHOTOSYNTHETIC PRODUCTION
15300
0.3
FOREST FIRE
0.8
0.82
ANIMALS
19
BIOSPHERE
A
DEEP HEAT
1.9
PRODUCTION OF OCEAN CRUST
FLOODS & EROSION
0.04
0.05
EARTHQUAKE
PRODUCTION OF CONTINENTAL CRUST
VOLCANOES
LITHOSPHERE
A
TIDE
RUN OFF
SNOW
OCEANIC CIRCULATION
34000
ICE
0.33
0.38
0.13
CURRENTS & VORTICES
HYDROSPHERE
OUTBOUND RADIATION

TABLE 7. GLOBAL DISASTER-AMPLIFIER RATIOS FOR CITIES AND NATURAL DISASTERS.

Disaster	Energy Flow in Disaster to Cities	Disorder Energy Flow of City	Disaster-Amplifier Ratio in Heat Calories	Disaster-Amplifier Ratio in Solar Calories	Note[a]
Storms	1.3×10^{-2} Cal $m^{-2}d^{-1}$	2.1×10^{-3} Cal $m^{-2}d^{-1}$	0.16	1.4	1
Floods	1.4×10^{-4} Cal $m^{-2}d^{-1}$	2.1×10^{-3} Cal $m^{-2}d^{-1}$	15	1.3	2
Earthquake	4.5×10^{-6} Cal $m^{-2}d^{-1}$	1.9×10^{-3} Cal $m^{-2}d^{-1}$	539	1.7	3

[a] The calculations that document this table are shown in Appendix I.

of the urban assets. This amounts to a loss of nearly 0.06 Cal $m^{-2}d^{-1}$ for urban systems due to fire.

The second major internal distructive force was revolution and war. War was modeled as the consumption of excess storages in urban systems, which was then fed back to produce disordering of the urban assets. The energy consumption of war and revolution was calculated by taking the ratio of the world military expenditures to the world gross national product. This ratio was multiplied by the world energy consumption to get war consumption. It was found that 0.05 Cal m^{-2} was consumed by war.

The destruction of urban assets by natural disasters, such as storms, floods, and earthquakes, was modeled as a stress on the cities of the world. The total loss due to these natural disasters was found to be 0.006 Cal $m^{-2}d^{-1}$ for urban systems. Global losses from each disaster were estimated and used as a basis for comparison of disaster severity. Order-disorder ratios for each disaster were calculated and are presented in Table 7. Global average energy flows in each disaster are listed along with order-disorder ratios in Calories, heat, equivalent, and Calories solar equivalent.

The Global Energy Web and Energy Quality of Disasters

The energy circuit made of the world in Figure 25 was evaluated to serve as a guide for energy quality calculation in this research. The model was powered by 7,000 Cal $m^{-2}d^{-1}$ of solar energy entering at the left and feeding through the web to the right. In each process, considerable energy was dissipated in the form of waste heat, which when collected produced 7,000 Cal $m^{-2}d^{-1}$ of infrared radiation outbound from the earth.

Energy quality factors for the major energy flow processes of the earth are summarized in Table 8. The energy flow in the process is presented in Cal $m^{-2}d^{-1}$ and the mean energy factor for each process in Calories of solar energy per Calorie of the process. Note that Table 8 is arranged in descending order of energy flow and thus ascending order with respect to energy quality. The energy quality of electromagnetic radiation was calculated by a different method. For infrared radiation the ratio of the average energy per photon was used. This was also equal to the ratio of the average temperature of the energy source. In all energy quality calculations solar energy was used as the reference.

In the sections that follow the quality factors developed based on the energy web of the biosphere were applied to specific case study order-disorder events.

Evaluation and Simulation of the Radiation Stress on a Tropical Rain Forest at El Verde, Puerto Rico

This section contains the results of evaluation and simulation of an order-disorder model of the effect of gamma ray irradiation on a tropical rain forest. Figure 26 is a much aggragated conceptual model of the tropical rain forest at El Verde, Puerto Rico. In the model, solar energy provides the necessary power to develop order in biomass and diversity from soil. Recycling is provided by respiration of plants, animals, and microbes. The structure built by the forest ecosystem was fed back to provide canopy mechanisms for the collection of solar energy. The model was evaluated at 20 m from the irradiation source. At this distance from the center of radiation it was observed that the structural

TABLE 8. ENERGY QUALITY FACTORS FOR GLOBAL PROCESSES AND DISASTERS

Global Process or Disaster	Global Mean Energy Flow Cal m^{-2} d^{-1}	Global Energy Quality Factor Cal Cal^{-1}	Note[a]
Solar energy to earth	7,000	1.0	2-1
Solar energy absorbed by earth	4,900	1.4	2-1
Surface radiation on earth	3,290	2.1	2-4
Evaporation	1,600	4.4	3-6
Weather	100	70	2-15
Wind and rain	15	4×10^2	2-16
Primary production of plants	7.8	9×10^2	4-6
Hurricanes	4	1.7×10^3	2-18
Tide	1.54	4.5×10^3	3-16
Animal respiration	0.65	1.1×10^4	4-9
Cities	0.45	1.5×10^4	6-2
Ice	0.39	2.0×10^4	3-23
Forest Fire	0.3	2.3×10^4	4-10
Waves	0.13	5.4×10^4	3-13
Fossil fuel	0.11	6.4×10^4	5-19
Urban fire	0.065	1.1×10^5	6-8
War	0.05	1.4×10^5	6-9
Uplift	0.05	1.4×10^5	5-14
Floods	0.04	1.7×10^5	5-17
Earthquake	0.001	4.7×10^6	5-16
Volcanoes	0.0005	1.4×10^7	5-22

[a] The calculations that document this table are shown in Appendix I.

Figure 26. Order-disorder model of gamma ray stress on tropical rain forest at El Verde, Puerto Rico. Solar energy, nutrients and biomass interact to produce plant sugar, which is transformed into biomass and structure. Biomass is recycled through litter to microbial and animal consumers. With the supplementary stress generated by the gamma radiation, additional biomass is recycled, the rate of which is a function of the radiation intensity.

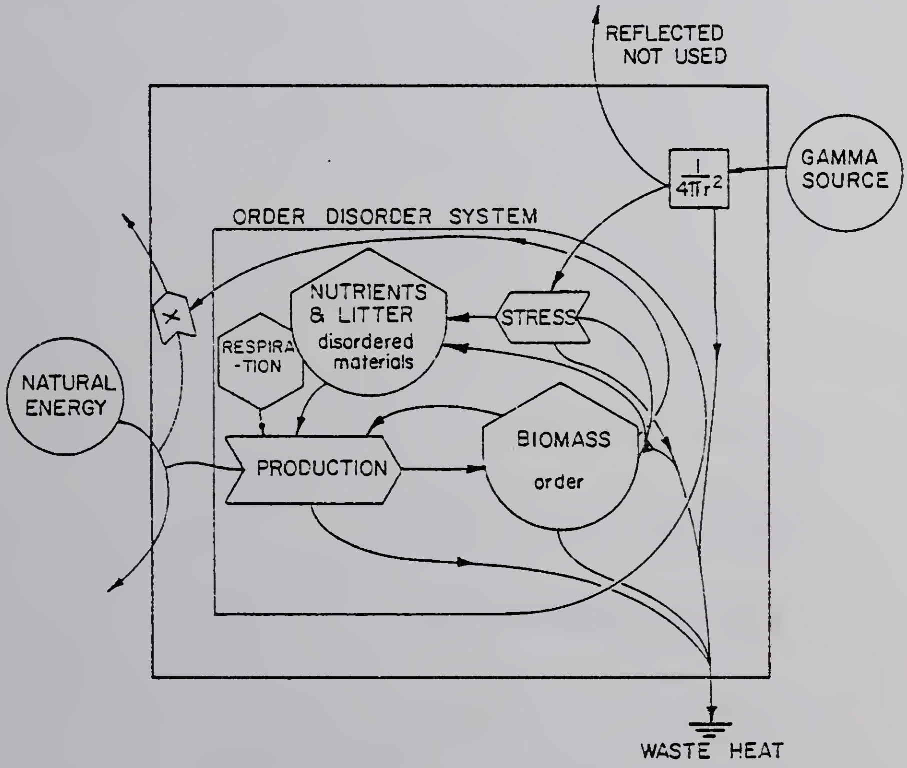
REFLECTED
NOT USED
$\frac{1}{4\pi r^2}$
GAMMA
SOURCE
ORDER DISORDER SYSTEM
NUTRIENTS
& LITTER
disordered
materials
STRESS
RESPIRA
-TION
×
NATURAL
ENERGY
PRODUCTION
BIOMASS
order
WASTE HEAT

loss due to radiation equaled the structure generated by primary production (Odum, 1970c).

Figure 27a is the energy circuit model used for the simulation of the order and disorder cycling process in the rain forest ecosystem. The storages and pathway are labeled with their mathematical coefficients in differential equation form. Figure 27b is the model with the storages and flows evaluated.

Evaluation of the Rain Forest Model

Table 9 summarizes the energy calculations necessary to evaluate the model in Figure 24, while detailed calculations are presented in Appendix I. All calculations were made in Calories to simplify simulation of the model. The solar insulation J was measured at the site to be 3,830 Cal $m^{-2}d^{-1}$ (Odum *et al.*, 1970).

The rain forest in El Verde, Puerto Rico, had a gross primary production of 32 g $m^{-2}d^{-1}$ organic matter, which was equivalent to 145 Cal $m^{-2}d^{-1}$ (Odum, 1970a). The production of organic matter by the photosynthetic process of the rain forest ecosystem was balanced by respiration of the plants, animals, and microbes. The loss due to respiration was equal to gross production at 20 meters (Odum, 1970c). The total standing stock of the biomass Q_1 was found to be 42 kg m^{-2} (Odum, 1970c).

The 10,000 curie cesium 137 source R was found to deliver 744 Cal d^{-1} in gamma rays. To calculate the radiation dose rate received by the forest ecosystem, the source was assumed to be a point source. By considering inverse square loss and radiation absorption by forest vegetation and atmosphere, the exposure rate at 20 m was calculated to

Figure 27. Evaluated order-disorder model of gamma ray radiation stress on tropical rain forest in El Verde, Puerto Rico. Table 9 documents the numerical evaluation of the model.

(a) Energy circuit model with mathematical coefficients and differential equation used in simulation.

(b) Evaluated energy circuit model.

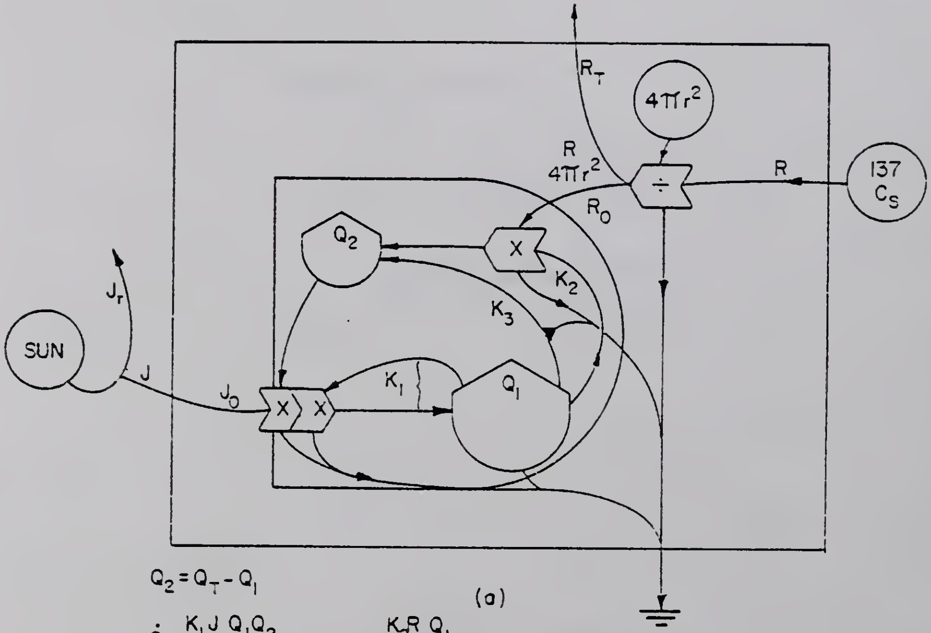

(a)

$$Q_2 = Q_T - Q_1$$

$$\dot{Q}_1 = \frac{K_1 J Q_1 Q_2}{1+K_0 Q_1 Q_2} - \frac{K_2 R Q_1}{(1+K_4 Q_1)\, 4\pi r^2} - K_3 Q_1$$

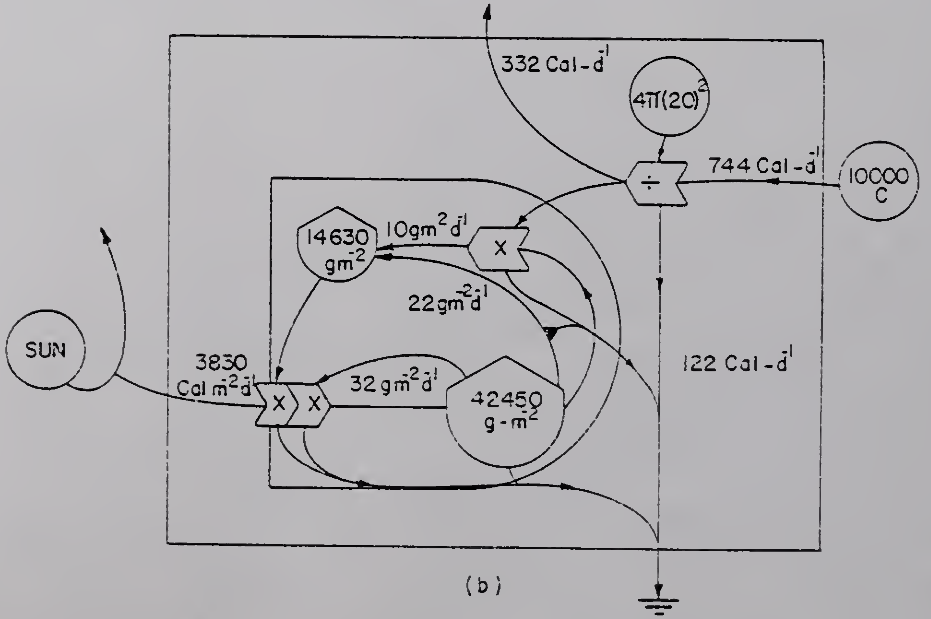

(b)

TABLE 9. GAMMA RADIATION AND SOLAR RADIATION STORAGES AND FLOWS FOR MODEL OF RAIN FOREST IN FIGURE 27.

	Value	Explanation	Note[a]
R	744.5 Cal/d^{-1}	Radiation energy flux from 10,000 Ci Cs 127 source	1
R_r	122.8 Cal/d^{-1}	Energy absorbed by 20 m of forest biomass and air	2
R_o	646.2 Cal/d^{-1}	Energy available at 20 m	3
4 r	$5.02 \times 10^{7}\ \text{cm}^{2}$	Inverse square factor for 20 m.	4
X	1.28×10^{-5} Cal $\text{cm}^{-2}\text{d}^{-1}$	Exposure at 20 m	5
X_t	0.55^{2} Cal $\text{m}^{-2}\text{d}^{-1}$	Total exposure of biomass per m^2 at 20 m	6
D	2.56×10^{-7} Cal $\text{g}^{-1}\text{d}^{-1}$	Absorbed dose per gram (66.2 rad/day) at 20 m	7
D_t	1.1×10^{-2} Cal $\text{m}^{2}\ \text{d}^{-1}$	Absorbed dose per m^2 of rain forest at 20 m	8
J	3,830 Cal $\text{m}^{-2}\ \text{d}^{-1}$	Energy used in photosynthesis (solar insulation)	9
	32 g $\text{m}^{-2}\text{d}^{-1}$	Net primary production of rain forest	10
$\frac{K_1\ J\ Q_1\ Q_2}{1 + K\ Q_1\ Q_2}$	145 Cal $\text{m}^{-2}\text{d}^{-1}$	Energy equivalent of gross primary production	11
Q_1	42,450 g m^{-2}	Biomass of rain forest	12
Q_2	14,630 g m^{-2}	Litter biomass of forest	13
$K_3\ Q_1$	22 g $\text{m}^{-2}\text{d}^{-1}$	Respiration of forest	14
$\frac{K_2\ R\ Q}{(1+K_4 Q_1) 4\pi r^2}$	10 g $\text{m}^{-2}\text{d}^{-1}$	Radiation induced disorder	15

---

[a] The calculations that document this table are shown in Appendix I.

Figure 28. Gamma radiation field and effects on tropical rain forest at El Verde.

(a) Summary of radiation field at close range as determined by dosimeters (Odum and Drewry, 1970).

(b) Graphs of optical-density characteristics for the South Control Center and the Radiation Center (Desmarais and Helmuth, 1970).

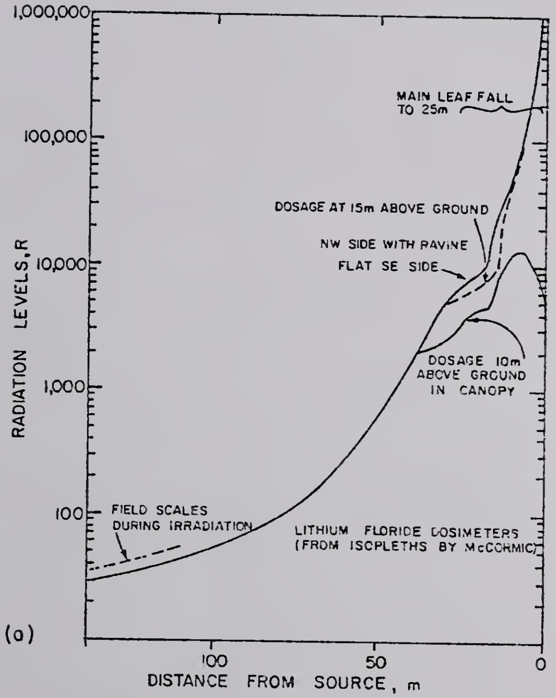
1,000,000
100,000
10,000
1,000
100
RADIATION LEVELS, R
MAIN LEAF FALL TO 25m
DOSAGE AT 15m ABOVE GROUND
NW SIDE WITH RAVINE
FLAT SE SIDE
DOSAGE 10m ABOVE GROUND IN CANOPY
FIELD SCALES DURING IRRADIATION
LITHIUM FLORIDE DOSIMETERS (FROM ISOPLETHS BY McCORMIC)
(a)
100
50
0
DISTANCE FROM SOURCE, m

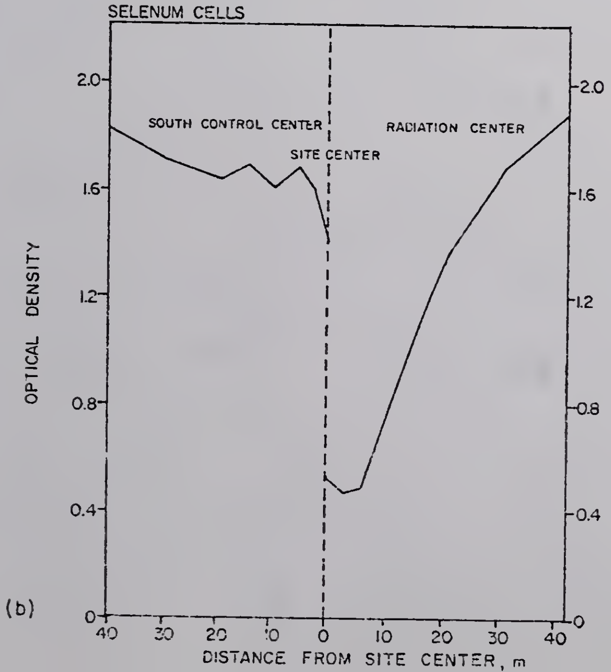
SELENUM CELLS
2.0
1.6
1.2
0.8
0.4
0
OPTICAL DENSITY
SOUTH CONTROL CENTER
SITE CENTER
RADIATION CENTER
(b)
40
30
20
10
0
10
20
30
40
DISTANCE FROM SITE CENTER, m

Figure 29. Results of simulation of order-disorder gamma ray model in Figure 27.

(a) Plot of order (biomass) Q_1 and disorder (litter) Q_2 in kilograms per meter squared versus time after radiation source is continuously activated in days for distance of 1, 2.5, 5, 10, 20, 30, and 50 m from the source.

(b) Plot of order (biomass) in kilograms per meter squared versus distance from the source after 93 days.

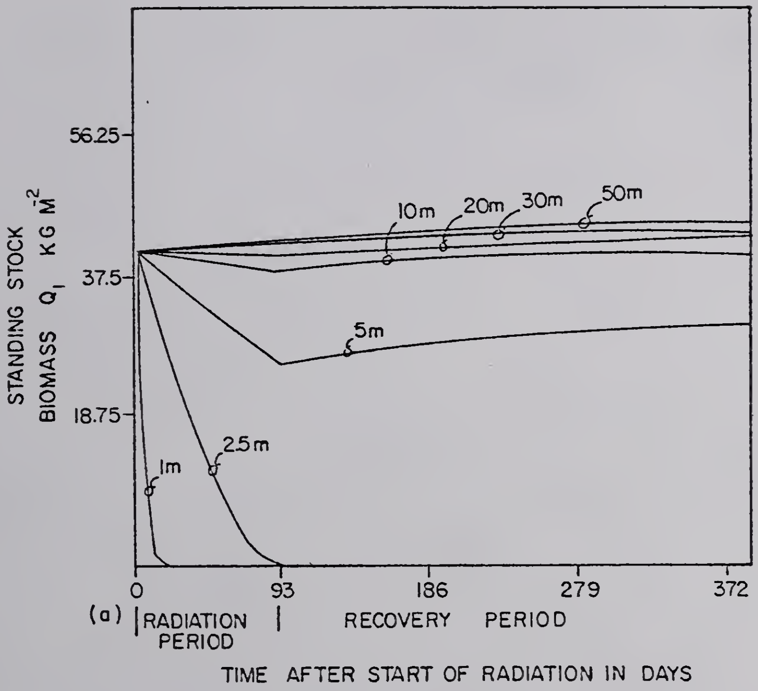
STANDING STOCK
BIOMASS Q_1 KG M^{-2}
56.25
37.5
18.75
10m
20m
30m
50m
5m
2.5m
1m
0
93
186
279
372
(a)
RADIATION PERIOD
RECOVERY PERIOD
TIME AFTER START OF RADIATION IN DAYS

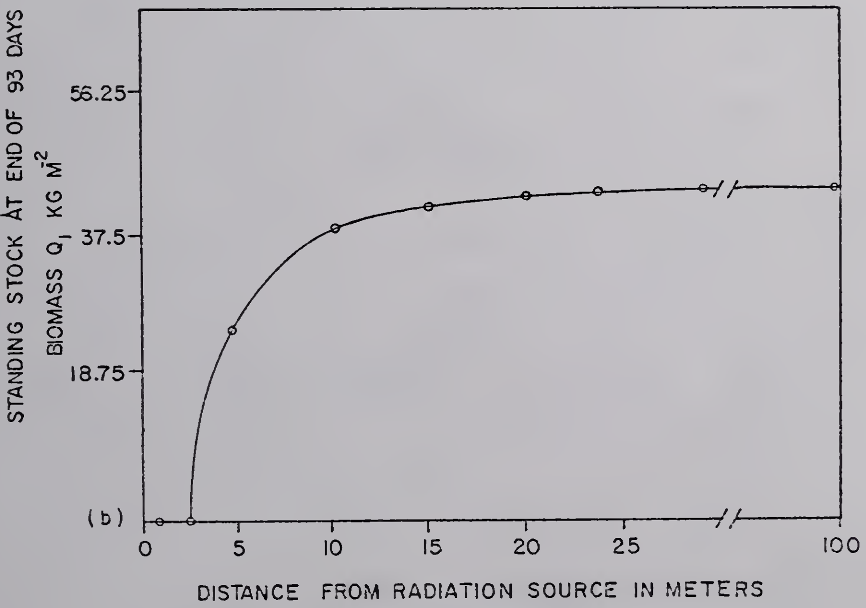
STANDING STOCK AT END OF 93 DAYS
BIOMASS Q_1 KG M^{-2}
56.25
37.5
18.75
(b)
0
5
10
15
20
25
100
DISTANCE FROM RADIATION SOURCE IN METERS

be 1.28×10^{-5} Cal $cm^{-2}d^{-1}$, which was also verified by comparison to field measurement. See Figure 28 from Odum and Drewry (1970). The absorbed dose at 20 m was calculated to be 2.5×10^{7} Cal g $m^{-2}d^{-1}$ based on a measured forest biomass of 42,450 g m^{-2} (Odum, 1970c).

Simulation of the Order-Disorder Process in the Rain Forest Ecosytem

Figure 29 demonstrates the result of the tropical rain forest order-disorder model simulation covering the 93-day radiation experiment at radius of 1, 5, 10, 20, 30, and 50 m from the source. At the end of the period of irradiation, the radiation source was turned off to let the system rebuild. Note that in the simulation results at 20 m, the growth of the forest was just offset by the radiation stress.

Figure 29b presents the simulated radiation dose and the disordering effect of the irradiation with distance. Biomass, as measured by optical density of the rain forest standing stock Q_1, is plotted in Figure 28b and compared with measurements of radiation dose (Figure 28a). Note the similarity between the measured and simulated biomass standing stock.

Calculation of Order-Disorder Energy Ratios for the Rain Forest

A previous calculation of the order-disorder ratio for the tropical rain forest system at El Verde was performed by Odum (1970c) comparing the dose rate to photosynthetic energy. Odum found 1 Cal of gamma energy was required to disorder what 10,000 Cal of photosynthetic energy could order. The order-disorder ratio for the tropical rain forest was also calculated from the evaluation of the model in Figure 27. The gross primary production of 137 Cal $m^{-2}d^{-1}$ was divided by the absorbed dose of 1.1×10^{-2} Cal $m^{-2}d^{-1}$. This yields an order-disorder ratio of 13,000 Cal of production per Cal of radiation.

The disaster-amplifier ratio was calculated by dividing the total loss of biomass due to the irradiation by the total absorbed dose over the 93-day exposure. At 20 m from the source 10 g $m^{-2}d^{-1}$ was disordered by the radiation. This amounts to a total loss of 3.9 x 10^3 Cal m^{-2} over the period of exposure. The total absorbed dose was 1 Cal m^{-2}. This yields a disaster-amplifier ratio of 3.9 x 10^3 Cal of biomass per Cal of radiation.

For compairson with other systems, ratios were also calculated in solar equivalents. The embodied solar energy in biomass was calculated from the quality factor for gross primary production in Table 8. Two methods were used to estimate a range of quality factors for gamma radiation.

The first method is based on the ratio of blackbody equivalent temperature of the cesium gamma source to the blackbody temperature of the sun. From Weins law the blackbody temperature of 6.6 x 10^5 ev gamma rays is 1.5 x 10^9°K. The blackbody temperature of the sun is 6,000°K (Gates, 1962). This gives a low estimate of the energy quality of the gamma radiation of 2.5 x 10^5 Cal solar per Cal radiation.

The second estimation is based on the ratio of the energy required to produce the 10,000 Ci cesium source to the 744 Cal d^{-1} of radiation produced by the source. The cesium source cost $25,000 in 1965 (Odum, 1970a). Using the ratio of 2.5 x 10^4 Cal coal equivalent per dollar (Odum and Odum, 1976) and a quality factor for Cal of 6.4 x 10^4 Cal solar per Cal coal from Table 8, yields a total of 4 x 10^{13} Cal solar energy required to produce the 10,000 Ci radiation source. The half life of cesium 137 is 30 yr (Gloyna and Ledbetter, 1969). Starting from 744 Cal d^{-1} a total of 8.1 x 10^6 Cal of radiation emitted over the life of the source. This results in a high estimate of the energy quality of the gamma radiation of 5 x 10^6 Cal solar per Cal gamma radiation.

With a low estimate of 2.5 x 10^5 Cal per Cal and a high estimate of 5 x 10^6 Cal per Cal an intermediate quality factor of 1 x 10^6 Cal solar per Cal gamma radiation was used. Applying the intermediate quality factor to the absorbed dose at 20 m gives an absorbed dose rate of 1 x 10^{-2} Cal solar $m^{-2}d^{-1}$ and a total dose of 9.3 x 10^5 for the 93 d exposure. Solar energy embodied in the gross primary production was calculated by multiplying the 137 Cal $m^{-2}d^{-1}$ production by the primary production quality factor in Table 8, yielding 1.23 x 10^5 solar Cal $m^{-2}d^{-1}$. This gives an order-disorder ratio of 12 solar Cal production per solar Cal of radiation. The disaster-amplifier ratio was also calculated in solar equivalents. The total loss of biomass was 3.5 x 10^6 solar Cal m^{-2} due to a total absorbed dose of 9.3 x 10^5 solar Cal. The disaster-amplifier ratio was thus 4 solar Cal biomass per solar equivalent Cal of radiation.

Evaluation and Simulation of the Johnstown Flood of 1889

Figure 30 is an energy circuit model of the failure of the South Fork Dam and the destruction of Johnstown, Pennsylvania, in 1889. The flow of water into the reservoir was modeled as the interaction of the land in the South Fork basin and the rain. The model was designed so that when the water in the spillway exceeded capacity the overflow was fed back to rupture the dam. The flood wave grew exponentially until the source of energy, the reservoir, was exhausted, generating an energy pulse. The pulse was transmitted down the Conemaugh Valley in

Figure 30. Energy circuit model of Johnstown, Pennsylvania, 1889, and the disruption generated by the catastrophic failure of the South Fork Dam. Table 11 documents the evaluation of the Johnstown.

$$\dot{Q}_1 - K_1 J Q_2 - K_3 Q_1 - K_4 Q_1 - K_3 Q_1 Q_3$$

$$\dot{Q}_3 = K_3 Q_1 + K_5 Q_1 Q_3 - K_6 Q_3 - K_7 Q_3 Q_4$$

$$Q_2 = Q_T - K_7 Q_1$$

$$\dot{Q}_4 = (K_{14} - K_{13}) Q_4 Q_5 Q_6 Q_7 - K_{10} Q_6$$

$$Q_5 = C - K_{11} Q_4$$

$$\dot{Q}_6 = K_8 R - K_9 Q_4 Q_5 Q_6 Q_7 - K_{10} Q_6$$

$$\dot{Q}_7 = -K_{12} Q_4 Q_5 Q_6 Q_7$$

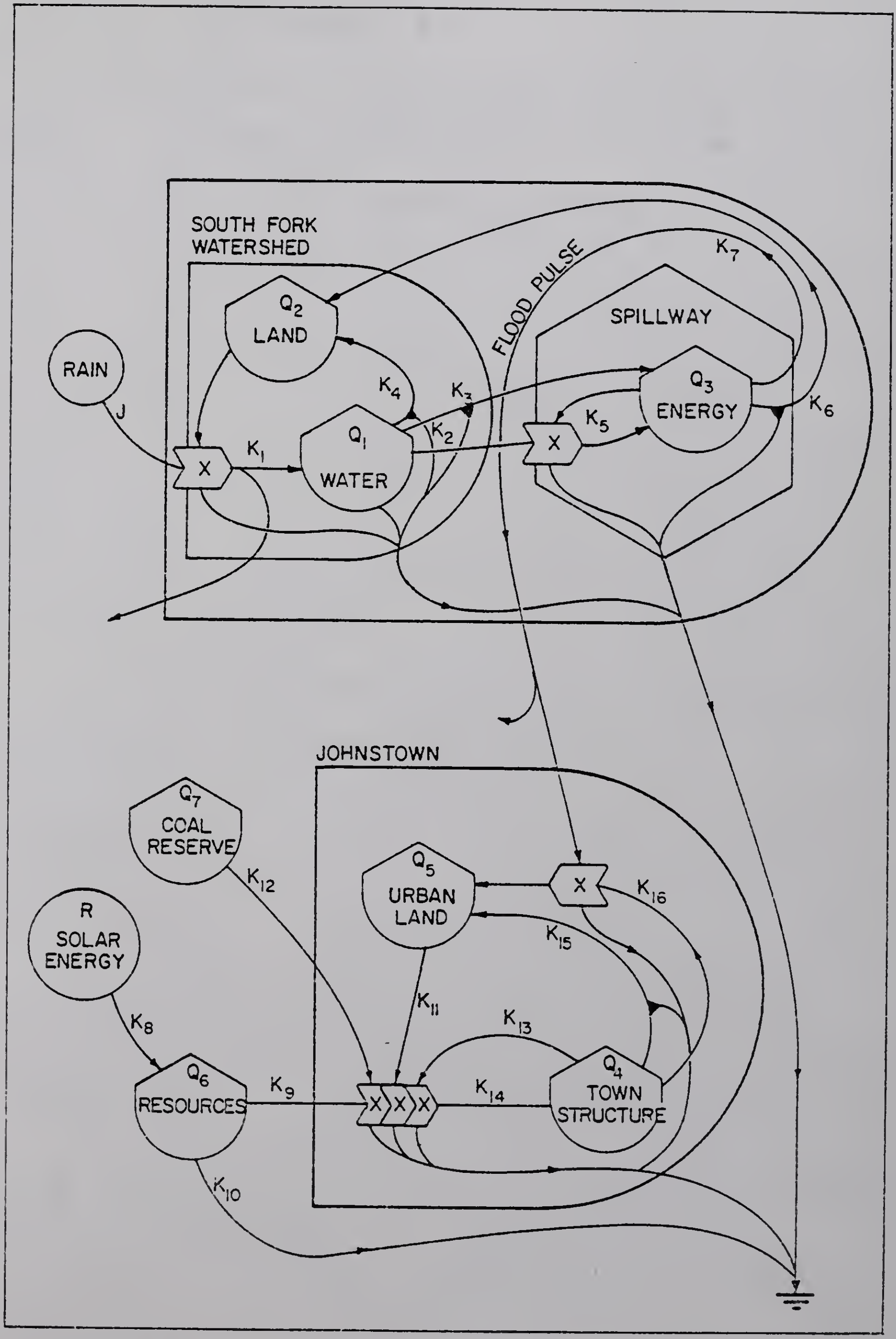
SOUTH FORK WATERSHED
FLOOD PULSE
K_7
SPILLWAY
Q_2
LAND
RAIN
Q_3
ENERGY
K_4
K_3
K_6
J
K_2
K_5
K_1
Q_1
X
X
WATER
JOHNSTOWN
Q_7
COAL RESERVE
Q_5
URBAN LAND
K_{12}
X
K_{16}
R
SOLAR ENERGY
K_{15}
K_{11}
K_8
K_{13}
Q_6
RESOURCES
K_9
X
X
X
K_{14}
Q_4
TOWN STRUCTURE
K_{10}

the form of a flood wave. The destruction of Johnstown was performed by using the pulse energy to disorder the town.

Evaluation of the Model

Table 10 documents the evaluation of the model Johnstown flood of 1889. To analyze and model the disruption and disorder created by the great flood, it was necessary to estimate the energy released. The flood was modeled as the interaction of the geologic processes of the earth and the hydrological system of the atmosphere that produces storms.

The South Fork reservoir Q drained $1.5 \times 10^8 m^2$. Not all of the $4 \times 10^{-6} m^3 sec^{-1}$ rainfall J was observed flowing into the reservoir in the form of runoff. Based on an observed rate of rise in the reservoir of $7 \times 10^{-5} m\ sec^{-1}$ (Engineering Society of Western Pennsylvania, 1889) and a reservoir surface area $1.69 \times 10^6 m^2$, a net increase of 118 m^3 sec^{-1} of water was stored in the South Fork reservoir. In addition, the spillway of the South Fork Dam K_6Q_3 was designed to release 99 m^3 sec^{-1} (Engineering Society of Western Pennsylvania, 1898). However, Shappee (1940) estimated the peak capacity to be 169 $m^3 sec^{-1}$. Combining the net increase in storage with the spillway loss yields a total inflow of 368 $m^3 sec^{-1}$, or approximately 58 percent of the rainfall.

The potential energy stored in a cubic meter of water in the South Fork reservoir calculated by equation 35.

$$E = 2.3 \times 10^{-4}\ mgh\ Cal\ m^{-3}, \qquad (35)$$

where m = mass of one m^3

h = elevation of South Fork reservoir with respect to Johnstown

g = acceleration of gravity

TABLE 10. EVALUATION, NAME, AND DESCRIPTION OF ENERGY FLOWS AND STORAGES FOR JOHNSTOWN FLOOD MODEL

Coefficients	Value	Coefficient Name	Discriptive Comment	Note[a]
J	4.1×10^{-6} m sec^{-1}	Rain	Rainfall rate during storm, 12 hr	1
$K_1 J Q_2$	368 m^3 sec^{-1}	Runoff	Water flow from South Fork Valley	2
$K_2 Q_1$	168 m^3 sec^{-1}	Overflow	Spillway overflow, max	3
$K_3 Q_1 Q_3$	133 m^3 sec^{-1}	Turbulence	Overflow at start of dam break	4
$K_4 Q_1$	34 m^3 sec^{-1}	Feedback	Turbulence from overflow	5
$K_6 Q_3$	99 m^3 sec^{-1}	Spillway flow	Water out of spillway, designed	6
Q_1	1.36×10^7 m^3	Reservoir	Designed capacity of reservoir	7
Q_3	1,690 m^3	Spillway capacity	Designed capacity of spillway	8
Q_2	1.55×10^8 m^2	Land	Land area of South Fork Valley	9
k_8	1/18.9 m	Slope	Reciprocal of depth of reservoir	10
Q_4	1.8×10^{12} Cal	Tangible assets	Total tangable assets of Johnston, 1889	11
Q_5	1.1×10^6 m^2	Land	Land area of Johnstown, 1889	12

---

[a] The calculations that document this table are shown in Appendix I.

TABLE 10. CONTINUED

Coefficient	Value	Coefficient Name	Descriptive Comment	Note[a]
Q_6	2.5×10^{13} Cal	Resources	Renewable natural resources, lumber and food	13
Q_7	3×10^{15} Cal	Coal reserve	Estimated Johnstown Coal Reserve	14
K_8R	2.8×10^{9} Cal d^{-1}	Renewable resource	Renewable resource production in Johnstown Valley	15
$K_9Q_4Q_5Q_6Q_7$	3.8×10^{8} Cal d^{-1}	Resource consumption	Use of renewable resources	16
$K_{10}Q_6$	2.4×10^{8} Cal d^{-1}	Respiration of natural system	Energy loss due to operation of natural system	17
$K_{11}Q_4Q_5Q_6Q_7$	3×10^{-7} m Cal^{-1}	Land consumption	Use of land by urban system	18
$K_{12}Q_4Q_5Q_6Q_7$	1×10^{9} Cal d^{-1}	Coal consumption	Consumption of fossil fuel	19
$K_{14}Q_4Q_5Q_6Q_7$	1.4×10^{9} Cal d^{-1}	Gross regional production	Total production of Johnstown	20
$K_{14}-K_{13}Q_4Q_5Q_6Q_7$	1.2×10^{9} Cal d^{-1}	Net regional production	Net production of Johnstown	21
$K_{15}Q_4$	8.9×10^{8} Cal d^{-1}	Depreciation and consumption	Average depreciation of Johnstown	22
$K_{16}Q_4Q_3$	1.65×10^{12} Cal	Catastrophic depreciation	Loss due to flood of 1889	23
Q_1	8×10^{10} Cal	Potential energy	Energy stored in reservoir	24
$K_7Q_3Q_4$	1.7×10^{9} Cal	Wave energy	Kinetic energy of flood	25

the gravitation potential energy was found to be 6.94×10^3 Cal m^{-3}.

The total energy consumption for Johnstown was estimated to be 1.4×10^9 Cal d^{-1}, of which 71 percent was coal and the remaining 29 percent was mainly lumber, firewood, and food. The net production of the city was 1.2×10^9 Cal d^{-1}, which was used to offset depreciation and consumption of 1.8×10^8 Cal d^{-1}. The remaining 4×10^7 Cal d^{-1} was consumed by the growth of the city. This would be an annual growth rate of 6 percent which was supported by the rapid industrial expansion of Johnstown between 1880 and 1889 reported in Engineering News (1889a). The tangible assets for Johnstown Q_4 were estimates based on the Historical Statistics of the United States (1975) and found to have an energy storage of 1.8×10^{12} Cal. This was approximately four times the annual energy consumption.

The failure of the South Fork Dam produced a wave that took 56 min to travel the 5.57×10^4m to Johnstown at an average speed of 7.66 m sec^{-1}. As the wall of water moved down the Conemaugh Valley, the water from the torrential rain lubricated the wave; however, the top of the water moved faster because of lower friction, creating a ball of water and debris which rolled down the valley. When the wave hit Johnstown, the height was observed to be 10 m. However, it was as high as 30 m in a narrow gorge. The kinetic energy of the 10 m wave which hit Johnstown traveling at a velocity of 7.66 m sec^{-1} was made up of two components. First, the linear motion term described by equation 36.

$$e_L = \frac{1}{2} mV^2 = 123 \text{ Cal } m^{-3}, \qquad (36)$$

which yields 123 Cal m^{-3} of kinetic energy. However, the turbulence generated by the rolling action of the wave also contained considerable kinetic energy as given in equation 37 (Kinsman, 1965).

$$E_t = 0.3\ H^2\ \mathrm{Cal}\ m^{-2} \qquad (37)$$

where H is the height of the wave in meters based on the observed 10 m wave height the turbulence was 32.3 Cal m^{-2}.

To calculate the kinetic energy of the flood wave the linear energy of 123 Cal m^{-3} was multiplied by the volume of water in the flood, $1.36 \times 10^7 m^3$ (Engineering News, 1889b), yielding a total linear kinetic energy release of 1.67×10^9 Cal. The total turbulent kinetic energy release was calculated by multiplying the area of flood wave $1.36 \times 10^6 m^2$ by the turbulent energy 32.3 Cal m^{-2}, which gave 4.4×10^7 Cal. Thus a total kinetic energy of 1.7×10^9 Cal was released in the flood. The kinetic energy $K_7Q_3Q_4$ of the flood was, therefore, 1.8 percent of the potential energy stored in the reservoir. Application of the energy quality factor for floods of 1.7×10^5 solar Cal per Cal yields 3×10^{14} Cal of solar energy embodied in the flood.

Simulation of the South Fork Dam Failure and the Destruction of Johnstown

Figure 31a is the results of the simulation of the dam failure with time. The total storage in the South Fork reservoir, the kinetic energy in the form of turbulence, and the rate of overflow over the dam or through the dam are plotted as a function of time. Note that once a critical overflow was reached, the growth of the kinetic energy in the dam failure wave was only limited by the quantity of water remaining in the reservoir to power the wave.

Figure 31. Simulation results of Johnstown flood of 1889 in Figure 30.

(a) Results of dam failure.

(b) Results of distruction of Johnstown.

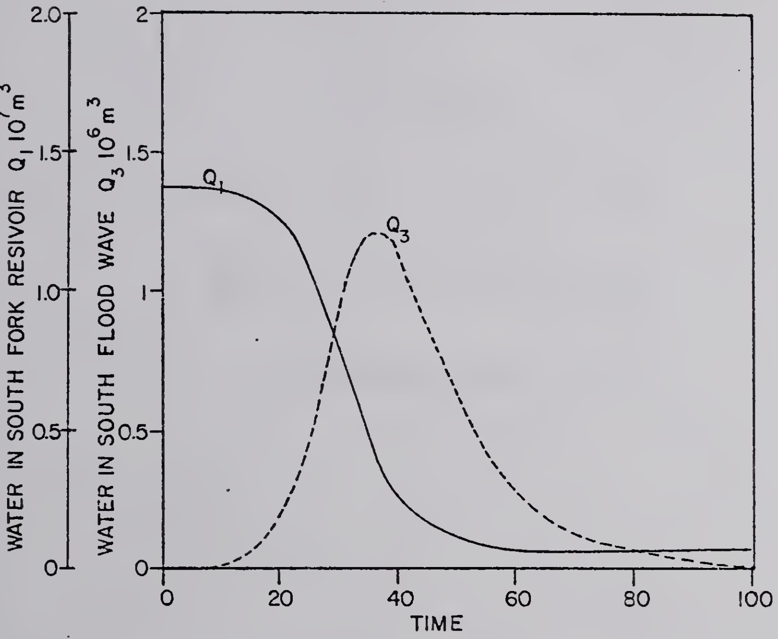
WATER IN SOUTH FORK RESIVOIR Q_1 $10^7 m^3$
WATER IN SOUTH FLOOD WAVE Q_3 $10^6 m^3$
2.0
1.5
1.0
0.5
0
2
1.5
1
0.5
0
Q_1
Q_3
0
20
40
60
80
100
TIME

(a)

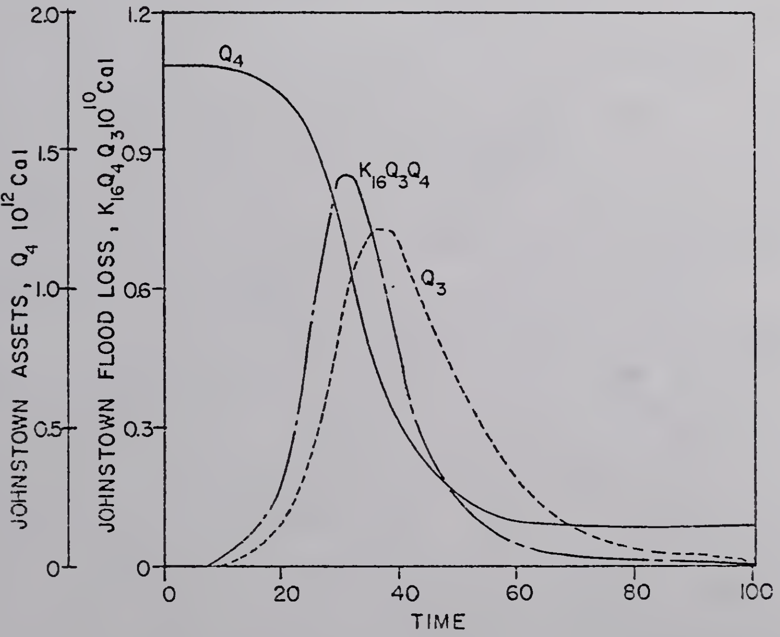
JOHNSTOWN ASSETS, Q_4 10^{12} Cal
JOHNSTOWN FLOOD LOSS, $K_{16}Q_4Q_3$ 10^{10} Cal
2.0
1.5
1.0
0.5
0
1.2
0.9
0.6
0.3
0
Q_4
$K_{16}Q_3Q_4$
Q_3
0
20
40
60
80
100
TIME

(b)

Figure 31b presents the results of simulation of the catastrophic destruction of Johnstown, Pennsylvania. The results of the simulation approximate qualitative descriptions of the event. Coefficients were calculated from the flow and storage evaluation in Table 10.

Disaster-Amplifier Ratios for Johnstown and the Flood

The ratio of the energy loss in the disaster to the energy in the flood was calculated in Calories heat equivalent and calories solar equivalent. The energy delivered to Johnstown by the flood was found to be 1.7 x 10^9 Cal. The total catastrophic depreciation undammage $K_{46}Q_4Q_3$ was 1.65 x 10^{12} Cal. Dividing the total destruction by the energy required to produce the disorder gave a disaster-amplifier ratio at 970 Cal of destruction to 1 Cal of flood energy.

For comparison purposes the disaster-amplifier factor was recalculated with both energy flows in solar equivalents. Energy quality factors for floods and cities were taken from Table 8. The embodied energy in the flood was 2.9 x 10^{14} solar Cal while the energy embodied in the loss of city structure was 2.4 x 10^{16} solar Cal. The disaster-amplifier ratio was thus 85 solar Cal of city per solar Cal of flood energy.

Evaluation and Simulation of the Guatemala Earthquake of 1976

Figure 32 is an energy diagram of the Guatemala earthquake and the destruction of El Progreso. The interaction of the North American Plate with the Caribbean Plate converges stress energy into the Motagua Fault system. When a threshhold is reached, excess energy is released in the form of an earthquake pulse. The seismic pulse is transmitted through the crust of the earth and coupled to secondary systems. The destruction

Figure 32. Earthquake order-disorder model for Guatemala earthquake. See Table 11 for energy flow and storage explanations.

$$\dot{Q}_1 = \frac{K_1 J\ Q_2}{K_0 Q_2 + 1} - K_3 Q_1 Q_3 - K_2 Q_1$$

$$Q_2 = C_e - K_{15} Q_2$$

$$\dot{Q}_3 = K_4 Q_1 Q_3 + K_7 Q_1 - K_6 Q_3 - K_0 Q_3 Q_4$$

$$\dot{Q}_4 = K_9 E\ Q_4 Q_5 - K_{10} Q_3 Q_4 - K_{11} Q_4$$

$$Q_5 = C_t - K_{13} Q_4$$

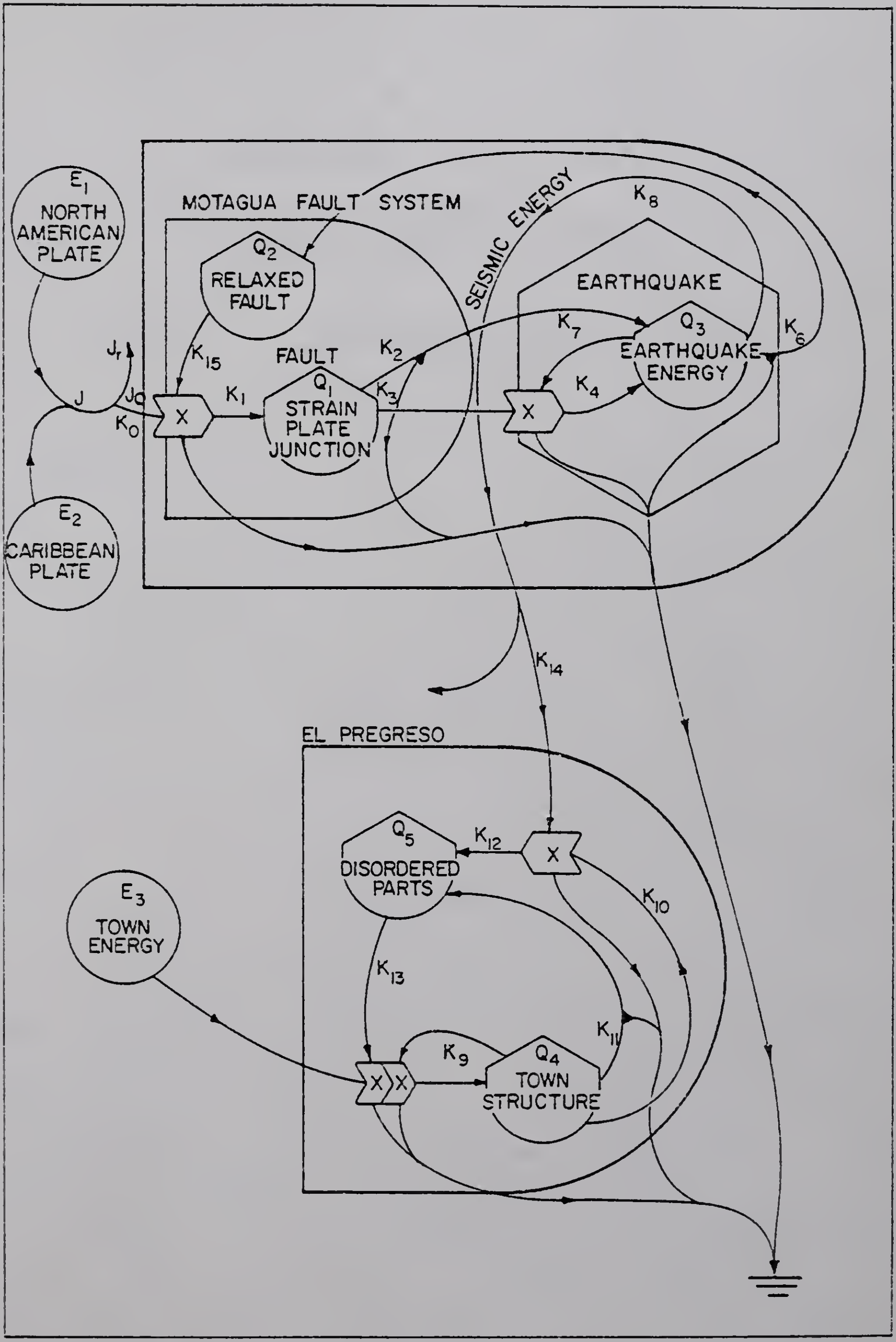
E_1
NORTH AMERICAN PLATE
E_2
CARIBBEAN PLATE
MOTAGUA FAULT SYSTEM
Q_2
RELAXED FAULT
FAULT
Q_1
STRAIN PLATE JUNCTION
SEISMIC ENERGY
EARTHQUAKE
Q_3
EARTHQUAKE ENERGY
J
J_r
J_O
K_0
K_1
K_2
K_3
K_4
K_6
K_7
K_8
K_{15}
X
K_{14}
EL PREGRESO
Q_5
DISORDERED PARTS
K_{12}
K_{10}
K_{13}
K_{11}
K_9
Q_4
TOWN STRUCTURE
E_3
TOWN ENERGY

of El Progreso is performed by disordering the structure of the town. The earthquake energy pulse provides the energy for the recycling process.

Evaluation of the Model

Results of evaluating the model are given in Table 11. The stress was a buildup of the Motagua Fault system as the North American Plate E_1 moved west at a rate from 2.1 to 2.2 cm yr^{-1} relative to the stationary Caribbean Plate (Jordan, 1975; Plafker, 1976). The total change in strain energy during the earthquake was estimated by multiplying the strain release per unit volume by the volume of fault relaxed. The United States Geological Survey found this to be a low stress drop event with between 3 and 18 bars of strain relieved by the rupture around the fault. The fault break was 240 km long, 7 km deep, and a slip of 3 m wide (Espinosa et al., 1976). This yields an estimated active fault volume Q_2 of 4.83×10^{16} cm^3. Releasing 3 bars of strain over the whole volume produced a spontaneous release of 3.1×10^{12} Cal during the earthquake. The result of this calculation was in good agreement with the 2.62×10^{12} Cal reported (Espinosa et al., 1976).

The change in strain energy, Q_1, was accounted for either by released seismic energy, E_s, and by work done, W, by sliding on the fault as shown in equation 37 (Dieterich, 1974):

$$Q_1 = E_s + W \qquad (37)$$

Many authors report methods for relating the seismic energy release, in ergs, to the magnitude of the quake on the Richter scale M. The recommended form is given in equation 38 (Gutenberg and Richter, 1969):

$$\log E_s = 9.4 + 2.14M - 0.054M^2 \qquad (38)$$

TABLE 11. EVALUATION, NAME, AND DESCRIPTION OF ENERGY FLOWS AND STORAGES FOR EARTHQUAKE MODEL IN FIGURE 32.

Coefficients	Value	Coefficient Names	Descriptive Comments	Note[a]
Q_1 (Max)	2.62×10^{12} Cal	Strain energy storage	Total strain energy stored in fault	1
Q_2 (Max)	4.83×10^{16} cm^3	Fault volume	Total volume of rock to be strained	2
T_1	2.62×10^{12} Cal	Threshold	Maximum value for Q_1 before earthquake	3
E_1	6.72×10^{-8} cm sec^{-1}	Strain energy source	Westernly motion of North American	4
E_2	0	Strain energy source	Stationary position of Caribbean	5
$\frac{K_1 J Q_2}{1 + K_0 Q_2}$	2.15×10^3 Cal sec^{-1}	Strain energy source	Annual buildup of strain in fault	6
$K_2 Q_1$	1.76×10^3 Cal sec^{-1}	Depreciation	Annual loss of strain energy in mini quakes	7
$K_3 Q_1 Q_3$ (Max)	5.43×10^{11} Cal	Main event	Total earthquake energy release	8
$K_8 Q_3$ (Max)	9.06×10^9 Cal sec^{-1}	Output	Seismic energy transmitted	9
(Max)	3.45×10^9 Cal sec^{-1}	Work	Energy lost in plate motion	10
K_{14}	7.61×10^6 cm sec^{-1}	Material strained	Quantity of material strained per year by plate motion	11
Q_3 (Max)	5.44×10^{11}	Monetary storage	Storage of kinetic energy in wave motion of earth	12

---

[a] The calculations that document this table are shown in Appendix I.

TABLE 11. CONTINUED

Coefficients	Value	Coefficient Names	Descriptive Comments	Note[a]
Q_4	2.14×10^5 Cal	Structure	Storage of gravitational potential motion of earth	13
Q_5	8.4×10^6 kg	Disorder	Total mass of houses in El Progreso when disordered	14
$K_{14}Q_3Q_4$	1.95×10^4 Cal sec^{-1}	Shock energy	Total earthquake energy transmitted to El Progreso structures and land (Table 2)	15
$K_{14}Q_3Q_4$	0.7 Cal sec^{-1}	Energy dissipated by structure	Geologic path of coupling of earthquake shock wave to structures	16
K_6Q_3	9.06×10^9 Cal sec^{-1}	Depreciation	Decay of kinetic energy stored in earth crust	17
$K_9E\ Q_4Q_5$	7.29×10^{-4} Cal sec^{-1}	Energy flow	Energy used in construction on maintenance structures in El Progreso	18
$K_{10}Q_3Q_4$	2.83×10^3 Cal sec^{-1}	Damage	Energy lost in El Progreso during earthquake	19
$K_{11}Q_4$	7.61×10^{-4} Cal sec^{-1}	Depreciation	Natural decay of urban structures of El Progreso	20
$K_{12}Q_3Q_4$ (Max)	9.66×10^4 kg sec^{-1}	Flow of disorder	Flow of material in earthquake	21
K_{13}	1.94×10^2 kg sec^{-1}	Material flow	Use of disordered material in construction	22

This gives a seismic energy release of 2.28 x 10^{22} ergs (5.44 x 10^{11} Cal) for the M = 7.5 earthquake under study (Espinosa et al., 1976). From equation 37, it was found that 75 percent of the energy released in the Guatemala earthquake was dissipated in moving the fault, while the other 25 percent was released as seismic energy.

The 2.2 cm yr^{-1} westward velocity of the North American Plate relative to the Caribbean Plate for 203 years yields a total offset of 446.6 cm. However, a maximum offset of 340 cm was observed with an average displacement of 108 cm (Plafker, 1976). Comparison of the average stress buildup motion to the average displacement gives an efficiency of 24.1 percent. The loss of the stress not accounted for in the earthquake was accounted for by many minor slips over the past several centuries. Harlow (1976) was able to show that over 100 of the mini-earthquakes occurring the year before the major event resulted from minor slips in the Motagua Fault(K_2Q_1).

Assuming that the mean of the mini-earthquake released 5.37 x 10^8 Cal of strain energy explained the difference between the calculated 446 cm and the observed 108 cm. The average mini-quake magnitude would be a little greater than four on the Richter scale. This magnitude is in agreement with reported shocks (Harlow, 1976). To build up the necessary storage of 2.62 x 10^{12} Cal to supply the earthquake in 207 years, 1.26 x 10^{10} Cal of energy is required to offset the depreciation due to losses in the fault resulting from minor slips. Therefore, a total of 6.6 x 10^{10} Cal yr^{-1} was delivered by the 2.1 cm yr^{-1} plate motion.

Table 12 summarizes the numeric calculation necessary to relate the known earthquake intensity to the distribution of siesmic energy

TABLE 12. ENERGY ABSORBED PER SQUARE METER OF ADOBE HOUSE BY ISOSEISMAL INTENSITY ZONES FOR GUATEMALA EARTHQUAKE OF FEBRUARY 4, 1976.

C1 I Modified Mercalli Intensity	C2 A Affected Land Area m^{-2}	C3 a· Acceleration m sec^{-2}	C4 a^2 Acceleration Squared	C5 Aa^2	C6 E_s Allocated energy ergs	C7 e Energy Dissipated ergs m^{-2}	C8 e Energy Dissipated Cal m^2	C9 e_n Energy Absorbed houses Cal m^{-2}
V	$6.04\text{x}10^{10}$	.14	.022	$1.32\text{x}10^9$	$2.44\text{x}10^{21}$	$4.04\text{x}10^{10}$	.9	$2.8\text{x}10^{-5}$
VI	$2.62\text{x}10^{10}$	.32	.1	$2.62\text{x}10^9$	$4.88\text{x}10^{21}$	$1.67\text{x}10^{11}$	4	$1.3\text{x}10^{-4}$
VII	$4\text{x}10^9$	.67	.46	$1.84\text{x}10^9$	$3.43\text{x}10^{21}$	$8.57\text{x}10^{11}$	20	$6.6\text{x}10^{-4}$
VIII	$2.37\text{x}10^9$	1.47	2.2	$5.2\text{x}10^9$	$9.7\text{x}10^{21}$	$4.10\text{x}10^{11}$	98	$3.2\text{x}10^{-3}$
IX	$1.25\text{x}10^8$	3.16	10	$1.25\text{x}10^9$	$2.33\text{x}10^{21}$	$1.86\text{x}10^{13}$	440	$1.46\text{x}10^{-2}$
Total	$9.31\text{x}10^{10}$			$1.22\text{x}10^{10}$	$2.23\text{x}10^{22}$			

dissipated in Cal m^{-2} for each isoseismal zone in Guatemala. Figure 33 is the results of a Log-log plot of the distribution of seismic energy throughout Guatemala. Double log coordinates were used so that the large range of values could be included.

Simulation of the Earthquake and Secondary Distribution

Figures 34a and 34b are the results of simulation of the catastrophic release of energy in the Guatemala earthquake and the secondary destruction of El Progreso as modeled in Figure 32. In Figure 35a the energy released is plotted as a function of time. Once the earthquake is triggered, the event grows exponentially until the strain in the fault is relieved. This generates a pulse of siesmic energy, which is then transmitted radially in a control action. Figure 34b is a plot of the destruction of El Progreso by the disordering action of the siesmic pulse.

Calculation of Disaster-Amplifier Ratios

With the distribution of earthquake energy known by zone for Guatemala and the percentage of destruction calculated for each zone, the relationship between earthquake energy dissipated and local disorder and distribution was examined.

The gravitational potential energy for a typical Guatemalan house was calculated from equation 39 (Spears and Zemansky, 1955) and found to be 97 Cal.

$$V_g = mgh, \tag{39}$$

where V_g is the gravitational potential energy, m is the mass of the house, g is the gravitational constant, and h is the mean height of the mass. The foundation area of the house was 6 m^2; therefore, the gravitational potential energy is 15 Cal m^{-2}.

Figure 33. Energy distribution in Guatemala from the major event, February 4, 1976 earthquake. Log-log plot of land area affected versus earthquake energy-dissipated.

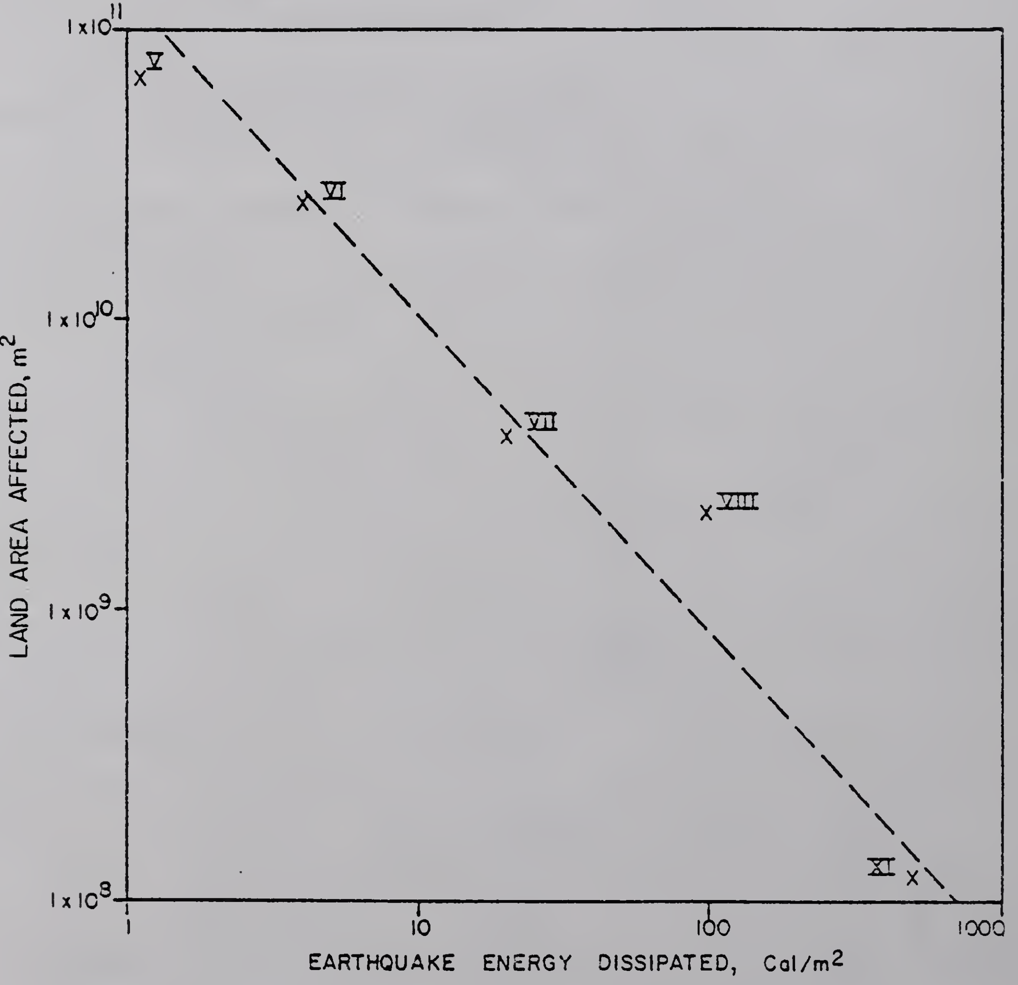
1 x 10^11
1 x 10^10
1 x 10^9
1 x 10^8
LAND AREA AFFECTED, m^2
1
10
100
1000
EARTHQUAKE ENERGY DISSIPATED, Cal/m^2
V
VI
VII
VIII
XI

Figure 34. Simulation results of earthquake model in Figure 32. Seismic energy release and destruction of El Progreso, Guatemala, versus time after earthquake.

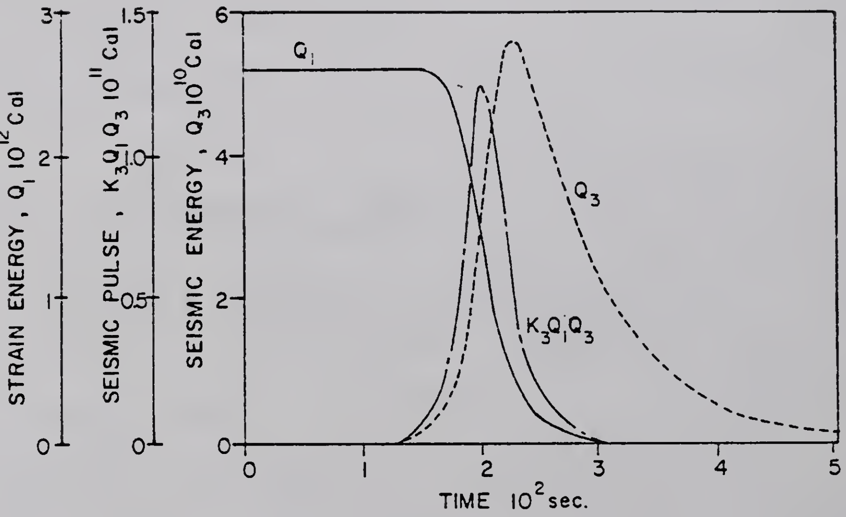
STRAIN ENERGY , Q_1 10^{12} Cal
0
1
2
3
SEISMIC PULSE , $K_3 Q_1 Q_3$ 10^{11} Cal
0
0.5
1.0
1.5
SEISMIC ENERGY , Q_3 10^{10} Cal
0
2
4
6
Q_1
Q_3
$K_3 Q_1 Q_3$
0
1
2
3
4
5
TIME 10^2 sec.

(a)

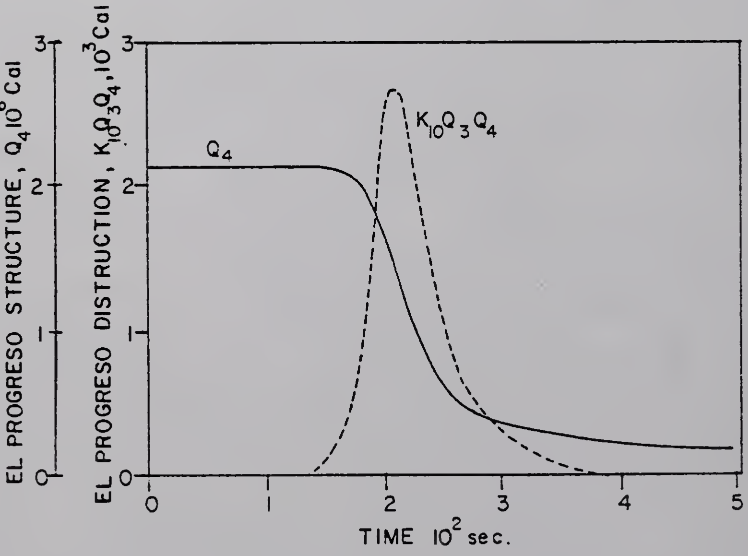
EL PROGRESO STRUCTURE, Q_4 10^6 Cal
0
1
2
3
EL PROGRESO DISTRUCTION, $K_{10} Q_3 Q_4$, 10^3 Cal
0
1
2
3
Q_4
$K_{10} Q_3 Q_4$
0
1
2
3
4
5
TIME 10^2 sec.

(b)

Figure 35. Structural damage of towns in Guatemala as a function of earthquake energy dissipated by the adobe houses.

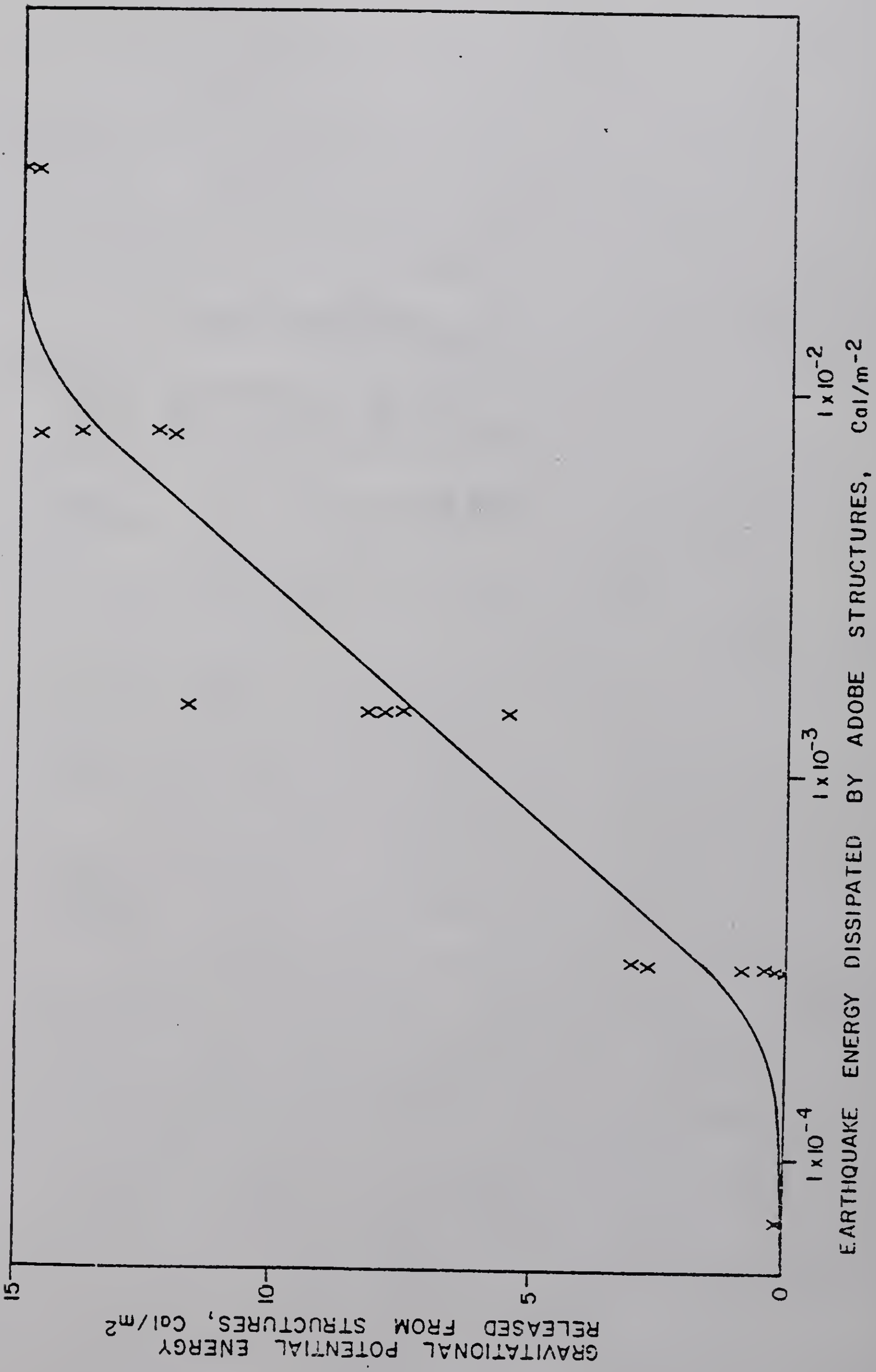
GRAVITATIONAL POTENTIAL ENERGY
RELEASED FROM STRUCTURES, Cal/m²
15
10
5
0
1 x 10⁻⁴
1 x 10⁻³
1 x 10⁻²
EARTHQUAKE ENERGY DISSIPATED BY ADOBE STRUCTURES, Cal/m⁻²

When the energy of the earthquake was dissipated over the land not all of the energy was absorbed in the man-made structures. The wave moved through a crust 7 km thick, so one might picture a house sitting on a column of earth 7 km high. A 1 m^2 column of earth would have a mass of 1.54×10^7 kg while a square meter of house has a mass of 512 kg. Since the houses are made of earth, linear distribution of energy was assumed throughout the entire column of earth crust and the house. Equation 40 gives the amount of energy absorbed in the house.

$$e_h = e_i \ (m_h/m_c), \tag{40}$$

where e_h is the energy absorbed by the house, e_i is the energy dissipated per square meter in zone i, m_h is the mass of the house, and m_c is the mass of the square meter column of earth crust. Column 9 of Table 12 shows energy absorbed per square meter of house based on the above method.

From the energy per unit area absorbed in the house and the energy per unit area stored in the structure, the effect of the two for towns throughout various intensity zones in Guatemala was compared. Table 13 summarizes the findings. The structural energy released by the earthquake was calculated by taking the gravitational potential energy stored in the structures of the town and converting it to kinetic energy based on the percentage damaged. The disaster-amplifier factor was then calculated for each city by dividing the gravitational kinetic energy released by the earthquake seismic energy absorbed by the structure. Figure 35 shows the results of relating the simulated destruction to earthquake seismic energy dissipated by adobe structures in Guatemala. It was found that on the average 1 Cal of earthquake wave energy released 7,716 Cal of gravitational potential energy by

TABLE 13. DISASTER-AMPLIFIER FACTORS FOR SECONDARY DISASTERS IN VARIOUS CITIES IN GUATEMALA.

Name	Intensity	Population	Damage Percent	Gravitation Potential Energy Release, Cal m^{-2}	Earthquake Energy Absorbed Cal m^{-2}	Amplifier Factors
El Progreso	VIII	11,040	951	14.25	$3.2x10^{-3}$	4,450
Guatemala	VII	700,504	45	6.75	$6.6x10^{-4}$	10,020
Chimattenango	VII	20,194	25	3.75	$6.6x10^{-4}$	5,680
Mixco	VIII	129,878	80	12.00	$3.2x10^{-3}$	3,750
Tecpan	VIII	24,181	100	15.00	$3.2x10^{-3}$	4,680
El Jicaro	VII	6,197	100	15.00	$3.2x10^{-3}$	4,680
San Agustin	VII	17,344	50	7.5	$6.6x10^{-4}$	11,000
Morazan	VIII	7,080	100	15.00	$3.2x10^{-3}$	4,600
Sanarate	VII	15,253	70	10.5	$6.6x10^{-4}$	15,000
Gualan	XI	23,378	99	15.0	$1.46x10^{-2}$	1,020
Esquipulos	V	19,304	1	.15	$2.8x10^{-5}$	5,333
Los Amates	VI	45,537	2	.3	$1.3x10^{-4}$	2,300
Villa Nueva	VI	--	8	1.2	$1.3x10^{-4}$	1,200
Amatitlan	VI	26,412	20	3	$1.3x10^{-4}$	23,000
Chinaurta	VIII	32,763	80	12	$3.2x10^{-3}$	3,750
San Maria de Jesus	VI	7,114	20	3	$1.3x10^{-4}$	23,000

toppling adobe houses. The magnitude of the earthquake energy dissipated per square meter was calculated from reported field intensities collected by the United States Geological Survey (Espinosa *et al*., 1976) and mapped in Figure 35. The damage data were reported by the Guatemalan National Reconstruction Committee (Comite de Emergencia, 1976).

The disaster-amplifier ratio was also calculated using Calories of embodied solar energy. The mean seismic energy absorbed per square meter of structure and the quantity of urban structure disorder were converted to solar Calories. The energy quality factors presented in Table 8 were used for this calculation. It was found that 25 solar Cal of structure were disordered by 1 solar Cal of seismic energy.

DISCUSSION

From models and measurements of disasters a general patternof pulsing was found for many aspects of nature. Interdependence of pulses was related through a world web model as a general theory of disasters.

The Dynamics of Pulsing Systems

The exponential surge model diagramed in Figure 2 was found to apply to all cases examined. It has an order-disorder model with a catastrophic consumer in the recycle loop. This model uses pulsing to improve material cycling between the storages of order and disorder in Figure 1, and accounts for the catastrophic properties of disasters. The transformation from a stable system to a pulsing action may be either self-activated or externally triggered.

The Cycling of Matter

Conservation of matter was incorporated in the models by requiring that the sum of the ordered and disordered matter equal a constant. Structure was built from disorder by ordering matter. Likewise disorder was created from order by recycling matter. In the basic exponential surge model, two recycle pathways exist. In the linear pathway the recycle process is continuous and proportional to the quantity of matter stored. When sufficient stocks are accumulated for catastrophic recycling to be supported, a catastrophic consumer is generated that is capable of very rapid recycle and energy pulse generation.

The ability to cycle matter may be a fundamental design principle of self-sustaining systems. When systems build up large storages of matter they may become sluggish and suffer from stagnation. Many forces, both internal and external, continually work to recycle the stored matter and prevent stagnation. The exponential surge model was used to diagram the systems of the global energy web, the Johnstown flood, and the Guatemala earthquake. The simulation results presented illustrate the material cycling character of this flexible configuration of the order-disorder model.

Energy Convergence and Storage

The exponential surge configuration of the order-disorder model presented in Figure 2 and used throughout this research, uses the ordered structure and the recycled matter in the form of disorder to converge energy and grow order from disorder. The ability to concentrate and store energy by transforming disordered matter to order is believed to be a property of self-sustaining systems. This model is capable of self-design in the sense that it can switch energy from developing order to control and recycle as either one of the other processes becomes limiting.

Exponential Surges and Energy Pulses

When the quantity of energy converged in the form of ordered structure is great enough to trigger catastrophic consumption, the exponential surge model catastrophically recycles the matter stored and releases its energy storage in a control action. The ability to generate control pulses is believed to be a common design principle of self-sustaining systems. The magnitude of the energy pulse released is proportional to the energy stored in the form of order.

The pulse width and height is set by the dynamic properties of the consumer module which catastrophically recycles the ordered matter.

System Control through Cascading

The catastrophic energy pulses generated by one system often control other systems. The diagram in Figure 3 illustrates this concept. Several possible control mechanisms exist. In some catastrophic events the disaster pulse energy provides the power to recycle the ordered structure by the interaction of the stored energy and the disaster pulses. In other cases the disaster pulse triggers a separate secondary disaster such as a dam failure or a fire. A fourth design principle suggested for self-sustaining systems is the ability to send and receive information in the form of energy pulses.

Dynamic Behavior of Energy Cycling Models

The application of the order-disorder model in Figure 18 to the disordering effect of radiation stress on a rain forest ecosystem approximated the dynamic nature of the actual system and was stable. When the model was applied quantitatively to the Johnstown flood and the Guatemala earthquake, it was found to have stable dynamic characteristics and to provide graphs replicating the observed events.

Global Energy Web

The energy circuit model of the world conceptually presented in Figure 18 and evaluated by sector in Figures 19, 21, 22, 23, and 24 connects many order-disorder models in a web. The global web allows energy flows including disasters to be put in relative prospective of importance and impact.

Energy Quality, A Universal Energy Conversion Factor

The energy quality factors computed were based on the weblike nature of energy flows of the earth's systems. The quality factors are the ratio of the total solar energy required to power the energy convergence process of the earth to the quantity of concentrated energy flowing in the system of interest. Through the evolutionary processes of the earth, the systems best adapted to the use of all pulsing energy sources present may have prevailed.

The necessity of each process to evolve until all available sources of energy are harnessed to maximize power may be the reason the atmospheric, oceanic, biological, geological, and urban sectors of the world's system have developed into a web. Once the web is formed and evolved to maximize power for the total system, no sector can compete by operating separetely because limitations in cycles would develop. Leibig's (1862) law of the minimum describes the behavior of processes without good recycle.

As solar energy is converged through the web of the earth, the energy flowing in a given process becomes less even though large quantities of dilute solar energy were necessary to power the concentration process. Thus the equality of the energy in areas of the flow decreases. Lotka's (1922) principle of maximum power suggests that systems which further converge high quality energy use it effectively to survive. Energy wasting systems are eventually replaced by systems that maximize power. For systems which have stood the evolutionary test of time, it is likely that the quantity of energy converged to produce the energy flow will be equal to the effect of the energy flow as a feedback amplifier. Thus energy quality is a universal way of comparing different forms of energy flowing in the weblike process of the earth showing which are valuable and have large requirements and impact.

Embodied Solar Energy, A Universal Measure

The solar energy embodied in a flow is calculated by multiplying the energy flow by the appropriate global quality factor. This calculation estimates the quantity of solar energy converged by the biosphere to produce a flow of interest. This transformation of the energy flows converts them to common units of measure, embodied solar Calories. This makes possible the comparison of two processes. Also the relative value of two interacting flows can be determined. Table 8 ranks energy flows according to their value.

Disater-Amplifier Ratios, A Measure of Control

When disaster-amplifier ratios were calculated for the evaluated models of the tropical rain forest, Johnstown flood, and Guatemala earthquake in Figures 27, 30, and 32, the control or disordering effect was greater than the quantity of energy delivered by the catastrophic pulsing action of the controlling system. Calculation of the disaster-amplifier ratio in heat equivalents ranged from 1,000 to 10,000. Lower amplifier factors ranging from 10 to 100 were found when calculations were made with the disaster energy pulse and the quantity of disorder generated both measured in embodied solar Calories.

The appropriate disaster-amplifier ratios multiplied by the quantity of energy embodied in a local hazard may be useful in estimating total risk from all hazards in specific locations. Risk maps constructed from plots of the aggregate risk potential may be of considerable utility for guiding local land use decisions.

The Frequency of Pulsing and Control

The ability of systems of man and nature to adapt to the pulsing environment is probably a function of the frequency of the pulsing action. Examples of adaptation are common. Structures built and ecosystems living in areas of daily tidal exchange with the sea show many characteristics of adaptation to the tidal pulsing; however, adaptation to less predictable pulses such as earthquakes is less pronounced. The magnitude and frequency of the pulsing action of the environment is believed to be of fundamental consequence in selecting which systems will survive the test of time.

Control of Global Cycles by Solar Pulses

Empirical evidence links 11-year solar cycles to the cycles of the global energy web. The physical mechanism for the linkage is not well known except for the upper atmospheric phenomena. Sunspot numbers are correlated with the aurora borealis. Auroral displays are produced when charged particles from the sun interact with the earth's magnetic field, resulting in particle acceleration and collisions with air molecules in the upper atmosphere (Eddy, 1976). Bray (1967) found significant correlation between sunspot and biological productivity through radiocarbon activity from 527 B.C. to 1964 A.D.

The high quality pulses generated by solar flares may couple to the order-disorder cycles of the earth, synchronizing the two processes. The appropriate disaster-amplifier factor for sunspots might be similar to the one calculated for the controlling effect of gamma radiation on the tropical rain forest in Figure 27. An energy quality factor for sunspots could be obtained by estimating the quantity of solar energy converged to produce a solar flare. The product of the disaster-amplifier ratio and the energy embodied in sunspot energy incident would then produce and estimate the degree of control over world's cycles by solar cycles.

Figure 36 is a conceptual diagram suggesting a mechanism for coupling the cycles of the sun to the cycles of the earth. Preliminary estimates based on disaster-amplifier ratios of gamma radiation and energy quality factors based on the blackbody temperature of solar flares point to sufficient energy in sunspot activity to control meteorological, biological, geological, and human cycles of the earth.

Disasters

Natural and man-made disasters have had considerable effect on the history of the earth. Many relatively smooth periods of slow physical and cultural changes have been violently disrupted and forever altered by the catastrophic release of energy in fires, wars, earthquakes, floods, and storms.

The Energy Cost and Benefit of Disasters

The results of the research in this work suggest that energy source-pulse systems provide benefits considerably larger than harm to the world environment. The ratio, of the quantity of work done to the energy required to produce the disordering, was greater than one in each case. Comparison between the continuously disordering effect of gamma radiation on a tropical terrestrial ecosystem, the two pulse disordering process of a flood and an earthquake suggest that the disordering pulse is more effective than an equivalent amount of energy expended on a continuous basis.

Figure 36. Conceptual model illustrating possible mechanisms for control of global energy cycles by Solar Pulsing.

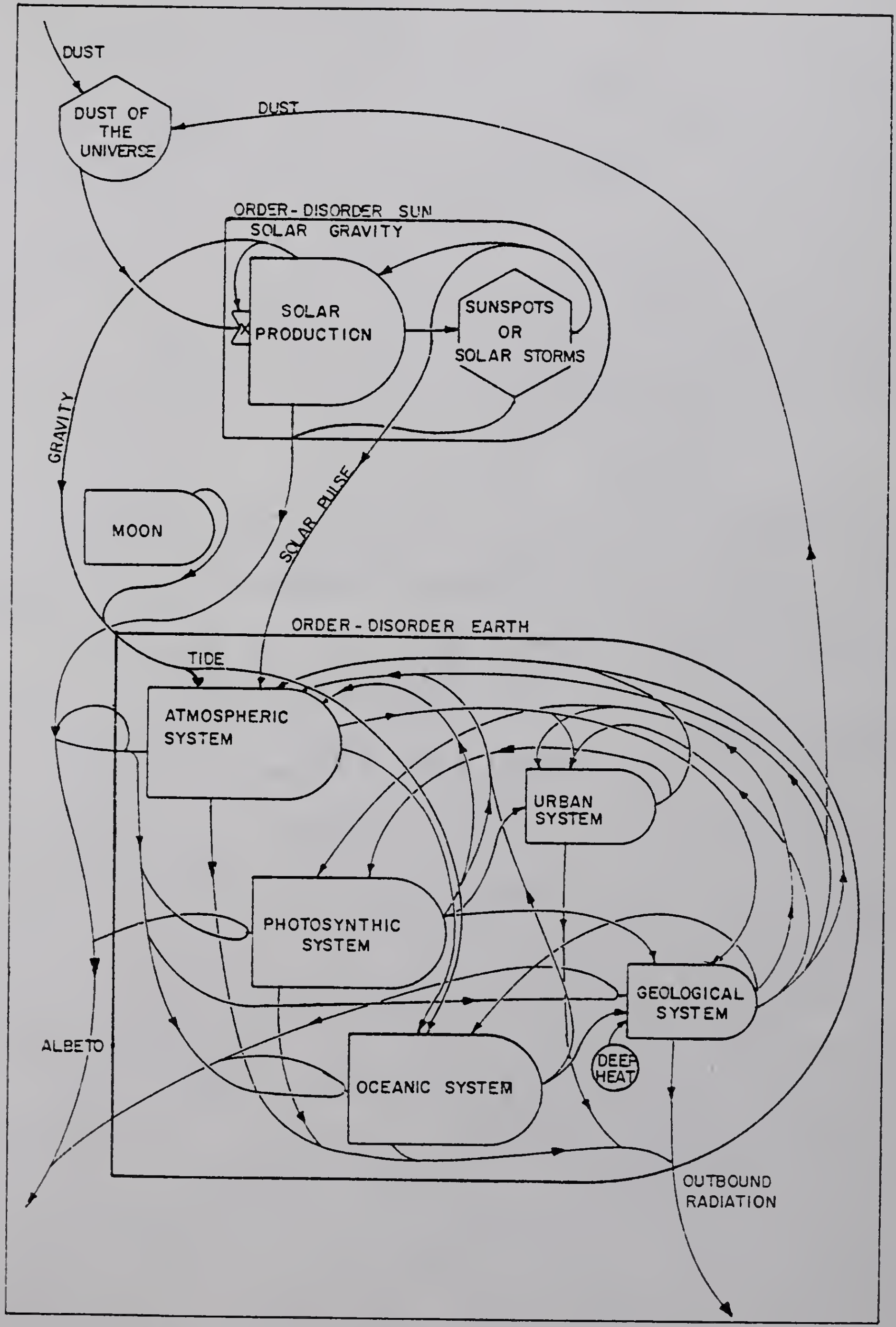
DUST
DUST OF THE UNIVERSE
DUST
ORDER-DISORDER SUN
SOLAR GRAVITY
SOLAR PRODUCTION
SUNSPOTS OR SOLAR STORMS
GRAVITY
MOON
SOLAR PULSE
ORDER-DISORDER EARTH
TIDE
ATMOSPHERIC SYSTEM
URBAN SYSTEM
PHOTOSYNTHIC SYSTEM
GEOLOGICAL SYSTEM
ALBETO
DEEP HEAT
OCEANIC SYSTEM
OUTBOUND RADIATION

When calculated, on the basis of Calories of heat equivalents, 1.1 x 10^{-2} Cal $m^{-2}d^{-1}$ of gamma radiation disordered the work of 145 Cal m^{-2} d^{-1} of photosynthetic energy or one Calorie of disorder was offset by 10,000 Calories of order. The same calculation, for the devastation of Johnstown by the failure of the South Fork Dam, yielded 1.7 x 10^6 Cal m^{-2} of devastation produced by 1.3 x 10^3 Cal m^{-2} of flood energy or approximately one Cal of disorder to offset 1,000 Cal of order. In the third case in El Progreso, Guatemala, 3.2 x 10^{-3} Cal m^{-2} of energy from the Guatemala earthquake of 1976 produced 14.5 Cal m^{-2} of release of gravitational potential energy of structure or approximately one Cal of earthquake energy absorbed the disordering of 7,700 Cal of gravitational potential energy. In each case the effect of one Calorie of disordering energy was far greater than the effect of one Calorie of ordering energy. However, the above ratios may be of little value since the calculation of the ratios were based on the heat equivalent Calories rather than a common denominator such as solar equivalents.

The Distribution of Disaster Pulses as a Control Device

The control action of energy pulses generated by the catastrophic disordering of energy concentrating systems of the earth is distributed conversely to the concentration gradient. As diagramed in the global model in Figure 18, energy is concentrated by all of the ordering processes of the earth, and when catastrophically released is fed back to control the system.

Throughout history, the occurrence of catastrophic events, both natural and man-made, have been used as milestones in time and space. Such terms as pre-World War I are common place in literature and every day conversation. Such references suggest that the control action of disaster pulses on the events of the world is generally recognized. Additional evidence for the acceptance of the large effect of disasters on the behavior of systems is implied by the deliberate hesitation of many analysts to model time periods which contain catastrophic events. Also a caveat is normally included with economic and population forecasts which specifically excludes the event of war or natural disaster from the projections.

The global model, developed and evaluated in this research and presented in overview form in Figure 10, addresses the control function of disasters on the world energy web. Many important material recycling processes are heavily dependent on energy pulses. Furthermore the recycling of materials helps to maximize the power of disordering systems which have stagnated.

Specific examples of higher productivity in natural systems after disordering have been sited by various researchers. For example, Lugo and Snedaker (1974) suggested that mangroves organized their extent of regrowth according to hurricane frequency to maximize productivity. The role of forest fire as a regenerative force in nature has been well documented by Komarek (1962) at the Tall Timbers Research Station. The long-term effect of disasters on the productivity of urban systems has also been shown to be positive. After extensive economic analysis of the long-term effect of disasters on communitites, Dacy and Kunrenther (1969) concluded that communities may benefit economically from disasters through rapid inflow of capital for rebuilding and the adoption of technological innovations to meet critical situations. The field research in El Progreso, Guatemala and Johnstown, Pennsylvania, support the positive benefit concept. In El Progreso, in addition to large quantities of immediate relief, an entirely new structural system, including water, sewerage, roads, and drainage, was installed and all of the government buildings were replaced with more modern and functional facilities. In the case of Johnstown, all three major floods have performed urban renewal functions and stimulated new economic investment. The rapid economic growth of Germany and Japan after heavy destruction from World War II are also examples of the positive benefit of recycling obsolete structure by externally driven catastrophic forces.

Common Aspects of Disaster and Disorder in Different Systems

As previously stated one of the objectives of this research was to develop an energy basis for disasters and to show that they were an essential part of the cycles of order and disorder of the systems of the earth. One of the ways this idea was addressed in this research was to demonstrate that a similar process of order, disorder, and pulsing exist throughout the major systems of the earth. All of the disaster generating models in this research use a common format for the energy convergence and catastrophic pulsing. Note the similarity in the energy convergence process for storms, floods, fires, war, earthquakes, and volcanoes as illustrated by Figures 18, 19, 21, 22, 23, and 24. This is further illustrated by the simulations of flood and earthquake destruction modeled in Figures 30 and 32, respectively.

Pulsing and Maximum Power

The field results in this research suggest that primary and lateral systems can be more productive if pulsed. To test the feasibility of this concept, a simple experiment was carried out.

Two order-disorder models with identical energy sources, differential equations, and coefficients were constructed as shown in Figures 37a and b. The model in Figure 36a was pulsed disordered every 25 time periods. The model in Figure 37b was allowed to grow undisturbed. See Figures 37c and d. Also plotted in Figure 37d is the result of the integration of the gross production of both systems (pathways marked P). The results are identical during the initial growth period. At the end of 25 time periods, system a was disordered and then allowed to rebuild. For this case, the total production was stimulated by the recycle generated by the pulse, producing a greater total production.

The results of this hypothetical case suggest that the pulse disordering of systems maximizes power by recycling the matter stored in the system which then may stimulate regrowth. The counter intuitive nature of this results raises many interesting questions about the role of pulses in systems of man and nature. Applications in the world possibly range from the pulse harvest of agricultural systems to possibly explaining the vitality of Germany and Japan post-World War II destruction.

Disaster Planning and Future Research

White and Haas (1975) have pointed out the critical need for analitical tools to support the development of urban policy in hazard prone areas. Several possible applications of the theory developed in this research to urban problems are: (1) demonstration of similarity between problems generated by natural and man made disaster situations; (2) calculation of the total risk expressed by specific community to all hazards;

Figure 37. A test of the effect of pulsing on the principle of maximum power.

(a) Pulsed order-disorder model. The gross production of the system is summed over time by Q_3.

$$\dot{Q}_1 = K_1E_1Q_1Q_2 - K_2Q_1 - SW$$

$$Q_2 = C - Q_1$$

$$\dot{Q}_3 = K_1E_1Q_1Q_2$$

(b) Order-disorder model, not pulsed, used as a control. The gross production of the system is summed over time by Q_7.

$$\dot{Q}_5 = K_1E_1Q_5Q_6 - K_2Q_5$$

$$Q_6 = C - Q_5$$

$$\dot{Q}_7 = K_1E_1Q_3Q_6$$

(c) Results of simulation of pulsed model a.

(d) Results of simulation of model b and plot of integral of production of models a and b.

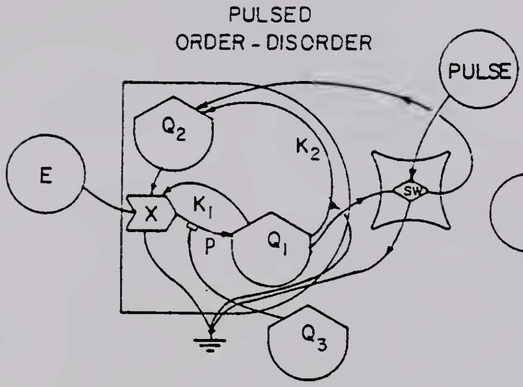
PULSED
ORDER - DISORDER
PULSE
E
X
K1
P
Q1
Q2
K2
SW
Q3

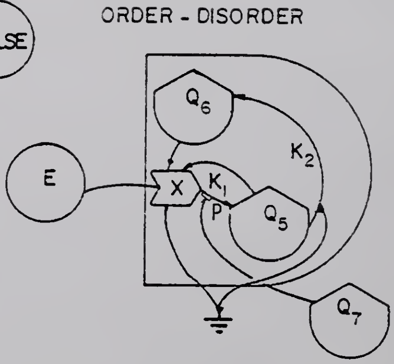
ORDER - DISORDER
E
X
K1
P
Q5
Q6
K2
Q7

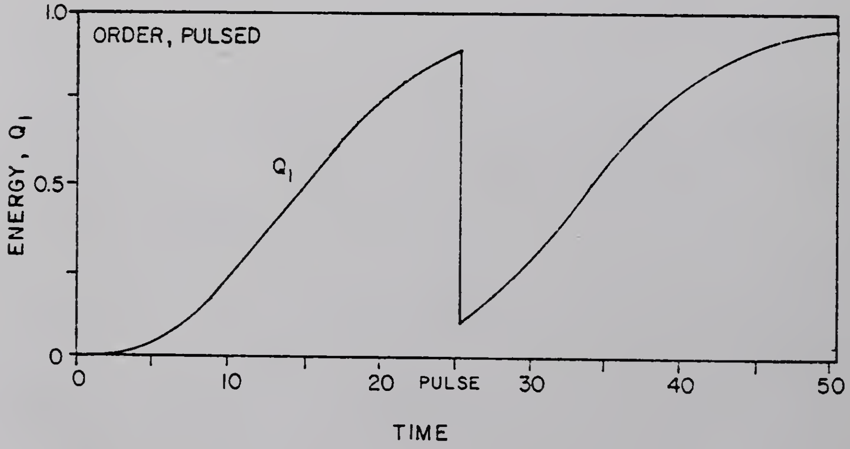
ORDER, PULSED
ENERGY, Q1
1.0
0.5
0
Q1
0
10
20
PULSE
30
40
50
TIME

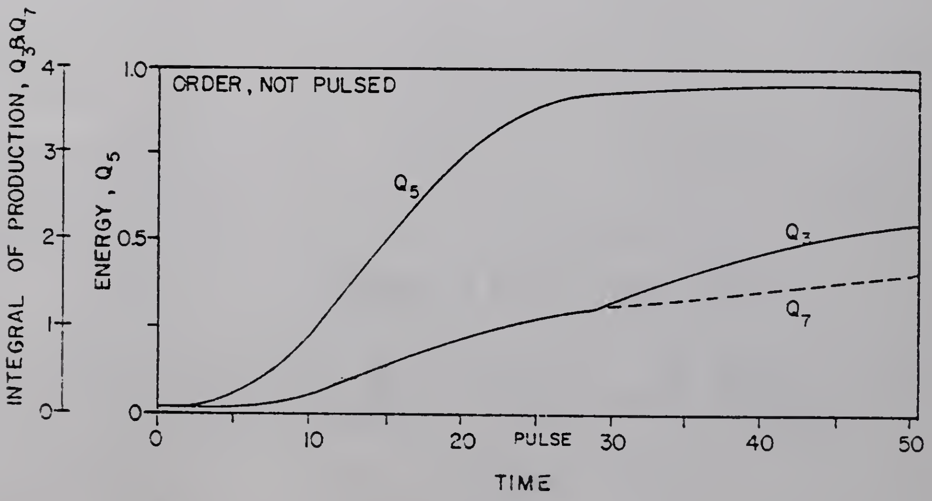
INTEGRAL OF PRODUCTION, Q3 & Q7
4
3
2
1
0
ORDER, NOT PULSED
ENERGY, Q5
1.0
0.5
0
Q5
Q3
Q7
0
10
20
PULSE
30
40
50
TIME

(3) simulation of effect of future disasters and effectiveness of disaster mitigation techniques; and (4) preparation of local maps of total risk.

Effective public policy can only be formed with an adequate understanding of the public. Too often the many types of disaster potentials that threaten the structure of communities are treated as separate and dissimilar events (White and Hass, 1975). An awareness of the similarity of disaster mechanism and disruptive effects is necessary to make efficient use of public resources. In addition the cascading of disasters renders planning for a specific type of disruption unrealistic. A well trained and integrated civil defense, fire, police, and emergency government agencies are essential to properly dealing with the multiple hazards of urban areas.

Disaster-amplifier ratios and the energy quality factors developed may have application in calculating the total risk a particular community faces. A quantitative understanding of the magnitude of the aggregate risk would provide a base for public policy decisions involving commitment of resources to disaster mitigation and preparedness.

Simulation of the possible effects of future disasters on a specific community in a manner similar to the models developed for El Progreso and Johnstown forms a quantitative basis for disaster planning. Models incorporating disaster mitigation techniques could be used to quantitatively evaluate various policy alternatives in disaster planning.

Local risk maps could be constructed by summing the result of converting spacial distribution of various forms of pulsing energy to embodied solar energy by using quality factors from Table 8 and disaster amplifier factors from appropriate cases. The resulting multi-hazard risk map could be used to more adequately allocate urban land between various uses. Possibly land uses with minimum structure would be allocated to high hazard areas.

It is recommended that a specific locality be selected for test application and further development of the energy basis for disasters.

APPENDIX I
NOTES TO TABLES 2-7, 9, 10 AND 11

Notes to Table 2

(1) Total solar flux received by Earth I_o per square meter of surface area.

$$I_o = \frac{Ap}{As} \times E$$

where Ap is the effective area of earth's plane

As is the surface area of the earth (Van Nostrands Scientific Encyclopedia, 1976)

E is the solar constant 19.4 Cal m^{-2} min^{-1} (Byers, 1974)

$$I_o = \frac{1.278 \times 10^{14} \text{ m } \times 19.4 \text{ Cal } m^{-2} min^{-1} \times 1.44 \times 10^{3} \text{ min } d^{-1}}{5.101 \times 10^{14} \text{ m}^{2}}$$

$$I_o = 7{,}000 \text{ Cal } m^{-2}d^{-1}$$

(2) Global average solar radiation absorbed by earth R_n (Vonder Haar and Suomi, 1971).

$$R_n = 3.4 \text{ Cal } m^{-2} \text{ } min^{-1} \times 1.44 \times 10^{3} \text{ min } d^{-1}$$

$$R_n = 4{,}900 \text{ Cal } m^{-2}d^{-1}$$

(3) Albedo radiation reflected by earth

Albedo A

$$A = 1 - \frac{R_n}{I_o} \cdot = - \frac{4{,}900 \text{ Cal } m^{-2}d^{-1}}{7{,}000 \text{ Cal } m^{-2}d^{-1}} = .30$$

$$R_a = 7{,}000 \text{ Cal } m^{-2}d^{-1} - 4{,}900 \text{ Cal } m^{-2}d^{-1}$$

$$R_a = 2{,}100 \text{ Cal } m^{-2}d^{-1}$$

(4) Surface radiation heat loss due to cooling and used by plants.

47% of solar flux (Houghton, 1954)

$$7{,}000 \text{ Cal } m^{-2}d^{-1} \times .47 = 3{,}290 \text{ Cal } m^{-2}d^{-1}$$

Notes to Table 2 - Continued

(5) Energy used in powering atmosphere

23% of solar flux I_o

$7{,}000 \text{ Cal m}^{-2}\text{d}^{-1} \times 0.23 = 1{,}610 \text{ Cal m}^{-2}\text{d}^{-1}$

(6) Global average infrared radiation R outbound, (Vonder Haar and Suomi, 1971).

$R_L = 3.4 \text{ Cal m}^{-2} \text{ min}^{-1} \times 1{,}400 \text{ m}^{-2} \text{ d}^{-1}$

$R_L = 4{,}900 \text{ Cal m}^{-2}\text{d}^{-1}$

(7) Energy stored in latent heat of world atmosphere

Total atmosphere water per m^2 (Skinner and Turekian, 1973)

$$\frac{(1.3 \times 10^4 \text{km}^3) \times (10^9 \text{m}^3 \text{km}^3) \times (10^6 \text{ g m}^{-3}) \times 0.574 \text{ Cal g}^{-1}}{5.10 \times 10^{14} \text{m}^2} =$$

$$1.46 \times 10^2 \text{ Cal m}^{-2}$$

(8) Mass of atmosphere based on mean pressure of 1.013×10^6 dynes cm^{-2} (Goody and Walker, 1972)

$$\text{Mass} = \frac{(1.013 \times 10^6 \text{ dynes cm}^{-2})(1 \times 10^4 \text{ cm}^2 \text{ m}^{-2})(\text{g cm sec}^{-2} \text{ dynes}^{-1})}{(981 \text{ cm sec}^{-2}) \qquad (1 \times 10^3 \text{ kg}^{-2})}$$

$\text{Mass} = 1.04 \times 10^4 \text{ kg m}^{-2}$

(9) Energy of global circulation and turbulence (Monin _et_ _al_., 1977).

$$\frac{(1 \times 10^{21} \text{ J})(2.30 \times 10^{-4} \text{ Cal J}^{-1})}{(5.1 \times 10^{14} \text{ m}^2)} = 470 \text{ Cal m}^{-2}$$

(10) Energy absorbed by atmosphere

23% of solar (Houghton, 1954)

$7{,}000 \text{ Cal m}^{-2}\text{d}^{-1} \times 0.23 = 1{,}610 \text{ Cal m}^{-2}\text{d}^{-1}$

(11) Evaporation from sea and land (Skinner and Turekian, 1971)

$3.83 \times 10^{20} \text{ g yr}^{-1}$

Evaporation from land: $0.63 \times 10^{20} \text{ g yr}^{-1}$

Notes to Table 2 - Continued

Average evaporation per square meter of earth

$$\frac{[(3.83 + .63) \times 10^{20}\ g\ yr^{-1}]}{(5.10 \times 10^{14} m^2) \times (365\ d\ yr^{-1})} = 2{,}400\ g\ m^{-2}d^{-1}$$

Evaporation energy

$2{,}400\ g\ m^{-2}d^{-1} \times .6\ Cal\ g = 1{,}400\ Cal\ m^{-2}d^{-1}$

(12) Turbulence (Byers, 1974)

50% of the kinetic energy of atmosphere in eddyflux

$0.5 \times 300\ Cal\ m^{-2}d^{-1} = 150\ Cal\ m^{-2}d^{-1}$

(13) Circulation (Byers, 1974)

50% of the kinetic energy of atmosphere in circulation

$0.5 \times 300\ Cal\ m^{-2}d^{-1} = 150\ Cal\ m^{-2}d^{-1}$

(14) Cooling due to radiation loss by atmosphere

Heat loss from atmosphere due to cooling by first law of thermodynamics

$2{,}720\ Cal\ m^{-2}d^{-1}$

(15) Poleward flow of energy in weather system, see Figure 20 (Vonder Haar and Suomi, 1971).

$100\ Cal\ m^{-2}d^{-1}$

(16) Total energy in winds, water, convection (Hubbert, 1971)

$15\ Cal\ m^{-2}d^{-1}$

(17) Heat loss in circulation and eddy flux of atmosphere by first law

$150\ Cal\ m^{-2}d^{-1} + 150\ Cal\ m^{-2}d^{-1} - (100\ Cal\ m^{-2}d^{-1} + 15\ Cal\ m^{-2}d^{-1})$

$= 185\ Cal\ m^{-2}d^{-1}$.

(18) Hurricane and cyclone energy (Dunn and Miller, 1964):

$$\frac{(9.5 \times 10^{15}\ Cal\ d^{-1})(9\ d\ hurricane^{-1})(9\ hurricane\ yr^{-1})}{(5.1 \times 10^{14}\ m^2)\ (365\ d\ yr^{-1})} = 4.1\ Cal\ m^{-2}d^{-1}$$

Notes to Table 3

(1) Solar energy 47% of total radiation (Weyl, 1970)

$7{,}000 \text{ Cal m}^{-2}\text{d}^{-1} \times .47 = 3{,}290 \text{ Cal m}^{-2}\text{d}^{-1}$

(2) Solar reflection 5% of total radiation (Weyl, 1970)

$7{,}000 \text{ Cal m}^{-2}\text{d}^{-1} \times .05 = 350 \text{ Cal m}^{-2}\text{d}^{-1}$

(3) Energy stored in heat of sea (Weyl, 1970)

$3.4 \text{ Cal cm}^{-2} \times 1 \times 10^4 \text{ cm}^2 \text{ m}^{-2} = 3.4 \times 10^4 \text{ Cal m}^{-2}$

(4) Mass of sea (Skinner and Turekian, 1973)

$$\frac{1.4 \times 10^{21} \text{ kg}}{3.61 \times 10^{14} \text{m}^2} = 3.88 \times 10^6 \text{ kg m}^{-2}$$

(5) Energy stored in sea gyres

Mean gyre velocity of 3.5 cm sec^{-1} (Monin _et_ _al_., 1977)

$$e = 1/2\, mv^2 = \frac{(3.88 \times 10^6 \text{ kg m}^2)(.035 \text{ m sec}^{-1})(2.38 \times 10^{-4} \text{Cal J } 1^{-1})}{2}$$

$e = 0.55 \text{ Cal m}^{-2}$

(6) Evaporation-energy loss in latent heat (Skinner and Turekian, 1973)

$$\frac{3.83 \times 10^{20} \text{ g yr}^{-1}}{(3.61 \times 10^{14} \text{ m}^2) \times (365 \text{ d yr}^{-1})} = 2.9 \times 10^3 \text{ g m}^{-2}\text{d}^{-1}$$

0.54 Cal g^{-1} energy for evaporation

$2.9 \times 10^3 \text{ g m}^{-2}\text{d}^{-1} \times 0.54 \text{ Cal g}^{-1} = 1{,}570 \text{ Cal m}^{-2}\text{d}^{-1}$

(7) Heating, solar energy consumed in heating of sea by conservation of energy, notes 1, 2, 6.

$(3{,}290 - 350 - 1{,}570) \text{ Cal m}^{-2}\text{d}^{-1} - 1{,}370 \text{ Cal m}^{-2}\text{d}^{-1}$

(8) Transport of heat in sea water toward the poles by tidal energy

$50 \text{ Cal m}^{-2}\text{d}^{-1}$ (Vonder Haar and Suomi, 1971)

Assume 50% by tide and 50% in wind drives surface current

$50 \text{ Cal m}^{-2}\text{d}^{-1} \times 0.5 = 25 \text{ Cal m}^{-2}\text{d}^{-1}$

Notes to Table 3 - Continued

(9) Wind pumped surface current

50 Cal $m^{-2}d^{-1}$ transport of heat toward the poles (Vonder Haar and Suomi, 1970).

Remaining 50% not transported by tide

$50 \text{ Cal } m^{-2}d^{-1} \times 0.5 = 25 \text{ Cal } m^{-2}d^{-1}$

(10) Heat pumped by wind driven waves 47% of cooling

Excess heat = $[3{,}290 + 1{,}570 + 50)] \text{ Cal } m^{-2}d^{-1} = 1{,}320 \text{ Cal } m^{-2}d^{-1}$

$(1{,}320 \text{ Cal } m^{-2}d^{-1} \times .47) = 620 \text{ Cal } m^{-2}d^{-1}$

(11) Heat lost due to surface cooling (not evaporation or wind generated) by law of energy conservation

1,320 Cal $m^{-2}d^{-1}$ excess heat

-620 Cal $m^{-2}d^{-1}$ wind driven wave cooling

700 Cal $m^{-2}d^{-1}$ surface cooling

(12) Surface current drive by wind

25 Cal $m^{-2}d^{-1}$ (see note 9)

(13) Energy dissipated by waves (Kinsman, 1965)

$$\frac{(7 \times 10^{26} \text{ ergs yr}^{-1}) \times (2.39 \times 10^{11} \text{ Cal erg}^{-1})}{(3.61 \times 10^{14} \text{ m}^2) \times (365 \text{ d yr}^{-1})} = 0.13 \text{ Cal } m^{-2}d^{-1}$$

(14) Wind cooling

620 Cal $m^{-2}d^{-1}$ (see note 10)

(15) Precipitation (Skinner and Turekian, 1973)

$$\frac{3.47 \times 10^{20} \text{g yr}^{-1}}{3.61 \times 10^{14} \text{ m}^2) (365 \text{ d yr}^{-1})} = 2{,}633 \text{ g } m^{-2}d^{-1}$$

(16) Energy input of tide dissipated by sea currents (Weyl, 1970)

$$\frac{(2.7 \times 10^{19} \text{ ergs sec}^{-1})(8.64 \times 10^{5} \text{ sec d}^{-1})(2.39 \times 10^{-11} \text{Cal erg}^{-1})}{(3.6 \times 10^{14} \text{m}^2)} =$$

1.54 Cal $m^{-2}d^{-1}$ (Skinner and Turekian, 1973)

Notes to Table 3 - Continued

(17) Energy input of wind (Hubbert, 1971)

$15 \text{ Cal m}^{-2}\text{d}^{-1}$

(18) Energy input to sea gyres (Monin *et al*., 1977)

Velocity of gyer at periphery 10 cm sec^{-1}

Mean gyer radius, 2,500 km

$$\frac{2 \ (2{,}500 \text{ km}) \ (1 \times 10^{5} \text{ cm km}^{-1})}{(10 \text{ cm sec}^{-1}) \ (8.64 \times 10^{4} \text{ sec d}^{-1})} = 1.8 \times 10^{3} \text{ d}^{-1}$$

$$E = \frac{0.55 \text{ Cal m}^{-2}}{1.8 \times 10^{3}\text{d}} = 3 \times 10^{-4}\text{Cal m}^{-2}\text{d}^{-1}$$

(19) Energy dissipated in gyers by first law of thermodynamics

Dissipation set equal to consumption

(20) Storage of energy in ice (Skinner and Turekian, 1973)

Volume of water in polar ice cap and glaciers

$$\frac{2.9 \times 10^{7} \text{ km}^{3} \times 1 \times 10^{9} \text{ m}^{3} \text{ km}^{-3} \times 1 \times 10^{6} \text{ g m}^{-3}}{5.1 \times 10^{14} \text{ m}^{2}} = 5.69 \times 10^{7} \text{ g m}^{-2}$$

(21) Mean residence time for water in ice caps and glaciers

4×10^{4} years

$$\text{Flow} = \frac{\text{storage}}{\text{mean residence time}} = \frac{5.69 \times 10^{7} \text{ g m}^{-2}}{(4 \times 10^{4} \text{ yr}^{1})(365 \text{ d yr}^{-1})} =$$

$3.9 \text{ g m}^{-2}\text{d}^{-1}$

(22) Rate of melting set equal to rate of buildup

$3.9 \text{ g m}^{-2}\text{d}^{-1}$

(23) Energy required to melt ice at $3.9 \text{ g m}^{-2}\text{d}^{-1}$ rate

Energy stored in ice relative to mean global temperature

Energy in ΔT $300° - 273°\text{K} = 23°\text{K}$

Specific heat of $1 \text{ Cal g}^{-1}° \text{ K}^{-1}$

$23°\text{K} \times 0.001 \text{ Cal}°\text{K}^{-1} = 0.023 \text{ Cal g}^{-1}$

$$+ \text{ heat of fusion } = \frac{0.079 \text{ Cal g}^{-1}}{0.1 \text{ Cal g}^{-1}}$$

Notes to Table 3 - Continued

$(3.9 \text{ g m}^{-2}\text{d}^{-1})(0.1 \text{ Cal g}^{-1}) = 0.39 \text{ Cal m}^{-2}\text{d}^{-1}$

Notes to Table 4

(1) Mean plant biomass 3.6 kg m^{-2} (Whittaker and Likens, 1975)

Energy storage 3.6 kg m^{-2} x 4,250 Cal kg^{-1} = 15,300 Cal m^{-2}

(2) Animal biomass 4.5 g m^{-2} x 4.25 Cal g^{-1} = 19 Cal m^{-2}

(Whittaker and Likens, 1975)

(3) Energy storage in fire 0.3 Cal $m^{-2}d^{-1}$

Energy flow (See note 10)

Assume mean storage time of 1 min for forest fire

$$\frac{0.3 \text{ Cal } m^{-2}d^{-1} \times 1 \text{ min}}{1{,}400 \text{ min } d^{-1}} = 2 \times 10^{-4} \text{ Cal } m^{-2}$$

(4) Mass of soil (Brady, 1974)

Mean bulk density approximately 1.3 g cm^{-1}

Mean soil depth approximately 50 cm

$$\text{Soil mass} = \frac{(1 \times 10^{4} \text{ cm}^{2} \text{ m}^{-2})(1.3 \text{ g cm}^{-3})(50 \text{ cm})}{1{,}000 \text{ kg}^{-1}} = 650 \text{ kg m}^{-2}$$

(5) See note 4 of Table 1

(6) Gross primary production 2 x net primary production (E. P. Odum, 1971)

3.9 Cal $m^{-2}d^{-1}$ x 2 = 7.8 Cal $m^{-2}d^{-1}$

(7) Respiration = gross production - net primary production (E. P. Odum, 1971) 7.8 Cal $m^{-2}d^{-1}$ - 3.9 Cal $m^{-2}d^{-1}$ = 3.9 Cal $m^{-2}d^{-1}$

(8) Net primary production 0.92 g $m^{-2}d^{-1}$ (Whittaker and Likens, 1975)

0.92 g $m^{-2}d^{-1}$ x 4.25 Cal g = 3.9 Cal $m^{-2}d^{-1}$

(9) Consumption by herbivorous animals (Whittaker and Likens, 1975)

0.147 x 4.25 Cal g^{-1} = 0.62 Cal $m^{-2}d^{-1}$

(10) Plant biomass consumed by fire

Fire statistics, U.S., 1974 -- (Statistical Abstract of the United States, 1975)

Notes to Table 4 - Continued

Area in data sample	5.86×10^{12} m^2 for U.S.
Number of fires	1.45×10^5 in U.S.
Area burned	1.13×10^{10} m^2 in U.S.
Mean area per fire	7.8×10^4 m^2 for U.S.

Plants consumed by fire

Mean continental standing stock of biomass = 12 kg m^{-2}

(Whittaker and Likens, 1975)

$$\text{Energy consumed} = \frac{\text{Area burned}}{\text{Area of sample}} \times \text{Energy stored per unit area}$$

$$\frac{(1.3 \times 10^{10} m^2\ yr^{-1}) \times (12.2\ kg\ m^{-2}) \times (4.25 \times 10^3\ Cal\ kg^{-1})}{(5.86 \times 10^{12}\ m^2) \quad (365\ d\ yr^{-1})} =$$

0.3 Cal $m^{-2}d^{-1}$

As cross check: Energy released for forest fire 3.67×10^9 Cal in U.S. (Sellers, 1965)

$(7.8 \times 10^4\ m^2$ per fire$) \times (12.2\ kg\ m^{-2}) \times (4.25 \times 10^3\ Cal\ kg^{-1}) = 4 \times 10^9$ Cal

Thus this estimates is in good agreement with Sellers, 1965.

(11) Transpiration

338 g $m^{-2}d^{-1}$ (Skinner and Turekian, 1973)

(12) Energy dissipated in fire (see note 10)

0.3 Cal $m^{-2}d^{-1}$

(13) Respiration of animals

0.62 Cal $m^{-2}d^{-1}$ Set equal to consumption by first law (see note 9)

(14) Animal biomass lost by fire

$$\frac{\text{area burned}}{\text{area sample}} \times \text{Energy stored in animal biomass per unit area}$$

$$\frac{(1.13 \times 10^{10}\ m^2\ yr^{-1})}{(5.86 \times 10^{12}\ m^2)} \times \frac{(19\ Cal\ m^{-2})}{(365\ d\ yr^{-1})} = 1. \times 10^{-4}\ Cal\ m^{-2}d^{-1}$$

Notes to Table 4 - Continued

(15) New soil (see Table 5, note 10)

$0.51 \text{ g m}^{-2}\text{d}^{-1}$

(16) Erosion

$0.55 \text{ g m}^{-2}\text{d}^{-1}$ (see Table 5, note 10)

(17) World detritus production (Schlesinger, 1977):

$$\frac{(3.75 \times 10^{10} \text{ mt yr}^{-1})(8.5 \text{ Cal g}^{-1})(1 \times 10 \text{ g mt}^{-1})}{(5.1 \times 10^{14} \text{ m}^2)\ (365 \text{ d yr}^{-1})} = 2.13 \text{ Cal m}^{-2}\text{d}^{-1}$$

(18) World detritus stock measured (Schlesinger, 1977) in carbon:

$$\frac{(1.4 \times 10^{12} \text{ mt})(8.5 \text{ Cal g}^{-1})(1 \times 10^{6} \text{ g mt}^{-1})}{5.1 \times 10^{14} \text{ m}^2} = 2.4 \times 10^{4} \text{ Cal m}^{-2}$$

Notes to Table 5

(1) Mass of ocean crust

$$Q_{12} = \frac{7 \times 10^{21}\ \text{kg}}{3.61 \times 10^{14}\ \text{m}^2} = 1.94 \times 10^7\ \text{kg m}^{-2} \qquad \text{(Clark, 1971)}$$

(2) Mass of mantle of earth

$$Q_{13} = \frac{4 \times 10^{24}\ \text{kg}}{5.1 \times 10^{14}\ \text{m}^2} = 7.8 \times 10^9\ \text{kg m}^{-2} \qquad \text{(Clark, 1971)}$$

(3) World Fossil Fuel Reserve (United Nations Statistical Yearbook, 1975)

1974 Known Resource

Bituminous coal 1.07×10^{12} mt x 6×10^6 Cal $\text{mt}^{-1} = 6.42 \times 10^{18}$ Cal

Lignite coal 3.4×10^{11} mt x 4×10^6 Cal $\text{mt}^{-1} = 1.36 \times 10^{18}$ Cal

Petroleum 7.5×10^{10} mt x 1×10^7 Cal $\text{mt}^{-1} = 0.75 \times 10^{18}$ Cal

Gas 5.9×10^{13} m^3 x 9×10^3 Cal $\text{m}^{-3} = \underline{0.53 \times 10^{10}\ \text{Cal}}$

9.06×10^{18} Cal

$$\frac{9.06 \times 10^{18}\ \text{Cal}}{5.1 \times 10^4\ \text{m}^{-2}} = 1.78 \times 10^4\ \text{Cal m}^{-2}$$

Bituminous coal 4.30×10^{11} mt x 6×10^6 Cal $\text{mt}^{-1} = 2.58 \times 10^{18}$

Lignite coal 1.60×10^{11} mt x 4×10^6 Cal $\text{mt}^{-1} = 0.64 \times 10^{18}$

Petroleum 7.3×10^{10} mt x 1×10^7 Cal $\text{mt}^{-1} = 0.75 \times 10^{18}$

Gas 5.9×10^{13} m^3 x 9×10^3 Cal $\text{m}^{-3} = 0.53 \times 10^{18}$

Chemical energy stored in earth's crust from organic deposits of oil, coal, gas, etc.

Coal and lignite	7.78×10^{18} Cal
Natural Gas	0.53×10^{18} Cal
Petroleum liquids	0.75×10^{18} Cal
Tar sands oil	0.44×10^{18} Cal
Shale oil	0.27×10^{18} Cal

Notes to Table 5 - Continued

$$Q_{14} = \frac{9.77 \times 10^{18} \text{ Cal}}{5.1 \times 10^{14} \text{ m}^{-2}} = 1.9 \times 10^{4} \text{ Cal m}^{-2}$$

(4) Stress energy stored in crust of earth generated by mean plate motion of 2 cm per year.

Annual release of seismic energy (Richter, 1958)

2.14×10^{14} Cal yr^{-1}

Assuming 11 yr average period for earthquakes

$$\frac{2.15 \times 10^{14} \text{ Cal yr}^{-1} \times 11 \text{ yr}}{5.1 \times 10^{14} \text{ m}^{2}} = 4.6 \text{ Cal m}^{-2}$$

(5) Mass continental crust of earth (Clark, 1971)

$$Q_{15} = \frac{1.6 \times 10^{22} \text{ kg}}{1.49 \times 10^{14} \text{ m}^{2}} = 1.07 \times 10^{8} \text{ kg m}^{-2}$$

(6) Storage of energy in volcanoes

9.6×10^{13} Cal yr^{-1} Energy released by volcanoes (Hayakawa, 1976)

Assume 1 hr turnover time

$$\frac{9.6 \times 10^{13} \text{ Cal yr}^{-1} \times 1 \text{ hr (turnover time)}}{(5.1 \times 10^{14} \text{ Cal m}^{-2}) \times (8.7 \times 10^{3} \text{ hr yr}^{-1})} = 2.2 \times 10^{-5} \text{ Cal m}^{-2}$$

(7) Storage energy in active earthquake

Annual energy release

2.15×10^{14} Cal yr^{-1} (Richter, 1958)

Assume average life of earthquake of one minute

$$\frac{2.15 \times 10^{14} \text{ Cal yr}^{-1} \times 1 \text{ min/earthquake}}{(5.1 \times 10^{14} \text{ m}^{2})\,(5.25 \times 10^{5} \text{ min yr}^{-1})} = 8 \times 10^{-7} \text{ Cal m}^{-2}$$

(8) Mantle flowing into ocean trench to form new ocean crust

$$\frac{(4.6 \times 10^{13} \text{ kg yr}^{-1})(10^{3} \text{ g kg}^{-1})}{(3.6 \times 10^{14} \text{ m}^{2})(365 \text{ d yr}^{-1})} = 0.35 \text{ g m}^{-2}\text{d}^{-1}$$

Ocean plates to recycle in 1.5×10^{8} yr (Clark, 1971)

Notes to Table 5 - Continued

$$\frac{(0.7 \times 10^{22}\ \text{kg})\ (10^{3}\ \text{g kg}^{-1})}{3.61 \times 10^{14}\ \text{m}^{2})(1.3 \times 10^{8}\ \text{yr}) \times (365\ \text{d yr}^{-1})} = 0.35\ \text{g m}^{-2}\text{d}^{-1}$$

(9) Ocean crust lost to mantle

$$\frac{7.6 \times 10^{13}\text{kg yr}^{-1})(10^{3}\ \text{g kg}^{-1})}{(3.61 \times 10^{14}\ \text{m}^{2}) \times 365\ \text{d yr}^{-1}} = 0.58\ \text{g m}^{-2}\text{d}^{-1}$$

balances new crust formed in note 8 and sediments in note 10

$$\frac{((4.6 \times 10^{13} + 3 \times 10^{13})\ \text{kg yr}^{-1})(10^{3}\ \text{g kg}^{-1})}{(3.61 \times 10^{14}\ \text{m}^{2}) \times 365\ \text{d yr}^{-1}} = 0.58\ \text{g m}^{-2}\text{d}^{-1}$$

(10) Global erosion driven by world stream flow (Clark, 1971)

$$\frac{3 \times 10^{13}\ \text{kg yr}^{-1}}{1.49 \times 10^{14}\,\text{m}^{2} \times 365\ \text{d yr}^{-1}} = 0.55\ \text{g m}^{-2}\text{d}^{-1};$$

however, sea is 2.4 times larger than land therefore sediments =

$$\frac{0.55\ \text{g m}^{-2}\text{d}^{-1}}{2.4} = 0.23\ \text{g m}^{-2}\text{d}^{-1}$$

(11) Stress by ocean plates

Average plate velocity (Clark, 1971)

2 cm yr^{-1}

(12) Stress energy buildup from 2 cm average motion of tectonic plates of the earth's crust (Clark, 1971)

(13) Stress energy consumed by earthquakes by conservation of energy.

Stress energy consumed = uplift + earthquakes + heat loss

Stress energy consumed = 0.05 + 0.005 + 0.1 = 0.155

(14) Energy required in uplift process

m = annual uplift 7×10^{13} kg yr^{-1}

g = $9.98 \times \text{m sec}^{-2}$

$$H = \frac{\text{continental crust-ocean crust}}{2} = \frac{40\ \text{km} - 7\ \text{km}}{2 \times 10^{-3}\,\text{km m}^{-1}} = 1.65 \times 10^{4}\ \text{m}$$

Notes to Table 5 - Continued

$$E = mgh = 7 \times 10^{13}\ \text{kg yr}^{-1} \times 9.88\ \text{m sec}^{-2} \times 1.65 \times 10^{4}\ \text{m} \times 2.39 \times 10^{-4}\ \text{Cal J}^{-1}$$

$$E = 2.75 \times 10^{15}\ \text{Cal yr}^{-1}$$

$$E = \frac{2.75 \times 10^{15}\ \text{Cal yr}^{-1}}{(1.49 \times 10^{14}\ \text{m}^2) \times 365\ \text{d yr}^{-1}} = 0.05\ \text{Cal m}^{-2}\text{d}^{-1}$$

(15) Energy dissipated in earthquake process

$$\frac{1 \times 10^{15}\ \text{Cal yr}^{-1}}{(5.1 \times 10^{14}\ \text{m}^2)\ 365\ \text{d yr}^{-1}} = 5.4 \times 10^{-3}\ \text{Cal m}^{-2}\text{d}^{-1}$$

(16) Global seismic energy released by earthquakes (Richter, 1958)

$$\frac{2.15 \times 10^{14}\ \text{Cal yr}^{-1}}{5.1 \times 10^{14}\ \text{m}^2) \times 365\ \text{d yr}^{-1}} = 1.15 \times 10^{-3}\ \text{Cal m}^{-2}\text{d}^{-1}$$

(17) Stress in earth's crust dissipated as heat, must exist by second law of thermodynamics taken as twice uplift as a minimum possible estimate (see note 14 for uplift calculation)

$$0.05\ \text{Cal m}^{-2}\text{d}^{-1} \times 2 = 0.1\ \text{Cal m}^{-2}\text{d}^{-1}$$

(18) Rate of formation of new soil set equal to erosion of soil

$$\frac{(3 \times 10^{13}\ \text{kg yr}^{-1})(1 \times 10^{3}\ \text{g kg}^{-1})}{(1.6 \times 10^{14}\ \text{m}^2)\ (365\ \text{d yr}^{-1})} = 0.51\ \text{g m}^{-2}\text{d}^{-1}$$

(19) Net production of fossil fuel

Working with an estimated coal rate of 3×10^{9} mt yr^{-1} (Hubbert, 1971). (Note: this estimate may be low)

$$\frac{(3 \times 10^{9}\ \text{mt yr}^{-1})(1 \times 10^{6}\ \text{g mt}^{-1})(6\ \text{Cal g}^{-1})}{(365\ \text{d yr}^{-1})(5.14 \times 10^{14}\ \text{m}^2)0.88\ (\text{coal \% of fossil fuel})} =$$

$$0.11\ \text{Cal m}^{-2}\text{d}^{-1}$$

Heat loss in fossil fuel production must exist by second law of thermodynamics. Minimum value assumed of two times production.

$$0.11\ \text{Cal m}^{-2}\text{d}^{-1} \times 2 = 0.22\ \text{Cal m}^{-2}\text{d}^{-1}$$

Notes to Table 5 - Continued

(20) Gross production of fossil fuel

Gross = Net + heat loss

Gross = (0.11 + 0.22) Cal $m^{-2}d^{-1}$ = 0.33 Cal $m^{-2}d^{-1}$

(21) World fossil fuel consumption

1937 1.9×10^9 Metric tons Coal equivalent

(Oxford Economic Atlas of the World, 1965)

$$\frac{(1.91 \times 10^9 \text{ T yr}^{-1})(1 \times 10^6 \text{ g T}^{-1})(5.5 \text{ Cal g}^{-1})}{(5.1 \times 10^{14} \text{ m}^2)(365 \text{ d yr}^{-1})} = 0.056 \text{ Cal m}^{-2}\text{d}^{-1}$$

1960 4.31×10^9 Metric tons Coal equivalent

(Oxford Economic Atlas of the World, 1965)

$$\frac{(4.13 \times 10^9 \text{ T yr}^{-1})(1 \times 10^6 \text{ g T}^{-1})(5.5 \text{ Cal g}^{-1})}{(5.1 \times 10^{14} \text{ m}^2)(365 \text{ d yr}^{-1})} = 0.127 \text{ Cal m}^{-2}\text{d}^{-1}$$

1971 7.14×10^9 Metric tons Coal Equivalent

(United Nations Statistical Year Book, 1975, 1976)

$$\frac{(7.14 \times 10^9 \text{ T yr}^{-1})(1 \times 10^6 \text{ g T}^{-1})(5.5 \text{ Cal g}^{-1})}{(5.1 \times 10^{14} \text{m}^2)(365 \text{ d yr}^{-1})} = 0.21 \text{ Cal m}^{-2}\text{d}^{-1}$$

1974 7.95×10^9 yr^{-1} (United Nations Statistical Year Book, 1975)

$$\frac{(7.95 \times 10^9 \text{ T yr}^{-1})(1 \times 10^6 \text{ g T}^{-1})(5.5 \text{ Cal g}^{-1})}{(5.1 \times 10^{14} \text{m}^2)(365 \text{ d yr}^{-1})} = 0.23 \text{ Cal m}^{-2}\text{d}^{-1}$$

Fossil fuel consumption (1970) (Hubbert, 1971)

$$\frac{(4 \times 10^{13} \text{KWH yr}^{-1})(859 \text{ Cal KWH}^{-1})}{(5.1 \times 10^{14} \text{m}^2)(365 \text{ d yr}^{-1})} = 0.18 \text{ Cal m}^{-2}\text{d}^{-1}$$

(22) Global energy released annually by volcanoes

$$\frac{9.6 \times 10^{13} \text{Cal yr}^{-1}}{(5.1 \times 10^{14}) \times 365 \text{ d yr}^{-1}} = 5.1 \times 10^{-4} \text{ Cal m}^{-2}\text{d}^{-1} \text{(Hayakawa, 1976)}$$

(23) Heat dissipated in volcanic process by second law must exist estimated twice volcanic release in note 20

$(5 \times 10^{-4} \text{ Cal m}^{-2}\text{d}^{-1}) \times 2 = 1 \times 10^{-3} \text{ Cal m}^{-2}\text{d}^{-1}$

Notes to Table 5 - Continued

(24) Energy consumed by volcanoes by law of energy consumption

$(1 \times 10^{-3} + 5 \times 10^{-4})$ Cal $m^{-2}d^{-1} = 1.5 \times 10^{-3}$ Cal $m^{-2}d^{-1}$

(25) Deep heat

$$\frac{1.9 \times 10^{17}\ \text{Cal yr}^{-1}}{(5.1 \times 10^{14}\ \text{m}^2) \times (365\ \text{d yr}^{-1})} = 1\ \text{Cal m}^{-2}\text{d}^{-1}$$ (Hayakawa, 1976)

(26) Energy storage in floods

Assume 1 hr turnover time (see note 19 for consumption)

$$Q_{11} = \frac{\text{consumption}}{\text{turnover time}} = \frac{0.04\ \text{Cal m}^{-2}\text{d}^{-1} \times 1\ \text{hr}}{24\ \text{hr d}^{-1}} = 1.7\ \text{Cal m}^{-3}$$

(27) Energy consumed by floods

Mass 10% of continental rain $(9.9 \times 10^{15}$ kg$)(0.1) = 9.9 \times 10^{14}$ kg

Elevation 1,000 m

$E = mgh = 9.9 \times 10^{14}$ kg $g^{-1} \times 9.9$ m $sec^{-2} \times 1{,}000$ m $\times 2.3 \times 10^{-4}$ Kg^{-1} $m^{-2}sec$ Cal =

$$E = \frac{2.3 \times 10^{15}\ \text{Cal yr}^{-1}}{(1.49 \times 10^{14}\ \text{m}^2) \times (365\ \text{d yr}^{-1})} = 0.04\ \text{Cal m}^{-2}\text{d}^{-1}$$

(28) Flow of water in world's rivers to produce erosion of continental crust to ocean crust

$$\frac{0.99 \times 10^{20}\ \text{g yr}^{-1}}{(3.6 \times 10^{14}\ \text{m}^2)\ (365\ \text{d yr}^{-1})} = 753\ \text{g m}^{-2}\text{d}^{-1}$$ precipitation on land

(Skinner and Turekian, 1973)

(29) Erosion to sea (Skinner and Turekian, 1973)

$$\frac{3 \times 10^{13}\ \text{kg yr}^{-1}}{(3.6 \times 10^{14}\ \text{m}^2)} = 0.23\ \text{g m}^{-2}\text{d}^{-1}$$

(30) Energy dissipated in floods set equal to energy consumption for conservation of energy (see note 19)

0.04 Cal $m^{-2}d^{-1}$

Notes to Table 6

(1) Energy storage of cities

8% depreciation rate

2% fire loss

1% war loss

0.5% disaster loss

11.5% total loss

$$\frac{\text{consumption}}{\text{depreciation}} = \frac{0.45 \text{ Cal m}^{-2}\text{d}^{-1} \times 365\text{d}}{0.115} = 1{,}400 \text{ Cal m}^{-2}$$

(2) Energy consumed by cities (Hubbert, 1971)

Consumption of forest fuel; 1970

0.18 Cal $m^{-2}d^{-1}$ (See note 21, Table 4)

Consumption of biomass, 1970 (Whittaker and Likens, 1975)

0.27 Cal $m^{-2}d^{-1}$

Total consumption 0.45 Cal $m^{-2}d^{-1}$

(3) Air pollution from cities

Release of 1/4.25 g Cal^{-1}

$$\frac{0.45 \text{ Cal}}{4.25 \text{ Cal g}^{-1}} = 0.1 \text{ g m}^{-2}\text{d}^{-1}$$

(4) Energy dissipated by cities equal consumption by conservation of energy less growth (see note 7)

0.45 Cal $m^{-2}d^{-1}$

(5) Operation of urban structure (Solow, 1954)

Estimated depreciation and obsolescence for capital assets

8% of stock per year

$$\frac{(1{,}400 \text{ Cal m}^{-2})(0.08) \text{ yr}^{-1}}{365 \text{ d yr}^{-1}} = 0.31 \text{ Cal m}^{-2}\text{d}^{-1}$$

Notes to Table 6 - Continued

(6) Fire loss estimated from U.S. data (United States Statistical Abstract, 1975)

$$\frac{\text{Total urban loss for 1965 due to fire}}{\text{National wealth}} \quad \frac{2.5 \times 10^{9}\ \text{yr}^{-1}}{14.5 \times 10^{16}} =$$

$$\frac{(1{,}400\ \text{Cal m}^{-2})(0.017)\ \text{yr}^{-1}}{365\ \text{d yr}^{-1}} = 0.065\ \text{Cal m}^{-2}\text{d}^{-1}$$

(7) Energy dissipated by fire set equal to consumption in note 6 $0.065\ \text{Cal m}^{-2}\text{d}^{-1}$

(8) Energy stored in urban fire. Assume 1 hr turnover time

$$\frac{0.065\ \text{Cal m}^{-2}\text{d}^{-1} \times 1\ \text{hr}}{24\ \text{hr d}^{-1}} = 2.7 \times 10^{-3}\ \text{Cal m}^{-2}$$

(9) Energy consumed by war (Statistical Abstract of U.S., 1975)

World Military Expenditures (1973) 2.7×10^{11} \$ yr^{-1}

World Per Capita GNP in 1968 dollars \$600 (Meadows *et al*., 1974)

World Population 3.78×10^{9} people (Statistical Abstract of U.S., 1975)

$$\frac{2.7\ \text{s}\ 10^{11}\ \$\ \text{yr}}{(660\ \$\ \text{people}^{-1})(3.78 \times 10^{-7}\ \text{people})} = 0.11$$

War consumption of energy $= 0.45\ \text{Cal m}^{-2}\text{d}^{-1} \times 0.11 = 0.05\ \text{Cal m}^{-2}\text{d}^{-1}$

(10) War dissipation set equal to consumption of $0.05\ \text{Cal m}^{-2}\text{d}^{-1}$ from note 9.

(11) Energy stored in war equipment assuming 5-yr lifetime of war equipment

$$\frac{0.05\ \text{Cal m}^{-2}\text{d}^{-1}\ 365\ \text{d yr}^{-1}}{0.2} = 90\ \text{Cal m}^{-2}$$

(12) Disaster losses for U.S. in 1964 dollars (Dacy and Kunreuther, 1969)

Notes to Table 6 - Continued

(1950-1965 averages)		Fraction of US GNP	Fraction of wealth
Storms	$2.3 \times 10^{8}\ \$\ yr$	0.005	0.0016
Floods	$2.1 \times 10^{8}\ \$\ yr^{-1}$	0.0045	0.0015
Earthquakes	$1.9 \times 10^{8}\ \$\ yr^{-1}$	0.014	0.0014
	6.3×10	0.014	0.0045

Where GNP = $4.6 \times 10^{10}\ \$\ yr^{-1}$

National wealth = $14.5 \times 10^{10}\ \$$

Energy loss due disaster

(0.45 Cal $m^{-2}d^{-1}$ consumption)(0.014 = 6.3 10^{-3} Cal $m^{-2}d^{-1}$)

Notes to Table 7

(1) Calculations for storm loss based on U.S. data

1950-1956 Average annual U.S. loss (Dacy and Kunreuther, 1969)

Storms

Hurricanes	1.7×10^8 \$$\text{yr}^{-1}$
Tornados	0.5×10^8 \$$\text{yr}^{-1}$
Strom total	2.2×10^8 \$$\text{yr}^{-1}$

$$\frac{2.2 \times 10^8 \ \$\text{yr}^{-1} \text{ (U.S. storm loss)}}{4.6 \times 10^8 \ \$\text{yr}^{-1} \text{ (U.S. GNP)}} = 4.8 \times 10^{-3}$$

Energy embodied in loss due to storms calculated based on energy consumption of cities

$(0.45 \text{ Cal m}^{-2}\text{d}^{-1}) \times (4.8 \times 10^{-3}) = 2.1 \times 10^{-3} \text{ Cal m}^{-2}\text{d}^{-1}$

Storm energy to cities $0.014 \text{ Cal m}^{-2}\text{d}^{-1}$ (Note 4)

Disaster-amplifier ratio in Calories heat equivalent

$$\frac{\text{Energy Disordered}}{\text{Storm flow}} = \frac{2.1 \times 10^{-3} \text{ Cal m}^{-2}\text{d}^{-1}}{0.014 \text{ Cal m}^{-2}\text{d}^{-1}} = 0.16 \text{ Cal Cal}^{-1}$$

Disaster-amplifier ratio in embodied solar energy

$$\text{Ratio in } \frac{(2.1 \times 10^{-3} \text{ Cal m}^{-2}\text{d}^{-1}\text{city})(1.5 \times 10^{4}) \text{ Cal Cal}^{-1}\text{city}^{-1}}{0.014 \text{ Cal m}^{-2}\text{d}^{-1} \ (1.7 \times 10^{3}) \text{ Cal Cal}^{-1}}$$

1.4 Solar Cal per Solar Cal

(2) Calculation for floods based on U.S. data

1950-1965 average annual flood loss (Dacy and Kunreuther, 1959)

Floods 2.1×10^8 \$$\text{yr}^{-1}$

$$\frac{2.1 \times 10^8 \ \$\text{yr}^{-1} \text{ (Flood loss)}}{4.6 \times 10^{10} \ \$\text{yr}^{-1} \text{ (GNP)}} = 4.6 \times 10^{-3}$$

Flood energy loss $(0.45 \text{ Cal m}^{-2}\text{d}^{-1})(4.6 \times 10^{-3})$

$= 2.1 \times 10^{-3} \text{ Cal m}^{-2}\text{d}^{-1}$

Flood energy to cities 1.4×10^{-4} (Note 4)

Notes to Table 7 - Continued

Disaster-amplifier ratio

$$\frac{2.1 \times 10^{-3} \text{ Cal m}^{-2}\text{d}^{-1}}{1.4 \times 10^{-4} \text{ Cal m}^{-2}\text{d}^{-1}} = 15 \text{ Cal Cal}^{-1}$$

Disaster-amplifier ratio in embodied solar energy

$$\frac{(2.1 \times 10^{-3} \text{ Cal m}^{-2}\text{d}^{-1})\ 1.5 \times 10^{4}}{(1.4 \times 10^{-4} \text{ Cal m}^{-2}\text{d}^{-1})(1.7 \times 10^{5})} = 1.3 \text{ Solar Cal per Solar Cal}$$

(3) Earthquake loss based on U.S. data (Dacy and Kunreuther, 1969)

1950-1965 averages

$$\frac{\text{Earthquake loss } 1.9 \times 10 \ \$\text{yr}^{-1}}{\text{GNP} \quad 4.6 \times 10 \ \$\text{yr}^{-1}} = 4.1 \times 10^{-3}$$

Energy loss $(0.45 \text{ Cal m}^{-2}\text{d}^{-1})\ (4.1 \times 10^{-3}) = 1.85 \times 10^{-3} \text{ Cal m}^{-2}\text{d}^{-1}$

Seismic energy to cities $3.4 \times 10^{-6} \text{ Cal m}^{-2}\text{d}^{-1}$ (Note 4)

$$\text{Disaster-amplifier ratio} = \frac{1.85 \times 10^{-3} \text{ Cal m}^{-2}\text{d}^{-1}}{3.4 \times 10^{-6} \text{ Cal m}^{-2}\text{d}^{-1}} = 539 \text{ Cal Cal}^{-1}$$

Disaster-amplifier ratio in embodied solar energy

$$\frac{(1.85 \times 10^{-3} \text{ Cal m}^{-2}\text{d}^{-1})(1.5 \times 10^{4})}{(3.4 \times 10^{-6} \text{ Cal m}^{-2}\text{d}^{-1})\ (4.7 \times 10^{6})} = 1.7 \text{ Solar Cal per Solar Cal}$$

(4) Disaster energy available tocities and urban places

World mean urban plus industrial area per person

500 m^2 (Meadows _et al_., 1974)

Fraction of world surface area urban

$$\frac{500 \text{ m}^2 \text{ per person} \times 3.5 \times 10^{9} \text{ people}}{5.1 \times 10^{14} \text{ m}^2} = 0.0034$$

Storm energy absorbed (Table 2, note 18)

$4 \text{ Cal m}^2 \times 0.0034 = 0.014 \text{ Cal m}^{-2}\text{d}^{-1}$

Flood energy absorbed (Table 5, note 17)

$0.04 \times 0.0034 = 1.4 \times 10^{-4} \text{ Cal m}^{-2}\text{d}^{-1}$

Seismic energy absorbed (Table 5, note 16)

$0.001 \times 0.0034 = 3.4 \times 10^{-6} \text{ Cal m}^{-2}\text{d}^{-1}$

Notes to Table 9

Documentation of Order-Disorder Model of Gamma Ray Radiation Stress

(1) Source = 1 x 10^4Ci of ^{137}Cs which has 0.662 MeV γ 97%

$\dot{X} = (1 \times 10^4 \text{ Ci})(3.7 \times 10^{10} \text{ dis sec}^{-1}\text{Ci}^{-1})(0.662 \times 0.92) \text{ MeV dis}^{-1}$

$(1.6 \times 10^{-6} \text{ erg MeV}^{-1})$

$\dot{X} = 3.6 \times 10^8 \text{ erg sec}^{-1} = 3.11 \times 10^{13} \text{ ergs d}^{-1} = 744.5 \text{ Cal d}^{-1}$

(2) Energy absorbed by forest air

biomass of rain forest = 42,450 g m^{-2} - canopy height = 20 m

(Odum, 1970c)

$$\frac{42{,}950 \text{ g m}^{-2}}{20 \text{ m} \times 10^6\text{cm}^3\text{m}^3} = 0.0021 \text{ g cm}^{-3}$$

density of air is 0.0012 g cm^{-3} thus total density is 0.0033 g cm^{-3}

with path of 25 m (2,500 cm) and absorption of 0.02 cm^2 g

$K = (2{,}000 \text{ cm})(0.0033 \text{ g cm}^{-3})(0.02 \text{ cm}^2\text{g}^{-1} = 0.132$

(3) Thus (0.132)(744.5 Cal d^{-1}) = 98.27 Cal d^{-1} absorbed

Therefore 744.5 Cal - 98.27 Cal d^{-1} = 646.2 Cal d^{-1}

(4) Inverse square effect:

$4\pi r^2 = 4 \times 3.14 \times (2{,}000 \text{ cm}^2) = 5.02 \times 10^7 \text{ cm}^2$

(5) Exposure per cm^2:

$$\frac{646.2 \text{ Cal d}^{-1}}{5.02 \times 10^7 \text{ cm}^2} = 1.28 \times 10^{-5} \text{ Cal cm}^{-2}\text{d}^{-1}$$

(6) $(1.28 \times 10^{-5} \text{ Cal cm}^{-2} \text{ d}^{-1})(43{,}950 \text{ g m}^{-2})(1 \text{ cm}^3\text{g}^{-1}) = 0.552 \text{ Cal}^{-2}\text{d}$

(7) Absorbed dose:

$(0.02 \text{ cm g}^{-1})(1.28 \times 10^{-5} \text{ Cal cm}^{-2}\text{d}^{-1}) = 2.56 \times 10^{-7} \text{ Cal}^{-1}\text{d}^{-1}$

$2.56 \times 10^{-7} \text{ Cal g d}^{-1} = 2.56 \times 10^{-7} \text{ Cal g}^{-1} \text{ day} \times 4.184 \times 10^{10} \text{ ergs Cal}^{-1}$

$= 1.07 \times 10^4 \text{ ergs}^{-1}$

$1.071 \times 10^4 \text{ ergs } 0.01 \text{ rad erg}^{-1}\text{d}^{-1} = 107.1 \text{ rad d}^{-1}$

Notes to Table 9 - Continued

(8) Total absorbed dose/m^2:

$(43{,}950\ g\ m^{-2})(2.56 \times 10^{-7} Cal\ g^{-1} d^{-1}) = 1.099 \times 10^{-2} Cal\ m^2\ d^{-1}$

(9) Solar insulation daily mean (Odum *et al.*, 1970)

$3{,}830\ Cal\ m^{-2} d^{-1}$

(10) Gross primary production of rain forest at El Verde (Odum, 1970c)

in g organic matter

$32\ g\ m^{-2}$

(11) Gross primary production of a rain forest (Odum, 1970c)

in energy units

$(32\ g\ m^{-2} d^{-1})\ (4.25\ Cal\ g^{-1}) = 145\ Cal\ m^{-2} d^{-1}$

(12) Biomass of rain forest in g organic matter (Odum, 1970c)

$42{,}450\ g\ m^{-2}$

(13) Litter biomass of forest (Odum, 1970c)

$14{,}630\ g\ m^{-2}$

(14) Respiration assumed, based on reported system response (Odum, 1970c)

$22\ g\ m^{-2} d^{-1}$

(15) Radiation induced disorder, assumed based on reported system response (Odum, 1970c)

$10\ g\ m^{-2} d^{-1}$ at 20 m from source

Notes to Table 10

Johnstown Flood

(1) Rainfall into South Fork basin

Rainfall 6 - 8 in/12 hr (Engineering Society of Western Pennsylvania, 1889)

using 7 in/12 hr

$7 \text{ in}/12 \text{ hr} \times 0.0254 \text{ m in}^{-1} \times 2.77 \times 10^{-4} \text{ hr sec}^{-1} = 4.1 \times 10^{-6} \text{msec}^{-1}$

Given a total basin area of 60 sq mi

$60 \text{ sq mi} \times 2.59 \times 10^{6} \text{ m}^{2} \text{ mi}^{-2} = 1.554 \times 10^{8} \text{m}^{2}$

Rainfall into basin therefore is

Rainfall x land area

$4.1 \times 10^{-6} \text{ m sec}^{-1} \times 1.554 \times 10^{8} \text{m}^{2} = 637 \text{ m}^{3} \text{ sec}^{-1}$

Shappee (1940) calculated 591 $\text{m}^{3} \text{ sec}^{-1}$

(2) Flow into reservoir

rate in = increased + rate out

rate in = $199 \text{ m}^{3} \text{ sec}^{-1} + 169.0 \text{ m}^{3} \text{ sec}^{-1} = 368 \text{ m}^{3} \text{ sec}^{-1}$

second reference gives 283 $\text{m}^{3} \text{ sec}^{-1}$ (Shappee, 1940)

(3) Water loss from reservoir - designed rate

3,500 $\text{ft}^{3} \text{ sec}^{-1}$ (Engineering Society of Western Pennsylvania, 1889)

$3{,}500 \text{ ft}^{3} \text{ sec}^{-1} \times 2.83 \times 10^{-2} \text{m}^{3} \text{ ft}^{-3} = 9{,}910 \text{ m}^{3} \text{ sec}^{-1}$

Spillway max, (Shappee, 1940) - 6,000 $\text{ft}^{3} \text{ sec}^{-1} = 169 \text{ m}^{3} \text{ sec}^{-1}$

(4) Water over top of dam, center

4,000 $\text{ft}^{3} \text{ sec}^{-1}$ (Shappee, 1940)

$4{,}000 \text{ ft}^{3} \text{ sec}^{-1} \times 2.83 \times 10^{-2} \text{m}^{3} \text{ ft}^{-3} = 133 \text{ m}^{3} \text{ sec}^{-1}$

(5) Turbulence from overflow (note 4 - note 6)

$133 \text{ m}^{3}\text{sec}^{-1} - 99 \text{ m}^{3}\text{sec}^{-1} = 34 \text{ m}^{3} \text{ sec}^{-1}$

Notes to Table 10 - Continued

(6) Spillway 10 m long (Shappee, 1940)

$99\ m^3\ \ sec^{-1}$

(7) Volume of South Fork reservoir (Engineering News, 1889)

$4.8 \times 10^8\ \ ft^3$

$4.8 \times 10^8\ \ ft^3 \times 2.83 \times 10^{-2}\ m^2\ ft^{-3} = 1.35 \times 10^7 m^3$

(8) Spillway storage capacity (Engineering News, 1889)

$1{,}690\ m^3$

(9) Land area of South Fork Valley (Engineering News, 1889a)

$1.55 \times 10^8\ m^2$

(10) Slope (Engineering News, 1889a)

Land covered by reservoir

Calculated by dividing reservoir capacity by depth.

Reservoir depth 62 ft

$62\ ft \times 0.3049\ m\ ft^{-1} = 18.9\ m$

(11) Tangible assets of Johnstown, Pennsylvania (Historical Statistics of the United States, 1976)

1889 U.S. per capita tangible assets

$$\frac{1.795 \times 10^{11}\ \text{(series F447)}}{7.59 \times 10^7\ \text{people}} = \$2{,}365\ \text{per person}$$

Johnstown Population (1889) 10,000 (McCullough, 1968)

Johnstown Tangible Assets (1889)

$$(\$2{,}365/\text{person})\ (10{,}000\ \text{people}) = 2.4 \times 10^7$$

$$\text{Energy value of 1889 dollar} = \frac{\text{Gross Energy Consumption}}{\text{Gross Product}}\ \begin{matrix}\text{(note 10)}\\ \text{(note 10)}\end{matrix}$$

$$\frac{(1.4 \times 10^9\ Cal\ d^{-1})\ (365\ d\ yr^{-1})}{(\$4.61 \times 10^6 yr^{-1})} = 1.1 \times 10^5\ Cal\ \$^{-1}$$

Energy value of Johnston ($\$2.4 \times 10^7$) ($1.1 \times 10^5$ Cal $\$^{-1}$) =

$$2.6 \times 10^{12}\ Cal$$

Notes to Table 10 - Continued

(12) Land area of Johnstown

1.10×10^6 m^2 (USGS Map, Johnstown, Pennsylvania, 1964)

(McCullough, 1968)

(13) Natural resources

Estimated forest area,

2×10^8 m^2 (USGS Map, Johnstown, Pennsylvania, 1964)

Mean biomass standing stock for deciduous temperate forest

30 kg m^{-2} (Whittaker and Likens, 1975)

Total standing stock

$(2 \times 10^8 \text{m}^2)(30 \text{ kg m}^{-2})(4.25 \times 10^3 \text{ Cal kg}) = 2.55 \times 10^{13}$ Cal

(14) Coal reserve, Johnstown

Est. $1 \times 10^4 \times 1889$ annual consumption

$1 \times 10^9 \text{ Cal d}^{-1} \times 365 \text{d yr}^{-1} \times 10^4 \text{yr} = 3 \times 10^{15}$Cal

(15) Net primary production of natural system (Whittaker and Likens, 1973)

Land area 2×10^8 m^2

Mean net primary production for deciduous temperate forest

$$\frac{(1{,}200 \text{ g yr}^{-1}\text{m}^{-2})(4.25 \text{ Cal g}^{-1})(2 \times 10^8\text{m}^2)}{365 \text{ d yr}^{-1}} = 2.8 \times 10^9 \text{Cal d}^{-1}$$

(16) Resource consumption

US consumption of timber products 1900

Historical Statistics of United States (1975)

$$\frac{(7.14 \times 10^9 \text{ft}^3 \text{yr}^{-1})(.0283 \text{ m}^{-3} \text{ ft}^{-3})\ (8 \times 10^5 \text{g m}^3)\ (4.25 \text{ Cal g}^{-1})}{(365 \text{ d yr}^{-}\ )\ 7.59 \times 10^7 \text{ people}}$$

2.4×10^4 Cal d^{-1} person^{-1}

Food energy U.S. per capita 1909 (Historical Statistics of U.S., 1975)

Notes to Table 10 - Continued

3.5×10^4 Cal d^{-1} $person^{-1}$

Firewood 44% value of forest products for 1900

Estimated consumption

$1. \times 10^4$ Cal d^{-1} person

Total renewable resource consumption

Timber products 2.4×10^4 Cal d^{-1} person

Fuel wood 1×10^4 Cal d^{-1} person

Food 0.3×10^4 Cal d^{-1} person

3.8×10^4 Cal d^{-1}person

Total consumption estimate for Johnstown 1889

$(3.8 \times 10^4 \text{ Cal } d^{-1}) \times (10{,}000 \text{ people}) = 3.8 \times 10^8 \text{ Cal } d^{-1}$

(17) Respiration of natural system

Production - Consumption

$2.8 \times 10^9 \text{ Cal } d^{-1} - 3.8 \times 10^8 \text{ Cal } d^{-1} = 2.4 \times 10^9 \text{ Cal } d^{-1}$

(18) Land consumption

Based on 50% land in valley occupied, low density in Johnstown (McCullough, 1968)

$$\frac{(1.1 \times 10^6 \ m^2)\ (.5 \text{ occupied})}{1.8 \times 10^{12} \text{ Cal}} = 3 \times 10^{-7} \ m^2 \text{Cal}^{-1}$$

(19) Johnstown coal consumption (Statistical Abstract of the United States, 1971)

Based on 1920 data

1.5×10^8 BTU/person $\times$ 0.252 Cal BTU^{-1} = 3.8 x 10 Cal yr^{-1} person

$$\frac{3.8 \times 10^7 \text{ Cal } yr^{-1}}{365 \ d \ yr^{-1}} = 10{,}000 \text{ people} = 1.0 \times 10^9 \text{ Cal } d^{-1}$$

(20) Energy value of gross regional production (1889)

Natural (note 6) = 0.38×10^9 Cal d^{-1}

Notes to Table 10 - Continued

$$\text{Fossil Fuel} = \frac{1.0 \times 10^9 \text{ Cal d}^{-1}}{1.4 \times 10^9 \text{ Cal d}^{-1}}$$

$$\frac{\text{Gross National Product}}{\text{Population}} = \frac{3.5 \times 10^{10}}{7.59 \times 10^7} \qquad \text{(1929 dollars)}$$

$(\$461 \text{ person}^{-1})(10{,}000) = \$4{,}610{,}000$

(21) Net regional product (Historial Statistics of U.S., 1975)

$$\frac{\text{Net National Product}}{\text{Population}} = \frac{\$3.1 \times 10^{10}}{7.89 \times 10^9} = \$408 \text{ person}^{-1}$$

$408 person x 1,000 people = $4,080,000

$$\frac{\text{Net regional product}}{\text{Gross regional product}} = \frac{4{,}080{,}000}{4{,}610{,}000} = 0.88$$

Net Johnstown consumption

$(1.4 \times 10^9 \text{ Cal d}^{-1})(0.88) = 1.2 \times 10^9 \text{ Cal d}^{-1}$

(22) Depreciation 8% (Solow, 1965)

Consumption 10%

$$\frac{(1.8 \times 10^{12} \text{ Cal})(0.18 \text{ gr})}{365 \text{ d yr}^{-1}} = 8.9 \times 10^8 \text{ Cal d}^{-1}$$

(23) Catastrophic destruction by flood

Damage $\$1.7 \times 10^7$ (Gilbert, 1977)

$(\$1.7 \times 10^7)(1.1 \times 10^5 \text{ Cal}_{he} \ \$^{-1}) = 1.9 \times 10^{12} \text{ Cal}_{he}$

To convert to solar calories

Johnstown energy consumption in solar equivalents

Biomass consumption (note 15)

Plant biomass quality factor (Table 8)

$(3.8 \times 10^8 \text{ Cal}_{he} \text{ d}^{-1})(1.7 \times 10^3 \text{ Cal}_{se} \text{ Cal}_{he}^{-1}) = 7 \times 10^{11} \text{Cal}_{se} \text{d}^{-1}$

Fossil fuel consumption (note 6)

Fossil fuel quality factor (Table 8)

$(1. \times 10^9 \text{ Cal d}^{-1})(6.4 \times 10^4 \text{ Cal}_{se} \text{ C}_{he}^{-1}) = 6.4 \times 10^{13} \text{Cal}_{se} \text{d}^{-1}$

Notes to Table 10 - Continued

Quality factor for Johnstown = $\frac{6.4 \times 10^{13}\ \text{Cal d}^{-1}\ \text{solar}}{1.4 \times 10^{9}\ \text{Cal d}^{-1}} =$

$$4.6 \times 10^{4}\ \text{Cal Cal}^{-1}$$

Solar energy embodied in flood destruction

Solar energy lost

$(19 \times 10^{12}\ \text{Cal})\ (4.6 \times 10^{4}\ \text{Cal}_{se}\ \text{Cal}_{he}^{-1}) = 8.6 \times 10^{16}\ \text{Cal Solar}$

(24) Gravitational potential energy of water in South Fork

Reference Johnstown

South Fork elevation 1,618 ft (McCullough, 1968)

Johnstown elevation 1,120 ft (McCullough, 1968)

$E = mgh = (1.36 \times 10^{10}\ \text{kg})(9.8\ \text{m sec}^{-2})(1{,}618-1{,}120\ \text{ft}) \times .304\ \text{m ft}^{-1}$

$E = 2.01 \times 10^{13}\ \text{joules} \times 4.186 \times 10^{-3}\ \text{Cal joules}^{-1} = 8.43 \times 10^{10}\ \text{Cal}$

Potential energy per m^{-3} in South Fork reservoir with respect to Johnstown

$E = mgh$

$E/m^{3} = (1{,}000\ \text{kg m}^{-3})(9.8\ \text{m sec}^{-2})(1{,}618\ \text{ft} - 1{,}120\ \text{ft}) \times 0.304\ \text{m ft}^{-1}$

$E/m^{3} = 1.65 \times 10^{6}\ \text{joules m}^{3} \times 4.186 \times 10^{-3} = 6.94 \times 10^{3}\ \text{Cal m}^{-3}$

Slope of Conemaugh Valley

South Fork of Johnstown

$$\text{Slope} = \frac{\text{elevation}}{\text{distance}} = \frac{(1{,}618\ \text{ft}-1{,}120\ \text{ft})\,0.304\ \text{m ft}^{-1}}{16\ \text{mi} \times 1{,}390\ \text{m mi}^{-1}} =$$

$$\frac{151.4\ \text{m}}{25744\ \text{m}}$$

Slope $5.88 \times 10^{-3}\ \text{m m}^{-1}$

(25) Wave energy

Wave height 33 ft x $0.304\ \text{m ft}^{-1} = 10.\ \text{m}$

Notes to Table 10 - Continued

Wave velocity $\frac{16 \text{ mi} \times 1{,}609 \text{ m mi}^{-1}}{56 \text{ min} \times 60 \text{ sec min}^{-1}} = 7.66 \text{ m sec}^{-1}$

Wave width 500 m (from USGS map)

Assuming all water in reservoir in rectangular wave

$$L = \frac{V}{A} = \frac{1.3 \times 10^7 \text{ m}^3}{500 \text{ m} \times 10 \text{ m}} = 2.6 \times 10^3 \text{ m}$$

Linear kinetic energy per m^3 of water

$$E = 1/2 \text{ m } V^2 = 1/2 \ (1{,}000 \text{ kg m}^{-3})(7.66 \text{ m sec}^{-1})^2$$

$$E = 2.933 \times 10 \ \frac{\text{kg m}^2}{\text{sec}} \text{ m} = 2.933 \times 10^4 \text{ joules} \times 4.186 \times 10^{-3}$$

$$\text{Cal joule}^{-1} \text{ m}^{-3} \ 122.81 \text{ Cal m}^{-3}$$

Turbulence wave energy

$125 \ H^2$ ergs cm^{-2} (Weyl, 1970)

where H is in cm

$$H = 30 \text{ ft} \times 30.48 \text{ cm ft}^{-1} = 1{,}040 \text{ cm}$$

$$Q_w = 125 \ (1{,}040)^2 \text{ ergs cm}^{-2} \times 10{,}000 \text{ cm}^2 \text{ m}^{-2} \times 2.39 \times 10^{-11} \text{ Cal erg}^{-1}$$

$$Q_w = 32.3 \text{ Cal m}^{-2}$$

Total wave energy (Engineering News, 1889b)

$$K \ (32.3 \text{ Cal m}^{-2})(1.36 \times 10^7 \text{ m}^2) = 4.4 \times 10^7 \text{ Cal}$$

(26) Total wave energy

Linear + turbulent

Linear

$$(122 \text{ Cal m}^{-3})(1.36 \times 10^7 \text{ m}^3) = 1.67 \times 10^9 \text{ Cal}$$

Turbulent

$$(32 \text{ Cal m}^{-2})(1.36 \times 10^6 \text{ m}^2) = \underline{4.4 \times 10^7 \text{ Cal}}$$

$$\text{Total flood energy} = 1.7 \times 10^9 \text{ Cal}$$

Notes to Table 11

Guatemala Earthquake

(1) Strain in bars - relating the 230 km rupture and the 108 cm average fault displacement (Plafker, 1976) of the Motagua Fault during the 1976 Guatemala Earthquake on Dieterich (1974) graphical representation of scaling laws of seismic energy yield three bar strain release. This point also matches observed seismic energy release on Dieterich's monograph.

E_T = strain per unit volume x volume (see note 2)

$E_T = 3$ bar x 4.83×10^{16} cm^3

$E_T = 3 \times 10^6$ dynes cm^{-2} x 4.83×10^{16}cm^3

$E_T = 1.3 \times 10^{23}$ dynes cm = ergs

$E_T = 2.62 \times 10^{12}$ Cal

(2) Volume of material under strain = V = lwh

lenght = 230 km, width = 3 m, height = 7 km. Plafker (1976) gives a volume of 4.83×10^{16} cm^3.

(3) Observed value of stored energy at time of rupture based on back calculation

2.62×10^{12} Cal (Espinosa *et al*., 1976)

(4) Strain energy source, westernly nation of North American Plate

2.12 cm yr^{-1} x 3.17^{-8} yr sec^{-1} = 6.72×10^{-8} cm sec^{-1} (Jordan, 1975)

(5) Strain energy source, Caribbean Plate

0 cm yr^{-1} = 0 cm sec^{-1} (Jordan, 1975)

(6) Annual buildup of strain energy =

$$\frac{\text{total buildup } E_S}{\text{time}} + \text{depreciation (7)}$$

Notes to Table 11 - Continued

(7) Depreciation on annual energy lost through minor fault slips; 100 small shocks of estimated average magnitude of 4 on Richter scale report (Harlow, 1976)

$R_s = 9.4 + 2.14$ or $- 0.054M^2$ (Gutenberg and Richter, 1969)

$E_s = 2.25 \times 10^{19}$ ergs

Depreciation = $100 \text{ yr}^{-1} \times 2.55 \times 10^{19} \text{ergs} = 2.25 \times 10^{21} \text{ergs yr}^{-1}$

Depreciation = $2.25 \times 10^{21} \text{ ergs yr}^{-1} \times 2.39 \times 10^{11} \text{ Cal erg}^{-1} =$

$3.17 \times 10^{-8} \text{ yr sec}^{-1} \times 5.37 \times 10^{10} \text{ Cal yr}^{-1} = 1.76 \times 10^{3} \text{ Cal sec}^{-1}$

(8) Total seismic energy released in main event

M = 7.5 (Espinosa _et al_., 1976)

where M is the magnitude on Richter scale

$E_s = 9.4 + 2.14M^2$ (Gutenberg and Richter, 1969)

$E_s = 2.28 \times 10^{22} \text{ ergs} = 5.44 \times 10^{11} \text{ Cal}$

Energy lost in plate motion

(9) $E_T = E_s + W$ (Dieterich, 1974)

where $E_T = 2.62 \times 10^{12}$ Cal

$E_s = 5.44 \times 10^{11}$ Cal

(10) $W = 2.07 \times 10^{11}$ Cal

(11) Material strained

$$\frac{4.83 \times 10^{16} \text{ cm}^3}{2{,}000 \text{ yr}} = 2.4 \times 10^{14} \text{ cm}^3 \text{ yr}^{-1} \times 3.17 \times 10^{-8} \text{ yr sec}^{-1} = 7.61 \times 10^{6} \text{ cm sec}^{-1}$$

(12) Momentary storage M earthquake pulse

1.3×10^{6} Cal

(13) Calculations for typical house

3 = 6 m, w = 4.25, h = 2.5 m, wall thickness = 0.3 m,

Notes to Table 11 - Continued

density of adobe = 1.538 kg m^{-3}, long wall volume = 2 (6x2.5x.3)

+ 2(4.25x2.5x.3) = 15.37 m^3

mass = 15.37 x 1.538 kg m^{-3} = 2.4 x 10^4 kg

average h = $\frac{2.5}{2}$

PE = mgh = 2.4 x 10^4 x 9.8 x 1.25 = 2.9 x 10^5 J

PE walls = 2.9 x 10^{12} ergs

Roof:

mass = 40 m^2 x 0.05 m thick x 1,922 kg m^{-3} = 3,840 kg

PE = mgh = 3,840 x 9.8 x 3 = 1.13 x 10^3 J

PE house = 4.07 x 10^5 J = 4.07 x 10^{12} ergs = 97.2 Cal

Area of contact = thickness x p = 0.6 m^2

PE house/m^2 = $\frac{97.2 \text{ Cal}}{6 \text{ m}^2}$ = 15 Cal m^{-2}

Dissipation of energy

Volume of earth under house = 6.25 m^2 x 7,000 m

= 4.37 x 10^4 m^3

density of plate = 2,800 kg m^{-3}

mass of plate = 1.2250 x 10^8 kg

mass of house = 2.42 x 10^4 kg

fraction house = 1.9 x 10^{-4}

(14) Mass of houses in El Progreso

(2,208 houses)(3,840 kg $house^{-1}$) = 8.4 x 10^6 kg

(15) Seismic energy transmitted to El Progreso

1.17 x 10^6 Cal (see Table 12) x 1.66 sec^{-1} = 1.95 x 10^4 Cal sec^{-1}

Notes to Table 11 - Continued

(16) Energy dissipated by structure of El Progreso is given by number of structures x area of structure x energy per unit area.

2,208 (houses assuming 5 people per house) x 6 m^2 (per house foundation) x 3.2×10^{-3} Cal m^{-2} x 1.66×10^{-2} sec^{-1} = 0.7 Cal sec^{-1} (10)

(17) Depreciation is calculated by total storage of wave energy/time of half life

5.44×10^{11} Cal x 1.66×10^{-2} sec^{-1} (Espinosa *et al*., 1976)

= 9.04×10^{9} Cal sec^{-1}

(18) Construction and maintenance of buildings in El Progreso

10% annual construction maintenance of stock assumed

2.3 x 10 Cal yr^{-1} (gravitational) x 3.17×10^{-8} yr sec^{-1}

= 7.29×10^{-4} Cal sec^{-1}

(19) Damage 95%

2.3 x 10 Cal (per event) 1.66×10^{-2} sec^{-1} = 3.83×10^{3} Cal sec^{-1}

(20) Depreciation of El Progreso

Based on construction rate plus 5% growth

2.14 x 10 Cal yr^{-1} x 3.17×10^{-8} yr sec^{-1} = 6.78×10^{-4} Cal sec^{-1}

(21) Disorder material (see note 13)

Mass of town times 95% damage

5.8 x 10 kg (per event) x 1.66×10^{-2} sec^{-1} = 9.66×10^{4} kg sec^{-1}

(22) Construction material

Mass of town times construction rate

6.13×10^{5} kg yr^{-1} x 3.17×10^{-8} yr sec^{-1} = 1.94×10^{-2} kg sec^{-1}

APPENDIX II
DYNAMO PROGRAMS

```
GAMMA RADATION MODEL     8/16/78

 *      GAMMA RADATION MODEL
 L      Q1.K=Q1.J+DT*(R1.JK-R2.JK-R3.JK)
 N      Q1=42450
 A      Q2.K=57080-Q1.K
 R      R1.KL=K1*J*Q1.K*Q2.K/(1+K0*Q1.K*Q2.K)
 C      J=2300
 C      K0=3.22E-9
 C      K1=7E-11
 *      RADATION SECTION
 A      R0.K=X-(R*1E2*6.6E-5)*X
 C      X=744.5
 R      R2.KL=CLIP(RX.K,0,93,TIME.K)
 A      RX.K=K2*R0.K*Q1.K/((1+K4*Q1.K)*(4*3.14*R*R*1E4))
 C      K2=1.35E2
 C      K4=1.436E-4
 R      R3.KL=K3*Q1.K
 C      K3=0.0005183
 C      R=20
 PRINT Q1,Q2,R1,R2,R3,J,R0
 PLOT  Q1=1,Q2=2(0,75000)/R1=*,R2=%,R3=+
 SPEC     DT=.1/LENGTH=365/PLTPER=7.3/PRTPER=73
 RUN
```

```
JOHNSTOWN FLOOD MAY 31 1889     8/01/78

 *    JOHNSTOWN FLOOD MAY 31 1889
 *    FAILURE OF THE SOUTH FORK DAM
 L   Q1,K=Q1,J+DT*(R1,JK-R2,JK-R3,JK)
 N   Q1=1,36E7
 R   R1,KL=(K1*J*Q2,K)/(K0*Q1,K+1)
 C   K0=1.57E-8
 C   J=7E-6
 C   K1=0,414
 R   R2,KL=K2*Q1,K
 C   K2=7.27E-6
 R   R3,KL=K3*Q1,K*Q3,K
 C   K3=9,87E-8
 L   Q3,K=Q3,J+DT*(R2.JK+R4,JK-R6,JK)
 N   Q3=990
 R   R4,KL=K4*Q1,K*Q3,K
 C   K4=2,52E-8
 R   R6,KL=K6*Q3,K
 C   K6=0,1
 A   Q2,K=L-K7*Q1,K
 C   L=1,55E8
 C   K7=0,053
 *   MODEL OF JOHNSTOWN 1889
 L   Q6,K=Q6,J+DT*(R8.JK-R9,JK-R10,JK)
 N   Q6=Q6I
 C   Q6I=2.5E13
 R   R8,KL=K8*R
 C   R=1,4E12
 C   K8=2E-3
 R   R9,KL=K9*Q4,K*Q5,K*Q5,K*Q7,K
 C   K9=2,55E-39
 R   R10,KL=K10*Q6,K
 C   K10=9,6E-6
 L   Q7,K=Q7,J+DT*(-R12,JK)
 N   Q7=3E15
 R   R12,KL=K12*Q4,K*Q5,K*Q6,K*Q7,K
 C   K12=6.75E-39
 L   Q4,K=Q4,K+DT*(R14,JK-R13,JK-R15,JK-R16.JK)
 N   Q4=1,8E12
 R   R13,KL=K13*Q4,K*Q5,K*Q6,K*Q7,K
 C   K13=1,35E-39
 R   R14,KL=K14*Q4,K*Q5,K*Q6,K*Q7,K
 C   K14=9,45E-39
 R   R15,KL=K15*Q4,K
 C   K15=4,9E-4
 R   R16,KL=K16*Q3,K*Q4,K
 C   K16=8E-8
 A   Q5,K=C-K11*Q4,K
 C   K11=3E-7
 C   C=1,1E6
 SPEC DT=0,01/LENGTH=100/PLTPER=2/PRTPER=10
 PRINT Q1,Q2,Q3,R1,R2,R3,R4,R6,Q4,Q5,Q6,Q7,R16
 PLOT Q1=1/Q2=2/Q3=3/R3=*
 PLOT Q3=3/Q4=4/R16=+
 RUN
```

```
EARTHQUAKE SIMULATION     3/14/78

 *   EARTHQUAKE SIMULATION
 L     Q1.K=Q1.J+DT*(R1.JK-R2.JK-R3.JK)
 N     Q1=Q1I
 C     Q1I==2.62E12
 R     R1.KL=K1*(E1-E2)*Q2.K
 C     K1=3.90E-2
 C   E1=2.12
 C   E2=0
 R     R2.KL=K2*Q1.K
 C     K2=2.04E-2
 R     R3.KL=K3*'      *Q1.K xQ6.K.
 C     K3= 2.04E-2
 A       Q2.K=CE-Q1.K
 C       CE=3E12
 L       Q3.K=Q3.J+DT*(R4.JK-R7.JK-R8.JK)
 N       Q3=0
 R       R4.KL=K4*Q1.K*SW.K
 C       K4=.2341
 R       R7.KL=K7*Q3.K*Q4.K
 C       K7=7.935E-5
 *       R8.KL=K8*Q3.K
 R     R9.KL=CLIP(K8*Q3.K.Q3.K/DT.Q3.K/DT.K8*Q3.K)
 C       K8=1.048E6
 L       Q4.K=Q4.J+DT*(R9.JK-R11.JK-R10.JK)
 N       Q4=Q4I
 C       Q4I=.214E6
 R       R9.KL=K9*E3*Q4.K*Q5.K
 C     E3=.23E6
 C     K9=10.94E-13
 R       R11.KL=K11*Q4.K
 C       K11=.1
 *       R10.KL=K10*Q3.K*Q4.K
 R     R10.KL=CLIP(K10*Q3.K*Q4.K,Q4.K/DT.Q4.K/DT,K10*Q3.K*Q4.K)
 C       K10=.383
 A     Q5.K=CT-Q4.K
 C     CT=1E6
 A     SW.K=PULSE(10..95E-5.20)
 PLOT  Q1=1/Q2=2/Q3=3/Q4=4/Q5=5
 PRINT Q1.Q2.Q3.Q4.Q5
 PRINT R1,R2,R3,R4,R7.R8.R9
 SPEC DT=1.9E-7/LENGTH=3.8E-5/PLTPER=1.9E-7/PRTPER=1.9E-7
 RUN
```

```
ORDER-DISORDER MODEL    11/29/76
 *   ORDER-DISORDER MODEL
 *   DYMANO MODEL FOR FIG. 3.2
 L     Q1.K=Q1.J+DT*(RT.JK-R1.JK-R2.JK)
 N     Q1=Q1I
 C     Q1I=.01
 R     RT.KL=K1*E1.K*QT.K
 A     QT.K=QTI
 C     QTI=1.0
 R     R1.KL=K1*E1.K*Q1.K
 A     E1.K=E1I
 C     E1I=1.0
 C     K1=0.2
 R     R2.KL=K2*E2.K*Q1.K
 A     E2.K=E2I
 C     E2I=1.0
 C     K2=.02
 A     Q2.K=QT.K-Q1.K
 A     Q1DOT.K=RT.JK-R1.JK-R2.JK
 A     GROWTH.K=Q1DOT.K/Q1.K
 SPEC  DT=.01/LENGTH=50/PLTPER=1.0/PRTPER=2.5
 PRINT  Q1,Q2,Q1DOT,GROWTH,QT,R1,R2
 PLOT  Q1=C,GROWTH=*,Q2=D,QT=T,R1=1,R2=2(0,1)
 RUN
```

```
AUTOCATALYTIC ORDER-DISORDER MODEL    11/29/76

 *   AUTOCATALYTIC ORDER-DISORDER MODEL
 *   DYMANO MODEL FOR FIG. 3.4
 L     Q1.K=Q1.J+DT*(RT.JK-R1.JK-R2.JK)
 N     Q1=Q1I
 C     Q1I=.01
 R     RT.KL=K1*QT.K*Q1.K
 A     QT.K=QTI
 C     QTI=1.0
 R     R1.KL=K1*Q1.K*Q1.K
 C     K1=0.2
 R     R2.KL=K2*E2.K*Q1.K
 A     E2.K=E2I
 C     E2I=1.0
 C     K2=.02
 A     Q2.K=QT.K-Q1.K
 A     Q1DOT.K=RT.JK-R1.JK-R2.JK
 A     GROWTH.K=Q1DOT.K/Q1.K
 SPEC  DT=.01/LENGTH=50/PLTPER=1.0/PRTPER=2.5
 PRINT  Q1,Q2,Q1DOT,GROWTH,QT,R1,R2
 PLOT  Q1=C,GROWTH=*,Q2=D,QT=T,R1=1,R2=2(0,1)
 RUN
```

LIST OF REFERENCES

Alexander, J. F. and N. G. Sipe. 1977. An Interdisciplinary Approach to Earthquake Redevelopment, A Case Study of El Progreso, Guatemala. Urban and Regional Planning Publication Series No. 9. University of Florida, Gainesville, Florida. 269 pp.

Alexander, J. F., N. G. Sipe, and H. T. Odum. 1976. A United States energy model economically driven by a global growth stimulation. Pages 1019-1023 in Modeling and Simulation Vol. II. Proceedings of Seventh Annual Pittsburgh Conf. University of Pittsburgh, Pittsburgh Pa.

Ambruster, J. T. 1978. Model of the flooding caused by the failure of the Laurel Run reservoir dam, 20 July, 1977, near Johnstown, Pa. Proceedings of American Meteorological Society Conf. on Flash Floods, Los Angeles, Cal. In press.

Ayre, R. S. 1975. Earthquake and Tsunami Hazards in the United States, A Research Assessment. University of Colorado, Boulder. 127 pp.

Balcarcel, M. A. and O. R. Orellana. 1978. El Progreso de Reconstruccion de Guatemala. Simposio Internacional Sobre El Terremoto de Guatemala del 4 de Febrero de 1976, Comite de Reconstruccion Nacional, Guatemala, C. A. 54 pp.

Berg, J., K. Gaskell, and V. Rigehat. 1964. Earthquake energy release and isostasy. Bulletin of the Seismological Society of America 54(2):777-784.

Bolin, B. 1970. The carbon cycle. Scientific American 223(3):124-32.

Bolt, B. A., W. L. Horn, G. A. MacDonald, and R. F. Scott. 1977. Geological Hazards. Springer-Verlag, New York. 330 pp.

Bonis, S. 1976. The 1974 eruption of Volcan de Fuego, Guatemala. (Abs.) EOS Am. Geophys. Union Trans. 57(4):345.

Brady, N. C. 1974. The Nature and Properties of Soil. 8th edition, Macmillan, New York, 639 pp.

Bray, J. 1967. Variation in atmospheric corbon-14 activity relative to sunspot-auroral solar index. Science 156(3775):640-642.

Brua, S. A. and C.P. Humphries. 1978. Hydrology of the 19-20 July 1977 Johnstown flood. Proceedings of the American Meteorological Society Conf. on Flash Floods in Los Angeles, Cal. In press.

Brune, J. N. 1968. Seismic moment, seismicity, and rate of slip along major fault zones. J. Geophys. Res. 73(2):777-784.

Budyko, M. T. 1969. The effects of solar radiation variations on the climate of the earth. Tellus 21:611-619.

Byers, H. T. 1974. General Meteorology. McGraw-Hill, New York. 461 pp.

Byram, G. M., H. B. Clements, M. E. Bishop, and R. M. Nelson. 1966. Final Report, Project Fire Model, An Experimental Study of Model Fires. Office of Civil Defense OCD-P5-6540. Washington, D.C. 44 pp.

Canog, M. J. 1972. Deoxyribonucleic acid in ecosystems. Ph.D. Dissertation. University of North Carolina, Chapel Hill. 355 pp.

Censo de Vivienda. 1973. Direccion General de Estadistica. Ministerio de Economia, Guatemala, C. A. 95 pp.

Charney, J. G. 1955. General circulation ocean currents by wind. Journal of Marine Research 14:477-518.

Chinnery, M. A. 1963. The stress changes that accompany strike-slip faulting. Bulletin of the Seismological Society of America 53(5):921-932.

Clark, S. P. 1971. Structure of the Earth. Prentice-Hall, Inc. Englewood Cliffs, N.J. 127 pp.

Cochrane, H. C. 1975. Natural Hazards and Their Disruption Effects. University of Colorado, Institute of Behavioral Sciences, Boulder. 135 pp.

Comite de Emergencia, Guatemala. 1976. Casualty and Damage Data. 150 pp.

Dacy, D. C. and H. Kunreuther. 1969. The Economics of Natural Disasters, Implications for Federal Policy. The Free Press, New York. 220 pp.

Desmarais, P. A. and B. T. Helmuth. 1970. Effects of ^{137}Cs radiation on vegetation, structure, and optical density at El Verde. Pages D77-D102 in H. T. Odum and R. F. Pigeon, eds. A Tropical Rain Forest, A Study of Irradiation and Ecology at El Verde, Puerto Rico. U.S. Atomic Energy Commission, Washington, D.C.

Dewey, E. R. 1971. Cycles, the Mysterious Forces that Trigger Events. Hawthorn Books, Inc., New York.

Dewey, J. W. and B. R. Julian. 1976. Main event source parameters from tales issue data. Pages 17-23 in The Guatemalan Earthquake of February 4, 1976, A Preliminary Report. USGS professional paper 1002. U.S. Govt. Printing Office, Washington, D.C.

Dienes, G. H. 1970. A kinetic model of radiation response to field irradiation. Pages 49-52 in H. T. Odum, and R. F. Pigeon, eds. A Tropical Rain Forest, A Study of Irradiation and Ecology at El Verde, Puerto Rico. U.S. Atomic Energy Commission, Washington, D.C.

Dieterich, J. H. 1974. Earthquake mechanisms and modeling. Pages 275-301 in The Guatemalan Earthquake of February 4, 1976, A Preliminary Report. USGS professional paper 1002. U.S. Govt. Printing Office, Washington, D.C.

Dunn, G. E. and B. I. Miller. 1964. Atlantic Hurricanes, Louisiana State University Press, Baton Rouge. 377 pp.

Eddy, J. A. 1976. The maunder minimum. Science 192(4245):1189-1201.

Ekman, W. W. 1905. On the influence of the earth's rotation on ocean currents. Ark. Mat. Astron. Eys. 2:1-53.

Engineering News. 1889a. The South Fork Dam and Johnstown disaster. 21:517-518.

Engineering News. 1889b. The work of the flood at Johnstown. 21:569-573.

Engineering Record. 1891. Report of the Special Committee of the American Society of Civil Engineers on the "Cause of the Failure of the South Fork Dam." 20:198.

Engineering Society of Western Pennsylvania. 1889. The South Fork Dam. Proceedings 5:89-99.

Ericksen, J. J. 1975. Scenario Methodology in Natural Hazard Research. University of Colorado Institute of Behavioral Sciences, Boulder. 125 pp.

Espinosa, A. F., R. Husid, and A. Quesada. 1976. Intensity distribution and source parameters from field observations. Pages 52-69 in The Guatemalan Earthquake of February 4, 1976, A Preliminary Report. USGS professional paper 1002. U.S. Govt. Printing Office, Washington, D.C.

Evaluacion de los daños causados por el terremoto. 1976. Su impacto sobre el desarrollo economico y social, y lineamientos para un programa inmediato de reconstruccion. Planificacion Economica, Guatemala. 125 pp.

FAA 1971. Yearbook of Forest Products. 1969-1970. Rome: Food and Agricultural Organization of the United Nations. United Nations Publication Service, New York. 822 pp.

Forrester, J. W. 1970. World Dynamics. Wright-Allen Press, Inc. Cambridge, Mass. 142 pp.

Friedman, D. G. 1975. Computer Simulation in Natural Hazard Assessment. University of Colorado Institute of Behavioral Sciences, Boulder. 192 pp.

Frisken, W. R. 1973. The Atmospheric Environment. John Hopkins University Press, Baltimore, Ma. 68 pp.

Gates, D. M. 1962. Energy Exchange in the Biosphere. Harper and Row, New York. 315 pp.

Gilbert, B. 1977. Floodtrap city: Johnstown, Pa. Audobon 79(6):2-10.

Gilliland, M. W. 1975. System models for phosphorus management in Florida. Pages 179-207 in F. G. Howell, J. B. Gentry, and M. H. Smith eds., Mineral Cycling in Southeastern Ecosystems. ERDA Symposium Series, Conf-740513. U.S. Energy Research and Development Administration, Washington, D.C.

Giron, R. A. 1976. Aplicacion del Catastro en la Reconstruccion de la Ciudad de El Progreso. Instituto Geografico Nacional, Guatemala, C. A. 39 pp.

Gloyna, E. F. and J. O. Ledbetter. 1969. Principles of Radiological Health. Marcel Oekker, New York. 473 pp.

Golley, F. B. 1972. Energy flux in ecosystems. Pages 69-90 in J. A. Wiens, ed., Ecosystem Structure and Function, Vol. 31. Annual Biological Colloquium, Oregon State Univ., Corvallis.

Goody, R. M. and J. C. G. Walker. 1972. Atmospheres. Prentice-Hall, Englewood Cliffs, N. J. 150 pp.

Gutenberg, B. and C. F. Richter. 1942. Earthquake magnitude, intensity, energy and acceleration. Bulletin of the Seismological Society of America 32:163-191.

Gutenberg, B and C. F. Richter. 1969. Earthquake magnitude, intensity, energy and acceleration. Pages 105-143 in Geologic Hazards and Public Problems, Conf. Proceedings, Office of Emergency Preparedness, Santa Rosa, Cal.

Haas, J. E., R. W. Kates, and N. J. Bowden. 1977. Reconstruction Following Disaster. M.I.T. Press, Cambridge, Mass. 331 pp.

Harbaugh, J. W. and G. Bonham-Carter. 1970. Computer Simulation in Geology. Wiley-Interscience, New York. 575 pp.

Harlow, D. 1976. Instrumentally recorded seismic activity prior to the main event. Pages 12-16 in The Guatemalan Earthquake of February 4, 1976, A Preliminary Report. USGS professional paper 1002. U. S. Government Printing Office, Washington, D.C.

Hayakawa, M. 1976. Energy balance of earth's crust estimated from geophysical data. Pages i and ii in Aoki and S. Iisuka, eds. Volcanoes and Tectonosphere. Tokyo University Press, Tokyo, Japan.

Hendershott, M. C. 1977. Numerical models of the ocean tides. Pages 47-96 in E. D. Goldbreeg, I. N. McCave, J. J. O'Brien, and J. H. Steele, eds. The Sea, Ideas and Observations on Progress in the Study of the Sea. John Wiley and Sons, New York.

Hirshleifer, J. and D. L. Shapiro. 1969. The treatment of risk and undertainty. Pages 505-530 in R. J. Haveman and J. Margalois, eds. Analysis and Evaluation of Public Expenditures: The PPB System, Vol. I. Markham, Chicago, Ill.

Historical Statistics of the United States. 1975. Department of Commerce. U. S. Government Printing Office, Washington, D.C.

Holland, W. R. 1977. Ocean general circulation models. Pages 3-45 in E. D. Goldberg, I. N. McCave, J. J. O'Brien, and J. H. Steele, eds. The Sea, Ideas and Observations on Progress in the Study of the Sea. John Wiley and Sons, New York.

Houghton, H. G. 1954. On the annual heat balance of the northern hemisphere. J. of Meteorology 11(1):1-9.

Hubbert, M. K. 1971. The energy resources of the earth. Scientific American 224(3):60-70.

Husid, R., A. F. Espinosa, and A. Quesada. 1976. Damage and engineering implication. Pages 67-69 in The Guatemalan Earthquake of February 4, 1976, A Preliminary Report. USGS professional paper 1002, U.S. Government Printing Office, Washington, D.C.

Jordan, T. H. 1975. The present-day motions of the Caribbean plate. J. Geophys. Res. 80(2):4433-4439.

Kahn, H. and A. J. Wiener. 1967. The Year 2000, A Framework for Speculation on the Next Thirty-Three Years. Macmillan, New York. 431 pp.

Kinsman, B. 1965. Wind, Waves, Their Generation and Propogation on the Ocean Surface. Prentice-Hall, Inc., Englewood Cliffs, N.J. 630 pp.

Komarek, E. V. 1962. Fire Ecology Proceedings of First Annual Tall Timbers Fire Ecology Conference. March, published by Tall Timbers Research Station, Tallahassee, Fla. 186 pp.

Liebig, J. von. 1862. Die Naturgesetze des Feldbaues. Braunschweigh, Vieweg 467 pp.

Lieth, H. 1975. Modeling the primary productivity of the world. Pages 237-263 in H. Lieth and R. H. Whittaker, eds. Primary Productivity of the Biosphere. Springer-Verlag, New York.

Lieth, H. and R. H. Whittaker. 1975. Primary Productivity of the Biosphere. Springer-Verlag, New York. 339 pp.

Lotka, A. J. 1922. Contribution to the energetics of evolution. Proceedings National Academy of Science 8:147-155.

Lugo, R. L. and S. C. Snedaker. 1974. The ecology of mangroves. Annual Review of Ecology and Systematics (5):39-64.

McCullough, D. G. 1968. The Johnstown Flood. Simon and Schuster, New York. 302 pp.

McDowell, A. 1976. Earthquake in Guatemala. National Geographic May 1976:810-829.

Meadows, D. L., W. W. Behrens, D. H. Meadows, R. F. Naill, J. Randers, E. K. Zahu. 1974. Dynamics of Growth in a Finite World. Wright Allen Press, Inc., Cambridge, Mass. 637 pp.

Michaelis, L. and M. L. Mentem. 1913. Die kinetik der invertin wirkung. Biochemische Zertschrift 49:333-369.

Mintz, Y. 1968. Very long term integration of primitive equations of atmospheric notion: An experiment in climate simulation. Meteorol. Monog., American Meteorological Society, Boston. 8:20-36 pp.

Monin, S. A., V. K. Kamenkovich, and V. G. Kort. 1977. Variability of the Oceans. J. L. Lumley, ed. (English translation from Russian). John Wiley, New York. 235 pp.

Murphy, P. G., R. R. Sharitz, and A. J. Murphy. 1977. Response of a forest ecotone to ionizing radiation. Pages 43-48 in J. Zavitkovski, ed. The Enterprise, Wisconsin, Radiation Forest Radioecological Studies. Energy Research and Development Administration. USAEC, Springfield, Va.

National Advisory Committee on Oceans and Atmosphere. 1972. The Agnes Floods: A Post-Audit of the Effectiveness of Storm and Flood Warning Systems of NOAA. U.S. Government Printing Office, Washington, D.C.

National Oceanic and Atmospheric Administration. 1977. Johnstown, Pennsylvania Flash Flood of July 19-20, 1977. A Report to the Administrator, Natural Disaster Survey Report 77-1. U. S. Department of Commerce, Rockville, Md. 40 pp.

Niler, P. P. 1977. One dimensional model of the seasonal thermocline. Pages 97-115 in E. D. Goldbreeg, I. N. McCave, J. J. O'Brien, and J. H. Steele, eds. The Sea, Ideas and Observations on Progress in the Study of the Sea. John Wiley and Sons, New York. 1048 pp.

North, G. R. 1975. Theory of energy-balance climate models. Journal of the Atmospheric Sciences 32(11):2033-2042.

Odum, E.P. 1971. Fundamentals of Ecology. W. B. Saunder Co., Philadelphia, Pa. 574 pp.

Odum, H. T. 1970a. The El Verde study area and the rain forest system of Puerto Rico. Pages B3-B32 in H. T. Odum and R. F. Pigeon, eds. A Tropical Rain Forest, A Study of Irradiation and Ecology at El Verde, Puerto Rico. U.S. Atomic Energy Commission, Washington, D.C.

Odum, H. T. 1970b. The AEC rain forest program. Pages C3-C22 in H. T. Odum and R. F. Pigeon, eds. A Tropical Rain Forest, A Study of Irradiation and Ecology at El Verde, Puerto Rico. U.S. Atomic Energy Commission, Washington, D.C.

Odum, H. T. 1970c. Summary, an emerging view of the ecological system at El Verde. Pages I191-I289 in H. T. Odum and R. F. Pigeon, eds. A Tropical Rain Forest, A Study of Irradiation and Ecology at El Verde, Puerto Rico. U.S. Atomic Energy Commission, Washington, D.C.

Odum, H. T. 1971. Environment Power and Society. Wiley-Interscience, New York. 331 pp.

Odum, H. T. 1972. Chemical cycles with energy circuit models. Pages 223-259 in O. Dyrssen and D. Jayner, eds. Nobel Symposium No. 20. John Wiley and Sons, New York.

Odum, H. T. 1973. Energy, ecology, and economics. Ambro 2:220-227.

Odum, H. T. 1974. The effects of herbicides in South Vietnam. National Academy of Sciences-National Research Council, Washington, D.C. 320 pp.

Odum, H. T. 1975. Marine ecosystems with energy circuit diagrams. Pages 127-150 in J. C. J. Nihoul, ed. Modelling of Marine Systems, Elsevier Scientific Publishing Co., Amsterdam.

Odum, H. T. 1978. Energy analysis, energy quality, and environment. Pages 53-87 in M. W. Gilliland, ed. Energy Analysis, A New Public Policy Tool. AAAS Selected Symposium #9. Westview Press, Inc, Boulder, Colo.

Odum, H. T. and G. Drewry. 1970. The cesium source at El Verde. Pages C23-C36 in H. T. Odum and R. F. Pigeon, eds. A Tropical Rain Forest, A Study of Irradiation and Ecology at El Verde, Puerto Rico. U.S. Atomic Energy Commission, Washington, D.C.

Odum, H. T., G. Drewry, and J. R. Kline. 1970. Climate at El Verde, Pages B347-B418 in H. T. Odum and R. F. Pigeon, eds. A Study of Irradiation and Ecology at El Verde, Puerto Rico. U. S. Atomic Energy Commission, Washington, D.C.

Odum, H. T. and E. C. Odum. 1976. Energy Basis for Man and Nature. McGraw-Hill, New York. 297 pp.

Odum, H. T. and R. F. Pigeon. 1970. A Tropical Rainforest. U.S. Atomic Energy Commission, Division of Technological Information TID-24270 (RRNC-138). 1561 pp.

Oliger, J.E., R. E. Welch, A. Kasahard, and W. M. Washington. 1970. Description of the NCAR global circulation model. National Center for Atmospheric Research, Boulder, Colo.

Olson, J. S. 1970. Carbon cycles and temperate woodlands. Pages 226-241 in D. E. Reichle, ed. Analysis of Temperate Forest Ecosystems. Ecological Studies. Springer-Verlag, New York.

Oxford Economic Atlas of the World. 1965. Third edition. Amen House, London, England.

Plafker, G. 1976. Tectonic aspects of the Guatemalan earthquake of February 4, 1976. Science 193(4259):1201-1208.

Plafker, G., M. Bonilla, and S. Bonis. 1976. Geologic effects. Pages 38-51 in The Guatemalan earthquake of February 4, 1976, A Preliminary Report. USGS professional paper 1002. U.S. Government Printing Office, Washington, D.C.

Pugh, A. L. 1970. DYNAMO User's Manual. Third Edition. M.I.T. Press, Cambridge, Mass. 100 pp.

Raxton, B. P. 1968. Order and disorder in land: Land evaluation. Pages 29-31 in Division of Land Research. CSYRO, Camberra, Australia.

Richey, J. E. 1970. The role of disordering energy in microcosms. Master's Thesis. University of North Carolina, Chapel Hill. 125 pp.

Richter, C. F. 1958. Elementary Seismology. W. H. Freeman and Co., San Francisco, Cal. 450 pp.

Rogers, G. W. 1970. Economic effects of the earthquake. Pages 58-76 in The Great Alaska Earthquake of 1974. Human Ecology. National Academy of Science, Washington, D.C.

Rosenberg, N. J. 1974. Microclimate: The Biological Environment. John Wiley and Sons, New York. 315 pp.

Rudolph, T. D. 1974. The Enterprise, Wisconsin, Radiation Forest Preirradiation Ecological Studies. USAEC, Washington, D.C.

Ryther, J. H. 1969. Photosynthesis and fish production in the sea. Science 166:72-76.

SCEP. 1970. Man's Impact on the Global Environment: Report of the Study of Critical Environmental Problems (SCEP). Massachusetts Institute of Technology, Cambridge. 319 pp.

Schlesinger, W. H. 1977. Carbon balance in terrestrial detritus. American Review of Ecology and Systematics 8:51-81.

Schneider, S. H. and C. Mass. 1975. Volcanic dust, sunspots, and temperature trends. Science 190(4216):741-746.

Schroeder, H. 1919. Die jährliche Gesamtproduktion der grünen Pflanzendecke der Erde. Naturwissenschaften 7:8-12.

Sellers, W. D. 1965. Physical Climatology. University of Chicago Press, Chicago, Ill. 272 pp.

Sellers, W. D. 1969. A climate model based on the energy balance of the earth-atmosphere systems. Journal of Applied Meteorology 8:392-400.

Shappee, D. N. 1940. A history of Johnstown and the great flood of 1889, A study of disaster and rehabilitation. Ph.D. Dissertation University of Pittsburg, Pittsburgh, Pa. 630 pp.

Skinner, B. J. and K. K. Turekian. 1973. Man and the Ocean. Prentice-Hall, Inc., Englewood Cliffs, N.J. 149 pp.

Smagorinsky, J. 1969. Problems and promises of deterministic extended range forcasting. Bull. Amer. Meteorol. Soc. 50:286-311.

Smagorinsky, J. 1974. Global atmospheric modeling and numerical simulation of climate. Pages 633-686 in W. N. Hess ed. Weather and Climate Modification. John Wiley, New York.

Solow, R. M. 1954. A contribution to the theory of economic growth. The Quarterly Journal of Economics. 70:55-94.

Solow, R. M. 1962. Technical progress, capital formation and economic growth. American Economic Review 52:76-86.

Spears, F. W. and M. W. Zemansky. 1955. University Physics. Addison-Wesley Publishing Co., Reading, Mass. 520 pp.

Spence, W. and W. Person. 1976. Tectonic setting and seismicity. Pages 4-11 in The Guatemalan earthquake of February 4, 1976, A Preliminary Report, USGS professional paper 1002. U.S. Govt. Printing Office, Washington, D.C.

Statistical Abstract of the United States. 1975. U.S. Bureau of the Census, Washington, D.C. 1050 pp.

Stommel, H. 1948. The westward intensification of wind-driven ocean currents. Transactions of American Geophysical Union 29:202-206.

Sverdup, H. U. 1947. Wind-driven currents in a baroclinic ocean, with application to the equatorial currents of the eastern Pacific. Proceedings of The National Academy of Sciences 33:319-326.

Tarr, A. C. and K. L. King. 1976. Puerto Rico Seismic Program. U.S. Geolo. Survey (open file report). 23 pp.

Thom, R. 1975. Structural Stability and Morphogenesis. D. H. Fowler, translator. W. A. Benjamin, Inc., Reading, Mass. 348 pp.

Thompson, J. N. 1976. The Lubbock Storm of May 11. A report prepared for the Committee on Earthquake Inspection of the National Academy of Engineering. National Academy of Sciences, Washington, D.C.

Thurow, L. C. and L. D. Taylor. 1966. The interrelation between actual and potential ratios of growth. Review of Economics and Statistics. 48:351-360.

United Nations Statistical Year Book. 1975. United Nations Publication Service, New York.

Van Nostrand's Scientific Encyclopedia. 1976. D. C. Considine ed. Van Nostrand Reinhöld Co., New York. 2370 pp.

Vonder Haar, T. H. and V. E. Suomi. 1971. Measurement of the earth's radiation budget from satellites during a five-year period. J. Atmos. Sci. 28(3):305-314.

Walker, D. A. 1976. Yearly seismic energy release; world totals versus ridge system totals. Science 193:886-888.

Walsh, J. J. 1972. Implications of a systems approach to oceanography. Science 176:969-975.

Weyl, P. K. 1970. Oceanography, An Introduction to the Marine Environment. John Wiley and Sons, Inc. New York. 535 pp.

White, G. F. and J. E. Haas. 1975. Assessment of Research on Natural Hazards. M.I.T. Press, Cambridge, Mass. 487 pp.

Whittaker, R. H. 1970. Communities and Ecosystems. Macmillan, New York. 162 pp.

Whittaker, R. H. and G. E. Likens. 1973. Primary production in the biosphere and man. Human Ecology 1:357-367.

Whittaker, R. H. and G. E. Likens. 1975. The biosphere and man. Pages 305-326 in H. Lieth and R. H. Whittaker, eds. Primary Productivity of the Biosphere. Springer-Verlag, New York.

Woodwell, G. 1963. Design of the Brookhaven Experiment on the Effects of Ionizing Radiation on a Terrestrial Ecosystem. USAEC Report BNL-6772. Brookhaven National Laboratory.

Woodwell, G. M. and A. L. Rebuck. 1967. Effects of chronic gamma irradiation on the structure and diversity of an oak-pine forest. Ecol. Monogr. (37):53-69.

Zavitkovski, J. 1977. The Enterprise, Wisconsin, Radiation Forest Radioecological Studies. Technical Information Center, Energy Research and Development Administration. NTIS,Springfield, Va. 210 pp.

Zavitkovski, J., T. D. Rudolph, and E. O. Bauer. 1974. Predicted effects of chronic gamma irradiation on northern forest communities. Pages 137-144 in T. D. Rudolph, ed. The Enterprise, Wisconsin Radiation Forest Preirradiation Ecological Studies. USAEC, NTIS, Springfield, Va.

Zavitkovski, J. and B. J. Salmonson. 1977. Effects of gamma radiation on biomass production of ground vegetation under broadleaved forests of northern Wisconsin. Pages 35-42 in J. Zavitkovski, ed. The Enterprise, Wisconsin, Radiation Forest Radioecological Studies. Technical Information Center, Energy Research and Development Administration. NTIS, Springfield, Va.

BIOGRAPHICAL SKETCH

John F. Alexander, Jr., was born in Tallahassee, Florida, on January 26, 1943. He grew up in Tallahassee where he attended and graduated from Leon High School. In September 1961, he entered the University of Florida as a student in Electrical Engineering. After one semester, he transferred to Florida State University as a student in Engineering Science.

Upon graduation with a Bachelor of Science with a major in engineering science in April 1965, he accepted the position of Electronics Design Engineer, a position he held until appointed as an instructor of Engineering Science in 1967. As a part time graduate student, he received the Master of Science with a major in engineering science in December 1971.

In 1972 he was employed as engineer of population with the Florida Department of Transportation. In 1974 he joined the Florida Division of State Planning as a senior planner and information systems manager.

In January 1975, he was appointed associate professor of Urban and Regional Planning at the University of Florida, the position held at present. While at the University of Florida, he has directed several research projects through the Urban and Regional Department and the Center for Wetlands.

While at the University of Florida, as a student in Environmental Engineering Science Systems Ecology program, course work for the Doctor of Philosophy was completed and he was graduated in 1978.

I certify that I have read this study and that in my opinion it conforms to acceptable standards of scholarly presentation and is fully adequate, in scope and quality, as a dissertation for the degree of Doctor of Philosophy.

H T Odum

Dr. Howard T. Odum, Chairman
Graduate Research Professor of
Environmental Engineering Science

I certify that I have read this study and that in my opinion it conforms to acceptable standards of scholarly presentation and is fully adequate, in scope and quality, as a dissertation for the degree of Doctor of Philosophy.

James F. Burns

Dr. James F. Burns, Professor
of Industrial and Systems Engineering

I certify that I have read this study and that in my opinion it conforms to acceptable standards of scholarly presentation and is fully adequate, in scope and quality, as a dissertation for the degree of Doctor of Philosophy.

Paul L D

Dr. Paul L. Doughty, Professor
of Anthropology

I certify that I have read this study and that in my opinion it conforms to acceptable standards of scholarly presentation and is fully adequate, in scope and quality, as a dissertation for the degree of Doctor of Philosophy.

Dr. Wayne C. Huber
Associate Professor of
Environmental Engineering Science

I certify that I have read this study and that in my opinion it conforms to acceptable standards of scholarly presentation and is fully adequate, in scope and quality, as a dissertation for the degree of Doctor of Philosophy.

Charles E. Roessler
Dr. Charles E. Roessler
Associate Professor of
Environmental Engineering Science

This dissertation was submitted to the Graduate Faculty of the College of Engineering and to the Graduate Council, and was accepted as partial fulfillment of the requirements for the degree of Doctor of Philosophy

August 1978

Hubert A. Bevis
Dean, College of Engineering

Dean, Graduate School

K544 [illegible]
NM5.2. 7.8. 3.095